Petrography, Metamorphism, and Geochemistry of the Bermeja Complex and Related Rocks in Southwestern Puerto Rico, and their Significance in the Evolution of the Eastern Greater Antillian Island Arc

A thesis presented to the Faculty
of the State University of New York
at Albany
in partial fulfillment of the requirements
for the degree of Master of Science

Victor J. B. Lee

1974

ACKNOWLEDGMENTS

The research described in this thesis was carried out at the Department of Geological Sciences, State University of New York at Albany under the direction of Dr. A. Miyashiro, to whom I am deeply grateful for having suggested the project and for his guidance during the study. I would also like to express my gratitude to Dr. P. H. Mattson, professor of the Department of Earth and Environmental Sciences, Queens College of City University of New York for his interest and support of this project.

I am indebted to the geologists in the Puerto Rico Branch, U. S. Geological Survey for their helpful advice and the use of field equipment, and to the Mario family and many other Puerto Rican friends for their hospitalities during a field trip in Puerto Rico during the summer of 1972. The kindness of Dr. P. H. Mattson in contributing some necessary samples of the Bermeja complex from his own collection is greatly appreciated. I would especially like to thank the faculty at the department of Geological Sciences, State University of New York at Albany - Drs. A. Miyashiro, G. W. Putman, S. E. DeLong, V. Dietrich, and P. J. Fox - for stimulating advice and discussions in the course of this study. My thanks are extended to Mrs. E. Bartlet for her excellent assistance with the X-ray and atomic absorption analyses, and to Dr. F. Shido, who kindly supplied rock standards used in the chemical analyses and verified the petrographic descriptions of the samples. I

am also indebted to Dr. S. E. DeLong for supplying the computer program for simple mass balance calculations and helpful suggestions in the trace element interpretation.

Preliminary versions of the manuscript have benefited from reviews by Drs. A. Miyashiro, G. W. Putman, and S. E. DeLong.

This research could not have been completed without the continuous spiritual encouragement of my wife, Teresa, and daughter, Victoria, to whom I owe a great deal of thanks and love.

TABLE OF CONTENTS

LIST OF TABLES

LIST OF FIGURES

I. INTRODUCTION AND PREVIOUS WORK

The eastern Greater Antilles and the Lesser Antilles on the northeastern and eastern margins of the Caribbean (Figure 1) is an island arc with attendant large gravity anomalies, volcanism, and earthquakes, at the boundary of the Atlantic and Caribbean plates. Features of island arc tectonics are well developed in the Greater Antilles, while they are yet in a more youthful stage in the Lesser Antilles.

The geology of the eastern Greater Antilles (consisting essentially of Puerto Rico and the Virgin Islands) is now fairly well documented. There has been a history of nearly continuous volcanism from the middle Cretaceous into the Tertiary, and subsequent slight deformation and metamorphism. The island of Puerto Rico is especially interesting for study of island arc evolution because volcanic rocks are exposed in large volume and represent a wide range of compositions.

In the southwestern part of Puerto Rico (Figure 2), serpentinized peridotite occurs in association with chert, pillow lava, spilite, and small blocks of amphibolite. This ultramafic complex comprises the oldest rocks of the island; within it relations between the lithologies are complex. Though it is widely believed that this ultramafic complex represents an exposure of oceanic crust and the underlying upper mantle which were created in a mid-oceanic ridge (Hess, 1960, 1964; Donnelly, 1971; Mattson, 1973a,b), the origin of this complex is actually rather obscure. An island arc

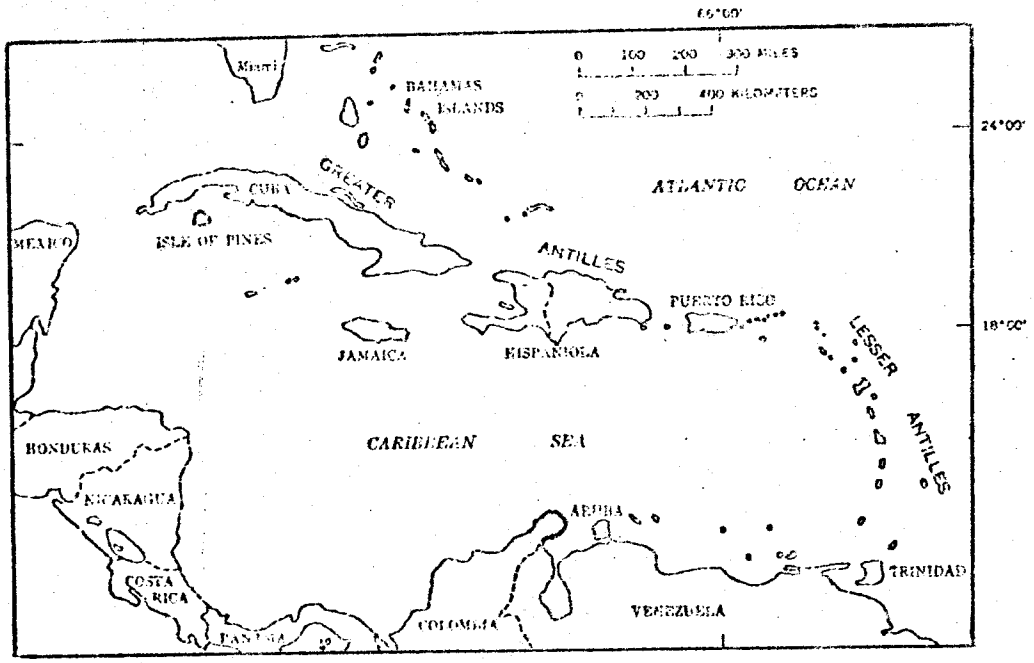

Figure 1. Map showing location of Puerto Rico in Caribbean area.

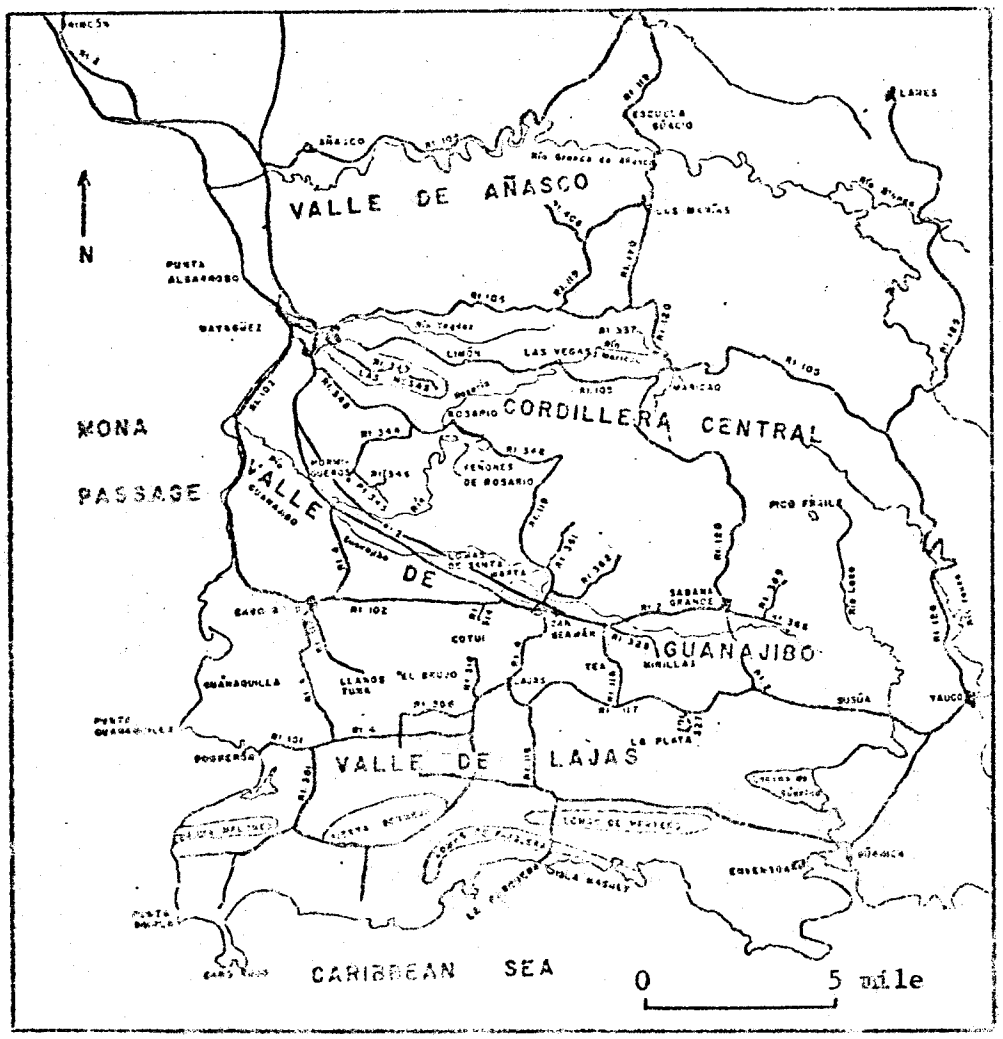

Figure 2. Map showing localities, highways, and topographic features of Southwestern Puerto Rico.

origin of such ultramafic complexes (ophiolite) was advocated by Challis (1969), White et al., (1971), and Miyashiro (1973b). Thus, it is desireable to find evidence to deduce a more refined conclusion about the origin of this complex and its significance in the prevailing hypotheses of plate tectonics and island arc evolution.

The present study focuses on an investigation of the petrography, metamorphism, and geochemistry of this complex and related rocks in southwestern Puerto Rico. In addition, secular compositional changes of the volcanic rocks in the Puerto Rico - Virgin Islands area were studied, so that the significance of this complex in the evolution of the eastern Greater Antillian arc system might be established.

The earliest geological reconnaissance reports on western Puerto Rico were by Mitchell (1922) and Hubbard (1923). Berkey (1915) and Meyerhoff (1933) made general surveys of the geology of Puerto Rico. The Princeton Caribbean Research Project dealing with the problem of island arc evolution was conceived and initiated by Hess and Maxwell (1953) (also see Hess, 1960, 1964, 1966). The pre-Oligocence sedimentary and igneous rocks, and the ultramafic complex of southwestern Puerto Rico has been studied by Mattson (1960). A report of a systematic study of the serpentinite from the AMSOC core hole in western Puerto Rico had been prepared by Burk (1964). Briggs and Akers (1965) prepared a hydrogeologic map of Puerto Rico. Lidiak (1965) discussed the petrology of the igneous rocks of north-central

Puerto Rico. Serpentinite dredged along the north wall of the Puerto Rico Trench, together with sedimentary rocks of Cenomanian and Eocene age was reported by Bowin et al., (1966). Mattson (1967) discussed the Cretaceous and lower Tertiary stratigraphy in west-central Puerto Rico. Studies of the amphibolite in the ultramafic complex of southwestern Puerto Rico had been made by Tobisch (1968). Otalora (1964) and Jolly (1970a) reported the presence of low grade metamorphism in south central Puerto Rico. Hart and Nalwalk (1970) studied the trace element relationships in submarine basalts from the Puerto Rico Trench. Mattson and Schwartz (1971) discussed the control of intensity of deformation in Puerto Rico. The geochemistry of the igneous rocks of the eastern West Indies was studied by Donnelly et al., (1971). A petrological report on the potassium - rich igneous rocks in south central Puerto Rico was made by Jolly (1971). Mattson et al., (1972) correlated the outcropping Paleocene and Eocene rocks in Puerto Rico with the Layer A in the Atlantic ocean and Layer A" and the Carib beds in the Caribbean Sea. The Caribbean serpentinites and their tectonic implications were reviewed by Dengo (1972). Mattson (1973a, b) proposed a nappe structure in the southwestern ultramafic complex, which has lately discussed by Walper (1973). The U. S. Geological Survey is currently mapping the entire island in detail. The stratigraphy of various parts of the island is reported by Kaye (1959), Beryhill et al., (1960), Briggs and Gelabert (1962), Mattson (1967),

Pease (1968), McIntyre et al., (1970), Donnelly (1970), and Seiders (1971).

The geology of the Virgin Islands had been studied by Donnelly (1960, 1966, 1972) and Hekinian (1971).

Ideas of the evolution of the eastern Greater Antilles arc are discussed by Donnelly (1964), Lidiak (1970), Donnelly et al., (1971), Mattson (1973a, b), and Donnelly (1973).

Molnar and Sykes (1969) and Malfait and Dinkelman (1972) discussed circum-Caribbean tectonics and the evolution of the Caribbean plate.

II. GEOLOGICAL SETTING AND THE PETROGRAPHY OF THE IGNEOUS AND METAMORPHIC ROCKS FROM SOUTHWESTERN PUERTO RICO

As shown in Figure 3, Puerto Rico can be clearly divided into three geologic belts, which in turn are divided into seven rock sequences that are separated from each other by unconformities or disconformities (Mattson and Schwartz, 1971). They range in age from recent to Albian or older. The northern and southern belts of the island, sequences 6 and 7 (Figure 3), consist primarily of middle Tertiary limestone, although epiclastic rocks and some blanket sand are also present (Briggs and Aker, 1965; Mattson and Schwartz, 1971). The bedding of both belts strikes east, with the north belt dipping gently toward the north and the south belt towards the south. These dips probably resulted from block tilting as the island emerged in the middle to late Miocene. The central belt of the island is made up of intrusive bodies and a thick pile of volcaniclastic rocks and some lavas that range in age from Albian to Eocene. The central belt is overlapped unconformably by middle Tertiary clastic and carbonate rocks of the northern and southern belt (sequence 6 and 7). The central belt (sequence 2 to 5) is divided into three tectonic blocks by large fault zones. The belt is composed of interfingering andesite, dacite, shoshonite and basalt, pyroclastic and epiclastic rocks, and some limestone (Mattson, 1960; Otalora, 1964; Lidiak, 1965; Briggs and Akers, 1965; Mattson, 1966; Jolly, 1970a, b, 1971;

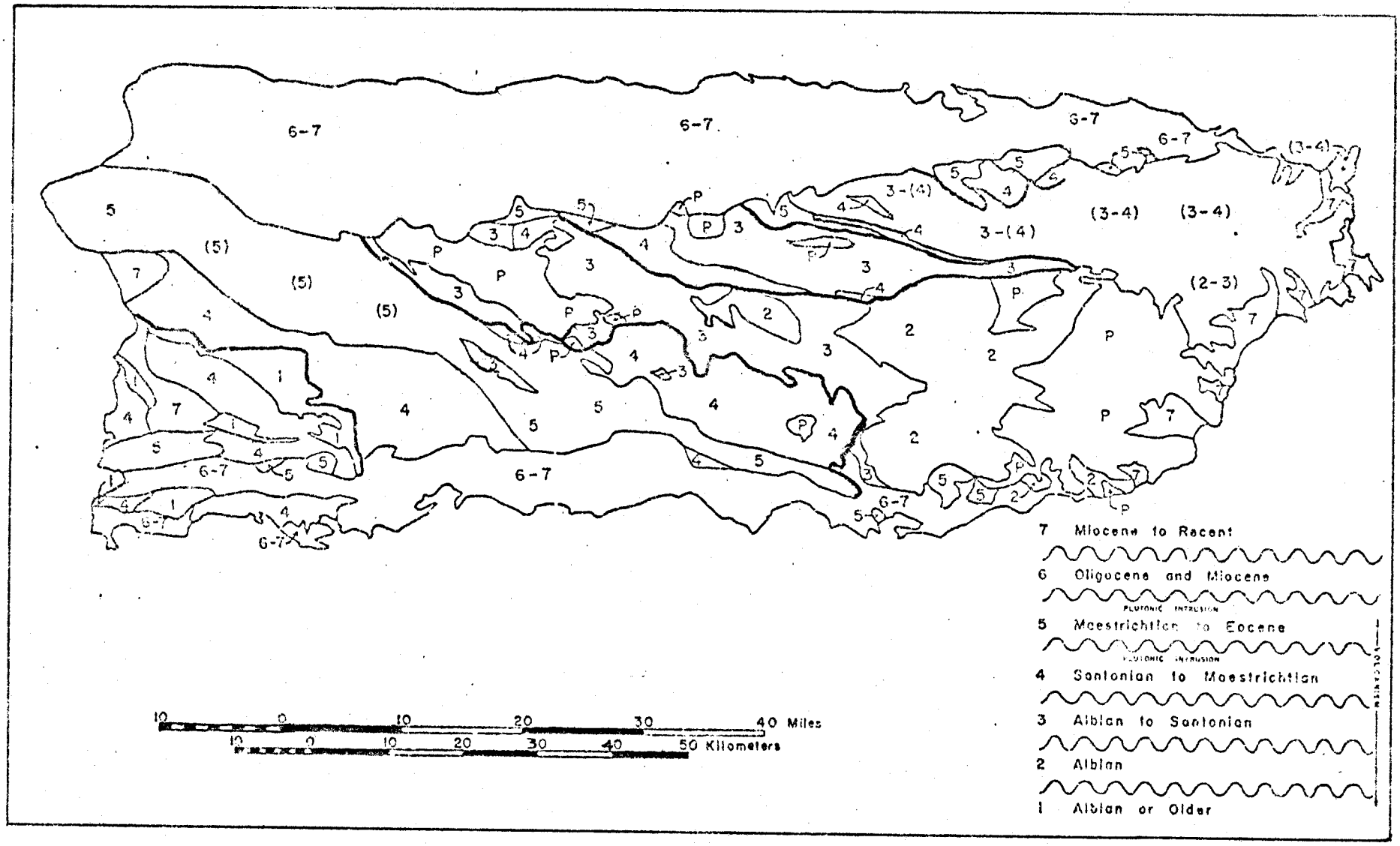

Figure 3. Generalized geologic map of Puerto Rico showing borders of sequences (light lines) ad tectonic blocks (heavy lines). P denotes granitic plutons (after Mattson, 1970).

Donnelly et al., 1971). Low grade regional metamorphism, possibly zeolite facies, prehnite pumpellyite facies and locally incipient greenschist facies has affected the rocks of sequence 2 and 3 (Otalora, 1964; Jolly, 1970a). Most primary textural features of the rocks are preserved, except in the fault zones and at the contact of the granitic intrusive bodies, where schistose texture can be found. The central block also contains several granitic plutons, mostly granodiorite and quartz monzonite. These intrude sequences 2 through 5 (Mattson and Schwartz, 1971; Donnelly et al., 1971).

Figure 4 shows the simplified structural features in Puerto Rico, which is very complicated in detail. The basic structural element of Puerto Rico is a broad anticlinal arch whose axis is approximately the long axis of the island. Thus, the deformation is limited to tilting of fault blocks, local drag or crumpling adjacent to major faults, and shallow-depth gravity sliding and thrusting. The rocks in all three blocks of the central belt have been moderately deformed. Deformation was brittle and faulting predominates, although some folding has occurred. Movements along the larger faults have been largely horizontal displacements, although vertical movement has occurred as well. Where the rock sequence is thin, as in the southwestern part of the island, folding is tight and folds are narrow. Where the rock sequences are thick, as in the central and eastern parts of the island, folding is gentle and folds are broad (Briggs

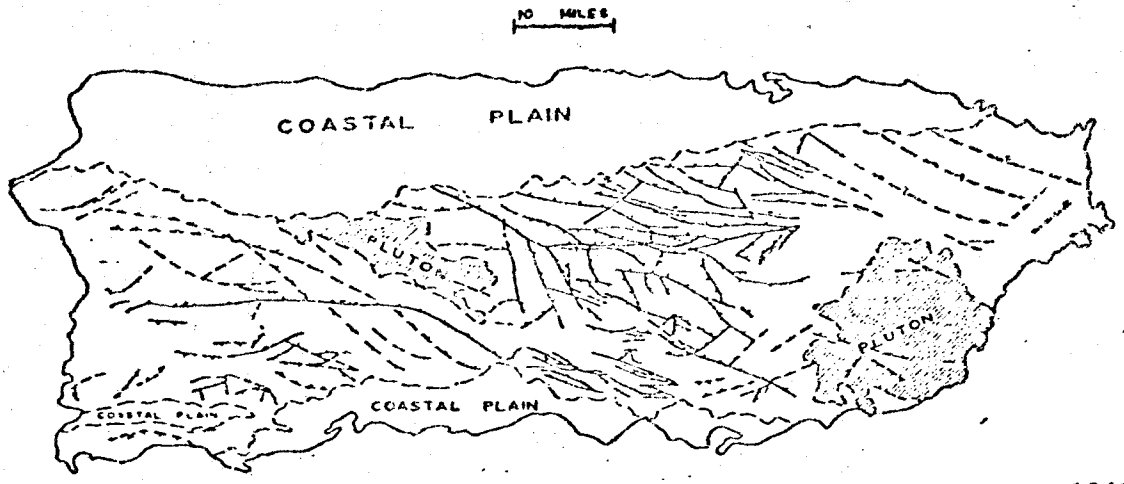

Figure 4. Simplified structural map of Puerto Rico (After Briggs, 1961).

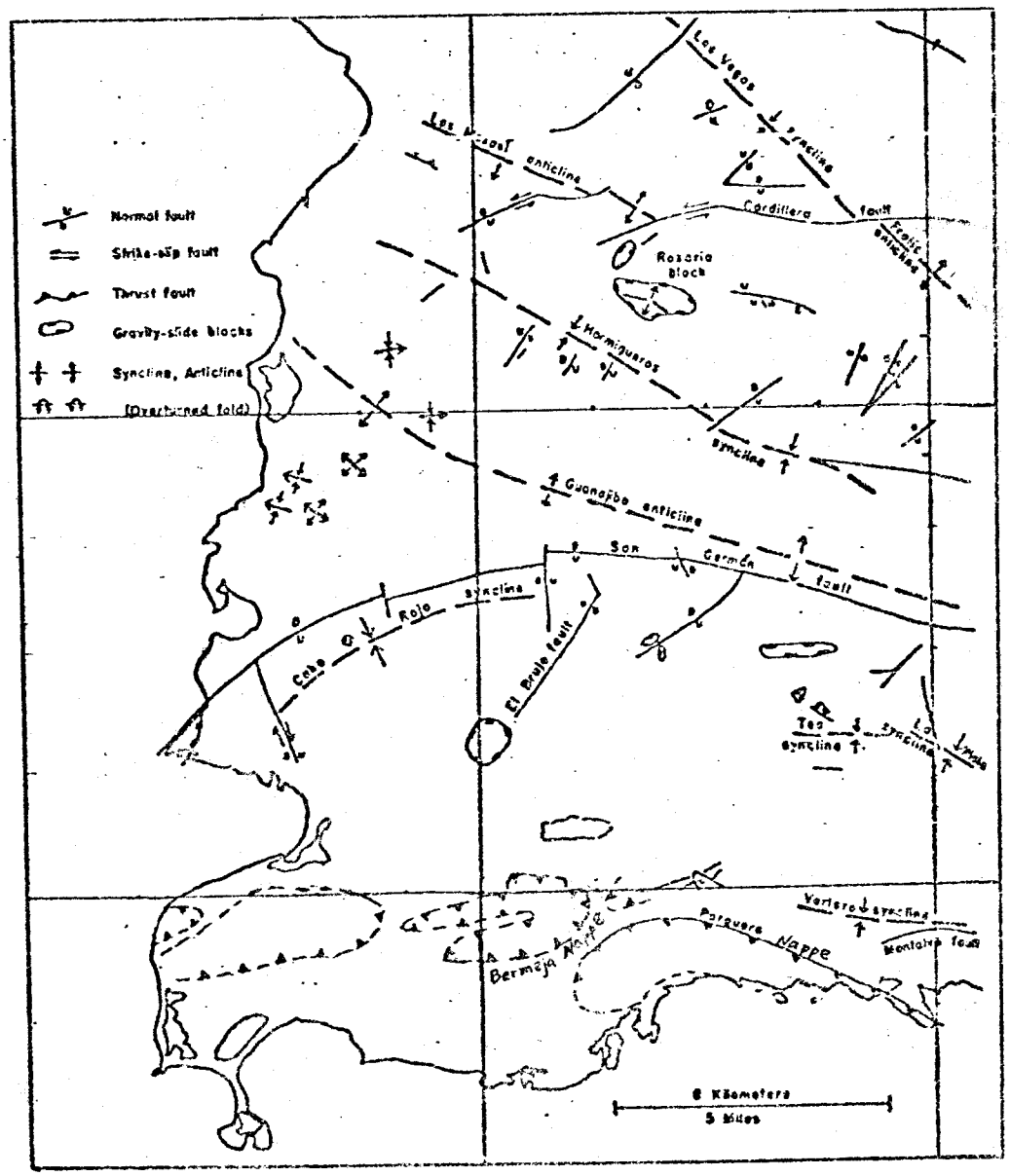

Figure 5. Structural map of Southwestern Puerto Rico (after Mattson, 1960, 1973).

and Akers, 1965; Mattson and Schwartz, 1971). Local gravity gliding has been demonstrated by Mattson (1960). The oldest rocks of the island occur in the Bermeja complex of southwestern Puerto Rico, which includes radiolarian chert, serpentinized peridotite, pillow lava, spilite, and amphibolite (Mattson, 1960, Burk ed., 1964; Tobisch, 1968; Donnelly et al., 1971, Mattson, 1973a, b). They are of Albian or older age.

A good survey of the geology of southwestern Puerto Rico was made by Mattson (1960), in which pre-Oligocene sedimentary and igneous rocks were emphasized, including the Bermeja complex. The complex is unconformably overlain by a broadly folded sequence of sedimentary and volcanic rocks, of Cenomanian or Santonian to Eocene age. A Maestrichtian unconformity subdivides this sequence with the Rio Loco formation and the Mayaguez group below, and the San German and Jicara formations above. A younger sequence, including the Juana Diaz, Ponce, Guanajibo, and San Juan formations, consists of tilted and uplifted Oligocene - Miocene limestone, gravels, and clays, Miocene limestone and clay and Pleistocene dune sands. A summarized structure map is shown in Figure 5. In this section of the report, the general geology of the igneous and metamorphic rocks from southwestern Puerto Rico is summarized, and their petrography is described.

A. Methods of Petrographic Analysis

Thin sections were prepared for most of the specimens sampled in a field trip to Puerto Rico during the summer of 1972, as well as for specimens of the Bermeja complex obtained from Dr. P. H. Mattson. One hundred specimens among the collection were selected later, and the thin sections were made by the use of Lakeside and Canadian balsam. A few volcaniclastic rocks and highly schistose rocks, which were found to be fragile, were impregnated in plastic materials before proceeding with the usual methods of thin section preparation. Refractive indices of the minerals were determined with reference to index oils, which were checked, immediately after the measurement, on a Abbe refractometer. A four-axis universal stage was used in the determination of the optic angle (2V) and extinction angle for some minerals (amphibole, pyroxene, and olivine). Emmons et al., (1953) noted that the measurement of extinction angles is less reliable in characterizing the composition of plagioclase than the measurement of the refractive indices. However, within an error of An $\pm$ 5, it is much quicker to estimate the composition of plagioclase on the universal stage, which can bring the symmetric extinction angles of plagioclase on the zone normal to (010) into measurement. Alteration of the plagioclase, however, is common in most rocks, and where secondary alteration obscures extinction, an error greater than An $\pm$ 5 may occur. wherever possible, measurements of the optic axial angles have been made between the two optic axes by rotation on a

single axis of the universal stage. Where both optic axis could not be reached by rotation about one axis (in the case of higher 2V, or no suitable grains available in the thin section), measurement has been made from one axis to a bisectrix position; this value has been doubled to give the optic axial angle. Because of less well defined extinction in hornblende, pyroxene, and olivine, the precision of 2V measurement is about $\pm 2^{\circ}$ in most rocks. In highly colored and strained (optically) hornblende, direct optic angle measurements are reproducible to $\pm 4^{\circ}$ (the precision is estimated by computing the standard error of the mean of several determinations). Measurements of $C\wedge Z$ of amphiboles by the use of universal stage vary by 1° to 3°, owing in part to strained extinction.

X-ray diffraction analysis using powder mounts was used to confirmed the presence of pumpellyite, prehnite, laumontite, and hydrogarnet for some specimens in which these phases were difficult to identify by optical methods. Usually, the portion of the rock of interest, from which the powder mount was prepared, were hand picked with the aid of the binocular after the specimen was partially crushed. The operating parameters of a Siemens Type F X-ray Diffractometer were set so as to achieve satisfactory peak resolution on the chart, using CuKA radiation, $\lambda = 1.5418$ Å, and nickel filter. The major reflections used for the identifications of these minerals are as followed: laumontite, $2\theta = 9.3$, 13, 21.3, 25.6, 26.8, 29.6, and 37.2 (?); prehnite, $2\theta =$

25.6, 27.2, 28.9, 31.8, 35.2, and 37.9; pumpellyite, 2θ = 23.4, 30.8, 32.7, and 36.7; hydrogarnet, 2θ = 33.3, 35, 36.5, 46.3, and 57.3.

The flake-like crystals with anomalous birefringence and greenish pleochroism are attributed to chlorite. However, smectite and various members of mixed-layer clay minerals also have a similar appearance in some cases. Identification of these minerals requires special techniques (Miyashiro, 1973c) and was not attempted.

B. Bermeja Complex

This ultramafic complex, containing the oldest rocks in the island, occurs only in the cores of the two northern anticlines (Las Mesas-Fraile and Guanajibo anticlines) and in Sierra Bermeja and Sierra Melones in southwestern Puerto Rico, being exposed in greatest variety in Sierra Bermeja and named the Bermeja complex by Mattson (1960). In the complex, serpentinitized peridotite occurs in association with minor amounts of spilite, radiolarian chert, pillow lava, and amphibolite. A geological map showing the central part of the Sierra Bermeja area is shown in Figure 6. Lying unconformably upon the complex are upper Cretaceous sedimentary and volcanic rocks of the Mayaguez group dated as Campanian and perhaps Santonian. Grains of chromite and pebbles of serpentinite and other rocks from this complex occur locally as the basal conglomerates in this sedimentary sequence, indicating that the Bermeja complex was eroded

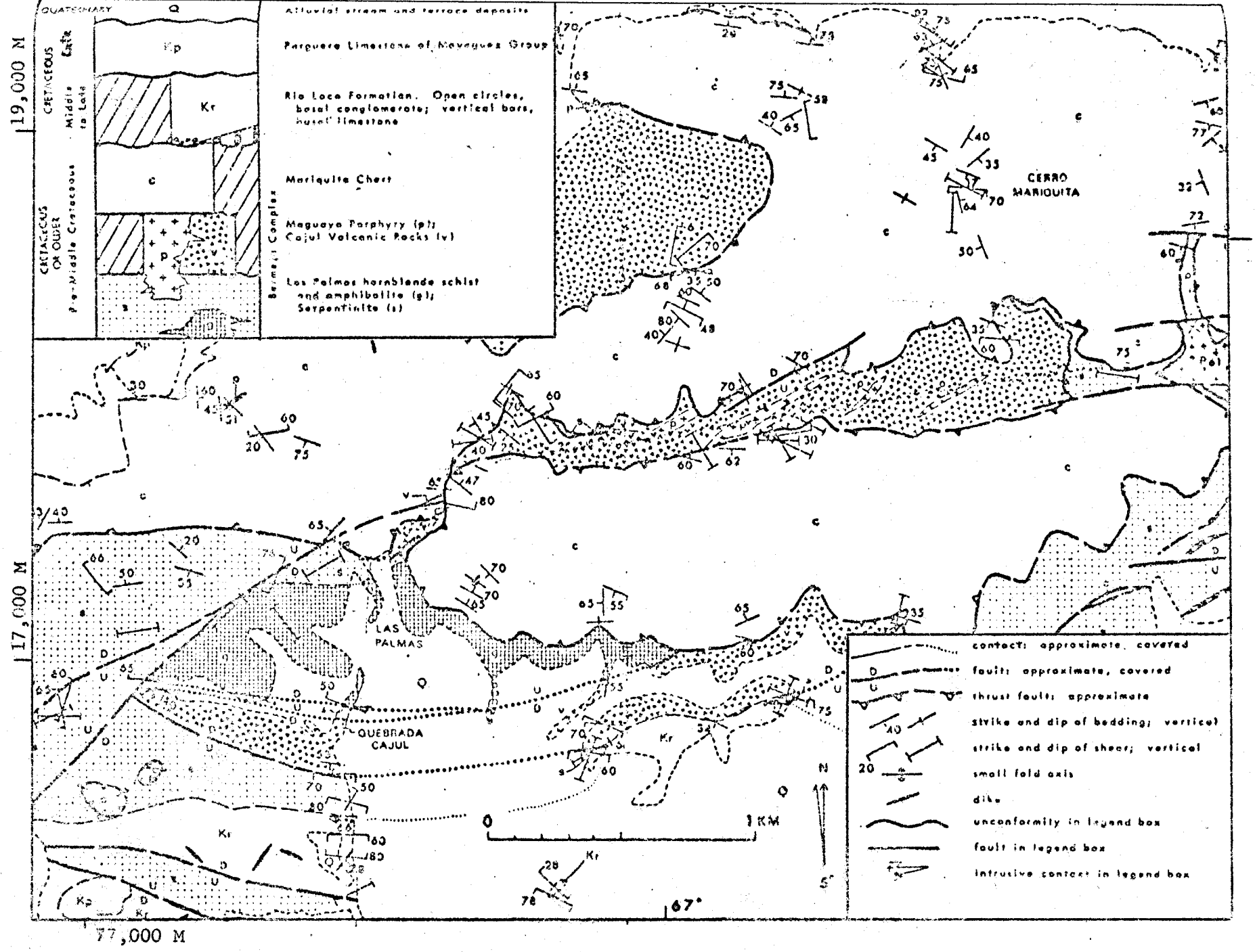

Figure 6. Geologic map of Central Sierra Bermeja, Puerto Rico (After Mattson, 1973).

during or before the age of the Mayaguez group (Mattson, 1960). In some places, a lava and volcanic formation lies below the well-dated Mayaguez group but unconformably on the Bermeja complex. Being correlated with the lower Cretaceous Albian foraminifera bearing Rio Loco formation of Otalora (1960) in central Puerto Rico, this volcanic unit was named the Rio Loco formation by Mattson (1960). Thus the Bermeja complex is certainly pre-Campanian and possibly Albian or even older. Although the relationship between rock types in the Bermeja complex has not been completely established, a diapiric intrusion of the serpentinite into the post-Albian rocks in the centers of Guanajibo and Las Mesas-Fraile anticline (Mattson and Schwartz, 1971) and a gravitational nappe structure in the Sierra Bermeja (Mattson, 1973a, b), in which a disharmonically deformed sheet of radiolarian chert forms the nappe overlying other rock types, with small lenses of serpentinite along the sole of the nappe, possibly as a lubricant were proposed.

1. Schistose Amphibolite and Massive Metabasaltic Dike

The amphibolite shows a markedly different metamorphic grade and style of deformation to the surrounding rocks, and is exposed mostly in the Sierra Bermeja and the Sierra Melones, where it occurs as a tectonic block in sheared serpentinite. The fragments of the amphibolite are dominant among many small serpentinite exposure (Mattson, 1973a), because the amphibolite is more resistant than ser-

pentinite. Amphibolite also occurs as pebbles in conglomerate near the base of the Campanian and Maestrichtian Mayaguez group (Mattson, 1960). The biggest body and the best outcrops of the amphibolite occur in the Las Palmas area (Figure 6), which is about 15 miles south of Mayaguez in the southernmost outcrop area of the Bermeja complex (Mattson, 1960, 1973a; Tobisch, 1968). Exposures of the amphibolite are available only along small streams and in some small road cuts. Most of the contact with the surrounding rocks is poorly exposed. Completely serpentinized peridotite is in part in intrusive contact and in part in fault contact with the amphibolite body. In the northern contact, a steeply dipping foliation, which is apparently defined by the planar arrangement of long axes of bastite pseudomorphs, is developed in the serpentinite (Tobisch, 1968). This planar structure, which weakens away from the contact in the serpentinite, was probably formed as the serpentinite was emplaced (Tobisch, 1968). Recrystallized chert and basalt which is interbedded with the volcaniclastic rocks, unconformably overlie some portions of the amphibolite.

Two main rock types, schistose amphibolite and massive metabasaltic dike, occur in the Las Palmas amphibolite body. A variable degree of development of foliation in the schistose amphibolite is formed by the preferred planar orientation of the long axes of hornblende, and to a lesser degree, flattened crystals of plagioclase and quartz. The structure features of this amphibolite body was described

a. Petrography of the Schistose Amphibolite

The average grain size of the schistose amphibolite is about 1 mm, with the long direction of the elongated and flattened crystals arranged more or less parallel to the foliation. The schistose amphibolite consists mainly of hornblende, plagioclase, and quartz, with small amounts of opaque minerals and with or without minor sphene, apatite, and zircon. The minerals are segregated into distinct layering, forming the white layers of plagioclase and quartz that alternate with dark green layers rich in hornblende. Close to the contact with the serpentinite, the schistose amphibolite locally may contain epidote minerals and prehnite in veinlets.

The hornblende has an average size of 1 mm, occuring in subhedral prismatic crystals with a preferred C-axis orientation parallel to the foliation and forming the dark colored layers. Cleavage is well developed, and C∧Z ranges from 14° to 25°, as determined on the universal stage. Pleochroism is X = pale yellow to pale greenish yellow, Y = yellowish green to deep yellowish green, and Z = pale to deep bluish green, and rarely to brownish green. Optical angles, measured on the universal stage, have a range of $2V_X$ 72° to 86° (measurement of 13 grains from different specimens). Slight optical straining (undulatory extinction) is consistent in most of the hornblende. n_X and n_Y are 1.644 to 1.660 and 1.666 to 1.682, respectively (measured on five

analyzed samples). Locally, minute crystals of sphene, apatite, or zircon are present as uncommon inclusions in the hornblende.

Plagioclase is usually subhedral to anhedral, and equant or slightly flattened somewhat parallel to the foliation, with an average length of 0.5 mm. It occurs mostly with quartz grains in the light layers that alternate with the dark hornblende-rich layers. Albite and other simple tiwns are weakly developed or absent. Weak zoning occurs in some plagioclase, but is not common. Optical undulatory extinction is not rare in the plagioclase; the composition by universal stage measurement, ranges from 20 to 40 percent An. The degree of alteration of the plagioclase varies from sample to sample, and ranges from none to moderate. The common alteration product is white micas or sericite, which clouds the plagioclase in varying degrees.

Quartz occurs as small crystals, 0.1 to 0.4 mm in diameter, usually in the light layer associated with the plagioclase. The grain is always anhedral with serrated edges, and sometimes slightly flattened. Undulatory extinction is consistently found in quartz crystals. C-axes of the crystals have weak preferred orientation subparallel to the foliation.

Accessory sphene, apatite, and zircon occur as small subhedral to euhedral crystals or granules about 0.05 mm in size in the interstitices between the main minerals, as well as common inclusions in hornblende. Magnetite is present as

a minor accessory mineral, commonly with rounded irregular edges and, locally, with slight elongation parallel to the foliation. It also occurs as inclusions in hornblende or interstitial to the main minerals. Tiny crystal aggregates of pale yellow epidote and/or colorless prehnite fill in veinlets in the schistose amphibolite near the contact with serpentinite. Thus epidote and prehnite can not be considered as part of the stable mineral assemblage. Apparently they were introduced as a result of the emplacement of the serpentinite. Some small anhedral quartz and locally euhedral garnet grains also occur in some veinlets.

b. Petrography of the Massive Metabasaltic Dike

The massive metabasaltic dike rocks are deep green in color and commonly porphyroblastic. The porphyroblasts of hornblende and plagioclase range from 0.5 to 1.5 mm in length. The groundmass commonly has a fine-grained intersertal texture, and consists of plagioclase, hornblende, and some epidote-group minerals. In most rocks, the original igneous porphyritic texture is somewhat preserved. The amount of original phenocrysts varies from less than 10 percent to 20 percent in the original rocks. Locally, a very weak foliation is defined by the subparallel arrangement of small prismatic hornblende grains. From field observation, which shows that the dike cuts the foliation in the schistose amphibolite, there is little doubt that the dike intruded the schistose amphibolite after the formation of its foliation. Tobisch

(1968) also found that protoclastic deformation in the schistose amphibolite body accompanied the injection of the dike.

Amphibole occurs in all the metabasaltic dike rocks and is evidently of metamorphic origin. The crystals are usually poorly shaped without well developed cleavage. Amphibole occurs in the porphyroblasts (0.5 to 1.5 mm) as subhedral to anhedral grains and as fibrous aggregates after the original phenocrysts (commonly clinopyroxene and a few of plagioclase), as well as small subhedral prismatic to fibrous crystals (smaller than 0.5 mm, mostly 0.2 mm) in the groundmass. The porphyroblastic amphiboles rarely rim relict colorless pyroxene and commonly show weak zoning. This zoning is indicated by variation in both the pleochroism and extinction angle within a single crystal. The pleochroism is generally much paler than that of the hornblende in the schistose amphibolite, although similar in scheme. In the porphyroblasts Z may gradually vary from bluish green on the rim to very pale yellow in the core for single amphibole crystals after original pyroxene phenocrysts, while the extinction angle $C \wedge Z$ also vary from 20° on the rim to 16° in the core, as measured on the universal stage. For the hornblende, in general, $2V_X$ ranged from 62° to 70°, n_X ranged from 1.644 to 1.646, n_Y ranged from 1.664 to 1.668. Rarely, tiny epidote minerals can be seen included in occasional single hornblende porphyroblasts. The fibrous amphibole variety, probably actinolite, has very weak pleo-

chroism, and is even colorless with low extinction angles (16^{o} to 18^{o}) and n_{γ} = 1.656. It commonly occurs as groups of subradiating tiny fibrous crystals in the porphyroblasts after pyroxene.

Although plagioclase grains are slightly to moderately replaced by tiny crystals of amphibole throughout and have no distinct crystal form, it is lath shaped ranging from 0.5 to 1.5 mm in length dispersed in the groundmass. Some twinning and weak zoning is still visible in a few crystals, with a composition as determined on the universal stage ranging from An_{33} to An_{35}. Replacement of plagioclase by epidote minerals is also common, rarely it is also replaced by chlorite. The relict clinopyroxene, possibly augite, is rimmed by prismatic or fibrous amphibole, and occurs only in small amounts in the core of some porpyroblasts.

Colorless to pale clinozoisite occurs in small prismatic crystals (usually less than 0.5 mm in length) and as small granules commonly replacing plagioclase, and in a few cases, relict augite phenocrysts. It also occurs in the groundmass, and very commonly as vein fillings. Some small, pale yellowish green epidote crystals also occur with clinozoisite, although this is not common. Magnetite granules (usually smaller than 0.05 mm) are dispersed throughout the dike rocks, occurring interstitial to other minerals in the groundmass, as inclusions in hornblende, and rarely in veinlets. The occurrence of prehnite in the dike rocks becomes important close to the contact of the amphi-

bolite with the serpentinite. Commonly it occurs as subradiating or fan shaped tabular crystal groups forming a monmineralic filling in significant numbers of veins or fractures near the contact. Subhedral tabular crystals of prehnite also replace plagioclase in the rock, and in some rare cases it forms a rock of essentially amphibole and prehnite. Other veinlet minerals are epidote, chlorite, and quartz.

2. Serpentinite

The serpentinite occurs in the cores of the two northerly west-northwest trending anticlines in southwestern Puerto Rico and as several small lenses beneath the Bermeja Nappe associated with chert, silicified volcanic rock, and amphibolites in Sierra Bermeja (Mattson, 1960, 1973a), and is well exposed in small and large road cuts. The serpentinite in most of the outcrops is intensively sheared, in some cases consisting of aggregates of highly polished slickenside-bounded serpentinite blocks set in matrices of finely divided crushed serpentine; zones of differential movement are present at most of the contacts with other rock types. Serpentinite is usually deep green, bluish green, or brownish green, or brownish black in fresh outcrops, but grayish brown or greenish white when weathered. Relict green colored crystals, usually pyroxene, are visible in some rocks both weathered and unweathered.

A systematic study of the 305 meter core of serpentinite exposed along the crest of the Guanajibo anticline

near Mayaguez was reported in Burk ed. (1964); the petrography of the core was studied by Mattson (1964). Rocks of the core include about two thirds serpentinized diopside harzburgite (original olivine content less than 95 percent, orthopyroxene dominant over clinopyroxene) and one third serpentinized dunite (original olivine greater than 95 percent). There is little relation between the degree of serpentinization and the present erosion surface (Mattson, 1964). Thirteen thin sections from the core specimens and eighteen from exposed serpentinites of the Bermeja complex were examined in this study. They consist mostly of secondary serpentine minerals, with varying small amounts of relict olivine, clinopyroxene, orthopyroxene, and accessory spinel.

The serpentinites exposed on the Las Mesas-Fraile anticline are serpentinized harzburgite. The completely serpentinized harzburgite[1] originally contains about 80 to 90 percent olivine, with bastite up to 2.5 mm. Exsolution lamellae in bastite can be seen only locally. Grains and veinlets of magnetite in some rocks form mesh textures or are present in serpentinized olivine cores. Pseudomorphs of pyroxene are common and appear heavily dusted. Translucent spinel is quite rare. Serpentine veins are very common. Small amounts of calcite replacement can be found in the serpentinite near the faulted contact breccia zone at the

---

1 Equivalent to Mattson's Type A (see Mattson, 1964)

south side of the anticline. The less serpentinized harzburgite[1] is similar to the completely serpentinized harzburgite but is about 80 percent serpentinized and originally contains about 70 percent olivine and 30 percent pyroxene (enstatite dominates diopside). The original enstatite, now partially serpentinized, may be up to 3 mm in length, while the diopside is less than 1.5 mm. Interstitial brown spinel, rimmed by magnetite, may be up to 2 mm. The serpentinite at the contact with the spilite near Mayaguez is strongly foliated with the contact at an angle to the foliation. No original minerals or relicts, or translucent spinel can be observed in it.

On the Guanajibo anticline, serpentinized dunite exposed near San German with breccia and microbreccia is found near the faults on the north side of the anticline, while serpentinized harzburigite is exposed near Punta Guanajibo. The completely serpentinized harzburigite on this anticline is similar to that in the northern anticline, except that translucent spinel (golden brown to grayish brown) is more common. The less serpentinized harzburgite has greenish brown spinel, up to 1 mm, rimmed by magnetite, exsolution lamellae of diopside in enstatite, and bastite, and is similar to that exposed in the northern anticline. Completely serpentinized dunite[2] exposed near San German,

---

1 Equivalent to Mattson's Type C (see Mattson, 1964)

2 Equivalent to Mattson's Type E (see Mattson, 1964)

originally consisted of less than 3 percent pyroxene (up to 1.5 mm). Mesh texture and yellowish brown to golden brown spinel (up to 2 mm and rimmed by magnetite) is generally common. Varing amounts of calcite occur in the interstitices between breccia fragments. Replacement by talc and iddingsite (?) is common in microbreccia.

Harzburgite[1], more than 95 percent serpentinized, is exposed as lenses in the Sierra Bermeja, commonly with the relicts of diopside, and less commonly enstatite and olivine. The bastite pseudomorphs may reach up to 8 mm in length, while the diopside may be up to 2 mm. The preferred orientation of their long axes defines the foliation. Minor amounts of magnetite occur as grains and veinlets, while golden brown to yellowish brown spinel, up to 1 mm, is rimmed by magnetite. Exsolution lamellae in the enstatite and bastite developed in some degree. Thin exsolved enstatite lamellae were found in one elongated clinopyroxene.

3. Spilite

Spilite is exposed in a large quarry about 0.7 mile east of Mayaguez on route 105 (Figure 2) (Mattson, 1960). The exposure consists of massive spilite and amphibolitized dolerite in contact with foliated serpentinite on the northmost margin of the quarry. Small veins of calcite, quartz, and epidote are common. Epidote can be abundant in larger

---

1 Equivalent to Mattson's Type A (see Mattson, 1964)

brecciated zones and then forms a massive yellowish green rock. Some spilite pebbles occur as basal conglomerates in the overlying Mayaguez group.

The spilite is grayish green and intersertal in texture with an average grain size of 0.5 mm. It consists of albite and predominately interstitial augite and chlorite, with minor amounts of opaque minerals and white micas. Small amounts of epidote, calcite, prehnite, hydrogarnet, and quartz are common locally.

The albitic plagioclase occurs usually as euhedral to subhedral phenocryst laths scattered irregularly throughout the rock, with an average length of 0.8 mm. It is commonly unzoned with albite, carlsbad and some combination twins. The composition, estimated by universal stage, ranges from 4 to 8 percent An. Slight alteration of the albite is common, with secondary white micas, chlorite, epidote, prehnite, and carbonate usually arranged along the cleavage or twin planes. Some small anhedral augite can be seen as inclusions in the albite laths. In some cases, a small amount of minute anhedral albite (?) can be found in veinlets associated with other low temperature minerals. Augite occurs as subhedral to anhedral grains of about 0.5 mm, filling the interstices between the plagioclase laths. Some grains have simple twins some show slight undulatory extinction, some are slightly bent. Measured values of $2V_Z$ of the augite are 50° to 53°; n_Y is 1.684 to 1.686. Minor alteration products of pyroxene are epidote, chlorite, prehnite, and

hydrogarnet (?).

One of the samples from the northmost outcrop of spilite on route 105, shows complete replacement of interstitial pyroxene by carbonate and platy chlorite. No relict pyroxene was observed, but its cleavage patterns are still preserved.

Chlorite occurs in tiny plates, fibrous aggregates, and/or as flakes, filling the cavities of veins radially and in the interstices of the phenocrysts. Most chlorite is pale green in color. It is in places altered into a mineral which shows yellow to yellowish green pleochroism and rather strong interference color. The interstitial chlorite is probably altered from original glass in the rock. The chlorite is sometimes found with small scattered granular grains of isotropic garnet embedded in it. Some six-sided euhedral pseudomorphs, consisting of prehnite aggregates rimmed with chlorite, can be seen in some thin sections, and these are probably altered from olivine?(about 0.4 mm grain size).

Epidote is pale yellowish green in color and weakly pleochroic, usually occuring as small (0.1 mm) subhedral prismatic crystals or as yellowish brown granular aggregates either associated with chlorite filling in the interstices in veinlets and cavities or as an alteration of plagioclase and pyroxene. In some cases the granular aggregate epidote is commonly associated with, or surrounded by, small grains of garnet.

Prehnite occurs as small (0.1 mm to 0.2 mm). colorless or pale yellowish brown aggregates that are sheaf-like, with moderate relief and wavy extinction, and are commonly associated with chlorite or calcite in the veinlets in some samples. Rarer occurrences are as an alteration of plagioclase, pyroxene, and possibly from olivine. Calcite occurs mostly in veins or amygdules, commonly rimmed by chlorite. It may also replace plagioclase and pyroxene.

The minute crystal of hydrogarnet (?) was associated with chlorite, and with some of the altered pyroxene. Fine grains and granules of sphene are predominantly associated with chlorite. Magnetite occurs as small granules mainly rimming the interstices. Small cubic grains (0.1 to 0.5 mm) of pyrite are common locally.

4. Amphibolitized Dolerite

The amphibolitized dolerite occuring in the northern spilite quarry is a massive, dark grayish green rock, which is holocrystalline granular, with relict subophitic texture and an average grain size of 0.8 mm. Dominant minerals include plagioclase and hornblende, with subordinate relict clinopyroxene (?), opaque minerals, and white micas.

Lath-shaped plagioclase is commonly twinned and strongly zoned. Plagioclase composition ranges from An_{75} in the core to An_{40} on the rim, as determined on the universal stage. Cores of individual crystals are clouded in varing intensity. All plagioclase contains minute inclusions of

hornblende and is altered to white mica flakes.

Pale yellowish green relict clinopyroxene, probably augite, is rare and only exists in the cores of grains, rimmed by secondary hornblende. Hornblende, having a pleochroism of X = pale yellow, Y = yellowish green, and Z = bluish green, occurs as subhedral to anhedral crystals, 0.5 to 1.0 mm in size, rimming the relict augite or as small subhedral prisms (0.2 to 0.1 mm) in the interstices of the plagioclase laths. The larger grains of hornblende are slightly zoned and commonly slightly clouded with tiny opaque minerals in the core. Irregular shaped opaque minerals occur in contact with or included in the hornblende. The optical angle ($2V_X$) of the hornblende ranges from 68° to 72°, and that of the relict clinopyroxene from 56° to 60°. The measured values of n_X and n_Y for the hornblende are 1.642 and 1.662, respectively.

5. Mariquita Chert

Exposed mostly on the high hill in the central part of the Sierra Bermeja, the chert is typically a fine grained, greenish gray (red-stained if weathered), medium-bedded radiolarian bearing rock, and is recrystallized into an aggregate of irregularly shaped quartz grains (usually smaller than 0.05 mm) with minor opaque minerals. Veins filled with quartz and/or epidote minerals, or locally with albite, are present (Tobisch, 1968; Mattson, 1973a). The original rock was apparently a fine-grained to aphanitic

radiolarian mudstone or claystone. Tectonic dislocation is suggested by the highly sheared serpentinite at the lower contact of the chert with serpentinite. At contacts of the chert with underlying Maguayo porphyry, and locally Cajul volcanic rocks, the chert is highly sheared and brecciated, also indicating a faulted lower contact. From these field relationships and a structural analysis, Mattson (1973a, b) proposed a gravitational nappe structure for a deformed sheet of the chert which moved northward with serpentinite beneath it serving as lubricant.

6. Cajul Volcanic Rocks

Feldspathic, finely crystalline, grayish green basaltic lava showing well defined pillow structure, and some coarse tuff exposed in western Sierra Bermeja have been named the Cajul volcanic rocks by Mattson (1973a). He also noticed that vague beds or interpillow bodies of red chert are common in the lava. The outcrops are usually sheared and deeply weathered. Except for the contact with the intrusive Mayguayo porphyry, faulted relationships occur at the contacts with all other rock units.

The lava is porphyritic to ophitic in texture, consisting mostly of plagioclase and clinopyroxene, with minor amounts of iron oxide, chlorite, white micas, quartz, calcite, epidote, and pumpellyite altered from the primary major minerals and groundmass, and also filling in vesicles and in veinlets.

Most plagioclase is in slender euhedral laths, average length 0.5 mm, up to 1 mm in some rare phenocrysts, and surrounded by anhedral clinopyroxene. Zoning and twinning are observed, although most plagioclase is extensively to moderately altered to a dusty appearance. The unaltered zoned plagioclase has a composition of An_{70} in the core to An_{50} on the rim, as determined on universal stage. Alteration minerals of the plagioclase are white micas, chlorite, and rarely calcite. There is less pale yellowish-green clinopyroxene than plagioclase, generally anhedral and interstitial to the plagioclase laths, and rarely present as subhedral phenocrysts. It is replaced by chlorite and rarely by calcite, usually starting inward from the rim. Fresch clinopyroxene usually shows undulatory extinction. Measurements of the optical angle by universal stage yield $2V_Z = 56^o$. Measured value of n_Y is 1.692.

Aggregates of various associations of epidote, chlorite, white micas, and quartz commonly replace the interstitial groundmass, and form veinlets of an average width of 0.5 mm. Amygdules are observed in some specimens, containing one or more of the following minerals: chlorite, epidote, quartz, calcite, and pumpellyite. Chlorite is generally yellowish green in color, rarely yellowish brown. It is the most abundant matrix mineral in the clastic rock, and is also widespread and abundant in the groundmass of the lava apparently as an alteration from the primary mafic minerals. Yellowish green to brownish green epidote occurs

as small granular or columnar aggregates, partly replacing plagioclase. It is also common in the amygdules and veinlets.

Pumpellyite displays blue-green to clear pleochroism, and is rarely brownish green. It occurs as an irregular mass or aggregate of small elongate prismatic crystals, usually with small anhedral quartz grains in the center of veinlets, and rarely as single grains in veinlets and amygdules. Pumpellyite within, or in contact with, quartz is usually well crystallized and displays a less brownish color. Association with epidote and calcite is less common. The iron oxides are usually interstitial to the major minerals, and also form subhedral elongated tiny crystals in the groundmass.

7. Maguayo Porphyry

Mattson (1973a) named the Mayuayo porphyry for a tan to greenish gray porphyritic rock, exposed mostly in the north-eastern Sierra Bermeja, with sparse to common feldspar and hornblende phenocrysts, and rarer phenocrysts of quartz and biotite in a microcrystalline aplitic groundmass. He also cited an extrusive or shallow intrusive origin for this porphyry, based on the observation of amygdules or vague flow layering in a few outcrops. The porphyry is in fault contact with the overlying chert. Contacts with other units are steep and show no evidence of contact metamorphism.

Euhedral plagioclase, ranging from 2 to 4 mm, is the most common phenocryst. The composition, determined by universal stage, is An_{38} to An_{42}. It is usually slightly to

moderately altered to white micas, chlorite, and rarely calcite, with a dusty appearance. Partial replacement by epidote and other common secondary minerals was observed in one specimen.

Hornblende phenocrysts have an average size of 1 mm, and are usually euhedral with well developed cleavages. The pleochroism is X = pale straw yellow, Y = greenish brown, and Z = brownish green. Zoning and twinning are common. Extinction angle (C∧Z) vary from 18° in the core to 15° on the rim, and $2V_X = 84°$ in the core, measured by universal stage. Measured values of n_X and n_Y are 1.652 and 1.676, respectively. The hornblende may be either very fresh or replaced by secondary minerals. A pseudomorphic association of greenish chlorite, brownish epidote, and calcite commonly replaces the hornblende, within which elongated epidote is always arranged parallel to and continuous along the cleavage traces of the original hornblende, with chlorite in between. Calcite occurs as anhedral patches scattered within the pseudomorph.

In some thin sections, biotite is common as phenocrysts. It is subhedral to euhedral averaging 0.5 mm, with tiny opaque minerals arranged along its cleavages. The biotite is yellowish brown or brownish green and displays strong pleochroism. It is partly to completely replaced by chlorite and calcite. Rarely, subhedral quartz grains, usually clear and unaltered, 1 to 4 mm in size occur as phenocrysts. The groundmass is aplitic in texture with a grain size less than 0.1 mm. Tiny pale green sericitic

mica is interstitial in the groundmass, with chlorite, calcite and occasionally epidote present as alteration minerals.

C. Rio Loco Formation

The Rio Loco formation is composed of bronzite andesite porphyry lava, more than half with pillow forms, and subordinate tuff, breccia, hornblende andesite, dacite (?), and limestone (Mattson, 1960). The formation occurs on the flanks of the Las Mesas-Fraile anticline and in the southeast part of the map area in Figure 2. It is approximately 300 m thick in the northern exposure. The Rio Loco formation lies stratigraphically between the Mayaguez group and Bermeja complex. Mattson (1960) described the bronzite andesite porphyry as consisting of about 40 percent phenocrysts, which include 20 percent of plagioclase, 10 percent diopsidic augite, and 10 percent bronzite, included in a glassy brown goundmass which contains embedded microlites of plagioclase, orthopyroxene, clinopyroxene, and magnetite, with amygdules of calcite, chlorite, and quartz. The plagioclase phenocrysts, averaging 1 mm long, occur as euhedral to subhedral twinned and zoned laths with an average composition of An_{64}. Diopsidic augite is subhedral and equidimensional, averaging 1 mm in size, commonly with cores of orthopyroxene. Bronzite is the usual orthopyroxene, occurring as subhedral laths averaging 0.6 mm long.

Samples from the north flank of the Las Mesas-Fraile

anticline, on route 105 near Limon, show strong secondary alteration, Most plagioclase phenocrysts are moderately to extensively altered to white micas and albite and partly replaced along cleavages by minor chlorite, calcite, quartz, opaque minerals, and sphene. Pseudomorphs, apparently after orthopyroxene, consist mostly of chlorite or dusty calcite with minor quartz and ore minerals. The groundmass has undergone extensive readjustment, with the lath-shaped to acicular plagioclase similarly alterated as the plagioclase phenocrysts. Abundant tiny grains of secondary chlorite with minute opaques are probably altered from the interstitial glass. Various associations of calcite, chlorite, quartz, and sodic plagioclase, with small amounts of white micas, sphene, and ore minerals in irregular aggregates fill in small veins.

Mattson (1960) found that while the northern and southern exposures of the lavas are mineralogically and texturally similar, the southern lavas have a larger percentage of phenocrysts, a smaller percentage of orthopyroxene phenocrysts, and about twice as many plagioclase phenocrysts.

D. Mayaguez Group

The Maygeuez group consists of bedded and massive fragmental limestone; thin to medium bedded forminiferal tuffaceous mudstone, siltstone, and tuff; and andesitic and basaltic volcanic rock including massive tuff, lava, and

breccia, comprising most of the rocks in southwestern Puerto Rico. Its thickness increase from 780 m on the south and southwest to 3800 m towards the northeast corner of the map area of Figure 2 (Mattson,1960). In most places it conformably overlies the Rio Loco formation, and locally lies unconformably upon the Bermeja complex. The age of the group ranges from Turonian or Santonian to Maestrichtian. Seven lithofacies formations have been recognized by Mattson (1960), eg: the Parguera, Brujo, and Melones limestones, the Yauco mudstone, the Maricao basalt, the Sabana Grande andesite, and the El Ray volcanic rocks. They occur in four major structures, namely the Las Vegas syncline, the Hormigueros syncline, the Tea syncline and Brujo structures, and the Parguera anticline and the Melones and Vertero synclines (?) (Figure 5).

The formations of volcanogenic origin, including the Yauco mudstone, the Maricao basalt, and the Sabana Grande andesite were studied and described here.

1. Yauco Mudstone

The Yauco mudstone consists of foraminiferal tuffaceous mudstone, minor tuff, and rare conglomerate and bedded chert, occurring in great thickness in the northern part of the map area of Figure 2 and as thinner lenses or tongues in the south. Fresh exposures are rare in the Las Vegas syncline. On the limbs of the Hormigueros syncline, the Yauco mudstone forms narrow belts, averaging 250 m in the north limb and ranging from 0 to 30 m in the south limb. It also occurs in

small synclines in the Guanajibo region. Good outcrops also exposed in the Tea syncline. The Yauco mudstone ranges from Turonian to Maestrichtian in age. Bedding in the Yauco mudstone generally parallels the contact with the underlying Rio Loco lava, but is truncated at the contact in some exposures, which was interpreted as evidence of local thrust faulting along the contact (Mattson, 1960).

Among the examined samples, one is porphyritic lava, with euhedral plagioclase laths and pseudomorphs after amphibole and other mafic minerals as phenocrysts ranging from 0.2 to 6.0 mm in size, being dispersed in the fine grained groundmass. The other specimens are coarse tuff and tuff, consisting mostly of porphyritic rock fragments, crystal fragments, and matrix materials. The porphyritic rock crystal fragments are usually angular to subangular, ranging from 0.05 to 2 mm in size. Feldspar occurs as euhedral laths in phenocrysts in the rock fragments and as broken fragments in the matrix. Small amounts of subhedral or broken pseudomorphs after smaller mafic minerals are present.

Most of the primary minerals are highly altered. Plagioclase is usually replaced by white micas and albite (?) with lesser amounts of one or more of the following: chlorite, calcite, epidote, quartz, laumontite, sphene (rare), and opaque minerals (rare). Rare small intermediate plagioclase relics (andesine) exist in some larger crystals. One thin section contains a few pseudomorphs apparently after olivine (less than 1 mm in length), consisting of calcite, chlorite,

and quartz. Partly to completely altered clinopyroxene and some pseudomorphs after mafic minerals are commonly present in the phenocryst-sized debris, as phenocrysts within rock fragments in the clastic rocks, and as phenocrysts in the lava. Most clinopyroxene has suffered extensive replacement by chlorite and opaque minerals, and in one thin section by laumontite. The relict clinopyroxene has an optical angle ($2V_Z$) approximate 50°; euhedral amphibole pseudomorphs in the lava consist entirely of opaques, chlorite, and epidote. Calcite, epidote, and white micas (?) form pseudomorphs after other mafic minerals. Very small amounts of a minute, dark yellowish brown, pleochroic mineral, probably pumpellyite, occuring as tiny subprismatic, subradiating fibrous aggregates, or as globular aggregates (less than 0.01 mm) was also observed in the pseudomorphs after mafic minerals.

The matrix of the volcaniclastic rocks is also extensively altered to an assemblage of mainaly chlorite, calcite, opaque minerals, and laumontite, with minor sericite and quartz. A trace amount of prehnite was observed in the matrix of one specimen, associated with chlorite, carbonate, and quartz. Some veins and voids are filled with calcite, chlorite, opaque minerals, and laumontite. The groundmass of the lava contains chlorite, opaque minerals, epidote, quartz, and other secondary phases.

2. Maricao Basalt

The Maricao basalt, consisting of lava and flow

breccia with minor breccia and tuff, occurs above, and as lenses in, the Yauco mudstone in the Las Vegas syncline and to a lesser extent in the Hormigueros syncline. Due to its lenticular occurrence within the Yauco mudstone, it is also considered to be of Turonian to Maestrichtian age, although no fossil evidence is available (Mattson, 1960).

The basalt porphyry contains various amounts of clinopyroxene and plagioclase as phenocrysts, ranging from 0.5 to 10.0 mm in size, which make up about 40 percent of the rocks. The greenish gray groundmass consists of magnetite, pyroxene and feldspar grains with an average size of 0.1 to 0.5 mm. Amygdules of various sizes are common. The plagioclase laths are moderately to extensively clouded with dusty alteration products. Relict calcic plagioclase is rare. Most rock specimens contain secondary albite. As other secondary phases, widespread or patchey sericite is abundant, chlorite is common along the cleavage traces of the plagioclase, and epidote and sphene are minor.

Pale green clinopyroxene phenocrysts are partially altered to chlorite, calcite, and opaque and rarely to sphene and pumpellyite. Optical angles ($2V_Z$) of the relict clinopyroxene range from 50° to 56°, measured on a universal stage. Measured values of n_Y range from 1.698 to 1.700. Small amounts of pseudomorphs, probably after olivine, contain chlorite and minor sphene, calcite, and opaque minerals. Within filled voids and veins, there are instances of one secondary phase embaying another, but most commonly, once

a mineral was deposited within a void, it remained unattacked;

Many amygdules and veins display a characteristic sequence of minerals from margins to core, which may represent the paragenesis of the phases. Parts of the following sequence of minerals from rim of the amygdules inward are typically present: (1) dark yellowish green chlorite, (2) faint green chlorite, (3) epidote (?), pumpellyite, quartz, (4) prehnite, (5) calcite, opaque minerals. Pumepllyite occurs as euhedral prismatic crystal aggregates, with an average length of 0.1 mm and displaying a distinct blue-green to clear pleochroism, or as slightly pleochroic, brownish green, globular or rectangular masses of submicroscopic crystals. Prehnite occurs in a typical form as subradiating to radiating faintly greenish to colorless masses, with the individual prisms reaching length of 0.5 mm. Primary constituents of the groundmass are tiny laths of plagioclase and opaque minerals. Secondary minerals are chlorite, calcite, and sphene, with minor pumpellyite and prehnite.

The volcaniclastic rocks consist mainly of lithic fragments of basalt porpyry of various sizes, small crystal fragments, in the matrix. The rock fragments have suffered a similar but stronger alteration than that of the basalt porphyry. Plagioclase phenocrysts in the fragments are heavily clouded and extensively altered to chlorite, white micas (sericite), calcite, epidote, pink prehnite, and blue-green pumepllyite. The matrix is altered to chlorite, calcite, sphene, epidote, prehnite, pumpellyite, and laumontite.

Laumontite usually occurs as anhedral to subhedral columnar crystals (smaller than 0.5 mm in length), as cement in the matrix or growing in amygdules or veins. The more extensive alteration of the volcaniclastic rocks than the lavas apparently occurred because they were more permeable and thus accessible to migrating fluids.

3. Sanbana Grande Andesite

Andesite breccia, flow breccia, and tuff with minor basalt lava forms the Sabana Grande andesite, which is well exposed in the Hormigueros syncline and less so in some small synclines in the Guanajibo regions, in a tongue in the Tea syncline, and in outcrops in the Yauco area (Mattson, 1960). Lava and tuff are common at the top of the unit, with breccia below. The sabana Grande andesite is between the Parguera limestone and Yauco mudstone, and can be dated as Turonian to Campanian, Mattson (1960) described lenses of poorly sorted conglomerate that contain rounded to subangular pebbles of radiolarian chert and metamorphic rocks (amphibolites), which are derived from the underlying Bermeja complex, at the base of the andesite in the Tea syncline and the Guanajibo anticlines. Sills and dikes of quartz diorite porphyry are intruded into the Sabana Grande andesite in the Tea syncline area. The general petrography of these rock types were described by Mattson (1960).

The andesite porphyry has equal amounts of phenocrysts and groundmass. The phenocrysts are composed mostly

of twinned and zoned plagioclase laths, 0.1 to 1.5 mm in length. They are commonly moderately altered to sericite, while chlorite, calcite, quartz, sphene, and pumpellyite may also replace it in some extensively altered crystals or pseudomorphs. Calcic plagioclase relicts are not rare, but only occur in the cores of grains. Although plagioclase is usually slightly zoned, the average anorthite content is about 35 percent. Partially altered pyroxene and euhedral pseudomorphs after it occur in minor amount as phenocrysts, averaging 1.0 mm in length. The pyroxene is pale green augite with an optical angle ($2V_Z$) of approximate 57°, as determined on a universal stage. Measured value of n_Y is 1.702. They are partially to completely replaced by chlorite, calcite, and quartz, with minor sphene, opaque minerals, and pumpellyite. The subhedral prismatic or blocky pumpellyite displays a distinctive blue-green pleochroism, and is smaller than 0.1 mm in grain size. A small amount of a euhedral to subhedral opaque mineral occurs as phenocrysts up to 0.2 mm in size. The groundmass contains small grains of opaque minerals and feldspar, and altered glass (?). The amygdules may be filled with laumontite, chlorite, calcite, quartz, and sphene.

The volcaniclastic rocks contain various amounts of rock fragments of andesite porphyry, broken crystals of plagioclase, pyroxene, and amphibole, and a fine grained matrix. Secondary alteration is more extensive than in the andesite porphyry. The plagioclase is moderate to extensively altered

to chlorite, sericite, epidote, and laumontite. Besides these secondary products, some pseudomorphs after plagioclase also contain pale yellow to brownish yellow epidote, and blue-green pumpellyite. Pale green clinopyroxene is slightly altered to chlorite and opaque minerals. Pseudomorphs after amphibole usually contain chlorite and calcite, with rare opaque minerals. The matrix and cavities are composed of various combinations of secondary chlorite, calcite, quartz, laumontite, epidote, sphene, and opaque minerals.

A specimen from an intrusive sill or dike is of quartz diorite porphyry. It was originally dominated by plagioclase, K-feldspar, and quartz, with subordinate biotite and apatite. Plagioclase occurs as phenocrysts, averaging 3 to 4 mm in length, commonly twinned with slight zonning. The composition is usually sodic andesine. K-feldspar is untwinned and very rarely zoned, occurring as phenocrysts of the same size as plagioclase. Both feldspars are usually moderate to extensively replaced by sericite and rarely by calcite, with unaltered feldspar only remaining in the center of some crystals. Euhedral quartz phenocrysts are 1 to 2 mm in size and rarely altered. The groundmass is composed of small grains (0.1 to 0.3 mm) of quartz and partially altered feldspar laths. Micas are widespread in the groundmass, usually interstitial to other minerals. They include sericite and olive-green pleochroic biotite. Biotite is usually in tabular or lamellar aggregates, sometimes associated with opaque minerals or intergrown with

white micas. Accessory apatite occurs as euhedral to subhedral prismatic crystals, averaging of 0.8 mm in size.

E. San German Formation

A thick sequence of andesitic volcanic rocks with interbedded conglomerate and lenses of massive limestone make up the San German formation. This formation, with a maximum thickness of 600 m near Cabo Rojo, thins from the west to a minimum of 100 m in the Lajas area and thickens further east in the Susua basin. The Contui limestone is the highest unit in the formation except southeast of Cabo Rojo, where about 150 m of andesitic volcanic rocks, with minor basalt lava, shale and conglomerate overlies it. The San German formation probably unconformably overlies the Mayaguez group and is conformably overlain by the Jicara formation. By means of foraminiferal age determination, the formation ranges from Campanian to Maestrichtian in age (Mattson, 1960).

The hornblende andesite porphyry contains about one third euhedral to subhedral plagioclase and hornblende phenocrysts, approximate 1 to 2 mm long. The rest is groundmass, containing altered minerals and small crystals of hornblende and plagioclase. Plagioclase laths are usually clouded with alteration products of white micas (sericite), albite, laumontite, chlorite, and minor calcite. Relict plagioclase is very rare and is usually calcic andesine.

The hornblende is usually twinned and has well developed cleavage, with an extinction angle $C \wedge Z$, of about 18°, $2V_X$ about 70°, $n_X = 1.660$, and $n_Z = 1.684$. Usually, the hornblende is unaltered, but slight alteration to chlorite and sphene occurs in a few cases. Inclusions of small plagioclase laths, euhedral apatite, and subhedral to euhedral opaque minerals in the hornblende are common. The hornblende displays strong pleochroism: X = greenish yellow, Y = dark greenish brown, and Z = dark brownish green. Besides the small altered plagioclase laths and hornblende, the groundmass is commonly replaced by interstitial chlorite, laumontite, quartz, and rare calcite.

In the basalt porphyry, euhedral plagioclase and clinopyroxene occur as phenocrysts, with an approximately equal amount of fine grained groundmass. Plagioclase laths are 0.2 to 2.0 mm in length, usually twinned and zoned, and are extensively altered to sericite, albite, chlorite, and rarely to calcite, epidote, and opaque minerals. No relict calcic plagioclase was observed. Colorless augite usually ranges from 0.5 to 1.5 mm in size, and is partially or completely replaced by chlorite, calcite, and sphene, and rarely by epidote and opaque minerals. The relict clinopyroxene has a optical angle ($2V_Z$) of 54°, measured on the universal stage. Measured values of $n_Y = 1.700$. The groundmass, commonly altered to chlorite and calcite, contains small crystals of altered plagioclase laths and pyroxene.

III. METAMORPHISM IN SOUTHWESTERN PUERTO RICO AND RELATIONS TO THE EASTERN GREATER ANTILLES

The study of metamorphism is one of the important tasks in an investigation of island arc evolution. The tectonic history of the interaction of two adjacent lithospheric plates can be recorded in the structural and metamorphic features in the rocks of an island arc, as well as in a continental margin. Structural features in an island arc area are revealed by studies of the surface structure, as well as through geophysical investigations. Much information can be hidden in the metamorphic rocks, which may contain clues to the physical conditions existing during part of the epoch of island arc evolution whether buried at depth or submerged in sea water, and of which we have little knowledge at this moment. Some models and hypotheses of island arc formation have been formulated or modified on the basis of the studies of exposed metamorphic belts in some island arcs and continental margins, especially in Japan.

In this section, the metamorphic features in the Bermeja complex of southwestern Puerto Rico and the exposed volcanogenic rocks in the same area will be discussed, and a review of the available published data of low-grade metamorphism in other parts of the eastern Greater Antilles will be made. A comparison with other metamorphic terranes and a brief discussion on the paragenesis follows.

A. Metamorphism in the Bermeja Complex

The oldest rocks exposed in the eastern Greater Antilles are the Bermeja complex, which probably represents examples of initial-stage island arc rocks under the exposed volcanic pile in most parts of Puerto Rico or the oceanic crust (see discussion in later sections). This unit is of special significance for the study of metamorphism, because it may reflect something of tectonic history of the initial stage of island arc formation.

1. Schistose Amphibolite and Massive Metabasaltic Dikes

The metamorphic features of these rocks and their relationships to possible tectonic events involving the schistose amphibolite as well as the intrusive metabasaltic dikes exposed in the Las Palmas area were described by Tobisch (1968). Regional metamorphism of a typical amphibolite facies first affected the schistose amphibolite. Most of the structural feature, including foliation, hornblende lineation, segregation bands, and small-scale folding, were formed during this stage of metamorphism. The metamorphic intensity decreased beofre the schistose amphibolite was intruded by the basaltic dikes, which were then metamorphosed in the epidote-amphibolite facies, with development of late stage kink-bands. Serpentinite bodies emplaced from depth caused local contact metamorphism or Ca-metasomatism in a narrow zone of the amphibolite bodies in

the Greenschist facies.

a. Regional Metamorphism

The main petrographic characteristics of the schistose amphibolite and the metabasaltic dike indicate features of the amphibolite facies and epidote amphibolite facies, respectively. The differences between the two rock types can be recognized by the mineral assemblages, the crystallization characters of hornblende, segregation bands, and the structural features.

The major constituent minerals of the schistose amphibolite unaffected by the contact metamorphism and metasomatism are hornblende, sodic andesine, and quartz. Accessories include apatite, opaque oxides, sphene, and zircon, and are stably associated with the main mineral assemblage. Apatite occurs in most specimens. Opaque oxides and sphene are common, but zircon appears only rarely. This mineral assemblage corresponds to the amphibolite facies and very close to or on the join hornblende-anorthite, as shown in Figure 7(c). The calciferous amphibole in this assemblage is bluish green, deep bluish green, and rarely brownish green hornblende, which usually has well formed crystal habit and well-developed cleavage. Therefore, the physical conditions of the metamorphism may correspond to those of the lower to upper amphibolite facies, accompanied by such tectonic stresses as are necessary to cause the foliations, lineations, folding, and quartzo-feldspathic

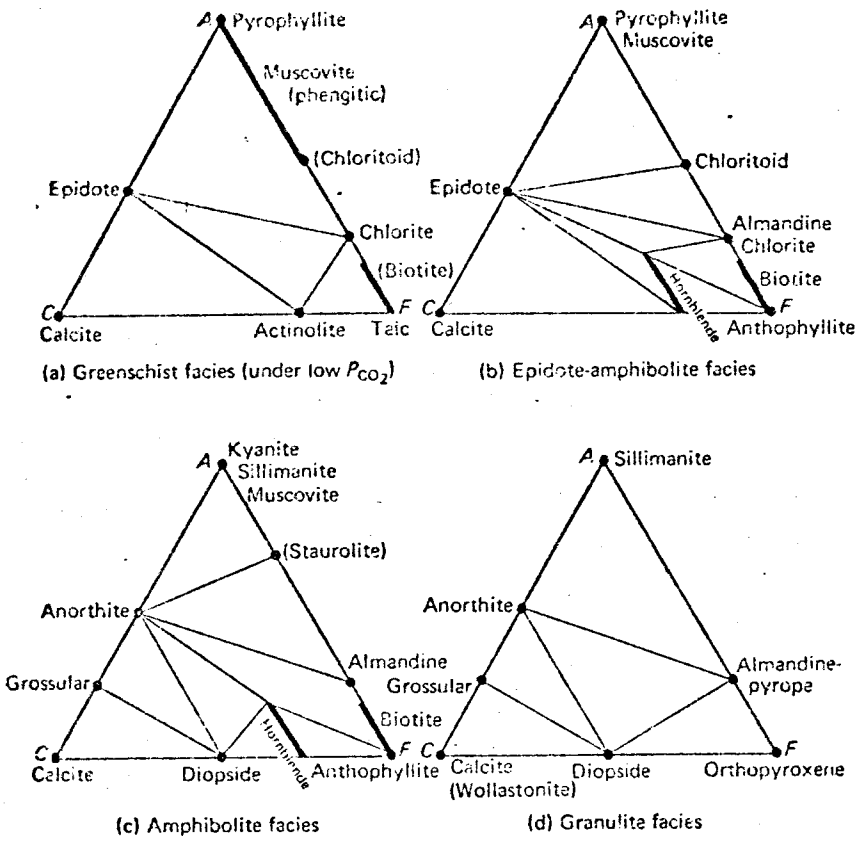

Figure 7. ACF diagrams for the medium-pressure facies series (Miyashiro, 1973c).

segregations in the schistose amphibolite.

The stable mineral assemblage in the dikes during regional metamorphism was hornblende, sodic andesine, and epidote. Opaque oxides and zircon occur rarely as accessories. Hornblende of this assemblage is a pale green to pale bluish green pleochroic variety. The stable assemblage falls in the field of the hornblende-epidote association of the epidote-amphibolite facies, as shown in Figure 7 (b). For the hornblende of the dike, the crystal habit and cleavage are less well developed, the grain size is smaller, and the pleochroism is weaker than in that of the schistose amphibolite. The existence of small relict clinopyroxene cores in the hornblende of the dike suggest that the physical conditions of epidote-amphibolite facies metamorphism lasted a relatively short period, before all minerals in the dike could be completely reconstituted. Thus, the schistose amphibolite was not, or only very slightly, affected under these new, and somewhat less intensive conditions. The tectonic stresses during this later stage of metamorphism appear to be weaker due to the absence in the metamorphosed dike of these structural and textural features which had existed in the schistose amphibolite.

b. Contact Metamorphism

Tobisch (1968) approximately defined a narrow contact zone, about 100 to 150 m in width on the margin of the amphibolite bodies, where he inferred an increased ther-

mal gradient due to the emplacement of the "hot serpentinite" into contact with the amphibolite body, after the major regional metamorphism ceased. Within this "contact zone", the equilibria among mineral phases are incomplete, with minerals belonging to the previous facies of regional metamorphism still persisting in these rocks. The possible equilibrium mineral assemblage may be albite to oligioclase (?) - epidote - chlorite - quartz - actinolite - (apatite - opaque oxides - sphene - prehnite (?)), which may belong to the epidote- chlorite - actinolite field of the greenschist facies (Figure 7 (a)), but some uncertainties still exist. Calcium-metasomatism is suggested by the appearance and abundance of prehnite in some parts of the "contact zone". More detailed work is obviously necessary in order to further clarify the picture of the effects of the serpentinite emplacement on this amphibolite body.

2. Amphibolitized Dolerite

The reconstitution of the metamorphic mineral assemblage was incomplete in the amphibolitized dolerite exposed in the spilite quarry near Mayaguez. The original igneous texture is preserved to some extent, but clinopyroxene is usually replaced by bluish-green hornblende. Small relict centers of augite are rare. The bluish green hornblende ranges 0.1 to 1 mm, usually with moderately developed cleavages. The mineral assemblage of hornblende - andesine - (quartz - opaque oxides) may be of the amphibolite facies

(anorthite - hornblende joint of Figure 7 (c)). However, this cannot be considered conclusive due to a lack of detailed petrographic data.

3. Spilite

The petrogenesis of spilite and the theories to explain the spilite problem are very diverse in nature (summarized by Amstutz (1968)), and will not be discussed here. As will be shown in a later section on geochemical data, the spilite of the Bermeja complex might have been subjected to metasomatism, mainly of alkali migration.

Generally, the original magmatic origin of the spilite of the Bermeja complex is recognizable by preserved textural features which differ in no marked way from those of normal extrusive mafic rocks. The original glassy groudmass has been effectively recrystallized into low-temperature mineral assemblages (chlorite, quartz, epidote, prehnite, hydrogarnet) under new physical conditions. Albite(secondary ?) is also commonly replaces in various extents by chlorite, white micas, prehnite, epidote, or calcite. These alteration assemblages may be caused by low-grade burial metamorphism. Alternatively, some of the secondary minerals (prehnite, epidote, calcite), may also be caused by Ca-metasomatism effects in proximity to the contact with the adjacent serpentinite. However, beyond the recognition of alteration effects, the genesis of this spilite is still obscure. In order to further evaluate the possible petrogenesis, more

field work to examine structural and petrologic features within the "spilite body" and the contact relationships with other rocks must be made.

4. Cajul Volcanics and Mayuayo Porphyry

All the examined rocks of Cajul volcanics and the Maguayo porphyry show at least some minor alteration to lower temperature assemblages.

In the Cajul volcanics, mostly plagioclase phenocrysts are moderately to extensively replaced by white micas or sericite, chlorite, and rarely calcite and epidote. Clinopyroxene usually persists unaltered or is only slightly replaced by chlorite and calcite. The interstial groundmass shows more extensive alterations to chlorite, epidote, white micas or sericite, quartz, or sphene. The amygdules and veinlet filling may contain chlorite, epidote, quartz, calcite and pumpellyite.

The Maguayo porphyry was subjected to a lesser degree but similar type of alteration as the Cajul volcanics. No clinopyroxene was found in the porphyry, and in stead, hornblende, either fresh or altered, and biotite, which is commonly altered, are common in the porphyry. The alteration, being similar to that of the low-grade metamorphism of the Upper Cretaceous volcanogenic rocks in southwestern Puerto Rico, will be discussed in more detail in the next section.

B. Metamorphism of the Post-Albian Rocks in Western Puerto Rico

In previous sections, the petrography and alteration of the igneous and pyroclastic rocks of the Rio Loco formation, Mayaguez group, and San German formation of southwestern Puerto Rico were discussed in some detail. In this ection, the type of regional distribution and of alteration, and the applicable low rank metamorphic facies of these rock units, and of the pyroclastic rocks exposed in the western part of the Yauco Quadrangle and the southwestern part of the Monte Guilarte Quadrangle (easternmost part of the map area of Figure 2), and the volcanoclastic rocks of the Rio Culebrinas formation in the Rincon Quadrangle (northwesternmost part of the map area of Figure 2), will be briefly discussed, while population of samples of these rock units in this study is too small to allow a definitive study of progressive low-grade metamorphism in this area, neverthless, the available limited petrographic data permit at least an introduction to the area immediately adjacent to the exposed Bermeja ultramafic complex. The features of low-grade metamorphism in other parts of the eastern Greater Antilles as currently known will also be summarized, and a comparison of other documented low-grade metamorphic terranes in other parts of the world and their paragenetic relations to the eastern Greater Antillean terrane will be discussed.

All the rock examined in the present study show at

least some minor alteration to low-temperature mineral assemblages. The amount of alteration or secondary phases is related to rock type; that is, pyroclastic rocks generally contain more secondary minerals than nearby lava flows. Greater alteration of pyroclastic rocks is expected because they generally were more permeable and thus accessible to fluid migration. It is also seen that minerals characteristic of the zeolite facies and prehnite-pumpellyite facies are typical in these rocks, and it will be shown that these secondary mineral assemblages are not clearly related to stratigraphic position or to the present depth of burial.

1. Alteration

Most primary mineral phases in the rocks show varying degrees of alteration. Although many secondary mineral associations are themselves in disequilibrium, in order to show the progressive sequence of alteration in the individual primary phases, the alteration of plagioclase, olivine, pyroxene, amphibole, groundmass, and of the matrix materials (in the pyroclastic rocks), as well as the filling of amygdules and veins will be considered separately.

a. Plagioclase Alteration

The least altered plagioclase occurs in the quartz diorite porphyry intruded in the Sabana Grande Andesite of the Mayaguez group.

With an increasing degree of alteration, the plagio-

clase has been slightly albitized. Thin rims of dusty albite and sericite are developed on the edge of the plagioclase phenocrysts, accompanied by the occurrence of various combinations of chlorite, calcite, sphene, epidote, opaque minerals, and quartz in minor amount. Relicts of the primary Ca-feldspar, however, commonly remain in the crystal centers, which is in contrast to the common style of (igneous) deuteric alteration where the cores of plagioclase (must calcic) are altered first with the more albitic outer zones remaining stable or approximate so with the alteration assemblage. Somewhat more altered plagioclase has been further replaced by combinations of the above minerals as well as laumontite.

The most altered plagioclase contain an extremely diversified suite of alteration phases. Prehnite and/or pumpellyite begin to replace the plagioclase phenocrysts, while secondary albite pervades all of the crystals. Only plagioclase phenocrysts of extremely coarse size have escaped complete alteration, with tiny isolated patches of calcic plagioclase remaining in crystal centers. Small quantities of the other alteration phases, including laumontite, are also present in these altered feldspars. Sphene and opaque minerals, however, are rare.

b. Olivine Alteration

Euhedral olivine pseudomorphs were only found in several thin section in keeping with the general sensitivity of olivines to alteration. No traces of relict olivine were

found in any of the rocks examined. The most common alteration product of olivine is greenish to pale greenish chlorite, commonly associated with the following minerals: calcite, quartz, epidote, and opaque minerals. In rare cases, calcite occurs as a major constituent in the olivine pseudomorph with minor amounts of other secondary minerals. In one thin section, a trace of pumpellyite (?) of the slightly brownish pleochroic type was found in associated with chlorite, epidote, and opaque minerals in the pseudomorphosed olivine.

c. Pyroxene Alteration

Clinopyroxene is usually unaltered or only slightly altered to secondary minerals. Pyroxene is extensively altered however, in some specimens. Pyroxene pseudomorphs are rarely found. Chloritization of pyroxene is common along edges and fractures in association with small amounts of sphene and calcite. More altered pyroxene contains mainly chlorite, calcite, sphene and opaque minerals, and rarely quartz and epidote. Subordinate amounts of pumpellyite of the bluish green and brownish (?) types also occurs in a few of the most altered pyroxene phenocrysts.

d. Amphibole Alteration

Primary amphibole occurs only in some andesite lavas (Sabana Grande andesite of the Mayaguez group and hornblende andesite porphyry of the San German formation). It usually persists unaltered, although some extensively altered

or pseudomorphosed amphiboles are found in the andesite fragments of the pyroclastic rocks. The possible alteration products are similar to those of clinopyroxene. The amphibole pseudomorph was usually recognized by means of the distinctive cleavage traces which were replaced by opaque minerals.

e. Alteration of Groundmass

The groundmass of the volcanic rocks and of the volcanic fragments of the pyroclastic rocks have undergone moderate to extensive secondary readjustment,and as noted above the latter contain more secondary minerals or are more extensively replaced than the former. Chlorite is the most common groundmass replacement mineral, with various combinations of sericite, sphene, calcite, quartz, epidote, opaque minerals, and laumontite present in lesser amounts.

f. Alteration of the Matrix Materials in the Pyroclastic Rocks

The pyroclastic rocks have been more extensively altered than the volcanic rocks of the studied specimens. In the least altered matrix of these rocks, chlorite is usually dominate,along with subordinate combinations of sericite, sphene, calcite, quartz, and opaque minerals. Laumontite coexists with combinations of the above secondary phases in the more altered matrices. Laumontite, as both a massive cement and a replacement product, may dominate the

mineralogy of some of these rocks. In the most extensively altered matrix materials, prehnite and pumpellyite become important, Chlorite, and small quantities of the combinations of sphene, calcite, quartz, epidote, and opaque minerals may coexist with prehnite and pumpellyite. In some cases, laumontite also occurs with these alteration products. In one thin section, prehnite exists without laumontite and pumpellyite.

g. Fillings of Amygdules and Veins

Within filled voids, parts of the following mineral sequence are commonly present in succession from margins to cores: (1) dark yellowish green chlorite, (2) faint green chlorite, (3) pumpellyite, quartz, (4) prehnite, (5) laumontite, (6) calcite. The completeness of the succession depending on the extent of alteration of the rocks. Laumontite, prehnite, and pumpellyite do not occur in the voids of the least altered rocks, but prehnite and pumpellyite are common in the amygdules of the most altered rocks. The variety and the amounts of secondary phases filling in voids of the rocks are usually greater than those altered from the primary crystal phases of the same rocks. Accordingly, equilibrium among the secondary phase (amygdules and altered crystals) and primary phases during alteration was not achieved.

2. Regional Distribution of Metamorphic Facies

The studied specimens of exposed rocks in the Las

Vegas, Hormiguera, and Tea synclines (in order, north to south) in the map area of Figure 5 will be discussed separately in this section. Because most secondary mineral phases of these rocks are not in total equilibrium, the term "mineral association" is used instead of "mineral assemblage".

The secondary mineral associations of the Upper Cretaceous igneous and pyroclastic rocks exposed in the Las Vegas syncline are shown in Table 1A. The approximate age, a columnar section, and the present stratigraphic thickness are shown in the left columns in the same table, in order to indicate the approximate stratigraphic level of the samples. The maximum depth of burial of the specimens examined, estimated from the present stratigraphic thickness, is about 4000 m. The varieties and the amounts of secondary minerals among the specimens do not vary clearly with the present depth of burial. Chlorite, white micas, and albite are the most common alteration products of these rocks, and sphene, carbonate, and epidote occur sporadically in small quantities. In most rocks, quartz coexists with other secondary minerals. Laumontite is locally in abundance, associated with most other secondary minerals. Varying amounts of prehnite and pumpellyite are common in some of these rocks (especially in the Maricao basalt), in which laumontite may or may not be present.

In the Homigueras syncline, the Sabana Grande andesite, occurring as lenses in the Yauco mudstone, contains an alteration association of mainly chlorite, sericite, albite,

Table 1A. Secondary mineral associations of the Upper Cretaceous igneous and pyroclastic rocks in the Las Vegas Syncline, southwestern Puerto Rico. Symbols as follows: a, abundant; c, common; s, minor; r, rare; -, absent.

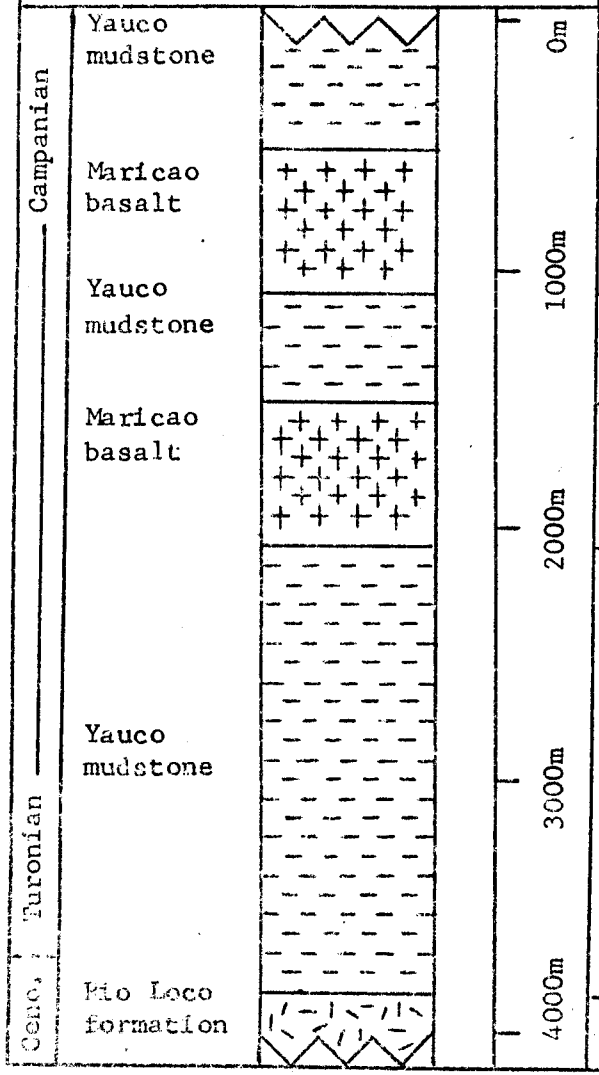

Sample no.	Chlorite	White micas	Albite	Sphene	Carbonate	Quartx	Laumontite	Epidote	Prehnite	Pumpellyite
Kmm-4	c	a	c	s	r	s	-	r	-	-
Kmm-5	c	a	c	s	-	s	s	r	s	r
Kmm-6	a	s	c	r	r	s	-	-	c	s
Kmy-2	-	s	c	r	s	s	c	r	-	-
Kmy-3	-	s	c	-	-	s	a	r	-	-
Kmm-3	c	-	c	s	s	s	-	-	s	r
Kmm-2	c	-	c	-	s	s	a	s	c	s
Kmm-1	c	a	c	s	c	s	c	s	s	r
Kmy-1b	c	a	c	-	s	s	-	-	-	-
Kmy-1a	c	a	c	-	c	s	-	r	-	-
K1-2	a	a	a	-	s	c	c	-	-	-

Table 1B. Secondary mineral associations of the Upper Cretaceous igneous and pyroclastic rocks in the Tea Syncline, southwestern Puerto Rico. Symbols as follows: a, abundant; c, common; s, minor; r, rare, -, absent.

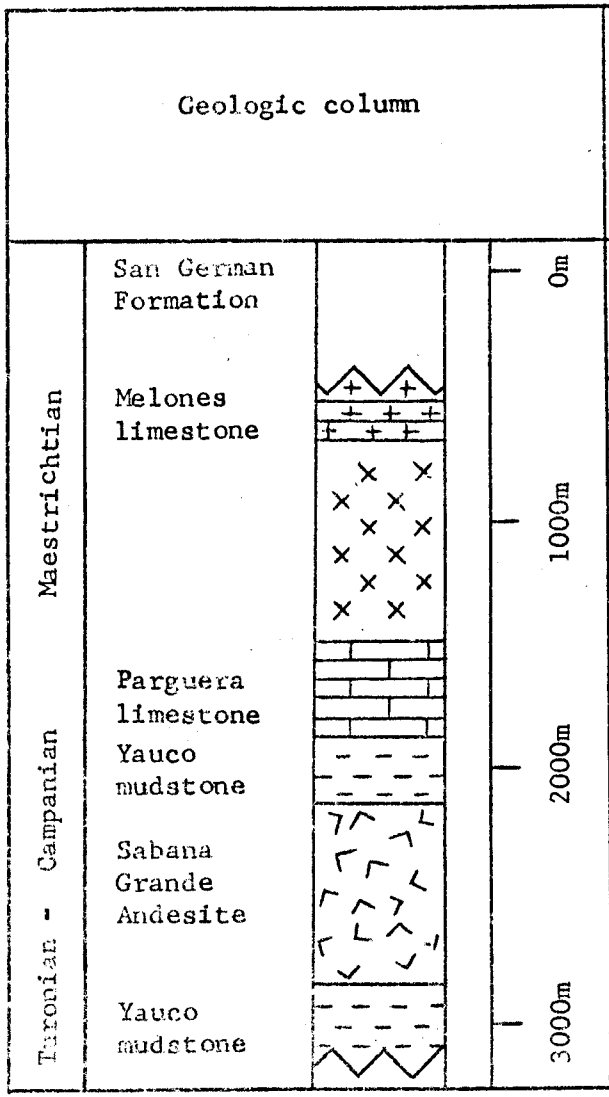

Sample no.	Chlorite	White micas (sericite)	Albite	Sphene	Carbonate	Quartz	Laumontite	Epidote	Prehnite	Pumpellyite
Ksv-2	c	c	c	s	s	s	-	r	-	-
Ksv-1	c	c	c	r	s	s	c	-	-	-
Kmy-4	c	c	c	-	-	s	c	r	-	s
Kms-7	-	a	-	-	r	a	-	-	-	-
Kms-6	c	c	c	s	s	s	-	r	-	-
Kms-3	s	c	c	s	s	s	c	-	-	r

quartz, and laumontite, with small amounts of sphene, calcite, or epidote. No prehnite or pumpellyite was found in the specimens examined, which are at an estimated stratigraphic depth of about 2000 m.

Secondary mineral associations for the studied specimens of the Mayaguez group and San German formation in the Tea syncline are shown in Table 1B. The associations usually contain abundant chlorite, sericite, and chlorite with occassional sphene, calcite, quartz, and epidote. Laumontite is locally abundant, but no prehnite was found; small amounts of pumpellyite may occur with laumontite and other secondary phases.

Thin sections were prepared and examined for the Upper Cretaceous rocks collected along route 128 between Yauco and Los Rabanos, on the eastern most part of the map area of Figure 2. Chlorite, sericite, albite, and quartz are common in all specimens. Calcite and epidote occasionally occur in small quantities; sphene is rare, and laumontite was found only in one specimen. Small amounts of prehnite and/or pumpellyite occur in most specimens, usually associated with epidote.

In northwestern Puerto Rico, the exposed Lower Tertiary Rio Culebrinas Formation contains as much as 3,000 m of andesite and dacitic tuff breccias, coarse tuffs, and thin-bedded volcanic sandstone and mudstone (McIntyre et al., 1970). Six specimens of the volcanogenic rocks of this formation, taken along route 2 in the Rincon Quadrangle in

the northwest part of the map area of Figure 2 were also microscopically examined. The alteration association is a common one, containing chlorite, sericite, albite, calcite, quartz, and laumontite. No epidote, prehnite, and pumpellyite were found.

In summary, chlorite, sericite, albite, calcite, and quartz are all common alteration products in Western Puerto Rico. Laumontite is in abundance in the southwestern part (Tea syncline and Homiguera syncline) and western part (Rio Calebrina formation on route 2) of this area. The occurrence of prehnite and pumpellyite is rare or limited to breciated zones in the rocks in this area. The mineral association, chlorite - laumontite - sericite - quartz - (- albite - calcite - sphene - prehnite (?) - pumpellyite (?)), may be of the zeolite facies (Coombs et al., 1959). Prehnite and pumpellyite are common in significant quantities in the northeastern part (Las Vegas syncline) and eastern part of southwestern Puerto Rico. Epidote commonly occurs in small amounts in these rocks. Laumontite is locally present in the prehnite-pumpellyite-bearing rocks, but not common. The mineral association prehnite - pumpellyite - albite - chlorite - sericite - quartz - (calcite - sphene - epidote - laumontite) may be considered as in transition from the zeolite facies to the prehnite-pumpellyite facies (Coombs, 1961). Therefore, the low-grade metamorphism in southwestern Puerto Rico may increase in intensity approximately from the zeolite facies in the southwestern part to the prehnite-

pumpellyite facies in the northeastern part. The secondary mineral associations are not, at least not clearly in terms of the data of Tables 1A-B, related to stratigraphic position or to the present depth of burial.

The large exposure of the younger Utuado pluton (see Figure 3) is about 20 miles northeast of the center of the studied area. Whether this intrusion might have slightly affected the thermal gradient during the low-grade metamorphism is problematical. Moreover, the metamorphism may have occurred before the plutonic intrusion. Obviously, no conclusion can be made without further work and data.

Simplified paragenesis account for the studied rocks is shown in Figure 8, in which the zeolite and prehnite-pumpellyite facies are approximately assigned in terms of the mineral associations. The transition between these metamorphic facies is, however, gradual, since most primary mineral are incompletely reconstituted. Thus, a determination of the boundary between the metamorphic facies (or zones) is difficult at best, and impossible at present, since the specimens examined in this study are limited in amount and regional distribution. More thorough sampling and detailed petrographic studies, as well as chemical analyses, are necessary to clarify the patterns of the low-rank metamorphism in southwestern Puerto Rico.

3. Low-Grade Metamorphism in Other Parts of the Eastern Greatern Antilles

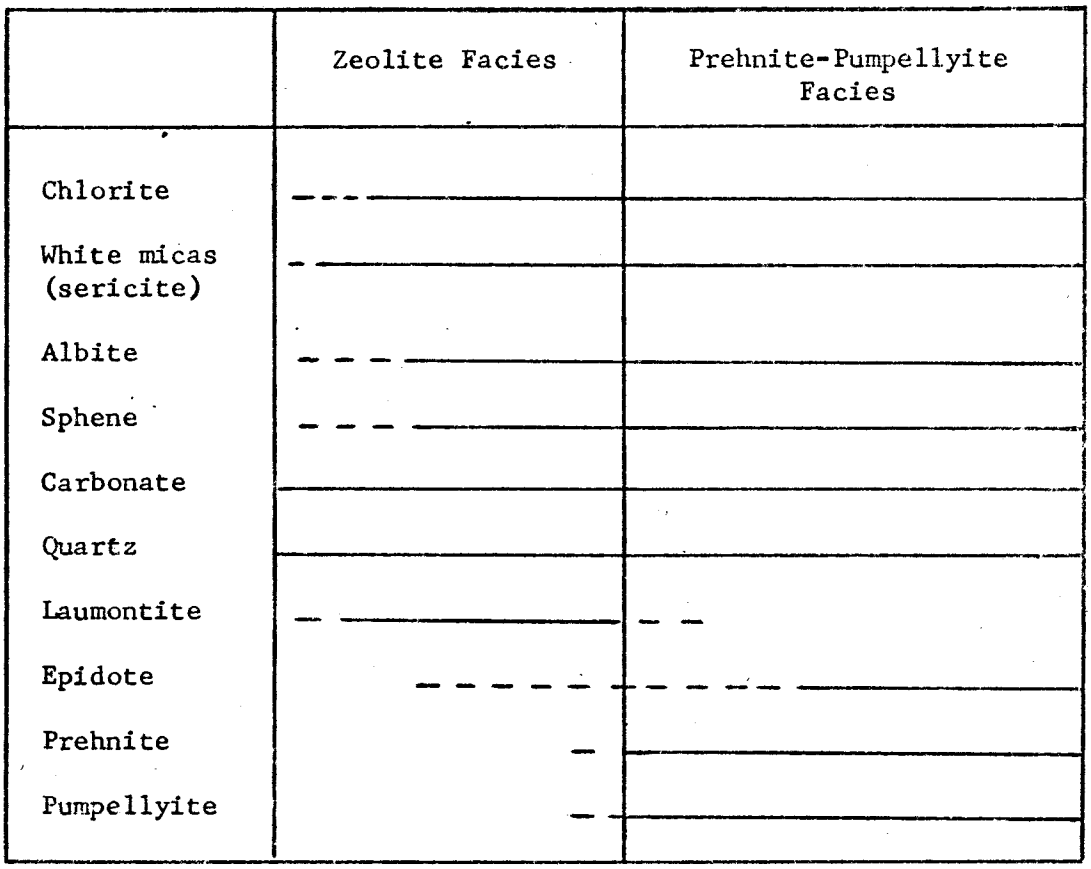

Figure 8. Progressive mineral changes of volcanic and pyroclastic rocks in southwestern Puerto Rico.

In order to discuss the metamorphism of the Eastern Greater Antilles in general, and to compare that in the area studied here, a summary of the low-grade metamorphism in different parts of the Eastern Greater Antilles as described by previous workers will be made.

The Water Island and Louisenhoj formations of the Virgin Islands appear to have been exposed to low-grade metamorphism of the prehnite-pumpellyite facies grading into the greenschist facies (Donnelly, 1966; Hekinian, 1971). The intermediate volcanogenic rocks in central Puerto Rico show regional low-grade metamorphism of the zeolite and prehnite-pumpellyite facies (Otalora, 1964; Lidiak, 1965; Glover, 1967; Jolly, 1970a).

In St. John of the Virgin Islands, the spilite-keratophyre association of the Water Island formation, probably of Pre-Albian age, lies unconformably below the Louisenhoj formation, which is an augite-andesite volcanic breccia of 7000 feet thickness. The Water Island formation is approximately 15,000 feet thick, of which spilite flows make up about one-fifth of the total. The sequences of low grade metamorphism in these formation described by Donnelly (1966), and Hekinian (1971) (Figure 9A) are a prehnite-pumpellyite and lower greenschist facies. The transition between the two facies is characterized by the disappearance of prehnite and pumpellyite, and a concomitant increase in actinolite with increasing stratigraphic depth in the Water Island formation.

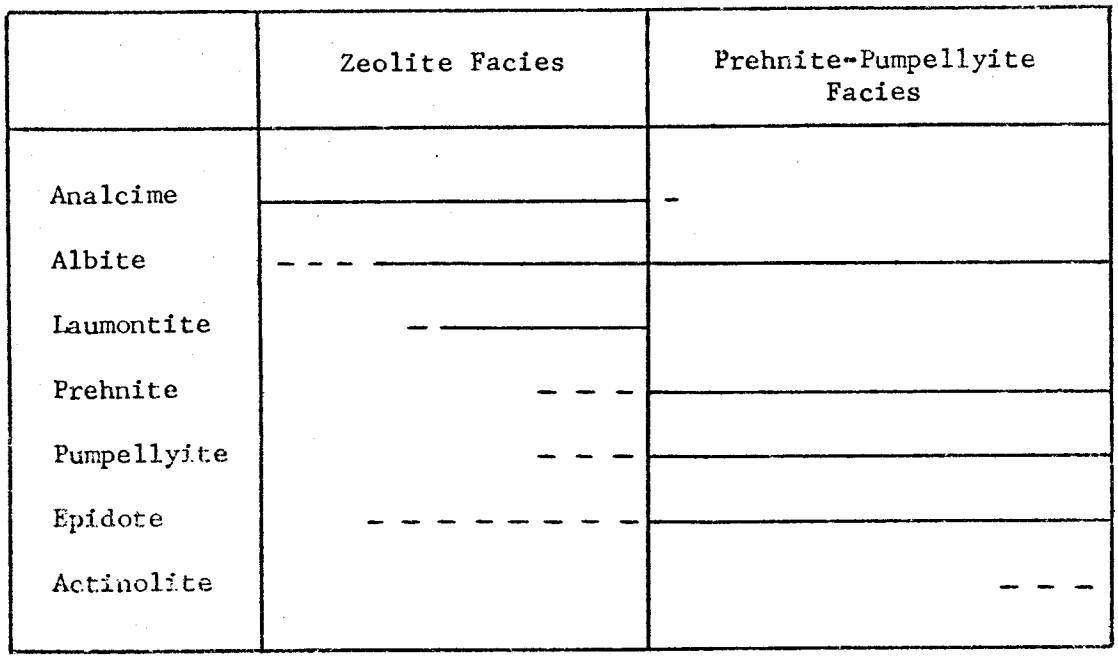

Figure 9B. Progressive mineral changes with metamorphism in intermediate volcanogenic rocks in central Puerto Rico (After Otalora, 1964; Jolly, 1970a).

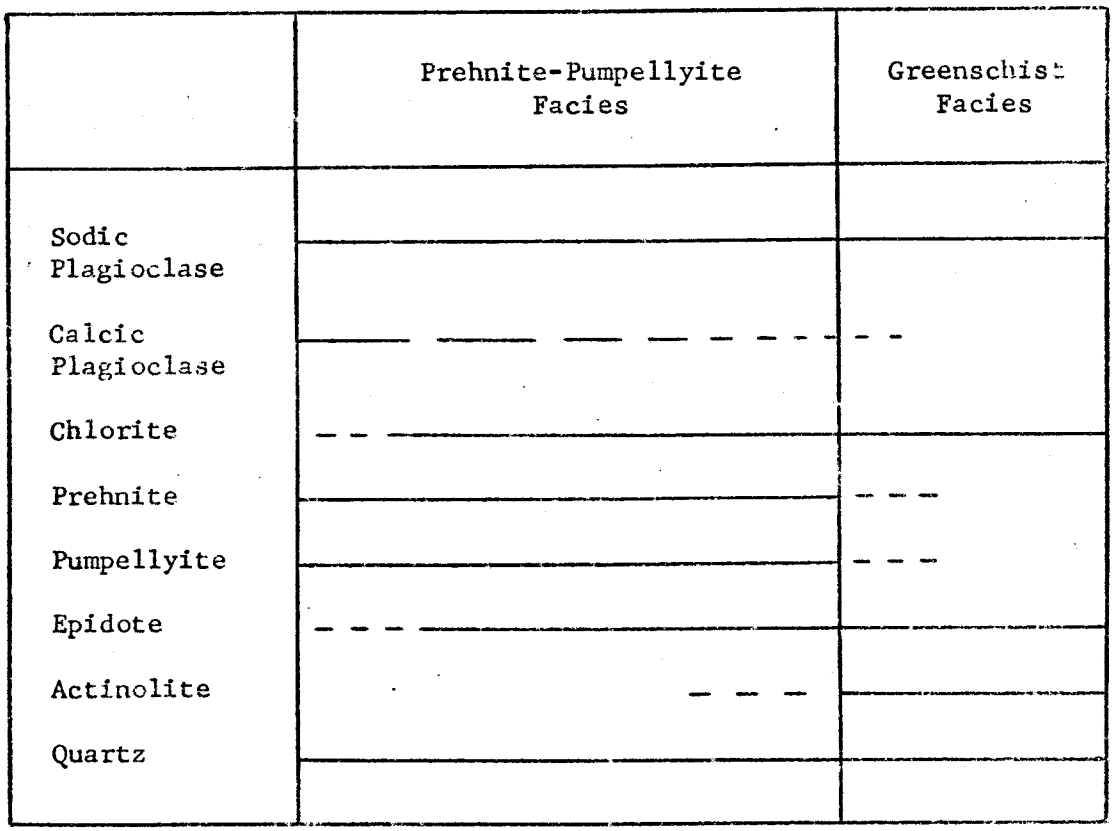

Figure 9A. Generalized progressive mineral changes with metamorphism in the Water Island and Louisenhoj Formations of the Virgin Islands (after Donnelly, 1966; Hekinian, 1971).

In central Puerto Rico, the metamorphic sequence produced in Upper Cretaceous intermediate effusive and pyroclastic volcanic rocks, which were altered in the zeolite and prehnite-pumpellyite facies, is shown in Figure 9B (Otalora, 1964; Lidiak, 1965; Jolly, 1970a). The primary texture of the rocks is preserved, and no schistosity has been developed. First, analcime and then, with increasing grade, laumontite, are characteristic of the zeolite facies. Epidote occurs sporadically in this facies. Heulandite associated with sericite and analcime was reported by Glover (1967) to be present in the Coamo and Cariblanco formations in the Coamo Quadrangle. The appearance of prehnite and pumpellyite at about 11,000 feet in terms of an estimate of the thickness of burial, marks the beginning of this facies. Calcic plagioclase (relict origin) is common in the zeolite facies while albitized plagioclase is characteristic of the higher-grade facies. Albite, quartz, chlorite, and calcite have been abundantly developed in both facies.

4. Comparison with Other Low Grade Metamorphic Terranes and their Paragenetic Relations

Low grade metamorphism of the zeolite and prehnite-pumpellyite facies occurs mainly in the lowest temperature parts of regional and ocean-floor metamorphic terranes, and recrystallization is usually incomplete within these facies. It appears that the paragenetic relations in the zeolite facies in different terranes are partly related to the

estimated geothermal gradient, based on recent petrographic and experimental studies. Thus, Miyashiro (1973c) classified these metamorphic terranes in terms of their apparent geothermal gradients into low, medium, and high pressure types.

In northeastern Maine, Coombs et al., (1970) have found a wide zone belonging to the prehnite-pumpellyite facies which probably represents the lowest temperature part of a low-pressure type metamorphism in the northern Appalachians. In the eastern Akaishi Mountains, Mogami area, and in the Tanzawa Mountains in Japan, the zeolite and prehnite-pumpellyite facies are well documented (Matsuda and Kuriyagawa, 1965; Utada, 1965; Seki et al., 1969), and are probably of the low-pressure metamorphic type. High geothermal gradients characterize these terranes, in which a great number of zeolites including mordenite, stilbite, yugawaralite, wairakite, heulandite, laumontite, and analcime occur.

In the Katsuyama area, Japan, a zone of the prehnite pumpellyite facies, which grades with increasing temperature into a zone of the glaucophane-schist facies, represents the lowest temperature parts of a high-pressure metamorphic terrane. A transitional zone between the typical glaucophane-schist facies into the prehnite-pumpellyite facies has been documented in the eastern and central parts of the Franciscan terrane in California (Ernst, 1965; Ernst et al., 1970).

A zeolite facies terrane in the Taringatura area (Figure 10), New Zealand is probably of the medium-pressure

Metamorphic Facies	Zeolite Facies		Prehnite Pumpellyite Facies
	Heulandite-Analcime Stage	Laumontite Stage	
Haulandite			
Analcime			
Laumontite			
Celadonite			
Smectite			
Chlorite			
Prehnite			
Pumpellyite			
Albite			
Quartz			

Figure 10A. Progressive mineral changes of volcanic graywackes and tuffs in the Taringatura area, New Zealand. (Coombs, 1954; Coombs et al., 1959)

Metamorphic Facies	Laumontite Facies	Prehnite-Pumpellyite Facies		Greenschist Facies
Mineral Zoning	I	II	III	IV
Laumontite				
Prehnite				
Pumpellyite				
Epidote				
Chlorite				
Actinolite				
Albite				
Quartz				
White micas				
Stilpnomelane				

Figure 10B. Progressive mineral changes in the central Kii Peninsula in the Sanbagawa metamorphic belt. (Seki et al., 1971)

type, with a lower geothermal gradient than that occurring during a low-pressure type metamorphism. In the central Kii Penisula (Figura 10B) in the high-pressure type Sanbagawa metamorphic belt of Japan, zeolite facies rocks, probably of the medium pressure type, occur with laumontite present as the only zeolite. The common varieties of zeolite present in low-grade metamorphism of the low-pressure type, i.e., mordenite, stilbite, yugawaralite, and wairakite, are absent in these medium-pressure terranes, partly as a result of the difference in geothermal gradient during these two types of metamorphism (Miyashiro, 1973c). In the Taringatura area (Figure 10A), the only zeolite minerals are heulandite, laumontite, and analcime, which are also the only three zeolite varities found in Puerto Rico volcanic and pyroclastic rocks. A few theoretical considerations and experimental studies of the stabilities of zeolites can be used to aid the interpretation.

Using a few basic assumptions and the available petrographic data, Miyashiro and Shido (1970) formulated a theoretical scheme for the stability relations of the zeolites. The stable assemblages of Ca-zeolite and Na-zeolite in the assumed systems An - SiO_2 - H_2O and Ne - SiO_2 - H_2O, respectively are shown in Figure 11A-B. It was assumed that an increasing temperature always tends to form a progressively dehydrated zeolite assemblage in the order as shown by (a) to (d) in the same figures. The low-pressure type metamorphism of the Tanzawa Mountains (Seki et al., 1969) may be roughly correlated

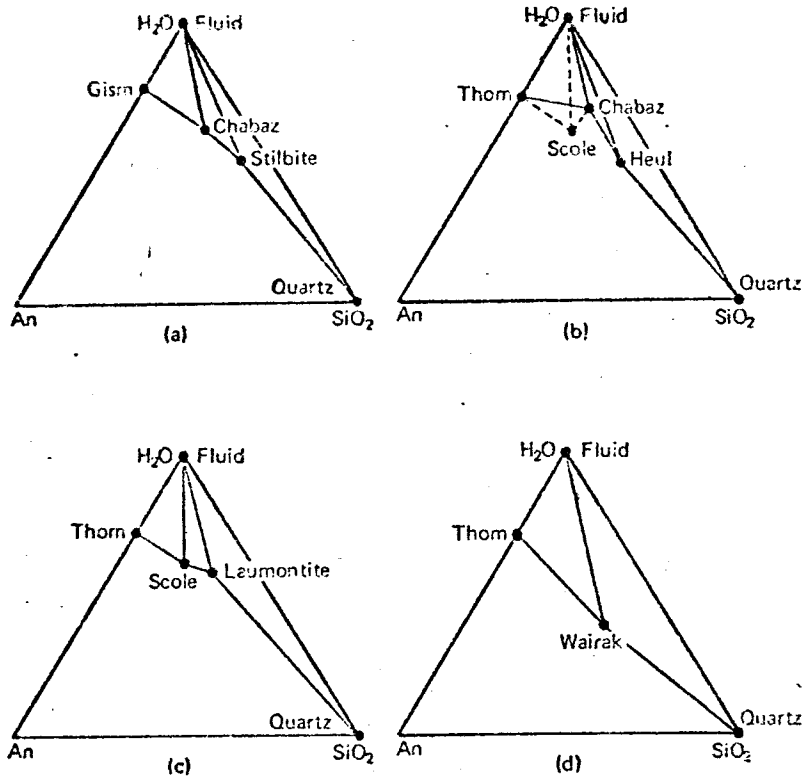

Figure 11A. Progressive dehydration of Ca-zeolite assemblages (Miyashiro and Shido, 1970). Abbreviations: An, anorthite; Chabaz, chabazite; Gism, gismondine; Heul, heulandite; Scole, scolecite; Thom, thompsonite; Wairak, wairakite.

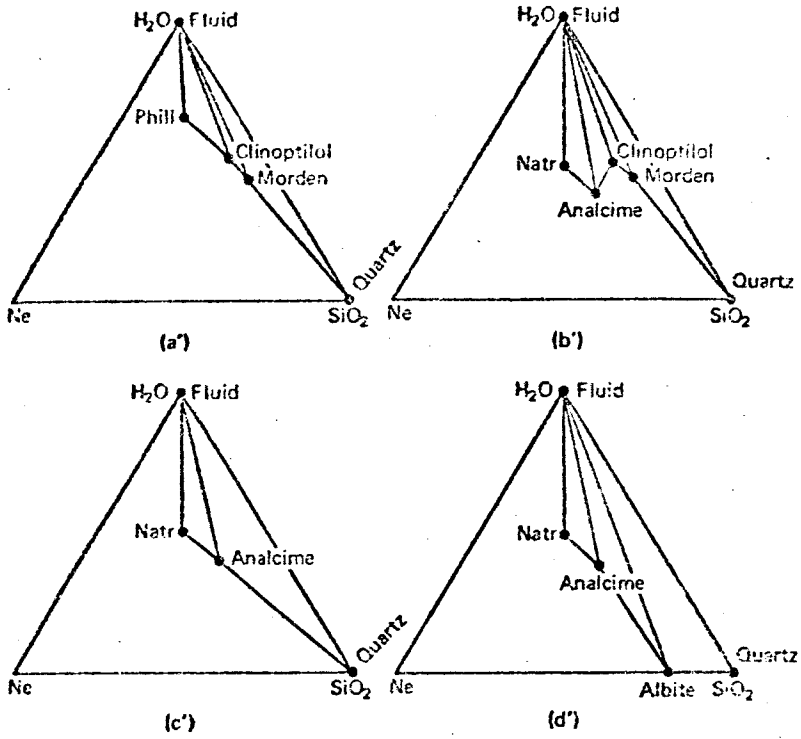

Figure 11B. Progressive dehydration of Na-zeolite assemblage (Miyashiro and Shido, 1970). Abbreviations: Ne, nepheline; Morden, mordenite; Clinoptilol, clinoptilolite; Phill, phillipsite; Natr, natrolite.

with all steps in the progressive dehydration of Ca- and Na-zeolite of Figure 11A-B. In an area of the medium-pressure type, where the geothermal gradient is low, e.g. the Taringatura area (Coombs et al., 1959), the most strongly dehydrated Ca-zeolite, wairakite (in Figure 11A9d)) does not occur. Instead, the zeolite assemblage in Figure 11A(c) with increasing temperature would grade directly into the prehnite-pumpellyite facies. The Puerto Rican zeolite facies rocks may also be correlated approximately with the assemblages of Figure 11A(b)(?), 11A(c), 11B(c'), and 11B(d')(?), which in turn then grade directly into the prehnite-pumpellyite facies. This may suggest that the physical conditions during low-grade metamorphism in the eastern Greater Antilles did not have a very high thermal gradient, and proceed approximately as a medium-pressure type.

Some experimental studies on the stabilities of zeolites, as shown in Figure 12A, can be applied as a mean of estimating the physical conditions of low-grade metamorphism. In central Puerto Rico, the amount removed by erosion above the studied rock sequences is unknown, but the maximum may be assumed to have been approximate 2 Km. (total thickness of Cariblanco and Coamo formations). Accordingly, the total depth of burial present during development of the sequence of secondary phases in this area may have been only about 5 Km. It is impossible,however, to determine at what depth the reaction analcime + quartz = albite + H_2O may have taken place, since the alterations commonly were incomplete (see

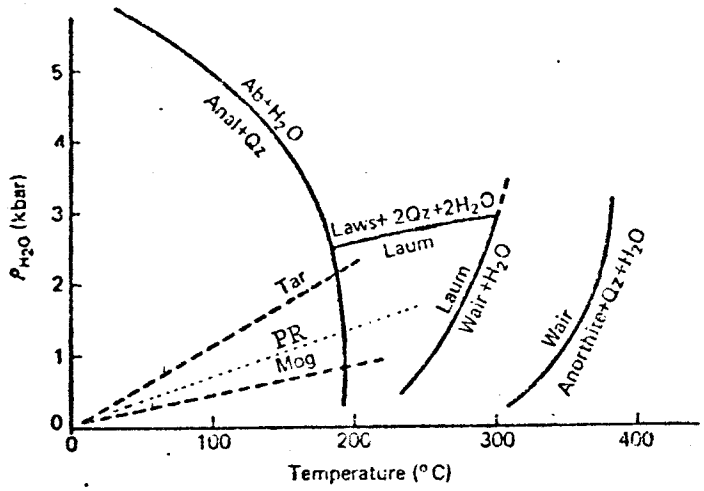

Figure 8A. Stability fields of the analcime + quartz assemblage and laumontite (Campbell and Fyfe, 1965; Liou, 1970). Broken lines 'Tar' and 'Mog' indicate possible geothermal curves of the Taringatura and Moagami areas (Miyashiro, 1973c). Dot line 'PR' indicates possible geothermal curve of Puerto Rico area. The high-temperature stability limit of laumontite is shown after Thompson (1970).

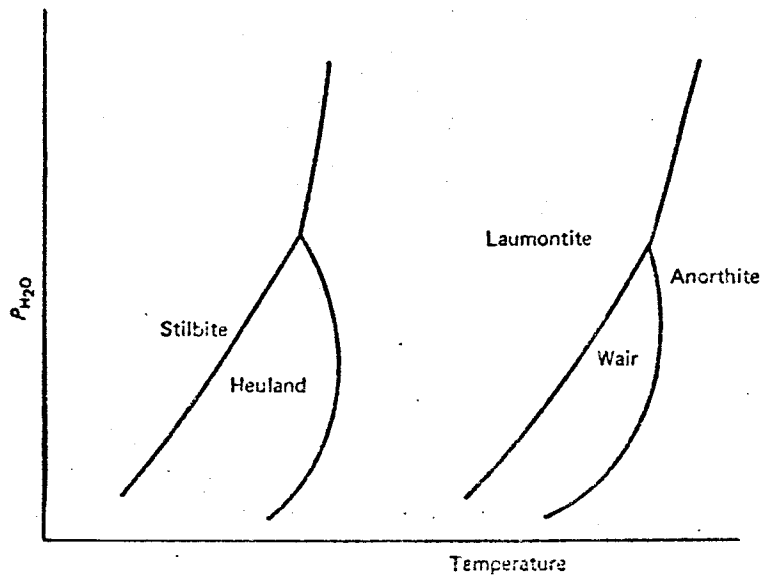

Figure 12B. Possible form of phase boundaries between Ca-zeolite in the presence of an aqueous fluid (after Miyashiro, 1973c). 'Heuland' and 'Wair' mean heulandite and wairakite.

Figure 8). The above reaction is regarded as taking place at about 180°C at low to moderate P_{H_2O} (see Figure 12A) and if it is assumed to have taken place at a depth of about 4 Km, the geothermal gradient is then roughly estimated at $45°C\ Km^{-1}$. Under these circumstances, the low grade metamorphism of the Puerto Rico area could be of the medium-pressure type, but close to the low-pressure type. Obviously, further work is required to confirm or modify this analysis, in particular the metamorphic features in other parts of the island, as well as the unknown effects on this metamorphism of the presence of numerous late-Cretaceous or Eocene plutonic intrusives in Puerto Rico should be studied.

C. Discussion

The general distribution of the regional metamorphic facies and their characteristic mineral assemblages in the Cretaceous volcanogenic rocks of the eastern Greater Antilles (Puerto Rico and Virgin Islands area), as discussed above in this section, are summarized in Figure 13.

The progressive mineral changes of regional metamorphism in these parts of the Greater Antillean island arc are shown in Figure 14. The range in metamorphic intensity (as represented by mineral facies) for various stratigraphic levels of the Greater Antilles are also shown in approximate order of increasing age. In general, the epoch of regional metamorphism in the Greater Antilles began at a Pre-Albian

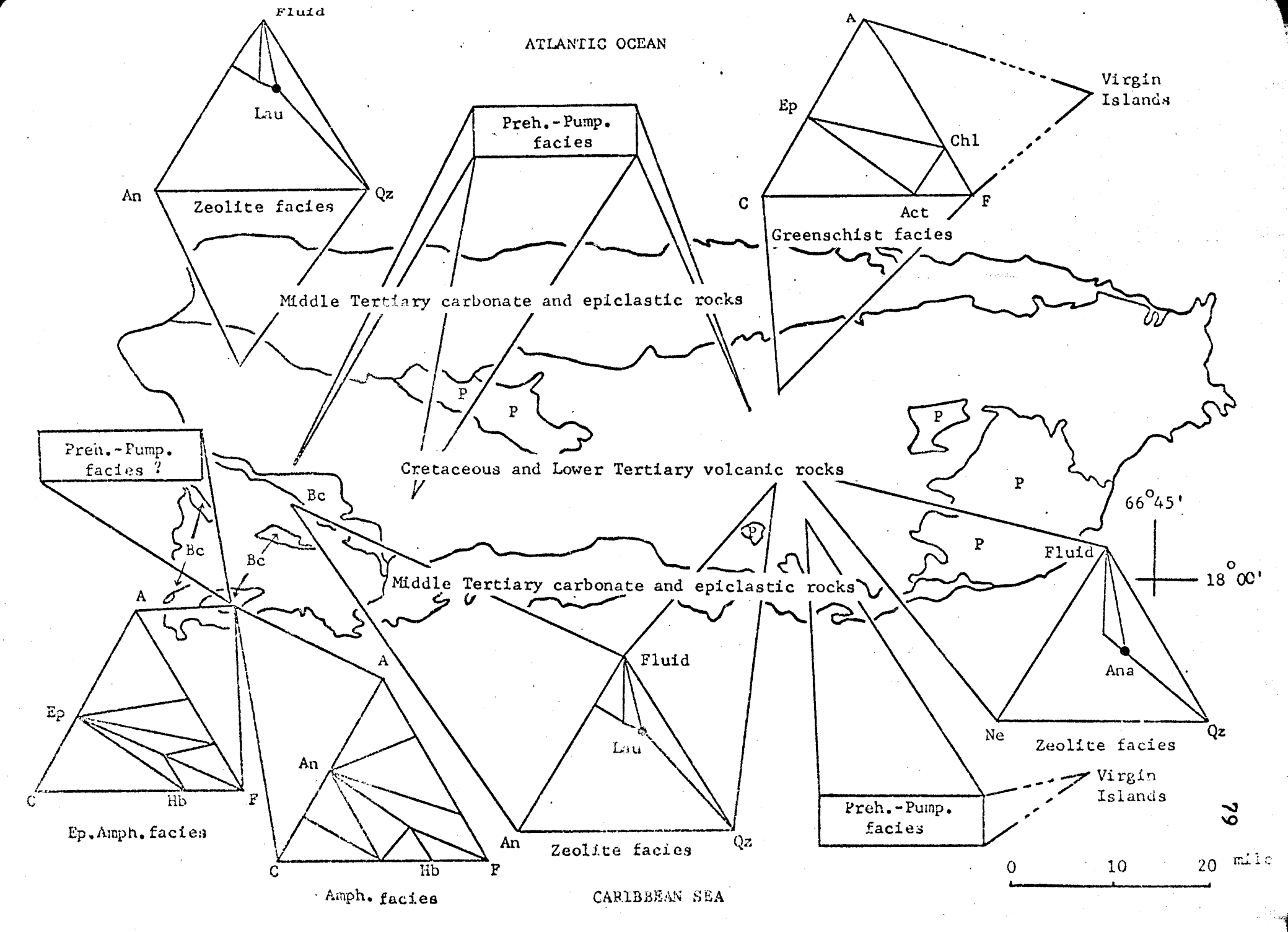
ATLANTIC OCEAN
Fluid
Lau
An
Zeolite facies
Qz
Preh.-Pump. facies
A
Ep
Chl
Virgin Islands
C
Act
F
Greenschist facies
Middle Tertiary carbonate and epiclastic rocks
P
Preh.-Pump. facies ?
Bc
Cretaceous and Lower Tertiary volcanic rocks
66°45'
18°00'
Middle Tertiary carbonate and epiclastic rocks
Fluid
Ana
Ne
Zeolite facies
Qz
Ep
Hb
F
Ep.Amph.facies
An
Amph. facies
Preh.-Pump. facies
Virgin Islands
0
10
20
miles
CARIBBEAN SEA
79

Figure 13. Simplified geologic map showing the general distribution of regional metamorphism and the mineral assemblages in Puerto Rico. "P" and "Bc" denote Lower Tertiary plutonic rocks and Pre-Albian Bermeja complex. "An" = Anorthite, "Hb" = Hornblende, "Amph." = Amphibolite, "Ep" = Epidote, "Act" = Actinolite, "Chl" = Chlorite, "Preh." = Prehnite, "Pump." = Pumpellyite, "Qz" =Quartz, "Lau" = Laumontite, "Ne" = Nepheline, "Ana" = Analcime. See Figure 7 for metamorphic facies. See Figure 11 for zeolite assemblages.

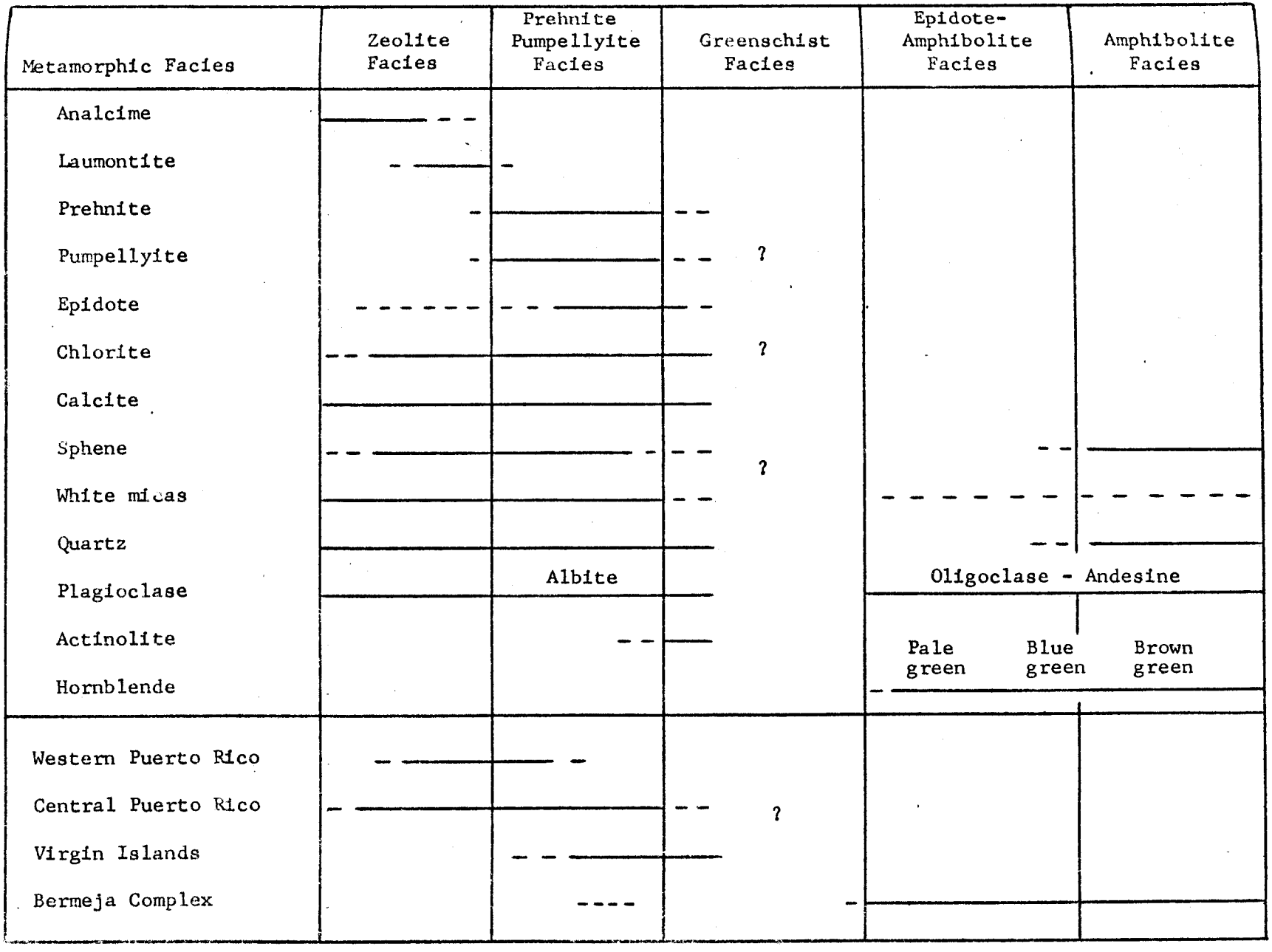

Figure 14. Mineral changes in the basic and intermediate volcanogenetic rocks in Central Puerto Rico (Otalora, 1964; Jolly, 1970a), Western Puerto Rico, and Virgin Islands (Donnelly, 1966; Hekinian, 1971), and the metamorphic rocks in Bermeja complex, southwestern Puerto Rico. Contact metamorphism is excluded in this figure.

age and ended probably in the Early Tertiary. The intensity of regional metamorphism appears to approximately decrease with decreasing age.

In the oldest Bermeja complex (which subsequently will be shown to represent either the rocks of the initial island arc stage or oceanic crust), of pre-Albian age and unconformably overlain by the younger rock sequences, was first subjected to high grade regional metamorphism of the amphibolite and epidote amphibolite facies with the developement of strong and moderate metamorphic textures, and later probably partly to low-grade metamorphism (?). The next younger rock sequences studied are those in the Virgin Islands, which were metamorphosed in the lower greenschist facies and the prehnite-pumpellyite facies. The younger Upper Cretaceous volcanogenic rocks in Central Puerto Rico, were altered during a low-grade metamorphism to the zeolite facies, the prehnite-pumpellyite facies, and probably to an incipient stage of the green-schist facies (?). The late Upper Cretaceous and Early Tertiary volcanogenic rocks in Western Puerto Rico were reconstituted in the zeolite and lower prehnite-pumpellyite facies.

If rocks stratigraphically between the Bermeja complex and the younger volcanic pile, and rocks similar to the Bermeja complex should exist in other parts of the eastern Greater Antilles they are likely hidden at depth under the thick volcanic pile or at least not yet found. Therefore, it is not unusual that there is an apparent gap

in the intensity of metamorphism between the incipient greenschist facies and the epidote amphibolite facies (Figure 14). The range in intensity of metamorphism may be continuous, and the whole metamorphic sequence may be due to the same epoch ranging from a Pre-Albian to Early Tertiary age. Alternatively, the gap in the intensity of metamorphism may separate two completely different types (and times) of metamorphism, as for instance, Miyashiro (1973a) proposed a paired metamorphism in island arcs. Evaluation of either of these possibilities will require more data, but nevertheless, I think that the unexposed rocks beneath the thick volcanic pile of Puerto Rico may be dominated by the more highly metamorphosed types, similar to those of the Bermeja complex, and probably of the greenschist to amphibolite facies.

IV. GEOCHEMISTRY OF THE BERMEJA COMPLEX

A. Analytical Methods

1. Sample Selection

Spilite, amphibolites, serpentinite, and amphibolitized dolerite from the Bermeja complex were chosen for geochemical study because of their uncertain petrogenesis in relation to the significant role they have played in the evolution of the Antilles Island arc. Specimens of the Cajul volcanic rocks and Maguayo porphyry from this complex were not analyzed. Microscopic examination showed that they had been subjected to strong secondary changes or alteration and would not suitably represent the composition of the original rocks.

Thin sections of the specimens examined under the microscope included four spilites, one amphibolitized dolerite from the northern spilite quarry near Mayaguez, twelve schistose amphibolites, four massive metabasaltic dikes in the schistose amphibolite at Las Palmas, and six serpentinites. On the basis of this examination, some samples were rejected for the chemical analysis, because they had veinlets and alteration or otherwise showed weathering effects.

Some spilites contain small prehnite - calcite veinlets of uncertain origin, which can in some cases be sawed away and not included in the samples prepared for the analysis. One spilite was rejected for analysis, however,

because it contained a higher density of veins that were found difficult to remove. Most plagioclase in the schistose amphibolites is slightly to moderately altered to white micas. This might represent some additional amount of alkali from exterior sources and bias the composition relative to the original parent rock. Five samples of schistose amphibolite with only slight plagioclase alteration, that was judged to be tolerable, were chosen for analysis, and seven were rejected. Most samples from massive metabasaltic dikes contain epidote veins. In two samples, the veinlets were sawed away with care. One sample was rejected because of an abundance of veinlets. Most rocks close to the contact zone with serpentinite are affected by metasomatism from the serpentinite body (Tobisch, 1968). In these specimens, prehnite appears in abundance. One massive metabasaltic dike rock was rejected for this reason. Three specimens of Cajul volcanic rocks and five specimens of Maguayo porphyry were also examined. The plagioclase phenocrysts in both rock types were all strongly altered to white micas, chlorite, and calcite. Secondary chlorite, epidote, quartz, calcite, and pumpellyite were also common in the groundmass, and as veinlets and amygdules. Therefore, these rocks were not accepted for chemical analysis. Among the serpentinites from the Las Palmas, AMSOC core hole near Punta Guanajibo (serpentinized diopside harzburgite, type C, 1947 m deep in AMSOC core hole, Mattson, 1964) was selected because it contains the highest amount of relic orthopyroxene, clinopyroxene, and olivine

among the samples examined in this study, and may thus preserve some portion of the original chemical features of the parent peridotite.

Thin section and petrographic data for the analyzed sample are listed in the AppendixA-E.

2. Sample Preparation

The undesired veinlets and the original contaminated rough surfaces of the rock samples were sawed away. Possible contamination caused by contact of the saw on the rocks was reduced to some extent by rubbing together two pieces of sawed slices cut from the same sample to remove the saw marks. This process was done on all sawed surfaces. Absolute freedom from contamination during the operation of the jaw crusher and the roller bar pulverizer cannot be expected. However, a small part of the "clean" rock sample was run through the "cleaned" jaw crusher and the roller bar in order to precontaminate them with the material of the same rock specimen. This portion of the sample was saved as reference. After pulverization, the sample was well shaken in a clean air-filled plastic bag to achieve a uniform distribution of the whole pulverized sample. The sample was split by rolling and quartering on clean sheets of paper. One split was ground in a tungsten carbide grinding container using the Spex Mixermill 8000 for 20 minutes. The powdered samples were used for major element analysis and trace element analysis.

3. Atomic Absorption Spectrometry

The Na_2O content of the analyzed samples was determined by atomic absorption spectrometry. About 5 ml of 48 % hydrofluoric acid was added to a platinum crucible, containing an accurately weighed sample of 0.1 g. It was heated on a hot plate at a rate to slowly evolve white fumes of the acid without boiling or splattering. When the sample was almost dry, a small portion of distilled water was added and the slow evaporation repeated. After this about 2 ml of nitric acid was added. Slow heating and evaporation led to a complete decomposition of the rock sample. Distilled water was then used to pick up and transfer the dissolved sample to a 100 ml volumetric flask. "Washing" the crucible with distilled water insured that all the decomposed sample was in the final solution. It was diluted to volume, using distilled water, and transferred to a polyethylene bottle. This provided a 0.1 % solution of the rock sample in distilled water. Sample solutions of suitable concentration for analyses were prepared by the dilution of 10 ml of the 0.1 % solution to 100 ml with distilled water, using a clean volumetric flask.

Trace analyses for Cr, Co, Ni, Cu, and Sr were done by atomic absorption spectrometry of rock sample solutions prepared similarly to that described above. Some samples were also analyzed by X-ray spectrometry as described in a later section. The instrumental conditions for the analyses

using a Perkin-Elmer 303 Atomic Absorption Spectrometer are shown in Table 2.

Multiple-element lamps were used for most elements, except for Na and Cu, when a single-element lamp was used. An air-acetylene flame was used throughout all analyses. Meter readings or recorder charts or both were made for each element. Standard solutions were prepared from stock solutions to cover the possible concentration ranges of the rock solutions to be analyzed. For Na analyses a calibration curve was constructed from standard solutions. In this method, the percent absorption for the standard solutions, read from the meter was converted to absorbance, which was plotted against established concentration. Then a calibration curve was drawn. The analysis of the unknown was done by obtaining the absorbance in like manner from the sample solution and applying this absorbance to the calibration curve to derive its concentration graphically. For the analysis of Cr, in order to avoid the effects of interference due to Fe, the method of standard additions was used. For the method of standard additions, two aliquots of each sample were taken. To one, 1 ml distilled water was added, to the other 1 ml of a known concentration of the analyte in the expected range. The absorbance for each solution was obtained and plotted against the added concentration incresment. The straight line between these points was then extrapolated through the zero absorbance axis. The intercept on the concentration axis then yields the concentration in the diluted

Table 2. Parameters for Atomic Absorption Spectrometry Analysis (Perkin-Elmer 303).

	Wavelength (Å)	Slit Setting (Å)	Light Source	Flame Type	Meter Expansion*	Standard Solutions (ppm)	Dilution factor for samples	Dilution for Standard Additions**
Na	5980	1.4	Na Hollow cathode Tube (10 mA)	Air-acetylene	1x10	.5,1.0 2.0,3.0	10,000	
Cr	3579	2.0	Co-Cr-Cu-Mn-Ni Hollow Cathode Tube (30 mA)	Air-acetylene	1x5 1x1 (B-2) 1x10 (BCR-1)		100	10mlS+1mlH_2O 10mlS+1ml10ppmCr 5mlS+1mlH_2O 5mlS+1ml12ppmCr 5mlS+5mlH_2O 5mlS+5ml20ppmCr
Co	2407	2.0	Co-Cr-Cu-Mn-Ni Hollow Cathode Tube (30 mA)	Air-acetylene	1x10	.25,.35, .5	100	5mlS+1mlH_2O 5mlS+1ml2ppmCo
Ni	2320	2.0	Co-Cr-Cu-Mn-Ni Hollow Cathode Tube (30 mA)	Air-acetylene	1x10 1x1 (B-2) 1x5 (S.A.)	.5,1.0 2.0 20.0 (B-2)	100	5mlS+1mlH_2O 5mlS+1ml6ppmNi
Cu	3247	7.0	Cu Hollow Cathode Tube (15 mA)	Air-acetylene	1x10 1x5 (S.A.) 1x2 (S.A.)	.1,.2,.5, 1.0;.12, .2,.6	100	5mlS+1mlH_2O 5mlS+1ml3ppmCu
Sr	4607	4.0	Ba-Ca-Sr-Mg Hollow Cathode Tube (20 mA)	Air-acetylene	1x10 1x2 (S.A.) 1x5 (S.A.)	1.2,2.4 5.9	100	5mlS+1mlH_2O 5mlS+1ml11.8ppmSr

* B-2:high Cr and high Ni; BCR-1:standard rock, having low concentration of Cr and Ni; S.A. : method of standard addition.

**See texts for details, "10mlS+1ml10ppmCr" indicates that"to one ml of sample, one ml of standard solution of 10 ppm Cr was added".

sample. Both the methods of the calibration standards and standard additions were used for other trace element analyses in order to compare the methods and to check the precision of the analytical results. The dilution factor for each rock solution was 100, using a 1.0 % solution of the rock sample. The further dilutions used in the method of standard additions are shown in the last column of Table 2.

4. X-ray Spectrometry

X-ray spectrometry was chosen as a second method for some of the trace element analyses. Two grams of each sample was compressed into a briquette, using 0.1 g pure ground boric acid as a binder. The effect of the binder is to reduce slightly the intensity of the X-ray spectrum. However, it makes the specimen more easily handled and stored, and facilitated the analysis under vacuum for some elements. The sample and binder were ground together to insure thorough mixing. The mix was fed evenly into the pellet press. A mixture of boric acid and graphite was used as backing material. A pellet with uniform and smooth analyzing surface and uniform sample thickness was produced. It was coated with clear lacquer on the margin to retard chipping and flaking. Duplicate pellets were made for each sample. Exactly the same procedure was followed to prepare pellets of standard rocks to achieve similar preparation conditions for both samples and standards.

Analyses were made using a Siemens SRS-1 X-ray

Spectrometer for Cr, Mn, Ni, Cu, and Zn. The instrumental conditions for the analysis of the various trace elements are summarized in Table 3A. K series X-ray spectral lines were used for these elements. The analytical line chosen for each element was that which had highest relative intensity and least interference from adjacent spectral lines. A tungsten target X-ray tube was used, with excitation as shown in Table 3A. LiF (110) analysing crystal was used for the analysis of Cr and Mn and LiF (100) was used for the other elements. Fine collimation (0.15^{o}) was used throughout the whole analysis to achieve good resolution. For the longer wavelength lines, CrKα and MnKα , a vacuum path was used to increase intensity. Secondary X-ray intensities were measured with a gas flow proportional counter using an argon-methane mixture (P10 gas). Shorter wavelengths (NiKα , CuKα , and ZnKα) were measured with a sintillation counter in an air path. The use of a pulse height selector becomes increasingly important with trace analysis in order to improve the peak to background ratio by rejecting harmonics and spurious pulses as well as possible higher order interference spectra. It is also important to remove pulses due to scattering and fluorescence from the analyzing crystal. The lower or base level of the pulse height selector was set within the range 7 to 7.5 volts. With the use of the scintillation counter, the channel widths were set at 8 volts. Because there may be slight drift in pulse voltage with counting rate with a flow proportional counter, a wider window, 10

Table 3A . Instrumental Conditions for the Trace Elements Analysis by the use of Siemens SRS-1 X-Ray Spectrometer.

	Analyte Line	X-Ray Tube			Analyzing Crystal	Collimator (o)	Spectrometer Path	Detector	Pulse-Height Selector (volts)	
		Target	Voltage (Kv)	Ampere (mA)					Base	Window
Cr	KA	W	48	34	(110)LiF	.15	Vacuum	Proportional	7	10
Mn	KA	W	48	34	(110)LiF	.15	Vacuum	Proportional	7	10
Ni	KA	W	48	34	(100)LiF	.15	Air	Scintillation	7.5	8
Cu	KA	W	48	34	(100)LiF	.15	Air	Scintillation	7.5	8
Zn	KA	W	48	34	(100)LiF	.15	Air	Scintillation	7.5	8

Table 3B. Stamdard Rocks used in the Quantitative Analysis of the Trace Elements by the use of X-Ray Spectrometry. The unit is ppm.

	BCR-1	CAAS	DTS-1	Knippa Basalt	PCC-1	T-1	V25-1-T2	W-1	Rock Base Addition Std. (A)	Rock Base Addition Std. (B)	Lower Limit of Detection
Cr	16	58			2640	24		120	+17.2	+34.1	20
Mn	1471	3096		1238	929	851	1316	1316	+49.6	+98.6	60
Ni		37	2435		2515	13		13			15
Cu	19	24	7		11	47		110			3
Zn	120	200	47		44	225		82			30

volts, was used. For the analysis of these elements the scaler was used. A fixed time interval of 6 to 12 seconds for accumulating counts was used for the analyses.

A background correction was applied to the analysis of each element. Positions of the background measurements were normally determined by examining X-ray 2θ scans of the peaks and vicinity. Background measurements on either side of the peak position were averaged to obtain the background at the peak position.

For the determinations of the trace elements by X-ray spectrometry a linear calibration method modified by mass absorption correction was used. The standard rocks used and the published recommended values for their trace element contents are shown in Table 3B. These standard rocks were chosen to provide a concentration range for the analyte similar to that of the samples to be analyzed. Two standards were prepared from a leached rock base by adding known amounts of the analyte to extend the range of the standard curve. A simple linear relationship between fluorescent intensity and concentration is not valid unless the mass-absorption coefficients for standards and samples are constant. The mass-absorption coefficient, which is a function of the bulk composition of a rock, is different for each selected standard rock and each sample, because of the gross variation in composition. For satisfactory analyses the application of an absorption correction as a function of bulk composition is necessary. Because the major components of the samples (see

"Geochemistry of Major Elements") and standards were known, the total mass-absorption coefficients for the selected standard rocks and samples at wavelengths of 1.5 Å and 2.0 Å were calculated from their major element compositions, using the values of mass-absorption coefficients given in Bertin (1969). These are shown in Table 4. For the measurements of NiKα , CuKα, and ZnKα, the mass-absorption coefficients at 1.5 Å were used for absorption correction, while for the measurements of CrKα and MnKα, the mass-absorption coefficients at the wavelength 2.0 Å were used. The count-rate corrected for background, C, was calculated for each standard rock and sample. The values, given by the products of net count-rate times mass-absorption coefficients, C x μ, were plotted against the known concentration for the standard rocks to establish the calibration curve. Hence, we were able to derve the concentration for the samples graphically.

For trace analysis, the count rate at the peak position, Cp, and of the background, Cb, differ only slightly, thus the counting time is generally equal for the line and background. The statistical lower limit of detection, i.e., peak minus background (3σ confidence), is then = 6 / m (Cb / T)$^{1/2}$, where T is the total measureing time and m is the number of counts per second obtained per unit of concentration for the element in the sample. This value (in terms of ppm) for the lower limit of detection for Cr, Mn, Ni, Cu, and Zn was calculated under the different instrumental conditions used and is shown in the last column in Table 3.

Table 4 . Calculated X-Ray Total Mass-Absorption Coefficients for the Standard Rocks and the Samples. μ (2.0Å) is used for the analysis of Cr (CrKA=2.291 Å) and Mn (MnKA=2.103 Å). μ (1.5 Å) is used for the analysis of Ni (NiKA=1.659 Å), Cu (CuKA=1.542 Å), and Zn (ZnKA=1.437 Å).

		Wavelength, Å	
		1.5	2.0
Standard Rocks	BCR-1	64.51	84.13
	CAAS	56.56	88.27
	DTS-1	43.49	57.80
	Knippa Basalt	60.66	86.02
	PCC-1	42.45	57.35
	T-1	46.07	76.54
	V25-1-T2	59.66	85.25
	W-1	61.14	86.15
Schistose Amphibolite	7917-85	61.95	84.10
	Ba-8a-1	60.99	79.50
	7917-66	66.36	86.21
	7917-45	65.93	85.15
	Ba-8a-4	67.26	80.91
Massive Metabasaltic Dike	Ba-10	57.39	83.32
	Ba-8b-2	57.43	83.39
Spilite	Ba-1b	51.26	76.43
	Ba-6	53.09	79.77
	Ba-3	55.04	77.20
Amphibolitized dolerite	Ba-7a	76.54	85.02
Serpentinite	B-2	39.99	54.17

B. Experimental Results

The mean value, $\bar{X}$, and the coefficient of variation, C.V. (%), were calculated for the various analyses in which duplicate determinations were made for each sample, and an additional determination was made in the case of duplicate samples. The following equations were used:

$$\bar{X} = (X_{n1} + X_{n2}) / 2$$

$$D_n^2 = ((X_{n1} - X_{n2}) / \bar{X}_n)^2$$

$$C.V.(\%) = ((\text{sum of } D_n^2) / 2 n)^{1/2} \times 100$$

where X_{n1} and X_{n2} are the duplicate measurements for one sample, n is the number of the sample, $\bar{X}_n$ is the mean, and C.V. is the coefficient of variation of the analyses. When an analysis of one element was made by two methods, the gross coefficient of variation was calculated in a similar way by considering the two averages or values obtained by the two methods, respectively, as duplicate measurements. The precision of the analytical techniques for the reported elements, calculated from the results shown in Table 8A-E and 9A-E by these equations is shown in Table 5.

1. Atomic Absorption Spectrometry

For analysis of Na, five amphibolite sample solutions were prepared without treating with nitric acid (see experimental methods). The results were apparently too low, probably because true solutions were not obtained. Next, one

Table 5. Precision of the analytical techniques for the reported elements, calculated from the results shown in Tables 8 A-E and 9 A-E by the equations shown in page .

	Analysis by Atomic Absorption Spectrometry		Analysis by X-ray Spectrometry		
	Coef. of variation by method of calibration via standard	Coef. of variation by methods of calibration via standard and standard additions	Coef. of variation determined on Pellet A	Coef. of variation determined on Pellet B	Coef. of variation determined on Pellets A and B
Na	3.3%				
Cr		11.9%	8.8%	6.4%	5.1%
Mn			4.1%	2.7%	3.7%
Co	6.5%	7.5%			
Ni	9.9%	8.1%			4.7%
Cu	8.9%	13.0%			16.4%
Zn					6.5%
Sr	11.7%	13.2%			

analyzed abyssal tholeiite was used as a standard and two samples of amphibolite were completely decomposed using the procedure as described on page 87. The results obtained on these three are shown in column three of Table 6. Ten rock samples were subsequently brought into solutions in the same manner. The results obtained on these are shown in column four of Table 6. Each value reported in these two columns are the mean of 1 to 3 replicate determinations. The next two columns show the normalized Na_2O % recalculated using a value for the standard rock (V25-1-T2) equal to the recommended value of 2.87. The suggested values of Na_2O% determined by atomic absorption are listed in the last column. The second column shows the Na_2O % reported for bulk rock analyses, which is systematically higher than the values determined here by atomic absorption, except for sample Ba-1b (spilite). The coefficient of variation, calculated from the duplicate determinations for samples 7717-85 and 7917-66, is 3.3 %. These analytical results for Na_2O content will be used in the discussion of the major element geochemistry.

Results of trace element analyses of two standard rocks, BCR-1 and V25-1-T2, analyzed at the same time as the twelve rock samples by atomic absorption spectrometry are shown in Table 7. Two analysis techniques were used, that of establishing a calibration curve from standard solutions, and the method of standard additions. Recommended values for BCR-1 are also given in this table for comparison.

Table 6. Quantitative Determination of Na_2O by Atomic Absorption Spectrometry.*

	Sample No.	%Na_2O from bulk Rock Analysis	%Na_2O by A.A. run #1	%Na_2O by A.A. run #2	Normalized %Na_2O** run #1	Normalized %Na_2O** run #2	Suggested Value for %Na_2O (Mean)
Schistose Amphibolite	1. 7717-85	3.3	2.96	2.97	3.2	3.0	3.1
	2. Ba-8a-1	3.3		2.97		3.0	3.0
	3. 7917-66	3.0	2.69	2.83	2.9	2.9	2.9
	4. 7917-45	2.9		2.63		2.7	2.7
	5. Ba-8a-4	3.3		2.97		3.0	3.0
Massive Metabasaltic Dike	6. Ba-10	3.2		2.97		3.0	3.0
	7. Ba-8b-2	3.4		2.9		2.9	2.9
Spilite	8. Ba-1b	5.5		5.53		5.6	5.6
	9. Ba-6	4.6		3.91		4.0	4.0
	10. Ba-3	5.2		4.04		4.1	4.1
Standard Rock	V25-1-T2**	2.87	2.69	2.83	2.87	2.87	

* Runs #1 and 2 were done on May 11 and May 14 of 1973, respectively.

* * V25-1-T2: Abyssal tholeiite, analyzed by F. Shido, used as standard.

* ** The %Na_2O determined by atomic absorption is recalculated so as to have the %Na_2O value for V25-1-T2 equal to the recommended value of 2.87.

Blanks mean no determination.

Table 7 . Atomic absorption trace element analyses of standard rocks BCR-1 and V25-1-T2, run during analyses of the rocks from Bermeja Complex and some recommended values (see Table for the analytical precisions).*

	BCR-1									
	Analysis by the method of: Calibration via standards			Standard additions			Mean (by two methods)	Recommended (Flanagan)**		Recommended (Abbey)***
	run #1	run #2	Mean	run #1	run #2	Mean		Mean	Std. Dev.	
Cr				14	18	16.0		14.7	4.2	16
Co	36	35	35.5		36		35.8	31.4	3.4	50
Ni	22	25	23.5		18		20.8	13.7	7.3	13
Cu	16	15	15.5		14		15.3	25.5	7.8	19
Sr	340				336		338.0	361.7	55.2	330
	V25-1-T2									
Cr				352						
Co	40	38	39.0							
Ni	180	175	177.5							
Cu	70	65	67.5							
Sr	90									

* Runs #1 and 2 were done in August and October of 1973, respectively.
** Flanagan, 1967, 18 determinations for each element.
*** Abbey, 1972.
All results are in ppm. Blanks mean no determination.

The precision of the analyses is shown in Table 5. My result for Cr is equal to the recommended value of 16.0 by Abbey (1972). My Co value is higher than the recommended value of 31.4 ± 3.4 ppm by Flanagan (1967), but is lower than the value of 50 ppm given by Abbey. My analyses of Ni give a average of 20.7 ppm, which is higher than both of the two recommended values which are close to 13 ppm. However, Flanagan's report gives a standard deviation of 7.3 ppm for a mean Ni content of 13.7 ppm. The value for Cu obtained in my analysis is lower compared with the two recommended values, while Sr is in good aggreement. There are no recommended values for these elements in sample V25-1-T2.

For the analyses, the values given for the method of calibration using standards are the mean of 1 to 3 replicate determinations. The results of the analyses for Cr, Co, Ni, Cu, and Sr in the twelve samples are shown in Tables 8A-E. Included are results obtained at different times and by different methods, The mean and coefficient of variation are reported to show the precision of the analyses for each sample and element.

Cr (Table 8A): Analyses of Cr were done by standard additions. The mean values for the samples range from 109.0 to 307.5 ppm, except for a high value of 2000 ppm for sample B-2 (serpentinite). The coefficient of variation for the analyses of Cr is 11.9 %.

Co (Table 8B): Co was analyzed by using standards for calibration. One sample of each rocm type, Nos. 2, 7, 9,

Table 8A . Quantitative analysis of Cr by atomic absorption using the method of standard additions*.

	Sample number	FeO*/MgO	run #1	run #2	Mean
Schistose Amphibolite	1. 7717-85	1.33	285	330	307.5
	2. Ba-8a-1	1.59	177	216	196.5
	3. 7917-66	1.70	198	192	195.0
	4. 7917-45	1.75	133	156	144.5
	5. Ba-8a-4	1.78	131	90	110.5
Massive Metabasaltic Dike	6. Ba-10	1.24	198	198	198.0
	7. Ba-8b-2	1.39	176	168	172.0
Spilite	8. Ba-1b	1.07	187	174	180.5
	9. Ba-6	1.12	154	204	179.0
	10. Ba-3	1.47	110	108	109.0
Amphibolitized dolerite	11. Ba-7a	1.10	286	288	287.0
Serpentinite	12. B-2		2000		2000.0
Coef. of variation					11.9 %

* Runs #1 and 2 were done in August and October of 1973 respectively.
All results are in ppm.
Blanks mean no determination.

Table 8B . Quantitative analysis of Co by atomic absorption spectrometry using the methods of calibration standards and standard additions.

	Sample number	FeO*/MgO	Analysis by the methods of: Calibration via standards run #1	run #2	Mean	Standard additions	Mean (by two methods)
Schistose Amphibolite	1. 7717-85	1.33	33	37	35.0		
	2. Ba-8a-1	1.59	27	28	27.5	27	27.3
	3. 7917-66	1.70	30	26	28.0		
	4. 7917-45	1.75	28	26	27.0		
	5. Ba-8a-4	1.78	30	25	27.5		
Massive Metabasaltic Dike	6. Ba-10	1.24	37	38	37.5		
	7. Ba-8a-2	1.39	25	29	27.0	24	25.5
Spilite	8. Ba-1b	1.07	32	33	32.5		
	9. Ba-6	1.12	33	31	32.0	33	32.5
	10. Ba-3	1.47	41	42	41.5		
Amphibolitized dolerite	11. Ba-7a	1.10	35	36	35.5	35	35.3
Serpentinite	12. B-2		52	53	52.5		
Coef. of variation for method of calibration via standards							6.5 %
Coef. of variation for both methods							7.5 %

Table 8C . Quantitative analysis of Ni by atomic absorption spectrometry using the methods of calibration standards and standard additions*.

	Sample number	FeO*/MgO	Analysis by the methods of: Calibration via standards run #1	run #2	Mean	Standard additions	Mean (by two methods)
Schistose Amphibolite	1. 7717-85	1.33	130	115	122.5	108	115.3
	2. Ba-8a-1	1.59	100	90	95.0	96	95.5
	3. 7917-66	1.70	100	85	92.5	78	85.3
	4. 7917-45	1.75	75	80	77.5	84	80.8
	5. Ba-8a-4	1.78	70	60	65.0	60	62.5
Massive Metabasaltic Dike	6. Ba-10	1.24	100	95	97.5	96	96.8
	7. Ba-8a-2	1.39	85	65	75.0	66	70.5
Spilite	8. Ba-1b	1.07	95	85	90.0		
	9. Ba-6	1.12	100	80	90.0	96	93.0
	10. Ba-3	1.47	95	85	90.0	72	81.0
Amphibolitized dolerite	11. Ba-7a	1.10	110	100	105.0	102	103.5
Serpentinite	12. B-2		2050	2000	2025.0		
Coef. of variation for the method of calibration via standards							9.9 %
Coef. of variation for both methods							8.1 %

Table 8D. Quantitative analysis of Cu by atomic absorption spectrometry using the methods of calibration standards and standard additions.

	Sample number	FeO*/MgO	Analysis by the methods of: Calibration via standards run #1	run #2	Mean	Standard additions	Mean (by two methods)
Schistose Amphibolite	1. 7717-85	1.33	63	67	65.0		
	2. Ba-8a-1	1.59	25	26	25.5		
	3. 7917-66	1.70	24	26	25.0		
	4. 7917-45	1.75	50	46	48.0	65	56.5
	5. Ba-8a-4	1.78	56	59	57.5		
Massive Metabasaltic Dike	6. Ba-10	1.24	85	81	83.0		
	7. Ba-8a-2	1.39	75	72	73.5	78	75.8
Spilite	8. Ba-1b	1.07	47	48	47.5		
	9. Ba-6	1.12	71	72	71.5		
	10. Ba-3	1.47	59	60	59.5		
Amphibolitized dolerite	11. Ba-7a	1.10	63	58	60.5	66	63.3
Serpentinite	12. B-2		20	30	25.0		
Coef. of variation for the method of calibration via standards							8.9 %
Coef. of variation for both methods							13.0 %

Table 8E. Quantitative analysis of Sr by atomic absorption spectrometry using the methods of calibration standards and standard additions.

	Sample number	FeO*/MgO	Analysis by the methods of: Calibration via standards run #1	run #2	Mean	Standard additions	Mean (by two methods)
Schistose Amphibolite	1. 7717-85	1.33	140	134	137.0		
	2. Ba-8a-1	1.59	100	98	99.0		
	3. 7917-66	1.70	110	84	97.0	72	84.5
	4. 7917-45	1.75	60	56	58.0		
	5. Ba-8a-4	1.78	90	92	91.0		
Massive Metabasaltic Dike	6. Ba-10	1.24	160	162	161.0	150	155.5
	7. Ba-8a-2	1.39	120	90	105.0		
Spilite	8. Ba-1b	1.07	80	98	89.0		
	9. Ba-6	1.12	100	126	113.0		
	10. Ba-3	1.47	80	94	87.0		
Amphibolitized dolerite	11. Ba-7a	1.10	190	218	204.0	228	216.0
Serpentinite	12. B-2		n.d.				
Coef. of variation for the method of calibration via standards							11.7 %
Coef. of variation for both methods							13.2 %

and 11, was analyzed by the method of standard addition in October. Results obtained at two different times and two different methods are very close for each sample. The largest mean value is 52.5 ppm for the serpentinite. The rest of the samples are less than 42 ppm. Coefficients of variation for the analyses by the method of calibration via standards is 6.5%. The coefficient of variation, calculated from the four samples analyzed by both methods is 7.5 %.

Ni (Table 8C): Most samples were analyzed for Ni by both methods at two different times, except Nos. 8 and 12 were not analyzed by the method of standard additions. The mean values, based on three determinations (excepting Nos. 8 and 12, two determinations), are within 62.5 to 115.3 for the basaltic rocks and 2025 ppm for the ultramafic rock (No. 12). The analyses using standards for calibration have a coefficient of variation of 9.9 %. For the analyses by both methods, the coefficient of variation is 8.1 %.

Cu (Table 8D): All samples were analyzed using standards for calibration, and in addition three samples of different rock types were also analyzed by the method of standard additions, yielding close agreement between values determined at two different times. However, the three determinations made by the method of standard additions give values which are systematically higher than those obtained by the other method. This bias might be due to preparation errors in making solutions. The means for the samples are in the range of 25.0 to 83.0 ppm. The coefficients of

variation using standards for calibration and for combing both methods are 8,9 % and 13.0 %, respectively.

Sr (Table 8E): The Sr analyses using standards that were made in October for the amphibolite and dike rocks tend to be lower values than those done in August by the same method. This systematical relationship is reversed for the spilite and amphibolitized dolerite. The time interval between the two series of analyses may have had different effects on solutions of these two groups of rocks. The determinations for one amphibolite and one dike by the method of standard addition also give lower values than those obtained on the same samples at two different times by the first method. This relationship is also reversed for the amphibolitized dolerite. The range of the means for the samples is 58 to 204 ppm, except for serpentinite, in which Sr was not detected. The coefficient of variation for the analyses using standards for calibration is 11.7 %. Three samples analyzed by both methods yield an overal coefficient of variation of 13.2 %.

2. X-Ray Spectrometry

Results of the analyses of Cr, Mn, Ni, Cu, and Zn by X-ray spectrometry are shown in Tables 9A-E. Analytical determinations were made on duplicate pellets prepared from each sample. Two determinations were made from most pellets for the analyses of Cr and Mn, while only single determinations were made of each pellet for the remaining elements. The

Table 9A. Quantitative X-ray spectrometric analysis of Cr by the method of linear calibration modified by absorption correction.

	Sample number	FeO*/MgO	Pellet A (1)	Pellet A (2)	Pellet A Mean	Pellet B (1)	Pellet B (2)	Pellet B Mean	Mean
Schistose Amphibolite	1. 7717-85	1.33	320	310	315.0	300	320	310.0	312.5
	2. Ba-8a-1	1.59	200			190	180	185.0	192.5
	3. 7917-66	1.70	220	200	210.0	210	220	215.0	212.5
	4. 7917-45	1.75	180	160	170.0	150			160.0
	5. Ba-8a-4	1.78	130	100	115.0	120			117.5
Massive Metabasaltic Dike	6. Ba-10	1.24	200	200	200.0	210	190	200.0	200.0
	7. Ba-8b-2	1.39	180			170			175.0
Spilite	8. Ba-1b	1.07	140	120	130.0	150	140	145.0	137.5
	9. Ba-6	1.12	180	170	175.0	190	160	175.0	175.0
	10. Ba-3	1.47	120	100	110.0	100	90	95.0	102.5
Amphibolitized dolerite	11. Ba-7a	1.10	230	230	230.0	240	220	230.0	230.0
Serpentinite	12. B-2		2100	2100	2100.0	2200	2100	2150.0	2125.0
Coef. of variation					8.8 %			6.4 %	5.1 %

Table 9B. Quantitative X-ray spectrometric analysis of Mn by the method of linear calibration modified by absorption correction.

	Sample number	FeO*/MgO	Pellet A (1)	Pellet A (2)	Pellet A Mean	Pellet B (1)	Pellet B (2)	Pellet B Mean	Mean
Schistose Amphibolite	1. 7717-85	1.33	1520	1480	1500	1500	1480	1490	1495
	2. Ba-8a-1	1.59	1640	1600	1620	1600	1580	1590	1605
	3. 7917-66	1.70	1840	1800	1820	1800	1800	1800	1810
	4. 7917-45	1.75	1640	1700	1670	1660	1640	1650	1660
	5. Ba-8a-4	1.78	1820	1780	1800	1800	1840	1820	1810
Massive Metabasaltic Dike	6. Ba-10	1.24	1400	1360	1380	1340	1320	1330	1355
	7. Ba-8b-2	1.39	1380	1340	1360	1320	1340	1330	1345
Spilite	8. Ba-1b	1.07	1280	1540	1410	1300	1260	1280	1345
	9. Ba-6	1.12	1320	1300	1310	1320	1300	1310	1310
	10. Ba-3	1.47	1320	1300	1310	1320	1290	1215	1308
Amphibolitized dolerite	11. Ba-7a	1.10	1300	1260	1280	1280	1260	1270	1275
Serpentinite	12. B-2		980	960	970	960	960	960	965
Coef. of variation					4.0 %			2.7 %	3.7 %

Table 9C. Quantitative X-ray spectrometric analysis of Ni by the method of linear calibration modified by absorption correction.

	Sample number	FeO*/MgO	Pellet A	Pellet B	Mean
Schistose Amphibolite	1. 7717-85	1.33	120	110	115.0
	2. Ba-8a-1	1.59	90	95	92.5
	3. 7917-66	1.70	90	95	92.5
	4. 7917-45	1.75	90	85	87.5
	5. Ba-8a-4	1.78	70	65	67.5
Massive Metabasaltic Dike	6. Ba-10	1.24	90	95	92.5
	7. Ba-8b-2	1.39	80	75	77.5
Spilite	8. Ba-1b	1.07	90	80	85.0
	9. Ba-6	1.12	90	85	87.5
	10. Ba-3	1.47	75	70	72.5
Amphibolitized dolerite	11. Ba-7a	1.10	100	90	95.0
Serpentinite	12. B-2		2300	2200	2250.0
Coef. of variation					4.7 %

Table 9D. Quantitative X-ray spectrometric analysis of Cu by the method of linear calibration modified by absorption correction.

	Sample number	FeO*/MgO	Pellet A	Pellet B	Mean
Schistose Amphibolite	1. 7717-85	1.33	64	58	61.0
	2. Ba-8a-1	1.59	30	32	31.0
	3. 7917-66	1.70	40	35	37.5
	4. 7917-45	1.75	60	62	61.0
	5. Ba-8a-4	1.78	76	53	64.5
Massive Metabasaltic Dike	6. Ba-10	1.24	63	65	64.0
	7. Ba-8b-2	1.39	64	60	62.0
Spilite	8. Ba-1b	1.07	33	19	26.0
	9. Ba-6	1.12	45	38	41.5
	10. Ba-3	1.47	52	40	46.0
Amphibolitized dolerite	11. Ba-7a	1.10	57	46	51.5
Serpentinite	12. B-2		n.d.	n.d.	
Coef. of variation					16.4 %

Table 9E. Quantitative X-ray spectrometric analysis of Zn by the method of linear calibration modified by absorption correction.

	Sample number	FeO*/MgO	Pellet	Pellet B	Mean
Schistose Amphibolite	1. 7717-85	1.33	110	98	104.0
	2. Ba-8a-1	1.59	136	118	127.0
	3. 7917-66	1.70	122	128	125.0
	4. 7917-45	1.75	116	120	118.0
	5. Ba-8a-4	1.78	144	142	143.0
Massive Metabasaltic Dike	6. Ba-10	1.24	76	78	77.0
	7. Ba-8b-2	1.39	76	84	80.0
Spilite	8. Ba-1b	1.07	64	60	62.0
	9. Ba-6	1.12	68	64	66.0
	10. Ba-3	1.47	80	74	77.0
Amphibolitized dolerite	11. Ba-7a	1.10	66	56	61.0
Serpentinite	12. B-2		40	36	38.0
Coef. of variation					6.5 %

mean and coefficients of variation were calculated from a total of 4 determinations for Cr and Mn for most samples and from 2 determination for Ni, Cu, and Zn in all samples.

Cr (Table 9A): The mean values of Cr content in the Bermeja rock samples are in the range 102.5 to 312.5 ppm. The serpentinite, sample B-2, has a high Cr concentration of 2125 ppm. The coefficient of variation for the analyses is 5.1 %.

Mn (Table 9B): For the analysis of Mn, the coefficient of variation is 3.7 %. The analyses fall within the range of 1275 to 1810 ppm, except for the serpentinite (B-2) which has a low value of 965 ppm.

Ni (Table 9C): Except for the high content of serpentinite (B-2) with 2250 ppm, the mean values for Ni concentration in the rocks analyzed are in the range 72.5 to 115.0 ppm. The coefficient of variation is 4.7 %.

Cu (Table 9D): The amphibolites and dike rocks have mean Cu content within the range 31.0 to 64.5 ppm. Cu was not detected in the serpentinite sample. The remaining rock types, spilite and amphibolitized dolerite, have mean Cu contents varying from 26.0 to 51.5 ppm. The coefficient of variation for the Cu analyses is 16.4 %.

Zn (Table 9E): The mean values of Zn content in the amphibolite samples are higher (range 104 to 143 ppm), than the rest of the rocks, in which the Zn content is less than 80 ppm. The coefficient of variation for the Zn analyses is 6.5 %.

3. Discussion

Precision of the analyses of Cr both atomic absorption spectrometry and X-ray spectrometry is reltatively good. The results of analyses for amphibolite, dike rocks, and serpentinite are in good agreement between the two methods. For spilite, however, the results by X-ray spectrometry are consistently lower than those by atomic absorption. Although corrections for matrix effects based on the mass-absorption of the bulk samples were applied to the X-ray data (page 95), other factors can affect the accuracy of the results. The effects of mineralogy, particle size distribution, and the physical packing of the sample, cannot be neglected, if there are differences in these factors between samples. For instance, chlorite is a dominant mineral in spilite, but is negligible in the other rocks analyzed. The presence of chlorite, which is a sheet slicate, commonly causes some problem in grinding, and tends to produce varying size distributions compared to the rocks without sheet silicate present in them, although all samples were ground in the same manner. The physical packing of the particles of the samples would also be affected by the presence of chlorite, even if the sample pellets are prepared by the same technique. Thus, it is probable that the theoretical correction for mass-absorption is not the only correction necessary for the X-ray analyses.

The precision for the analysis of Co by atomic absorption and Mn by X-ray fluorescence is good. However, in

the preparation of the sample, use of the Spex Tungsten Carbide Mill may introduce some Co contamination, which is a factor at low concentration levels. We are not certain to what extent Co contamination might occur in our samples (Thompson and Bankston, 1970). The precision for the analysis of Ni by atomic absorption and X-ray is good to fair for individual methods, but for the spilites a discrepancy between the results of the two methods occurred, similar to the case of Cr analysis. This has been discussed above. In the analysis of Cu, the precision by the X-ray method is poor due to the target contamination and short counting time, while the analysis of Cu by atomic absorption yields good precision. However, in spilite of this the greatest discrepancy between the X-ray and atomic absorption results again occurs for the spilite samples. The precision for the analysis of Sr by atomic absorption is fair. The analysis of Zn by X-ray spectrometry generally has good precision.

C. Geochemistry of the Major Elements

The discussion in this section is based on the new major element analyses of the schistose amphibolite, massive metabasaltic dike, spilite, amphibolitized dolerite, and serpentinite from the Bermeja complex. The Cajul volcanic rocks and Maguayo porphyry from the complex are excluded from our discussion, inasmuch as they were subjected to strong secondary changes. The existing analytical data of this complex and other related rocks reported in the literature

were used to supplement my results, because these new analyses were of a limited FeO*/MgO range. Here, FeO* means total iron expressed as FeO, i.e., Σ (FeO + 0.9 Fe_2O_3). CIPW norms were calculated from the analyzed data, and diagrams showing the variations in the major elements were constructed, with their significant features emaphasized. All of the analyses in the tables have a Fe_2O_3 content higher than 1.5 %, probably owing to metamorphism, and possibly weathering before and/or after metamorphism. In the study of slightly weathered abyssal rocks, Miyashiro et al., (1970) and Kay et al., (1970) suggest that the partial reduction of total Fe_2O_3 to give Fe_2O_3 = 1.5 % as a common degree of oxidation may serve to approximate the composition of the original fresh rocks. Therefore, the CIPW norms were also calculated from the modified data after assigning a value of 1.5 % for Fe_2O_3 to them.

1. Schistose amphibolite

Five new chemical analyses for the major elements of the schistose amphibolite are presented in Table 10A, as well as seven analyses from the literature (Mattson, 1960; Renz and Vorspyck, 1962; Tobisch, 1968; Donnelly et al., 1971). These are listed in order of increasing FeO*/MgO ratio. The sampling locality, field observations, and petrography for the newly analyzed samples are given in Appendix A. The new major element data are in good agreement with most of the existing analyses in the literature. Some variations exist

Table 10A. Major Elements Analyses of the Schistose Amphibolite from Las Palmas.

	1.	2.	3.	4.	5.	6.	7.	8.	9.	10.	11.	12.
Specimen no.	PR-336	T-3	7717-85	TD-1691	Ba-8a-1	7917-66	T-2	7917-45	Ba-8a-4	TD-1707	T-1	R.V.-1
FeO*/MgO	0.92	1.16	1.33	1.38	1.59	1.7	1.73	1.75	1.78	2.06	2.2	2.89
SiO_2	46.36	49.71	49.0	50.2	53.9	48.2	48.31	48.7	47.6	48.9	51.58	48.7
TiO_2	1.34	1.3	1.1	1.2	1.3	1.75	1.2	1.7	1.6	2.2	2.3	2.6
Al_2O_3	14.5	14.13	14.3	13.0	13.2	14.0	14.43	14.1	14.4	12.4	12.72	13.4
Fe_2O_3	2.09	3.41	4.0	9.9	3.9	3.8	4.71	4.25	5.0	14.8	4.51	16.2
FeO	8.17	7.52	7.4		7.95	9.15	8.62	8.95	9.55		9.62	
MnO	0.21	0.2	0.19		0.22	0.23	0.22	0.22	0.25		0.31	
MgO	10.94	9.12	8.3	7.2	7.2	7.4	7.42	7.3	7.9	7.2	6.21	5.6
CaO	10.4	11.03	10.6	12.3	7.8	10.8	10.12	10.1	8.6	12.3	8.21	8.6
Na_2O	1.95	2.61	3.1	2.8	3.0	2.9	2.41	2.7	2.8	2.8	2.6	2.4
K_2O	0.34	0.31	0.3	0.2	0.1	0.35	0.35	0.15	0.1	0.2	0.14	tr.
H_2O^+	3.26	0.09	1.3		1.1	1.0	1.5	1.2	1.6		1.2	
P_2O_5	0.1	0.29	0.11		0.13	0.16	0.26	0.17	0.13		0.26	
Total	99.66	99.72	99.70		99.80	99.74	99.55	99.54	99.57		99.66	

FeO* means total iron as FeO, i.e., FeO + 0.9 Fe_2O_3.

Nos. 3, 5, 6, 8, and 9: This study (see Appendix A).

No. 1: In road cut on route 301 between Sierra Melones and Sierra Bermeja, on south edge of Valle de Lajas (Mattson, 1960).

No. 2: Near the north contact with serpentinite at Las Palmas, containing hornblende, sodic andesine with accessary sphene, zircon, and apatite. Veinlet bearing epidote crosscutss foliation. (Tobisch, 1968)

No. 4: At Las Palmas (Donnelly, et al., 1971).

No. 7: In the road cut in the west part of the amphibolite body at Las Palmas, containing hornblende sodic andesine and quartz with accessary sphene, zircon, apatite and opaque mineral (Tobisch, 1968).

No. 10: At Las Palmas (Donnelly et al., 1971).

No. 11: In the stream cut at Las Palmas, containing hornblende sodic andesine and quartz with accessary opaque mineral, sphene, apatite, and zircon (Tobisch, 1968).

No. 12: Renz and Verspyck (1962).

Table 10B. . Original CIPW norms of the schistose amphibolite from Las Palmas*.

		1.	2.	3.	5.	6.	7.	8.	9.	11.
Specimen no.		PR-336	T-3	7717-85	Ba-8a-1	7917-66	T-2	7917-45	Ba-8a-4	T-1
Q					7.97		0.75	0.57		8.47
or		2.01	1.83	1.77	0.59	2.07	2.07	0.89	0.59	0.83
ab		16.5	22.09	26.23	25.39	24.54	20.39	22.85	23.69	22.0
an		29.81	25.93	24.22	22.26	24.15	27.52	25.91	26.43	22.63
di	wo	8.82	11.23	11.55	6.51	11.85	8.76	9.64	6.42	6.85
	en	5.78	7.42	7.53	3.99	7.0	5.31	5.78	3.87	3.88
	fs	2.43	3.01	3.21	2.15	4.26	2.98	3.35	2.21	2.69
hy	en	8.19	11.58	5.57	13.94	5.25	13.17	12.4	14.18	11.59
	fs	3.44	4.7	2.38	7.49	3.19	7.39	7.18	8.09	8.03
ol	fo	9.31	2.61	5.30		4.32			1.14	
	fa	4.31	1.16	2.49		2.89			0.71	
ap		0.23	0.67	0.25	0.3	0.37	0.6	0.39	0.3	0.6
il		2.55	2.47	2.09	2.47	3.32	2.28	3.23	3.04	4.37
mt		3.03	4.94	5.8	5.65	5.51	6.83	6.16	7.25	6.54

* Original CIPW norms was not calculated for sample Nos. 4, 10, 12, because total iron was determined as FeO.

Table 10C. CIPW norms (Fe_2O_3 = 1.5 %) of the schistose amphibolite from Las Palmas.

		1.	2.	3.	4.	5.	6.	7.	8.	9.	10.	11.	12.
Specimen no.		PR-336	T-3	7717-85	TD-1691	Ba-8a-1	7917-66	T-2	7917-45	Ba-8a-4	TD-1707	T-1	R.V.-1
Q						5.26						5.07	1.71
or		2.01	1.83	2.77	1.18	0.59	2.07	2.07	0.89	0.59	1.77	0.83	
ab		16.5	22.09	26.23	23.69	25.39	24.54	20.39	22.85	23.69	22.0	22.0	20.31
an		29.81	25.93	24.22	22.31	22.26	24.15	27.52	25.91	26.43	21.28	22.63	25.79
di	wo	8.82	11.23	11.55	16.16	6.51	11.85	8.76	9.64	6.42	12.45	6.85	7.05
	en	5.61	6.62	6.43	9.13	3.39	6.03	4.32	4.83	3.14	5.84	3.13	2.79
	fs	2.66	4.06	4.67	6.36	2.94	5.53	4.28	4.61	3.17	6.46	3.67	4.34
hy	en'	7.12	7.87	1.71	6.03	14.54	1.97	8.69	8.44	7.76	7.07	12.34	11.16
	fs	3.38	4.83	1.24	4.2	12.64	1.81	8.62	8.05	7.85	7.82	14.5	17.39
ol	fo	10.17	5.77	8.78	1.94		7.31	3.83	3.45	6.15	3.52		
	fa	5.31	3.9	7.03	1.49		7.38	4.19	3.62	6.86	4.29		
ap		0.23	0.67	0.25		0.3	0.37	0.6	0.39	0.3		0.6	
il		2.55	2.47	2.09	2.28	2.47	3.32	2.28	3.23	3.04	4.18	4.37	4.94
mt		2.17	2.17	2.17	2.17	2.17	2.17	2.17	2.17	2.17	2.17	2.17	2.17

The norms were calculated after partial reduction of Fe_2O_3 to constant value of 1.50 %.

between the rocks studied, with the major variations found for Fe, Mg, Al, and Ti, and minor variations in the other elements.

The degree of advance in the fractional crystallization of basaltic magma may be measured by increases in the FeO*/MgO ratio. The existing data for amphibolites in the literature give FeO*/MgO ratios ranging from 0.92 to 2.89, while those of the new analyses fall in a smaller range from 1.33 to 1.78. As shown in Figure 15A, the SiO_2 content, with few exceptions (Nos. 1 and 5), remains within a narrow range (around 49 %) and very slightly increases with the increasing FeO*/MgO ratio for the schistose amphibolite. Nos. 1 and 5 represent the two extremes, with SiO_2 contents of 46.36 % and 53.9 % respectively. The FeO* content and FeO*/MgO ratio were plotted in Figure 15B, and a clear positive correlation can be seen. Figures 15C-E show the plots of the MgO, TiO_2, and P_2O_5 content versus FeO*/MgO ratio, respectively, which show the sympathetic variation in these elements. With an increase of the FeO*/MgO ratio, the TiO_2 content tends to increase, and the MgO content decreases. If the sample No.2, which was taken near the contact with the serpentinite and has extremely high P_2O_5 content among the schistose amphibolite, is not considered, there is a tendancy for the P_2O_5 content to increase with an increase of the FeO*/MgO ratio. A variation trend of Al_2O_3 with the FeO*/MgO ratio is not well defined in Figure 15F, however, a weak negative correlation between them appears to exist. A $(Na_2O + K_2O)$ - FeO - MgO plot for

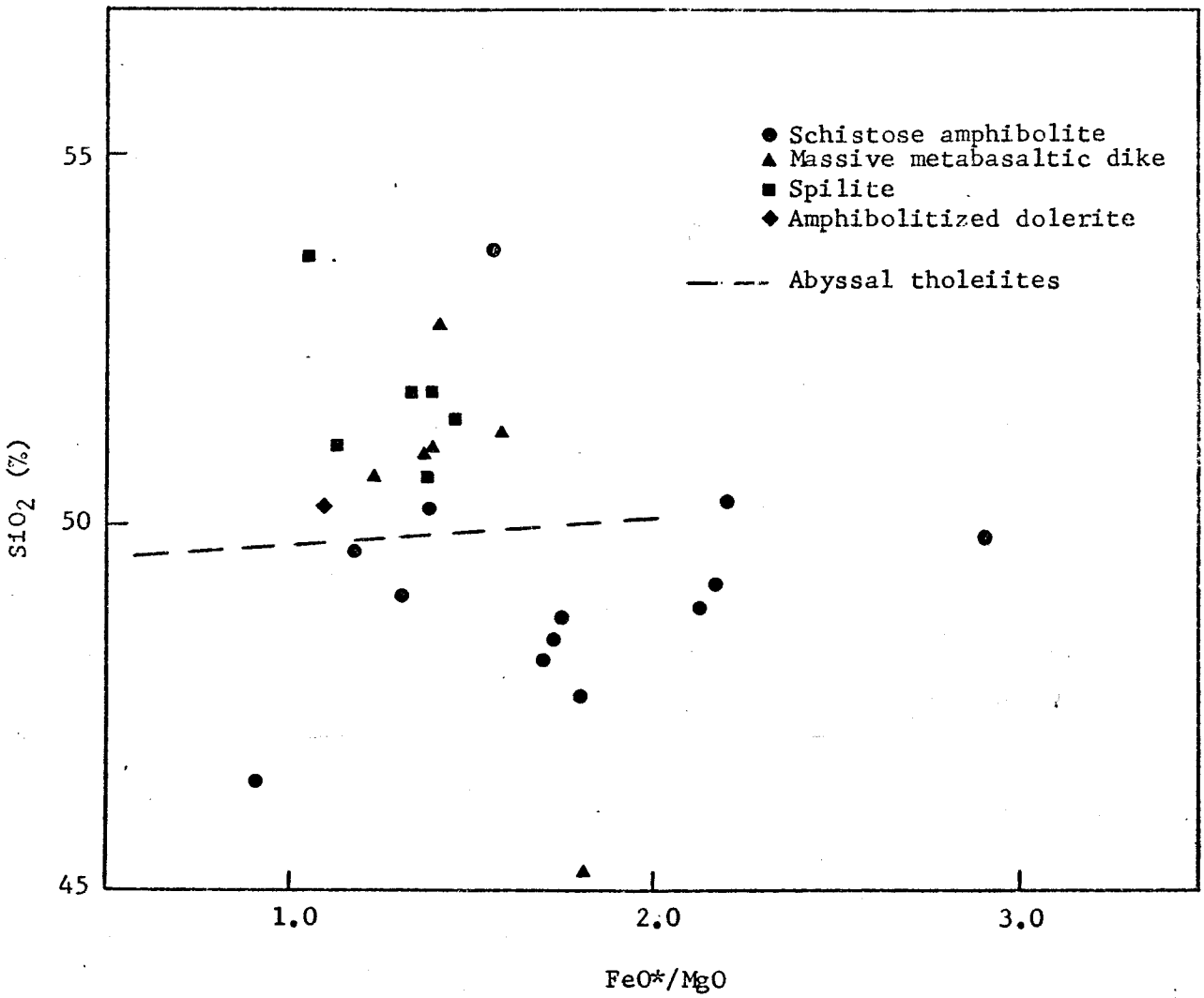

Figure 15 A. Changes of SiO_2 content (anhydrous) with FeO*/MgO ratio in the schistose amphibolite, massive metabasaltic dike, spilite, and amphibolitized dolerite of the Bermeja complex. Dash line is the average compositional trend of abyssal tholeiites.

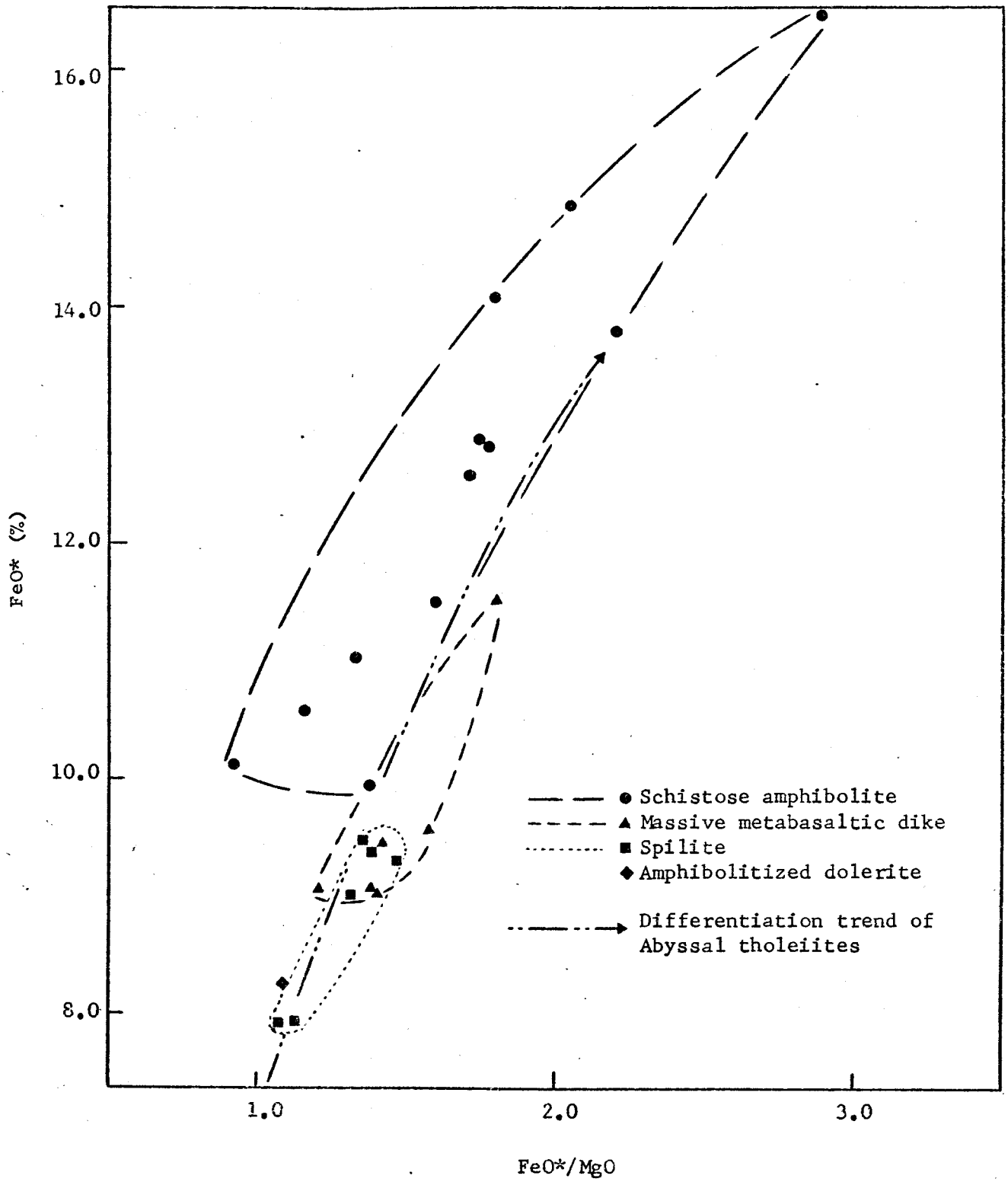

Figure 15 B. Changes of FeO* content with FeO*/MgO ratio in the schistose amphibolite, massive metabasaltic dike, spilite, and amphibolitized dolerite of the Bermeja complex. The encircled areas are composition fields, which are arbitrarily drawn.

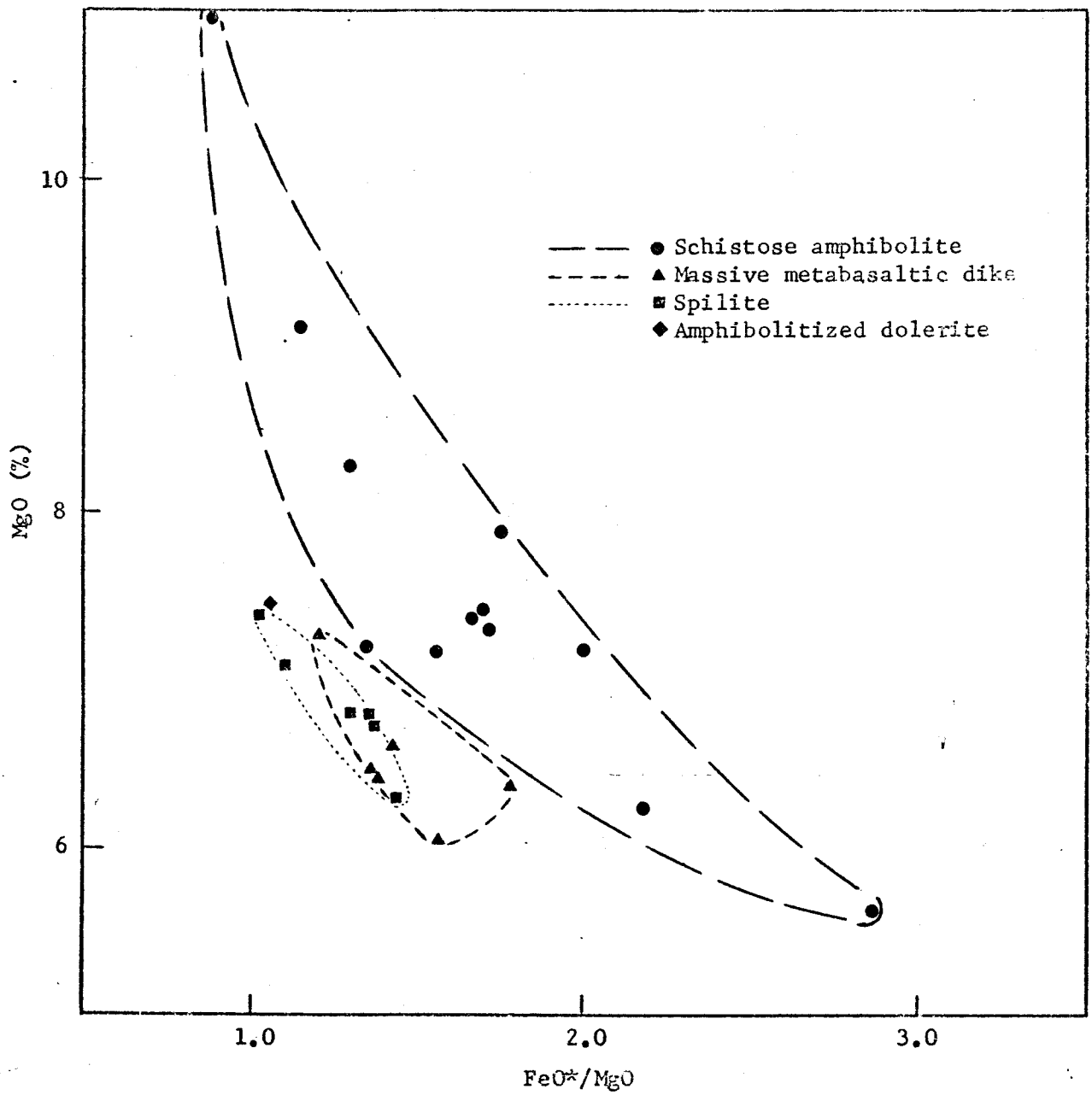

Figure 15 C. Changes of MgO content with FeO*/MgO ratio in the schistose amphibolite, massive metabasaltic dike, spilite, and amphibolitized dolerite of the Bermeja complex. The encircled areas are composition fields, which are arbitrarily drawn.

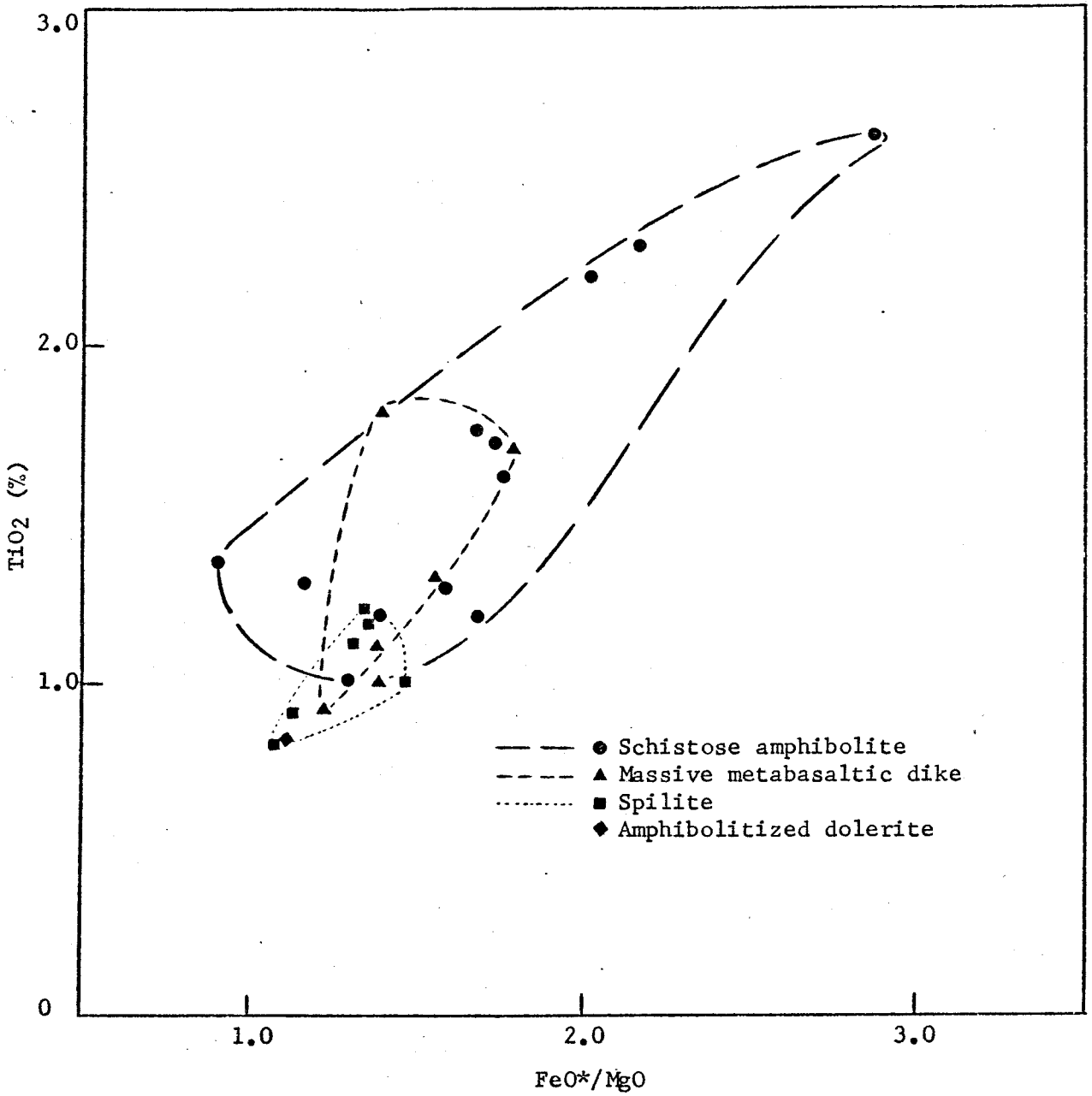

Figure 15 D. Changes of TiO_2 content with FeO*/MgO ratio in the schistose amphibolite, massive metabasaltic dike, spilite, and amphibolitized dolerite of the Bermeja complex. The encircled areas are composition fields, which are arbitrarily drawn.

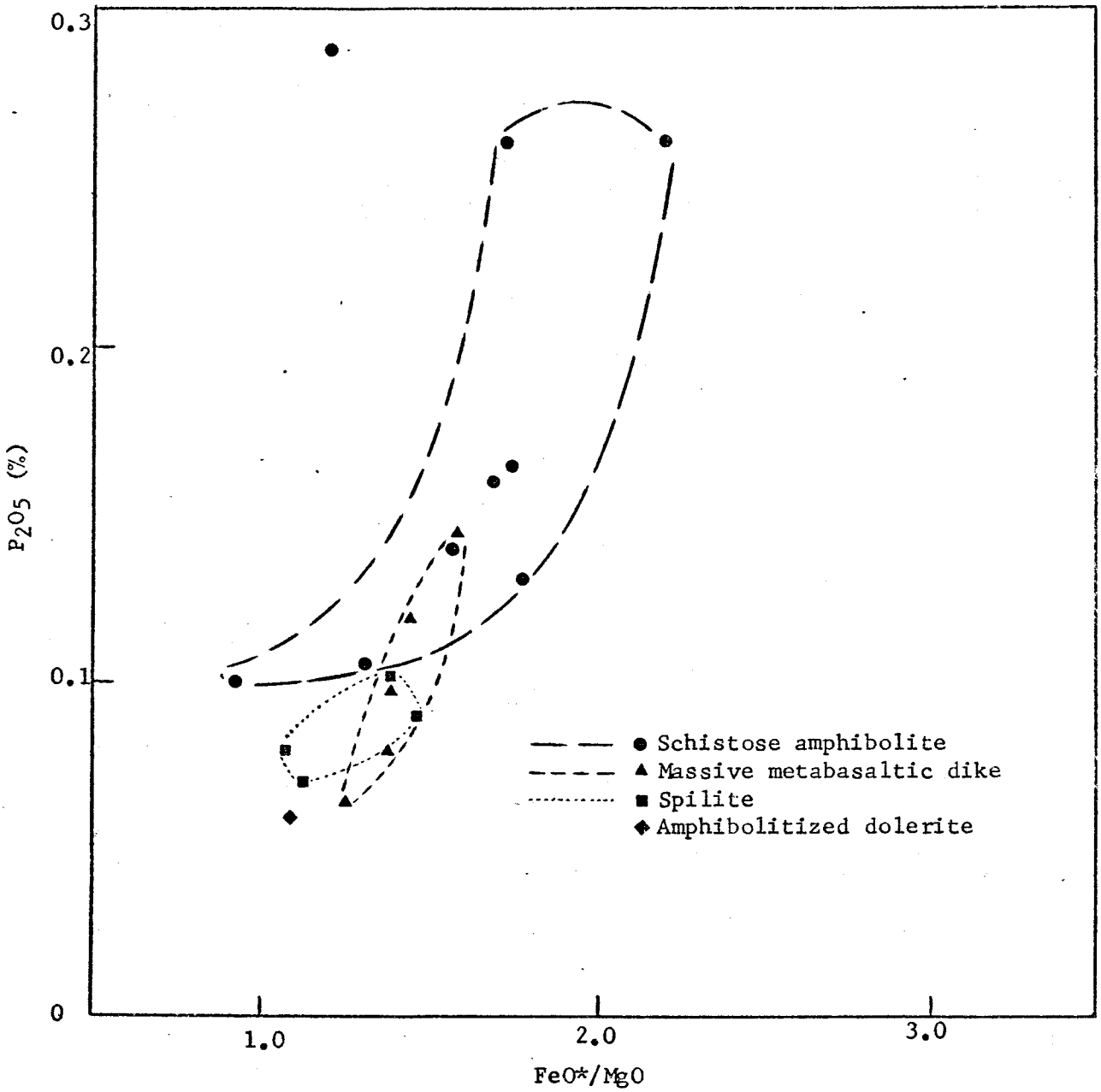

Figure 15 E. Changes of P_2O_5 content with FeO*/MgO ratio in the schistose amphibolite, massive metabasaltic dike, spilite, and amphibolitized dolerite of the Bermeja complex. The encircled areas are composition fields, which are arbitrarily drawn. Sample No. 2 of the schistose amphibolite, which was taken near the contact with serpentinite has extremely high P_2O_5 content is not included in the composition field.

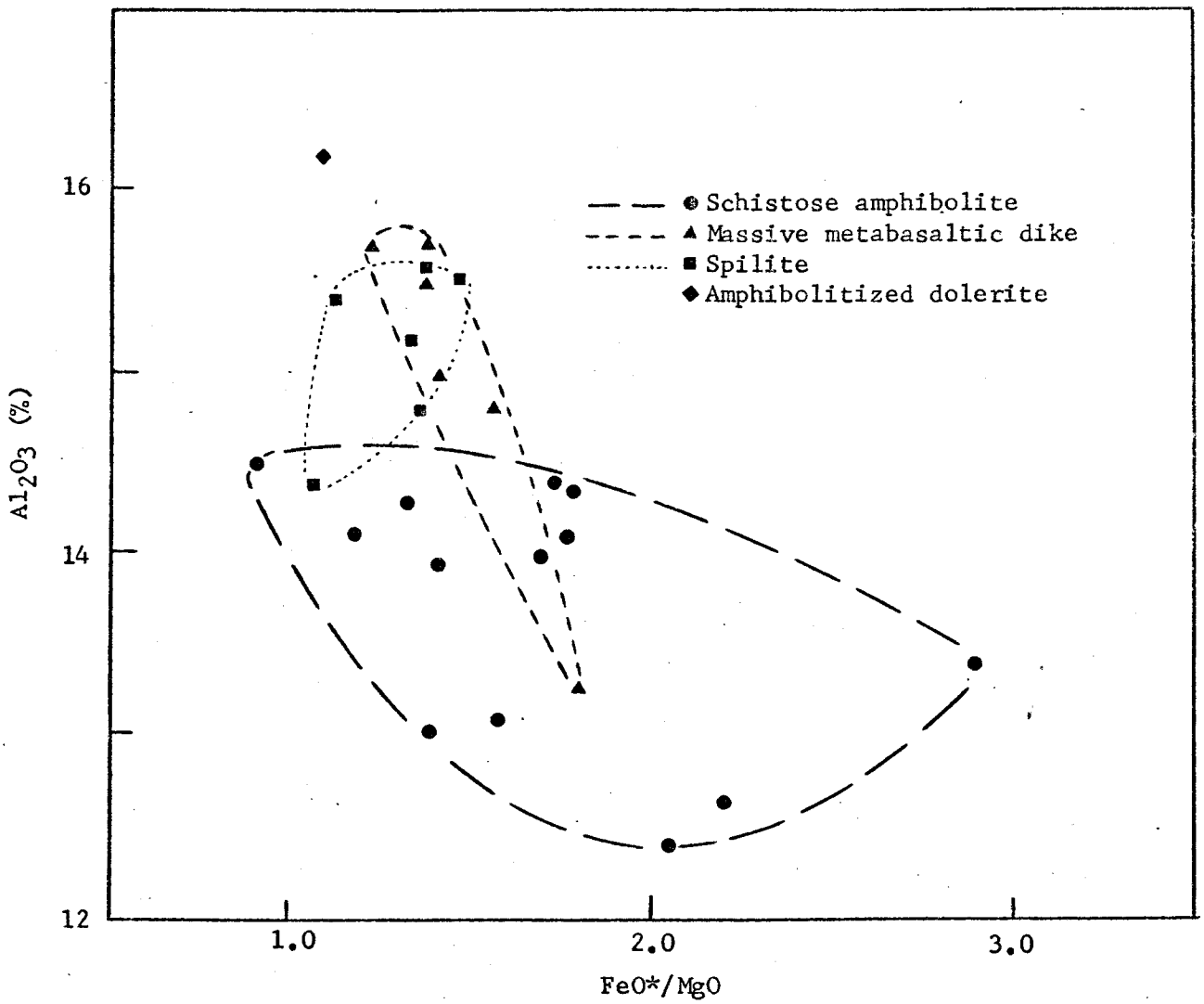

Figure 15 F. Changes of Al_2O_3 content with FeO*/MgO ratio in the schistose amphibolite, massive metabasaltic dike, spilite, and amphibolitized dolerite of the Bermeja complex. The encircled areas are composition fields, which are arbitrarily drawn.

the schistose amphibolite is shown in Figure 16, in which a clear tendency for iron enrichment can be easily defined in a field elongated parallel to the MgO - FeO* side, that is, in the direction of tholeiitic trends of differentiation. A plot of Na_2O/K_2O ratio against ($Na_2O + K_2O$) is shown in Figure 17, in which the schistose amphibolite is distributed within a small area ($Na_2O + K_2O$ about 2.5 to 3.5 %, Na_2O / K_2O ratio varying from 6 to 3.5). Figure 18A-B show the relations of Na_2O and ($Na_2O + K_2O$) versus SiO_2, respectively. Both Na_2O and ($Na_2O + K_2O$) contents remain in restricted ranges with the changes of SiO_2 content. The average trends for the schistose amphibolite show a slight increase of Na_2O and ($Na_2O + K_2O$) contents with increasing SiO_2 content.

The CIPW norms of the schistose amphibolite are represented in Table 10B-C. Both the original norms and modified norms are plotted on a diopside - hypersthene - olivine - nepheline - quartz diagram in Figure 19, representing the fields of quartz tholeiite, olivine tholeiite, and alkali olivine basalt of Yoder and Tilley (1962). Most of the analyses fall within the olivine tholeiite normative field. The modified recalculation using 1.5 % Fe_2O_3 moves two of four which are in the quartz normative field into that of olivine tholeiite. No analysis of the schistose amphibolite is nepheline normative.

2. Massive Metabasaltic Dike

Two new analyses (Nos. 1 and 2) were added to the

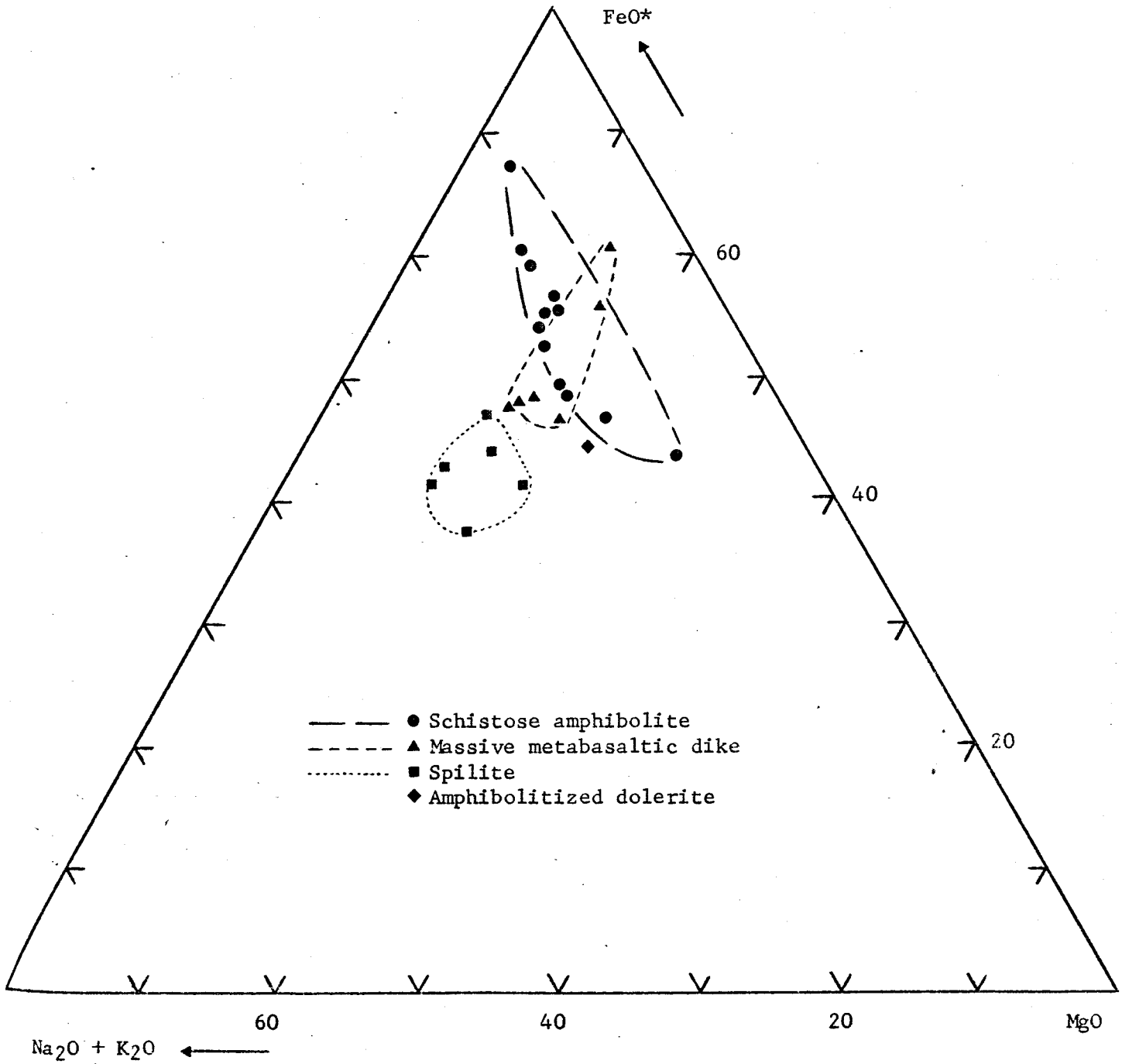

Figure 16. MgO - FeO* - (Na_2O+K_2O) diagram for the schistose amphibolite, massive metabasaltic dike, spilite, and amphibolitized dolerite of the Bermeja complex. See the text for the differentiation trend of the massive metabasaltic dike. The encircled areas are composition fields, which are arbitrarily drawn.

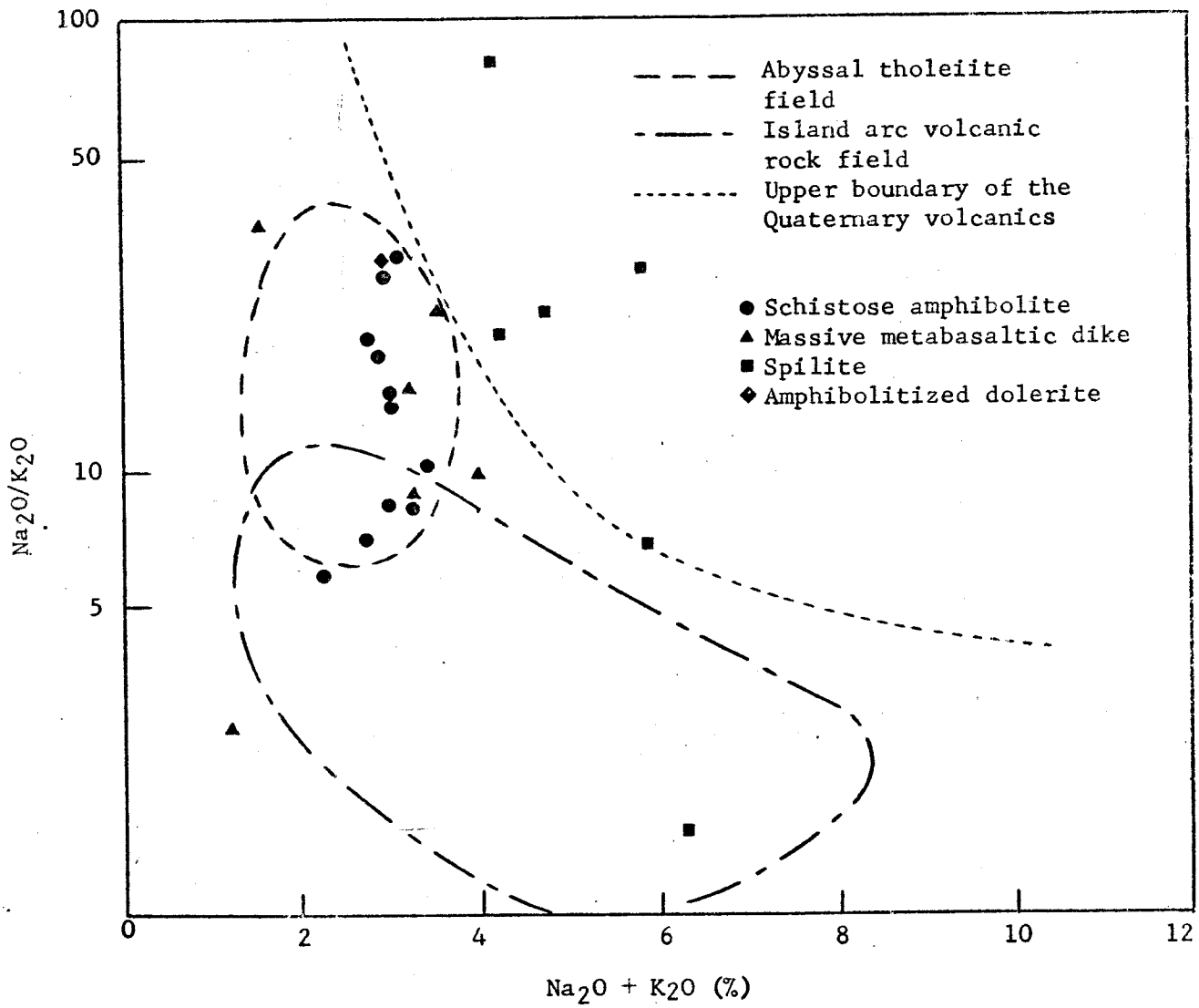

Figure 17. (Na_2O+K_2O) versus Na_2O/K_2O relation in the schistose amphibolite, massive metabasaltic dike, spilite, and amphibolitized dolerite of the Bermeja complex. The compositional fields for the abyssal tholeiite and island arc volcanic rock and the upper boundary of the Quaternary volcanics are also shown.

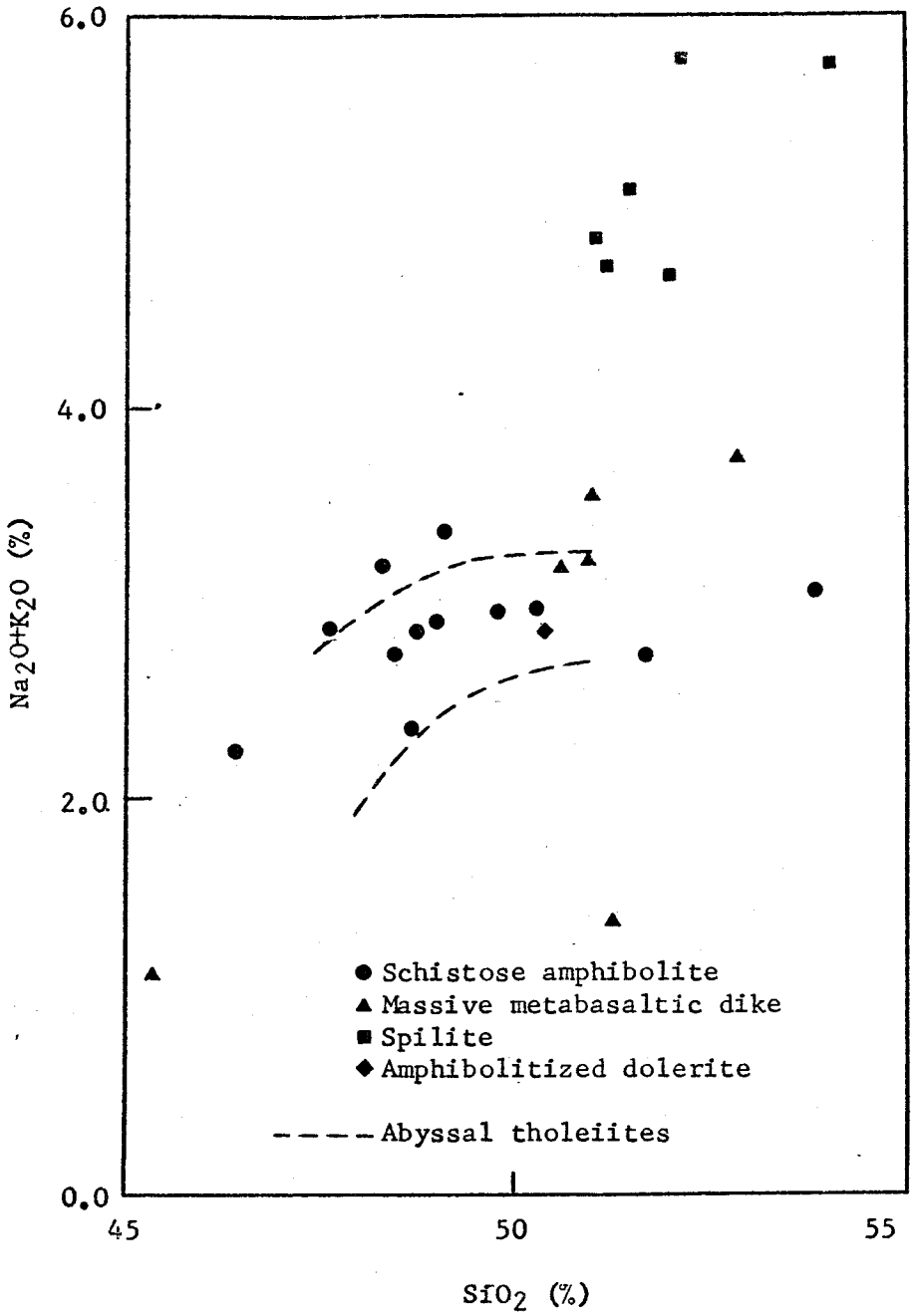

Figure 18A. SiO_2 versus Na_2O+K_2O relation in the schistose amphibolite, massive metabasaltic dike, spilite, and amphibolitized dolerite of the Bermeja complex. The data for the abyssal tholeiites are from Table 2 and 3 in Miyashiro et al., (1969a) and Table 2, 4, and 5 in Shido et al., (1971).

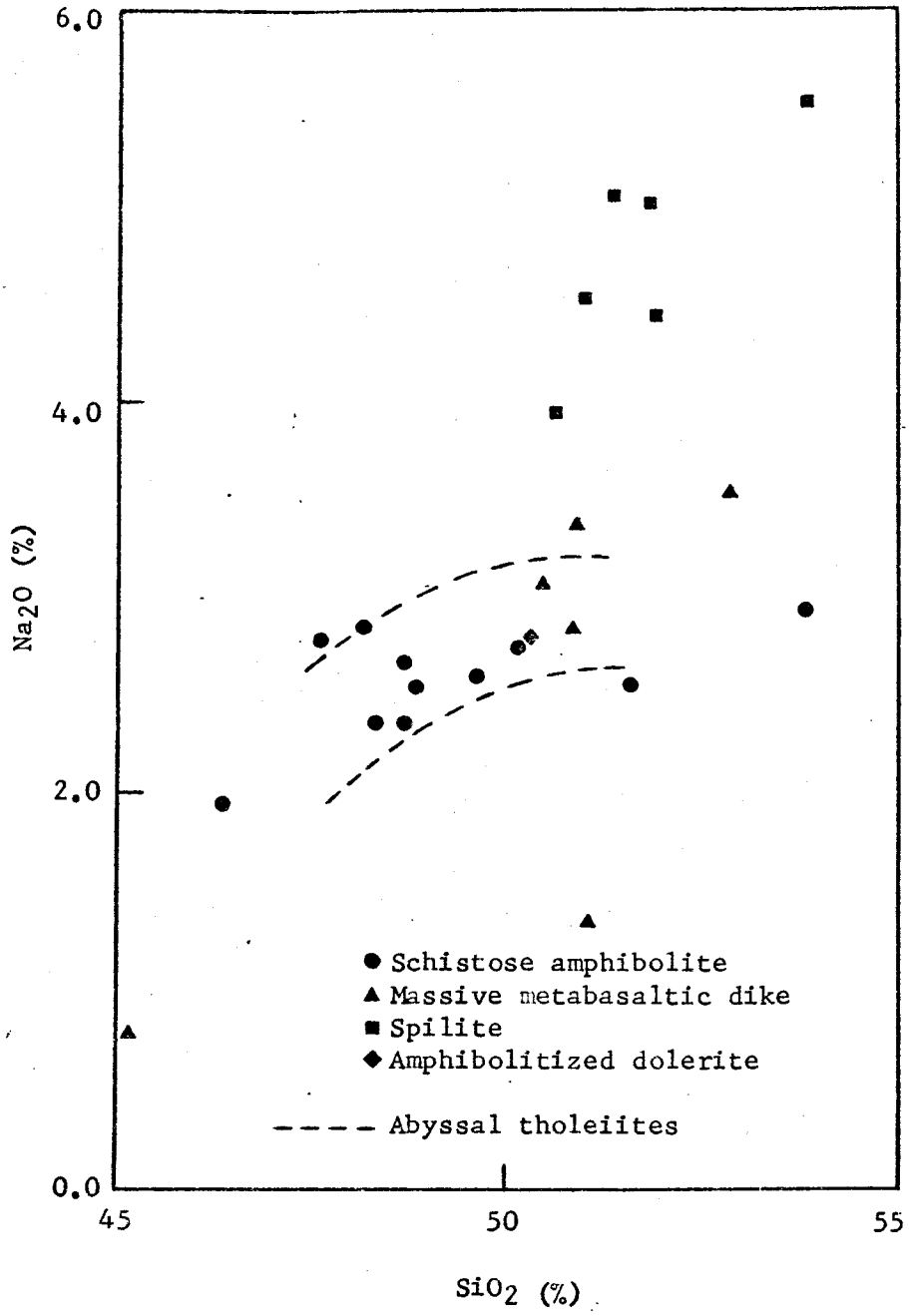

Figure 18B. SiO_2 versus Na_2O relation in the schistose amphibolite, massive metabasaltic dike, spilite, amphibolitized dolerite of the Bermeja complex. The data for the abyssal tholeiites are from Table 2 and 3 in Miyashiro et al., (1969a) and Table 2, 4, and 5 in Shido et al., (1971).

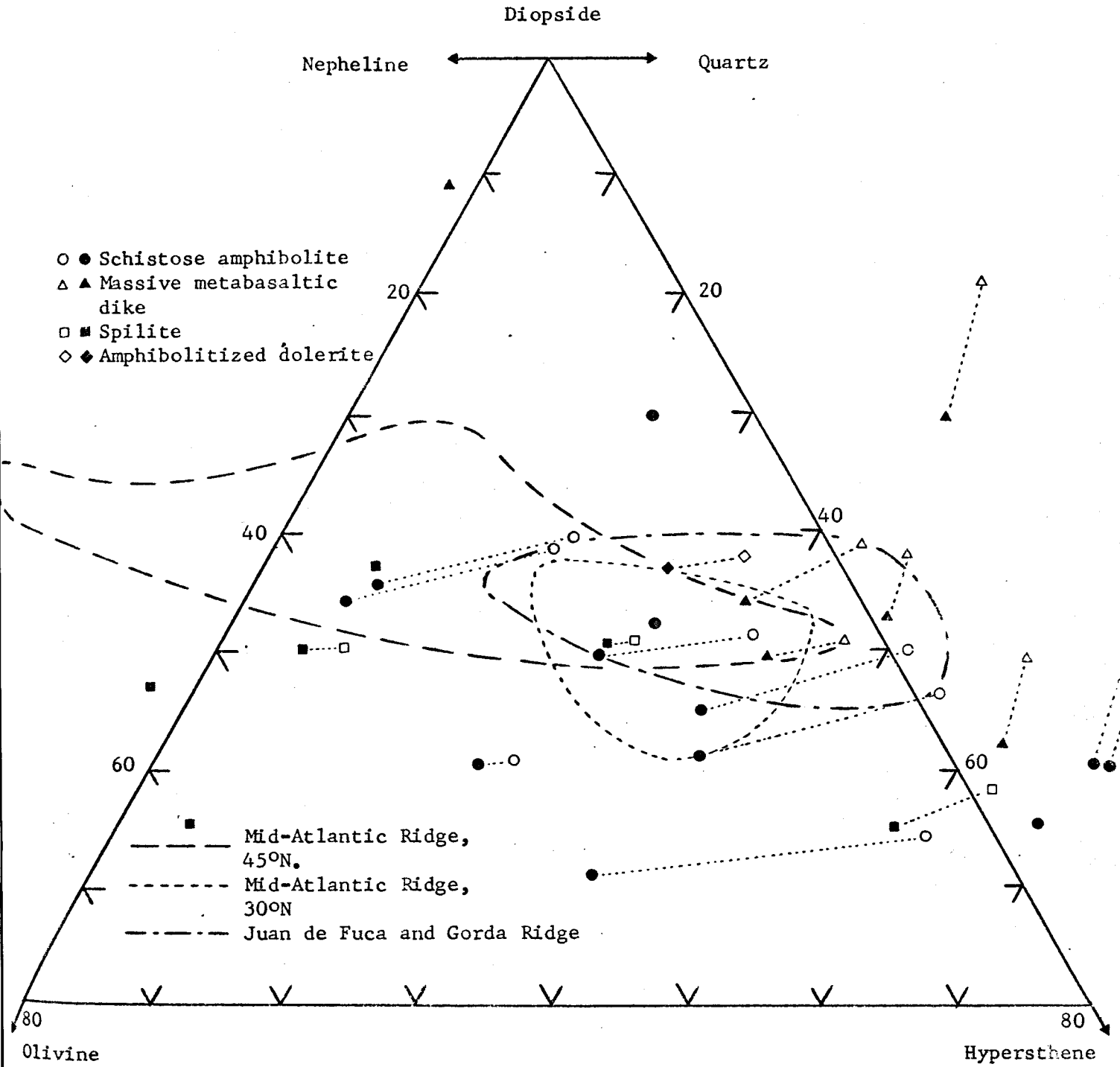

Figure 19. Normative mineralogy of the schistose amphibolite, massive metabasaltic dike, spilite, and amphibolitized dolerite plotted on a diopside-hypersthene-olivine-nepheline-quartz diagram. Open symbols are calculated from the original analyses. Solid symbols are from the analyses recalculated using 1.5 % Fe_2O_3. The data for the abyssal basalts are from Figure 2 in Kay et al., (1970).

four previous analyses of the massive metabasaltic dikes which are intruded the schistose amphibolite. These data were taken from the literature (Tobisch, 1968; Donnelly et al., 1971) and are given in Table 11A. The new analyses with FeO*/MgO ratios of 1.24 and 1.39 are on the lesser or early differentiation side of all the analyzed samples. In general, for all the analyzed samples of the massive metabasaltic dikes, the ranges of variation of the major elements, except SiO_2 and alkalies, are rather small compared with those of the schistose amphibolite as shown in some of the variation diagrams (Figures 15B-F and 16). This is probably due to the smaller range of differentiation within the parental rocks compared to that of the amphibolite. The FeO*/MgO ratio ranges from 1.24 to 1.8. These rocks are relatively widely distributed in the FeO*/MgO - SiO_2 diagram of Figure 15A. The metabasaltic dike shows enrichment in FeO* in Figure 15B. The trend has a similar slope to that of the schistose amphibolite. The clear differentiation trends of the MgO, TiO_2, P_2O_5 contents are easily observed in Figures 15C-E, respectively. In the metabasaltic dike the P_2O_5 content increases more rapidly with increasing differentiation than that for the schistose amphibolite of similar differentiation index (FeO*/MgO). In Figure 15F, the Al_2O_3 content of the dike rocks decreases rapidly with increasing differentiation, thus a trend with a steep slope can be seen clearly for the metabasaltic dike. In general, the Al_2O_3 content is higher in the massive metabasaltic dike than in the schistose amphibolite at an equi-

Table 11A. Major Elements Analyses of the Massive Metabasaltic Dike from Las Palmas.

	1.	2.	3.	4.	5.	6.
Specimen no.	Ba-10	Ba-8b-2	T-4	T-6	T-5	TD-1720
FeO*/MgO	1.24	1.39	1.40	1.43	1.58	1.80
SiO_2	50.6	50.9	50.93	52.76	51.07	45.2
TiO_2	0.92	1.0	1.1	1.81	1.3	1.7
Al_2O_3	15.7	15.5	15.74	14.97	14.82	13.3
Fe_2O_3	2.35	2.9	3.31	2.91	4.01	11.5
FeO	6.95	6.45	6.02	6.83	5.91	
MnO	0.16	0.16	0.17	0.18	0.19	
MgO	7.3	6.5	6.42	6.63	6.01	6.4
CaO	10.6	10.5	10.43	8.24	13.42	17.9
Na_2O	3.0	2.9	3.41	3.62	1.4	0.8
K_2O	0.2	0.35	0.15	0.37	0.04	0.3
H_2O^+	1.9	2.0	2.01	1.51	1.60	
P_2O_5	0.07	0.09	0.10	0.12	0.15	
Total	99.75	99.25	99.79	99.95	99.92	

FeO* means total iron as FeO, i.e., FeO + 0.9 Fe_2O_3.

Nos. 1 and 2: This study (see Appendix B)

No. 3: In the stream cut at Las Palmas, containing hornblende, sodic andesine, and epidote (Tobisch, 1968).

No. 4: In the small road cut in the west part of the amphibolite body at Las Palmas, containing sodic andesine, hornblende, and epidote (Tobisch, 1968).

No. 5: Near the north contact with serpentinite, containing amphibole, plagioclase (albite and some sodic andesine), quartz, minor epidote and prehnite, and some prehnite veinlets and quartz veinlets (Tobisch, 1968).

No. 6: At Las Palmas (Donnelly et al., 1971).

Table 11B. Original CIPW norms of the massive metabasaltic dike from Las Palmas.*

		1.	2.	3.	4.	5.
Specimen no.		Ba-10	Ba-8b-2	T-4	T-6	T-5
Q			2.09	0.94	3.26	9.66
or		1.18	2.07	0.89	2.19	0.24
ab		25.39	24.54	28.85	30.63	11.85
an		28.78	28.24	27.2	23.51	34.04
	wo	9.75	9.71	9.98	6.93	13.18
di	en	6.01	6.08	6.51	4.45	8.82
	fs	3.17	3.04	2.78	2.02	3.38
	en	11.35	10.11	9.48	12.06	6.15
hy	fs	5.99	5.05	4.04	5.46	2.36
	fo	0.57				
ol	fa	0.33				
ap		0.16	0.21	0.23	0.28	0.35
il		1.75	1.9	2.09	3.44	2.47
mt		3.41	4.2	4.8	4.22	5.81

* Original CIPW norms was not calculated for sample No. 6, because the total iron was determined as FeO.

Table 11C. CIPW norms (Fe_2O_3 = 1.5 %) of the massive metabasaltic dike from Las Palmas.

		1.	2.	3.	4.	5.	6.
Specimen no.		Ba-10	Ba-8b-2	T-4	T-6	T-5	TD-1720*
Q			0.51		1.67	6.85	
or		1.18	2.07	0.89	2.19	0.24	1.77
ab		25.39	24.54	28.85	30.63	11.85	4.8
an		28.78	28.24	27.2	23.51	34.04	31.82
di	wo	9.75	9.71	9.98	6.93	13.18	23.8
	en	5.65	5.44	5.61	3.97	7.08	12.12
	fs	3.64	3.88	3.96	2.64	5.66	11.1
hy	en	9.6	10.75	7.98	12.54	7.89	
	fs	6.18	7.68	5.64	8.34	6.31	
ol	fo	2.05		1.68			2.68
	fa	1.46		1.31			2.7
ap		0.16	0.21	0.23	0.28	0.35	
il		1.75	1.9	2.09	3.44	2.47	3.23
mt		2.17	2.17	2.17	2.17	2.17	2.17

* TD-1720 contains 1.06 % of nepheline in the modified CIPW norms.
The norms were calculated after partial reduction of Fe_2O_3 to constant value of 1.50 %.

valent FeO*/MgO ratio, while FeO* is lower. The secondary phases formed during metamorphism or alteration, especially during contact metamorphism, could cause some migration of the more mobile alkalies and alkaline earths in the original parental rocks of the metabasaltic dike (Tobisch, 1968). Thus, an iron-enrichment trend is not found in the AFM diagram of Figure 16. As shown in the (Na_2O / K_2O) - (Na_2O + K_2O) diagram of Figure 17, the dike rocks have a relatively wide range of total alkalies (Na_2O + K_2O ~ 1.5 to 4.0 %) and Na_2O / K_2O ratios (~ 3 to 40). The variations of Na_2O and Na_2O + K_2O contents with SiO_2 content for the dike rocks are relatively large as shown in Figures 18A-B. Although not shown in these diagrams the CaO content also varies over a wide range. Sample No. 5, which was taken near the contact with the serpentinite, has a high CaO content. This is probably due to calcium metasomatism following the emplacement of the serpentinite, or during the serpentinization process. Analysis of sample No. 6 also yields uncommonly high CaO content. Unfortunately, the sampling locality is unknown and the relationship to possible contact metamorphism, or alteration is therefore not clear. The remaining four analyses, which are from samples further away from the contact and therefore expected to be free from contact metasomatic effects, have CaO contents similar to those of most samples of the schistose amphibolite. In the AFM diagram, the analyzed metabasaltic dikes fall on both sides of the iron enrichment trend of the schistose amphibolite, with samples

Nos. 5 and 6, on the ferromagnesian side. If we exclude these two samples which may have been affected by contact metasomatism, a short trend of iron enrichment can be seen in Figure 16.

The CIPW norms are shown in Tables 11B-C, and are plotted in the diopside-hypersthene - olivine - nepheline - quartz diagram of Figure 19, in which the metabasaltic dike samples are relatively widely distributed. Most of these analyses are quartz normative for the original CIPW norms. One is moved into the olivine tholeiite field and one is nepheline normative after assigning a value of 1.5 % for Fe_2O_3 to the original data. The wide distribution of all the analyses of the metabasaltic dike in Figure 19 may be due to the effects of metasomatism and alteration.

3. Spilite and Amphibolitized Dolerite

The major element composition of the spilite and the amphibolitized dolerite from the quarry one Km east of Mayaguez is shown in Table 12A. Three analyses of spilite (Nos. 3, 4, and 5) were taken from the literature (Mattson, 1960; Donnelly et al., 1971), the other three analyses of spilites (Nos. 1, 2, and 6) and one amphibolitized dolerite (Nos. 7) were made in the course of this study. The newly analyzed spilite have a wider range of FeO*/MgO ratio (1.07 to 1.47) than that of the previous analyses (1.32 to 1.39). Thus, some chemical variation features became more clearly defined in the spilites with the new data. As shown in Figure

Table 12 A. Major Element Analyses of the Spilite (sample Nos. 1 to 6) and amphibolitized dolerite (sample No. 7) from Mayaguez.

	1.	2.	3.	4.	5.	6.	7.
Specimen no.	Ba-1b	Ba-6	TD-1838	TD-1830	PR-42	Ba-3	Ba-7a
FeO*/MgO	1.07	1.12	1.32	1.38	1.39	1.47	1.10
SiO_2	53.7	51.0	51.8	50.7	51.84	51.3	50.1
TiO_2	0.83	0.92	1.1	1.2	1.21	1.0	0.83
Al_2O_3	14.4	15.4	15.2	14.8	15.54	15.5	16.2
Fe_2O_3	1.85	1.8	9.0	9.4	2.47	2.65	2.25
FeO	6.25	6.3			7.12	6.9	6.25
MnO	0.16	0.15			0.17	0.17	0.18
MgO	7.4	7.1	6.8	6.8	6.74	6.3	7.5
CaO	6.7	9.0	8.9	6.5	6.05	7.7	11.8
Na_2O	5.6	4.0	4.5	3.8	5.07	4.1	2.8
K_2O	0.2	0.2	0.2	2.5	0.75	0.05	0.1
H_2O^+	2.8	3.5			2.7	3.1	1.8
P_2O_5	0.08	0.07			0.1	0.09	0.05
Total	99.97	99.44			99.76	98.86	99.86

Nos. 1, 2, and 6: This study (see Appendix C).

No. &: This study (see Appendix D).

Nos. 3 and 4: Rosario Quarry, 2 Km east of Mayaguez (Donnelly et al., 1971).

No. 5: Quarry on Route 106 1 Km east of Mayaguez (Mattson, 1960).

Table 12B. Original CIPW norms of the spilite (sample Nos. 1,2,5, and 6) and the amphibolitized dolerite (sample No. 7) from Mayaguez.*

		1.	2.	5.	6.	7.
Specimen no.		Ba-1b	Ba-6	PR-42	Ba-3	Ba-7a
Q					0.45	
ne						
or		1.18	1.18	4.43	0.3	0.59
ab		47.39	33.85	42.9	34.69	23.69
an		13.57	23.48	17.43	23.74	31.34
di	wo	8.0	8,65	4.98	5.79	11.22
	en	5.06	5.43	3.02	3.47	7.19
	fs	2.44	2.71	1.68	2.02	3.3
hy	en	1.86	6.81	2.19	12.22	9.02
	fs	0.9	3.4	1.22	7.12	4.14
ol	fo	8.07	3.83	8.11		1.73
	fa	4.28	2.11	4.98		0.88
ap		0.19	0.16	0.23	0.21	0.12
il		1.58	1.75	2.3	1.9	1.58
mt		2.68	2.61	2.17	3.84	3.26

*Original CIPW norms was not calculated for sample Nos. 3 and 4, because the total iron was determined as FeO.

Table 12C. CIPW norms (Fe_2O_3 = 1.5 %) of the spilite (sample Nos. 1 to 6) and the amphibolitized dolerite (sample No. 7) from Mayaguez.

		1.	2.	3.	4.	5.	6.	7.
Specimen no.		Ba-1b	Ba-6	TD-1838	TD-1830	PR-42	Ba-3	Ba-7a
Q								
ne					0.99			
or		1.18	1.18	1.18	14.78	4.43	0.3	0.59
ab		47.39	33.85	38.08	30.32	42.9	34.69	23.69
an		13.57	23.48	20.69	15.95	17.43	23.74	31.34
	wo	8.0	8.65	9.8	6.81	4.98	5.79	11.22.
di	en	4.93	5.29	5.67	3.87	2.81	3.16	6.8
	fs	2.61	2.87	3.68	2.64	1.97	2.42	3.81
	en	1.34	6.25	1.68		0.84	10.73	7.54
hy	fs	0.71	3.39	1.09		0.59	8.21	4.22
	fo	8.52	4.3	6.72	9.15	9.2	1.26	3.04
ol	fa	4.97	2.57	4.81	6.89	7.1	1.06	1.87
ap		0.19	0.16			0.23	0.21	0.12
il		1.58	1.75	2.09	2.28	2.3	1.9	1.58
mt		2.17	2.17	2.17	2.17	2.17	2.17	2.17

* The norms were calculated after partial reduction of Fe_2O_3 to constant value of 1.50 %.

15A, the SiO_2 contents(ranging from 50.7 to 53.7 %) do not vary regularly in respect to the FeO*/MgO ratios for the spilites. In general, for a given FeO*/MgO ratio the SiO_2 content of the spilite is higher than that of the amphibolite and of the metabasaltic dike of the complex. The SiO_2 content of the amphibolitized dolerite is 50.1 %, which is lower than that of spilite but higher than most amphibolite.

The enrichment of FeO* for the spilite (in respect to FeO*/MgO ratio) can be clearly seen in Figure 15B. This trend is continuous toward that of the massive metabasaltic dike, which overlaps on the more differentiated end. This continuous iron enrichment trend of spilite and dike rock occurs at a lower FeO* content than in the schistose amphibolite trend at an equivalent FeO*/MgO ratio. The amphibolitized dolerite sample lies on the trend defined by spilite and dike. The same relationships can be observed in the FeO*/MgO - MgO diagram of Figure 15C, except that the trends of variation are negatively correlated.

The variation trend of the spilite, showing a slight increase of TiO_2 with FeO*/MgO ratio, has a similar slope as those defined by the amphibolite and dike (Figure 15 D). The plotted point of the amphibolitized dolerite is again on the spilite trend. P_2O_5 content increases with the extent of differentiation for spilite, forming a trend having a similar slope to that of the amphibolites but at a somewhat lower value for the same range of FeO*/MgO ratio, as shown in Figure 15E. The amphibolitized dolerite

has the lowest P_2O_5 content among the analyzed basaltic rocks, however, it is close to the spilite trend.

Al_2O_3 contents of spilites vary from about 14.8 to 16.1 %. No variation trend with differentiation can be defined on the Al_2O_3 - FeO*/MgO diagram of Figure 15F. The distribution field overlaps that of the metabasaltic dike rather than the amphibolite field. Generally, the spilite has a higher content of Al_2O_3 than amphibolite at an equivalent FeO*/MgO ratio. Again, the amphibolitized dolerite has a high Al_2O_3 content which is close to the spilite field. In the AFM diagram of Figure 16, as could be expected, the distribution field of the spilite falls on the alkali side compared to the other rock types analyzed, but no other trend can be recognized for spilites in this diagram. The point for the amphibolitized dolerite is more or less continuous on the MgO rich end of the iron enrichment trend of the metabasaltic dike.

As shown in Figure 18A-B, both Na_2O and $Na_2O + K_2O$ seem to increase with increasing SiO_2, with the spilite containing more alkali as compared with the other rock types analyzed. Plotting the Na_2O/K_2O ratio against $Na_2O + K_2O$ (Figure 17) can be used to interpret the character of the alkali content to some extent. Most spilite points fall outside the field for the Quaternary volcanic rocks from various parts of the world, with a higher Na_2O/K_2O ratio. For this reason, we believe the spilites likely have been subjected to metasomatism, at least in respect to the migration of alkalis,

during or after the magmatic stage. As can be seen in the same figure, the spilites are distributed in a steep narrow belt, with a wide range of Na_2O/K_2O ratios (about 1 to 100), and a relatively small range in total alkalis. Based on the fact that the Na_2O concentration is much higher than the K_2O concentration (by about a factor of 15) in the spilite, the migration of K_2O may be the main reason for such a distribution trend with a steep slope. However, this is not conclusive. Other types of alkali migrations are also possible and cannot be ruled out.

The CIPW norms for the spilite and the amphibolitized dolerite are shown in Table 12B-C. The plots of the CIPW norms (Fe_2O_3 = 1.5 %) are all distributed over a wide area within the olivine tholeiite field of the diopside -hypersthene - olivine - nepheline - quartz diagram of Figure 19, except for No. 4 which is in the nepheline normative field.

The spilite of the Water Island Formation, which is recognized stratigraphically lowest group of volcanic rocks in the eastern West Indies, is chemically similar to the spilite of the Bermeja complex. Although they show a wider range of FeO*/MgO ratio (about 1 to 2.7), the tholeiitic series have similar variation trends as these of the Bermeja complex spilite (more discussions will be in the later sections). The younger spilitic lava flows exposed in central Puerto Rico are mostly Upper Cretaceous in age and are chemically distinct from the spilites belonging to the Bermeja complex. In general, they are more differentiated

(FeO*/MgO ratio from about 1 to 5) than the spilite from the Bermeja complex, and are rich in K_2O (generally 2 to 5 %) and depleted in Na_2O compared to the spilites from the Bermeja complex.

4. Discussion of the Major Element Chemistry of the Basaltic Rocks

The major element chemical analyses for the amphibolite, dike rocks, spilite, and amphibolitized rocks have been shown in the previous sections. The increases in FeO*, TiO_2, and P_2O_5 and the decrease in MgO with the increasing fractionation (FeO*/MgO ratio) of these basaltic rocks, are similar to those of abyssal tholeiites (Miyashiro et al., 1969a; Shido et al., 1971). However, the tholeiitic rocks generated in the early stage of island arc magmatism are also characterized by these features, except that the TiO_2 content is generally, but not necessarily, lower than that of the abyssal tholeiite (Jakes and Gill, 1970; Jakes and White, 1971; Jakes and White, 1972; Miyashiro, 1973b). Although the schistose amphibolites show a slight decrease in Al_2O_3 with increasing FeO*/MgO ratio, similar to the trend of abyssal tholeiite, they are lower by about 1 % in Al_2O_3 content than most low alumina abyssal tholeiite analyses in the literature (Miyashiro et al., 1969a; Shido et al., 1971). Morever, the previous analyses of the amphibolites (Nos. 10, 11, and 12) give FeO*/MgO ratios higher than the upper limit of 1.9 in common low-alumina abyssal tholeiites.

The chemical variation trends for the abyssal tholeiites and the amphibolite with FeO*/MgO ratios smaller than 1.9 are similar, and extend continuously to these three analyses of amphibolite with high FeO*/MgO ratios. Abyssal tholeiites with such high FeO*/MgO ratios have not been commonly found in the mid-oceanic ridge. However, tholeiitic gabbros from the Mid-Atlantic Ridge show remarkable differentiation, with the range of their FeO*/MgO ratios, 0.32 to 2.84, being much wider than that of the analyzed abyssal tholeiites (Miyashiro et al., 1970; Thompson, 1973) and covering that of the schistose amphibolite. This rock type may also be considered as one of the possible parental rocks for the schistose amphibolite. On the other hand, the abyssal basalt may react with sea water and cause an increase in the Fe*/MgO ratio by an increase of FeO* and decrease of MgO in the rocks during their travel from the mid-oceanic ridge to the continental margin (Hart, 1970). In such cases, the metamorphic derivative of the weathered abyssal tholeiite may have a high FeO*/MgO ratio, as the schistose amphibolites have. However, this possibility is still largely unevaluated. The variations of Na_2O and $Na_2O + K_2O$ with SiO_2 content for amphibolite are similar to those of the abyssal tholeiite as shown in Figures 18A-B. Moreover, in the Na_2O/K_2O - ($Na_2O + K_2O$) diagram of Figure 17, most schistose amphibolite points fall within the small field of abyssal tholeiites. However, until the migration of alkalies during any secondary process is understood, these features of the alkalies offer

no evidence to solve the problem of the genesis of these rocks.

As mentioned above in this section, island arc tholeiite is also similar to abyssal tholeiite in most features of its major element chemistry. Some island arcs mainly composed of the rocks of the tholeiitic series are represented by the Kermadecs (Brothers and Searle, 1970; Brothers and Martin, 1970), Tongas (Bauer, 1970; Baker et al., 1971; Bryan et al., 1972), and North Marianas (Tanakadate, 1940; Schmidt, 1957; Stark, 1963). These low-K tholeiites of island arcs usually have slightly lower TiO_2 and Na_2O contents than common abyssal tholeiites. However, there is a long submarine history for these arcs prior to their evolution to the stage for which the chemical data were available. For this initial period of island arc formation, we have no data. Thus, by a reasonable extrapolation the initial stage arc tholeiites may also have TiO_2 and Na_2O contents similar to those for common abyssal tholeiites (Miyashiro, in press). However, in considering this possibility, necessarily the present approach to interpreting the genesis of the tholeiitic rocks from the Bermeja complex becomes increasingly more difficult. The chemical variation during the evolution of an island arc will be discussed in more detail in the later sections, with emphasis also on the chemical features of the earliest developed rocks of the tholeiitic series. So far, there is still not enough evidence to certify whether these particular tholeiitic rocks of the Bermeja

complex originated as a basement in the early stage of island arc magmatism or were at a mid-oceanic ridge and were moved to their present location by sea floor spreading.

Before the genesis of the analyzed tholeiitic rocks becomes clear, let us summarize the similarities between the rock types and also the significant differences in chemical features. The rocks can be divided into two groups as shown in the variation diagrams. Group I, including only the schistose amphibolite, has a higher FeO* and P_2O_5 and lower MgO and Al_2O_3 at an equal FeO*/MgO ratio than group II which includes the massive metabasaltic dike, spilite, and amphibolitized dolerite. Except for the variation of alkalies, each group defines separate variation trends, within which the rock types of the same group have continuity. The variation behavior of FeO*, MgO, TiO_2, and P_2O_5 are more or less similar between two groups.

Although the SiO_2 contents do not vary regularly with FeO*/MgO ratio for each rock type of group II, a trend can be defined, if all rock types are considered together. In this case, the SiO_2 content increases with increasing FeO*/MgO ratio for group II, while remaining almost constant for group I. The spilite of group II is believed to have been subjected to secondary migration of alkalies, which tends to obscure any trends relative to alkali contents as in Figures 16, 17, and 18A-B. However, the differentiation trends of other oxides - FeO*, MgO, TiO_2, and SiO_2 - which usually suffer relatively little change during such secondary

spilitization processes, tend to confirm the view that two groups of parental magmas are present, both tholeiitic in character.

In the field observation, there is no doubt that the metabasaltic dike of the group II intruded the schistose amphibolite of group I in Las Palmas area. Therefore, the rock types of the group II must be younger than group I.

In general, these tholeiitic rocks appear to have preserved their original composition quite well in respect to FeO*, MgO, TiO_2 contents, while other components were changed somewhat during metamorphism and/or other secondary processes.

5. Serpentinites

Thirteen chemical analyses of the AMSOC serpentinite core were given by Hess and Otalora (1964). One specimen (B-2) from this core was analyzed in this study. Results are given in Table 13. The analyses are in order of decreasing CaO content. Serpentinites from the north wall of the Puerto Rico trench were studied by Bowin et al., (1966), from which two analyses are also shown in Table 13.

The CaO content of the AMSOC serpentinite ranges from 0.07 % to 2.38 % by weight. In Figures 20A-H, Al_2O_3, TiO_2, Na_2O, FeO, MgO, FeO*/MgO, Fe_2O_3/FeO, and H_2O^+ were plotted against CaO, respectively. As shown in Figure 20A, the Al_2O_3 content tends to decrease with decreasing CaO content. The TiO_2 content appears to decrease with decreasing CaO content,

Table 13. Major Element Analyses of the Serpentinite from AMSOC core and Puerto Rico Trench (Nos. 15 and 16)*.

	1.	2.	3.	4.	5.	6.	7.	8.
Specimen no.	A-11	A-3	A-16	A-19	A-2	A-10	A-18	
SiO_2	39.27	38.46	37.41	37.75	37.29	37.40	37.47	38.21
TiO_2		0.09	0.04	0.04	0.04	0.04	0.04	0.09
Al_2O_3	2.45	1.82	2.20	1.75	1.74	1.91	2.58	1.86
Fe_2O_3	3.95	3.98	5.01	4.15	5.43	4.12	4.09	4.15
FeO	3.99	3.72	3.36	3.64	2.37	3.23	3.11	3.48
MnO	0.09	0.09	0.09	0.09	0.09	0.09	0.10	0.10
MgO	36.61	36.41	36.25	36.61	36.53	37.00	36.10	36.48
CaO	2.38	2.38	2.03	1.99	1.65	1.51	1.46	1.07
Na_2O	0.21	0.29	0.21	0.43	0.26	0.37	0.32	0.32
K_2O								
H_2O^-	0.81	1.37	1.62	1.30	2.08	1.55	2.30	1.71
H_2O^+	10.00	10.97	11.12	11.13	12.41	12.41	12.15	12.32
P_2O_5	0.06	0.05	0.05	0.07	0.08	0.04	0.09	0.05
Cr_2O_3	0.37	0.36	0.34	0.36	0.34	0.39	0.32	0.39
NiO	0.29	0.21	0.33	0.39	0.31	0.35	0.39	0.21

Table 13. (continued)

	9.	10.	11.	12.	13.	14.	15.	16.
Specimen no.	A-6	A-14	B-2	A-13	A-7	A-8	D2-2	D10-6
SiO_2	37.20	33.11	38.90	34.29	33.51	31.57	42.59	39.34
TiO_2		0.04						
Al_2O_3	1.94	0.0	0.90	1.88	1.01	0.0	0.41	0.61
Fe_2O_3	4.64	5.37	5.1	4.21	5.33	7.24	5.44	7.25
FeO	2.52	2.76	2.95	2.36	2.15	1.93	2.14	0.94
MnO	0.10	0.07	0.12	0.09	0.09	0.09	0.04	0.04
MgO	36.73	41.01	37.0	38.47	40.76	41.37	37.09	37.28
CaO	0.99	0.67	0.5	0.37	0.11	0.07	0.29	0.15
Na_2O	0.48	0.24	0.0	0.43	0.18	0.37	0.29	0.24
K_2O			0.0					
H_2O^-	2.30	1.59		2.03	2.12	1.99	0.86	2.08
H_2O^+	12.70	14.10	13.9	14.54	14.02	15.26	10.99	11.32
P_2O_5	0.06	0.07	0.0	0.08	0.04	0.07	0.07	0.05
Cr_2O_3	0.38	0.45	0.21	0.42	0.42	0.24	0.25	0.40
NiO	0.31	0.37	0.29	0.47	0.30	0.37	0.21	0.43

* Nos. 1 to 14 are AMSOC serpentinite.

Nos. 15 and 16 are serpentinite from Puerto Rico trench.

The analyses are arranged in the order of decreasing CaO for Nos. 1 to 14 and 15 and 16.

Nos. 1 to 10 and 12 to 14 from Hess and Otalora (1964).

No. 11: This study (see Appendix for petrographic data).

Nos. 15 and 16 from Bowin et al., (1966).

Blanks mean "smaller than 0.005 %".

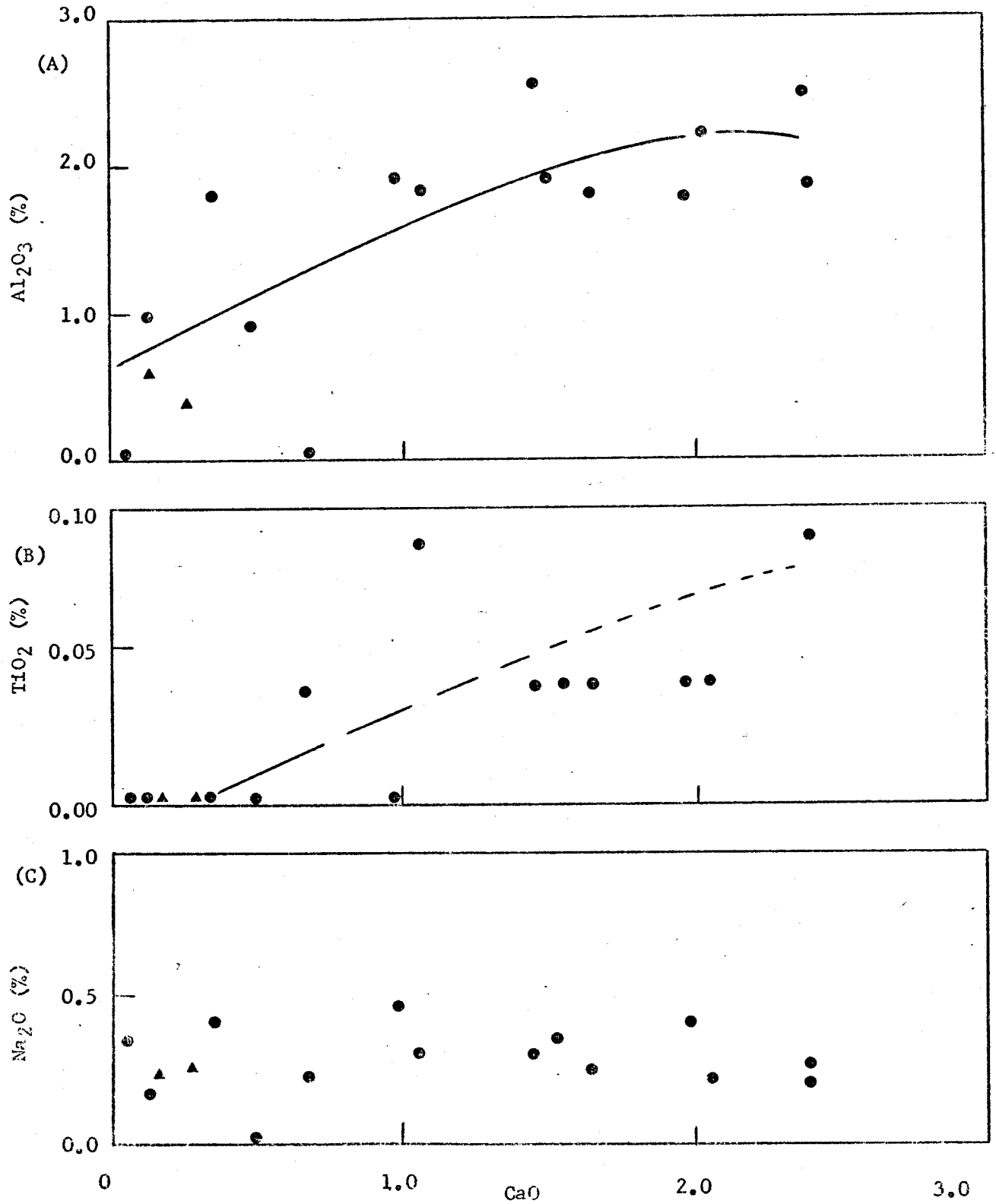

Figure 20 A-C. CaO versus Al_2O_3, TiO_2, and Na_2O relations in the serpentinites from the Bermeja complex (filled circle) and Puerto Rico trench (filled triangle).

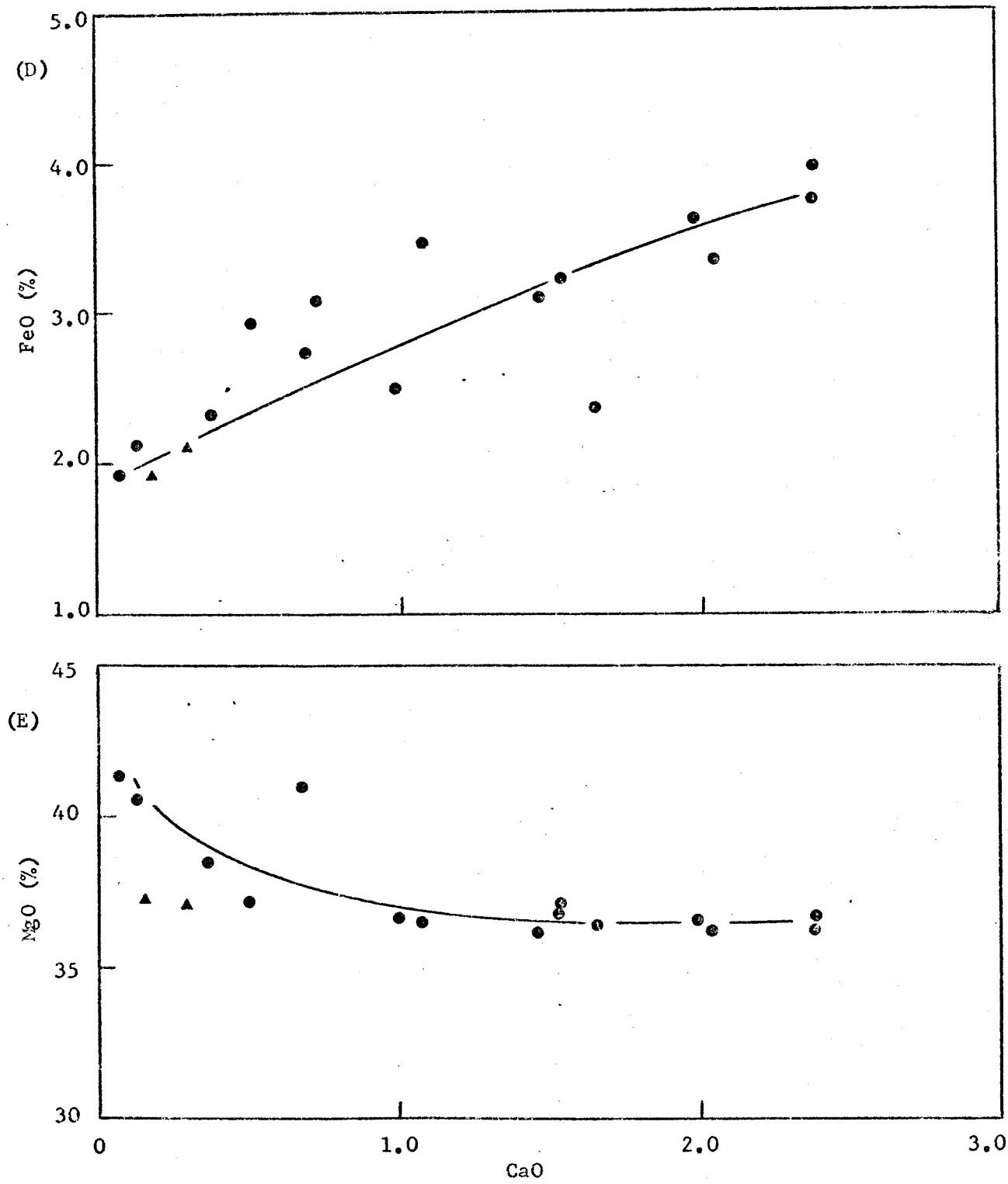

Figure 20D-E. CaO versus FeO and MgO relations in the serpentinites from the Bermeja complex (filled circle) and Puerto Rico trench (filled triangle).

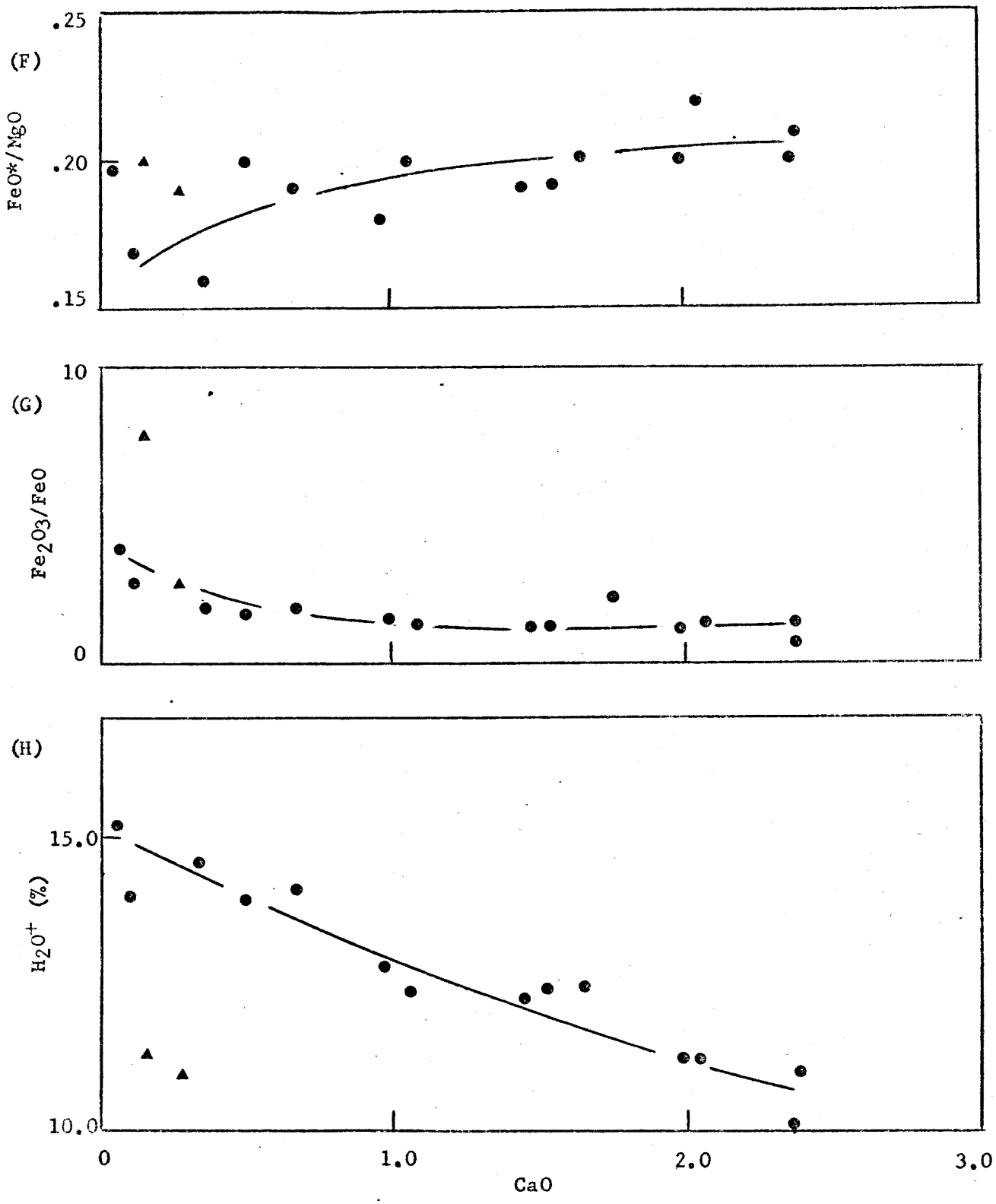

Figure 20 F-H. CaO versus FeO*/MgO and Fe_2O_3/FeO ratios and H_2O^+ content relations in the serpentinites from the Bermeja complex (filled circle) and Puerto Rico trench (filled triangle).

as shown in Figure 20B, but in a very irregular manner. The Na_2O content varies from 0.18 to 0.48 % by weight, except for sample No.11 (B-2), in which it was not detected. No correlation between Na_2O content and CaO content can be seen in Figure 20C. The FeO content decreases and the MgO content tends to increase with decreasing CaO content as shown in Figure 20D-E. Hence, the FeO/MgO ratio decreases with decreasing CaO content. Figure 20 F shows that the FeO*/MgO ratio also tends to decrease with decreasing CaO. The Fe_2O_3/FeO ratio is high, ranging from 0.9 to 3.8, and tends to increase with decreasing CaO (Figure 20G). Miyashiro (1966) recognized that serpentinites in metamorphosed regions are generally lower in this ratio than those in unmetamorphosed regions, showing a different degree of oxidation. The H_2O^+ content increases with decreasing CaO content as shown in Figure 20 H. Cr_2O_3, MnO, P_2O_5, and NiO are generally unchange with varying CaO content. In general, the new analyses of the core specimen fall well within the variation trends defined by the other 13 analyses of AMSOC serpentinite, on the low CaO side.

Two highly serpentinized peridotites from the north wall of the Puerto Rico trench, about 200 miles north northeast of the nearest exposed serpentinite bodies in the Bermeja complex, were also plotted in Figure 20A-H. Both analyses appear to have lower H_2O^+ contents than the AMSOC serpentinites having similar CaO content, as shown in Figure 20H, and higher SiO_2 content than all the analyses of the AMSOC serpentinites

Except for the H_2O^+ and SiO_2 contents, these two serpentinites from the trench are close to the average variation trends of the AMSOC serpentinite shown in the previous figures.

Although the AMSOC serpentinites are generally low in CaO and Al_2O_3 content, the highest contents of these constituents in the serpentinites are somewhat similar to the CaO and Al_2O_3 contents of the high temperature peridotite (Green, 1967) and the high calcium group of olivine nodules in basalts (Harris et al., 1967), both of which commonly are suggested as solid masses brought up from the upper mantle. Based on the recalculated water free average composition of the AMSOC serpentinites, Hess and Otalora (1964) suggested a chemical resemblance between these serpentinites and mantle material.

Serpentinites from the Mid-Atlantic Ridge (Miyashiro et al., 1969b) show chemical compositional trends similar to the AMSOC serpentinites, in that the Al_2O_3 content tends to decrease with decreasing CaO. A similar relationship also occurred in the relatively fresh peridotite from St. Pauls' Rocks (Tilley, 1947, 1966; Melson et al., 1967; Hess, 1955). In this case the positive correlation between Al_2O_3 and CaO contents may be regarded as representing heterogeneity in the mantle peridotite. The high-temperature peridotite intrusion in the Lizard area (Green, 1964) also shows a similar trend of chemical variation, but with a slightly higher Al_2O_3 content. Most of the AMSOC serpentinites as well as Mid-Atlantic Ridge serpentinites have lower CaO and

Al_2O_3 content, compared to the majority of the peridotites of St. Pauls' Rocks and the Lizard. Miyashiro et al., (1969b) regarded the decrease of CaO content accompanied by that of Al_2O_3 in these low CaO content serpentinites from the Mid-Atlantic Ridge to be ascribed partly to the removal of these components during serpentinization. Based on the petrographic observations of the analyzed AMSOC serpentinites (Mattson, 1964; Hess and Otalora, 1964), with the increasing serpentinization of the analyzed samples, the CaO content shows a tendency to decrease with the exception of my new analyses. Hence, the compositional variations with CaO content of the AMSOC serpentinite may be partly due to the various degrees of serpentinization. The occurrence of hydrogarnet (identified in X-ray pattern) in the brecciated serpentinite forming a light colored band in the serpentinites, probably represents the secondary enrichment of Al_2O_3 and CaO, extracted from the rocks during serpentinization. Therefore, the compositional variations of the serpentinite from the Bermeja complex and Puerto Rico trench are probably due mainly to chemical migration during serpentinization, but perhaps partly to heterogeneity of upper mantle peridotite from which the serpentinites were derived.

D. Geochemistry of the Trace Elements

1. Trace Element Distribution in the Basaltic Rocks of the Bermeja Complex

Analytical techniques and results using atomic absorption spectrometry and X-ray fluorescence have been discussed in detail in previous sections. Table 14 lists analytical results for Cr, Co, Ni, Cu, and Sr determined by atomic absorption, and for Mn and Zn as determined by X-ray. The precision of the analyses is shown in Table 5 expressed as the coefficient of variation. Comparative data for Cr, Ni, and Cu as determined by X-ray spectroscopy can be found in Tables 9A,C, and D.

In the previous section treating the major element chemistry, we have noted that there appear to be two groups of basaltic rock each having similar major element variation trends in the analyzed rocks from Bermeja complex. These trends show increasing total Fe, TiO_2, and P_2O_5, and decreasing MgO concentrations with increasing FeO*/MgO ratio. However, group I rocks (schistose amphibolite) have higher total iron, MgO, TiO_2, and P_2O_5, and lower Al_2O_3 than those of group II (massive metabasaltic dike, spilite, and amphibolitized dolerite) at equivalent FeO*/MgO ratios. The variation trend for the group I rocks is also better defined in the AFM diagram than that of group II. The SiO_2 contents range to higher values at lower FeO*/MgO ratios for group II than group I. Similar trends can also be observed in terms of the trace elements. In Figure 20A-B, Cr and Ni contents are plotted against FeO*/MgO ratio of the sample. For the amphibolite, dike rocks, and spilite, Cr and Ni decrease in concentration with increasing FeO*/MgO ratio. Overall, higher

Table 14. Trace Element Analyses of Rocks from the Bermeja Complex, Puerto Rico*.

	Sample number	FeO*/MgO	Cr	Mn	Co**	Ni	Cu	Zn	Sr
Schistose Amphibolite	1. 7717-85	1.33	310	1500	35	120	65	105	135
	2. Ba-8a-1	1.59	195	1610	27	95	25	125	100
	3. 7917-66	1.70	195	1810	28	85	25	125	85
	4. 7917-45	1.75	145	1660	27	80	55	120	60
	5. Ba-8a-4	1.78	110	1810	28	65	60	145	90
Massive Metabasaltic Dike	6. Ba-10	1.24	200	1360	38	95	85	75	155
	7. Ba-8b-2	1.39	170	1350	26	70	75	80	105
Spilite	8. Ba-1b	1.07	180	1350	33	90	50	60	90
	9. Ba-6	1.12	180	1310	33	95	70	65	115
	10. Ba-3	1.47	110	1310	42	80	60	75	85
Amphibolitized dolerite	11. Ba-7a	1.10	285	1280	35	105	65	60	215
Serpentinite	12. B-2		2000	970	53	2025	25	40	n.d.

* All results are in ppm. For precision, see Table included in the Experimental Results. Cr, Co, Ni, Cu, and Sr are determined by atomic absorption spectrometry. Mn and Zn are determined by X-ray spectrometry.

** For the contamination of Co, see the Analytical Methods and Experimental Results.

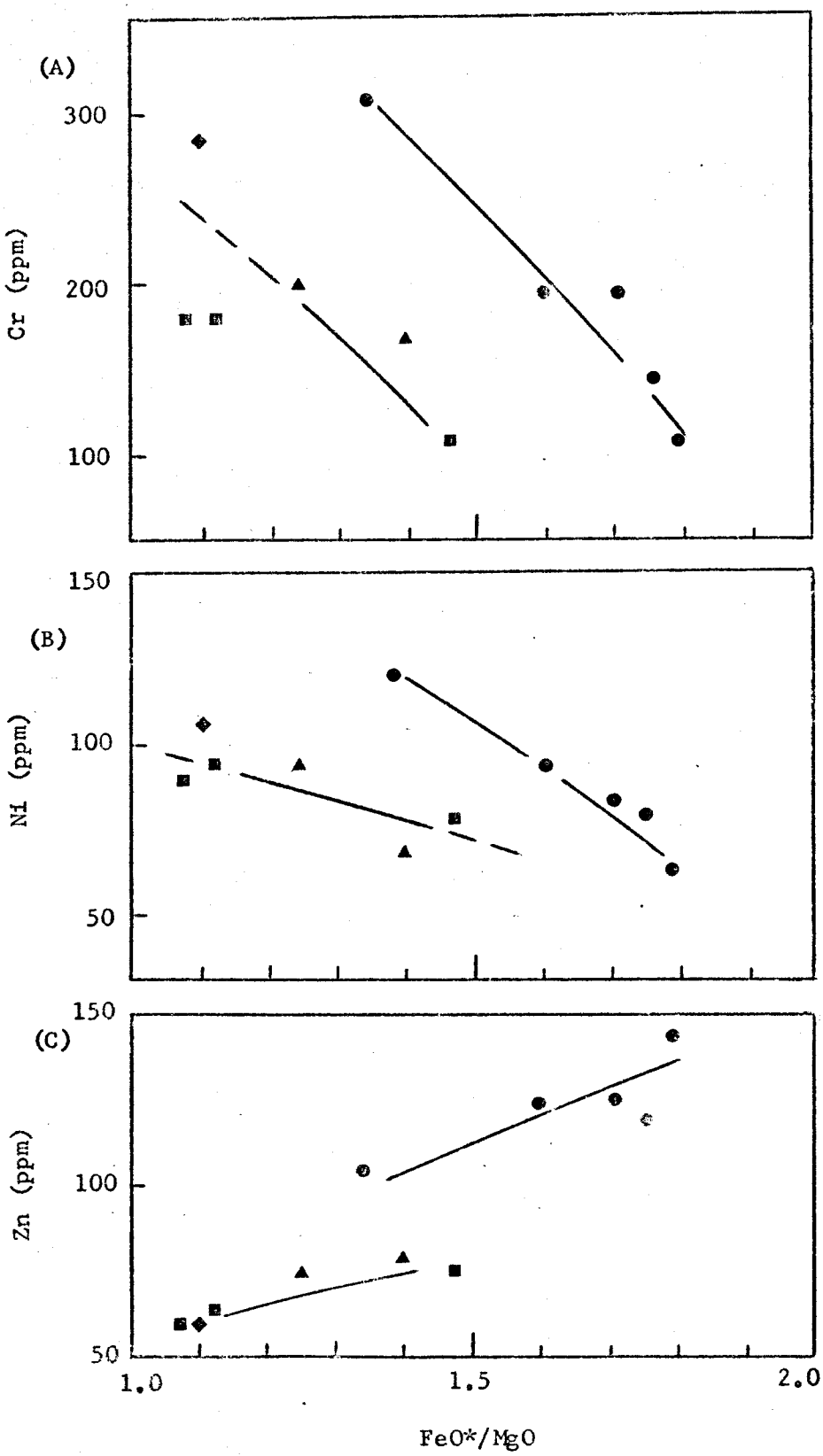

Figures 21 A-C. Changes of Cr, Ni, and Zn contents with FeO*/MgO ratio in the schistose amphibolite (●), massive metabasaltic dike (▲), spilite (■), and amphibolitized (◆) of the Bermeja complex.

concentrations of Cr and Ni are present in the trends defined by the amphibolite than those of the dike rocks and spilite. Moreover, the dike and spilite trends overlap and can be regarded as one trend; values for the amphibolitized dolerite appear related to this latter trend. Hence the analyzed basaltic rocks from the Bermeja complex appear to also consist of the same two group in terms Cr and Ni contents. Zn contents tend to increase with increasing FeO*/MgO ratio in terms of two groups, as shown in Figure 20C. The trends have a similar slope, however, group I has a higher Zn content than group II at a similar FeO*/MgO ratio. No distinctive trends are noted for Mn, Co, Cu, and Sr contents over the range of FeO*/MgO ratios possessed by either group. Overall, group I may be somewhat lower in Sr content compared to group II.

2. Discussion of the Significances of Cr and Ni Distribution in Basaltic Rocks from the Bermeja Complex

The large fractionation effects for Cr and Ni in basaltic rocks are generally considered to reflect the precipitation of the mineral olivine (Henderson and Dale, 1970; Gunn, 1971; Thompson et al., 1972). Hence, the observed variation trends of Cr and Ni in the basaltic rocks from the Bermeja complex may represent in some measure original features of the fractional crystallization (mainly of olivine) of their parental magma, if metamorphism and/or secondary processes had only minor effects on the distribution of these elements. During fractionation the Cr content in a magma

is apparently controlled by olivine crystallization, but to what extent this is influenced by inclusion of Cr-spinel in the olivine is still not clear. Gunn (1971) and Thompson et al., (1972) agree in a value for the partition coefficient K (olivine/liquid) of about 10 for Ni and 5 for Mg in oceanic basalts. The octahedral site preference of Ni over Mg is consistent with crystal field theory predication for the olivine lattice (Burns, 1970; Henderson and Dale, 1970). As shown in Figure 21 A-B, the slope of the FeO*/MgO - Cr distribution is identical in both groups of basaltic rocks from the Bermeja complex. However, the (FeO*/MgO) v.s. Ni trends for each group appear to have somewhat different slopes. Although not shown in the diagram, it is noted that the MgO - Cr trends for both groups have similar slopes, while these for MgO - Ni show distinctly different slopes. The steep slope of group I indicates a higher rate of decrease in Ni content with decreasing MgO (MgO/Ni $\approx$ 240) than the gentle slope of group II (MgO/Ni $\approx$ 400). A possible explanation is that in group II, Ni and Mg contents may be influenced or controlled by two crystallizing phases, olivine and clino - pyroxene, the latter having a markedly lower Ni/Mg ratios.

In a silicate melt, Ni and Cr may be fractionated by crystallization of olivine and clinopyroxene. In Figure 22A, the Ni contents and Cr/Ni ratios of individual samples are normalized relative to the sample in each group of basaltic rocks of the Bermeja complex with the highest Ni content (7717-85 and Ba-7a from groups I and II, respectively).

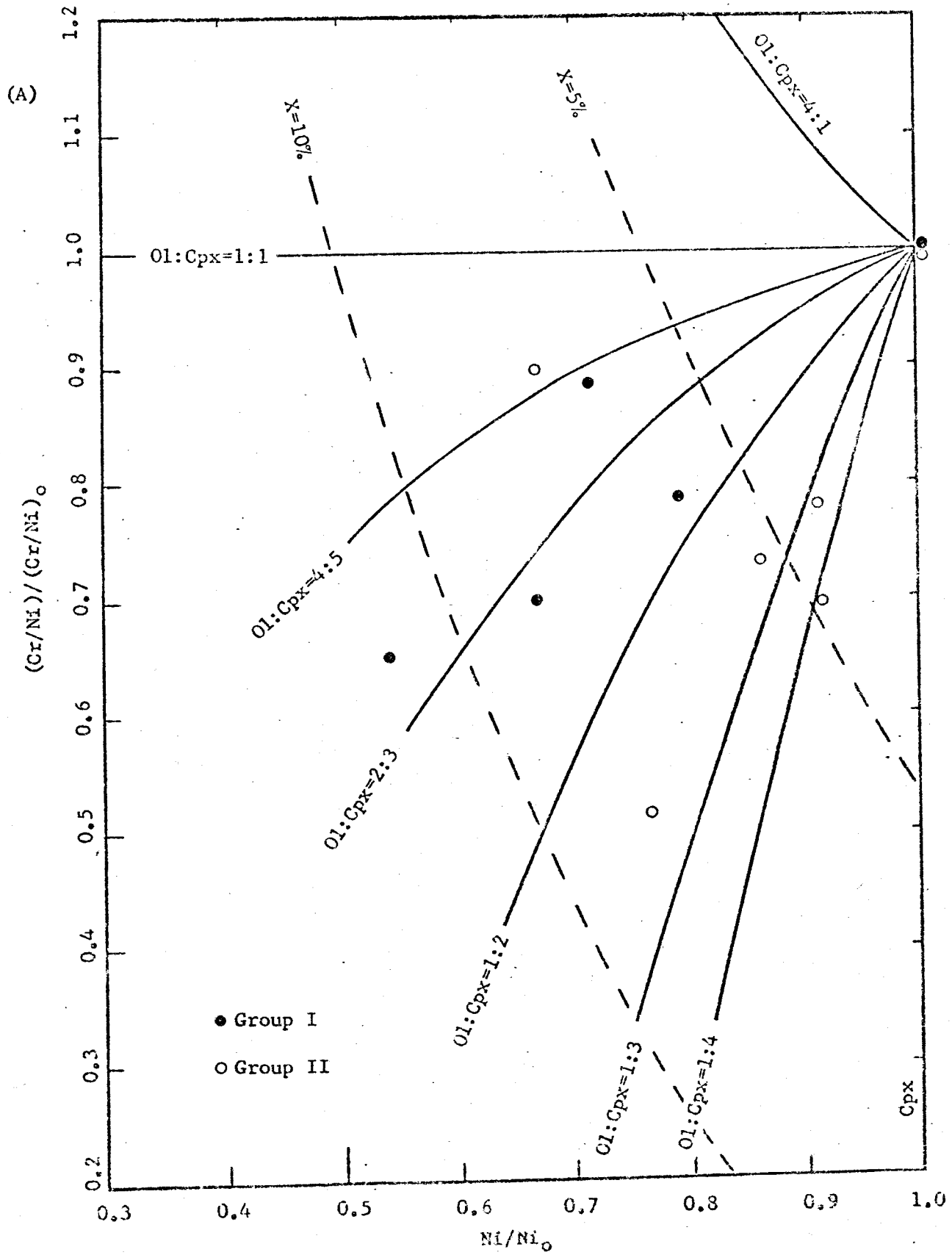
(A)
(Cr/Ni)/(Cr/Ni)o
Ni/Nio
X=10%
X=5%
Ol:Cpx=4:1
Ol:Cpx=1:1
Ol:Cpx=4:5
Ol:Cpx=2:3
Ol:Cpx=1:2
Ol:Cpx=1:3
Ol:Cpx=1:4
Cpx
Group I
Group II
1.2
1.1
1.0
0.9
0.8
0.7
0.6
0.5
0.4
0.3
0.2
0.3
0.4
0.5
0.6
0.7
0.8
0.9
1.0

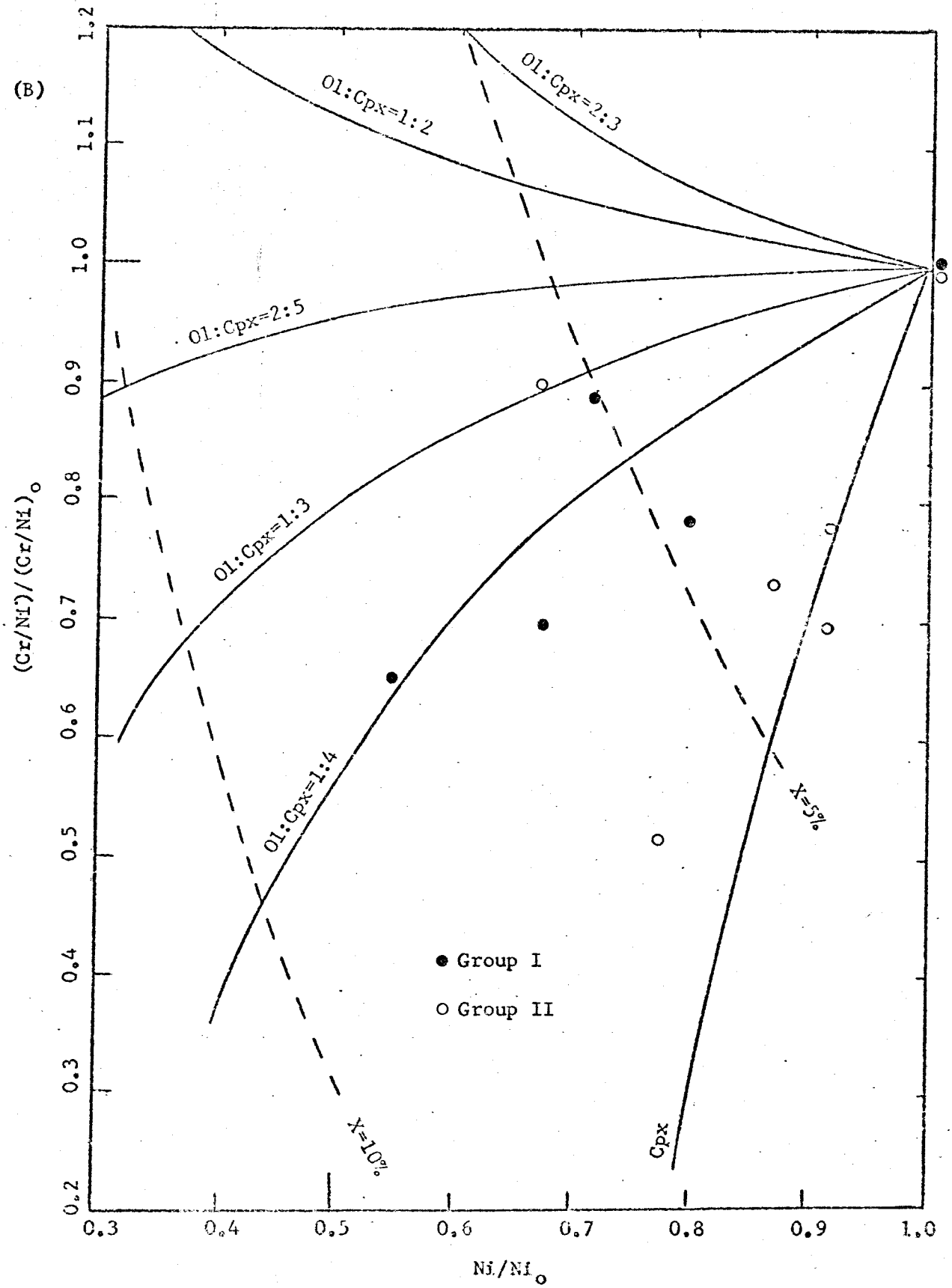
(B)
Ol:Cpx=1:2
Ol:Cpx=2:3
Ol:Cpx=2:5
Ol:Cpx=1:3
Ol:Cpx=1:4
X=10%
X=5%
Cpx
Group I
Group II
(Cr/Ni)/(Cr/Ni)o
Ni/Ni o
0.2
0.3
0.4
0.5
0.6
0.7
0.8
0.9
1.0
1.1
1.2

Figure 22 A-B: Cr/Ni vs. Ni for metabasaltic rocks of the Bermeja complex (normalized to sample of highest Ni content in each group). Filled circle = Group I: schistose amphibolite. Open circle = Group II: massive metabasaltic dike, spilite, and amphibolitized dolerite. Solid curves are calculated fractional crystallization trends based on simple mass balance relations. Broken curves are the percentages of crystallization (X = 5 to 10%). The partition coefficients used in Figure A and B are $D_{Cr}^{1/ol} = 1.0$, $D_{Ni}^{1/ol} = 0.1$, $D_{Cr}^{1/cpx} = 0.1$, and $D_{Ni}^{1/cpx} = 1.0$ and $D_{Cr}^{1/ol} = 1.0$, $D_{Ni}^{1/ol} = 0.06$, $D_{Cr}^{1/cpx} = 0.1$, and $D_{Ni}^{1/cpx} = 0.3$, respectively.

Based on simple mass balance relations comparison curves showing fractional crystallization behavior are constructed to show the effect of crystallization of olivine and clinopyroxene and various combinations of the two. For the elements Cr and Ni, the depletion or enrichment of Ni and the decrease or increase of the Cr/Ni ratio in the residual liquid are given by the relations:

$$Ni/Ni_o = (1-x/D_{Ni}^{l/ol}-y/D_{Ni}^{l/cpx})/(1-x-y)$$

$$(Cr/Ni)/(Cr/Ni)_o = (1-x/D_{Cr}^{l/ol}-y/D_{Cr}^{l/cpx})/(1-x/D_{Ni}^{l/ol}-y/D_{Ni}^{l/cpx})$$

where x = weight fractionation of olivine that crystallized;

y = weight fractionation of clinopyroxene that crystallized;

$D_a^{l/xtal}$ = liquid/crystal partition coefficient for element a;

The subscript "o" designated the initial concentration or ratio in the liquid.

Using the liquid/solid partition coefficients adopted by Gast (1968; $D_{Cr}^{l/ol} = 1.0$, $D_{Ni}^{l/ol} = 0.1$, $D_{Cr}^{l/cpx} = 0.1$, and $D_{Ni}^{l/cpx} = 1.0$) it is noted from Figure 22A that the crystallization of olivine and clinopyroxene in proper proportions can imitate the Ni - Cr/Ni depletion observed in the two groups of rocks, and usually less than 10 percent crystallization of these two minerals. Under the assumed conditions, group I would generally require crystallization of a lesser proportion of clinopyroxene than group II. Curves calculated with an alternate set of Ni partition coefficients ($D_{Ni}^{l/ol} = 0.06$, $D_{Ni}^{l/cpx} = 0.3$) gave the results shown in Figure 22B.

These latter calculations suggest a higher proportion of clinopyroxene and a smaller percentage of crystallization (less than 8 %) than those shown in Figure 22A.

Other values of the assumed partition coefficients and the presence of other mineral phases that might be involved in Cr - Ni crystal fractionation (especially spinel) are conceivable, of course, but the main point here is to show that it is possible that some of the basaltic rocks of the Bermeja complex could have been derived(relative to rocks representing the most Ni - Cr enriched types of each group) by only a small degree of crystallization of olivine and clinopyroxene in reasonable proportions, as far as Ni and Cr are concerned. If this mechanism was operative for the basaltic rocks of the Bermeja complex in general, then it is likely that group II was more influenced or controlled by clinopyroxene crystallization than was group I.

3. Discussion of the Application of Trace Element Distribution Data to the Petrogenesis of the Bermeja Complex

In terms of major elements, the basaltic rocks from the Bermeja complex are tholeiitic in character, but whether these particular metamorphosed tholeiitic rocks originated at a mid-oceanic ridge or in an island arc setting is still not conclusively shown. In the past some authors have stated that there were some consistent differences between the mid-ocean and island arc tholeiites, especially in terms of trace

element distribution. Jakes and Gill (1970), for example, concluded that island arc volcanics are distinctively low in Ni and Cr concentrations, compared with those in the abyssal tholeiites at any given silica content. The distribution fields of Cr and Ni concentrations in abyssal tholeiites from the Mid-Atlantic Ridge, continental margin and island arc volcanics from the calc-alkalic series of New Zealand and Japan, calc-alkalic and tholeiitic series rocks of Hakone, Japan, and the calc-alkalic series of northern Chile are shown in Figures 23A-B, respectively. In these figures, the Cr and Ni concentrations of the volcanic rocks generated at two different environments tend to decrease with increasing FeO*/MgO. The Cr and Ni concentrations in the abyssal tholeiites from the Mid-Atlantic Ridge are high (about 140 to 800 ppm and 70 to 250 ppm, respectively), compared to the majority of the island arc and continental margin volcanics. Moreover, practically all the abyssal tholeiites have FeO*/MgO ratios smaller than 2.0. However, if volcanic rocks from island arcs and continental margins with FeO*/MgO ratios smaller than 2.0 are compared with abyssal tholeiites, the two groups of rocks overall would show similar Cr andNi contents. Therefore, the negative correlation trends shown in both figures for the abyssal tholeiites and island arc and continental margin volcanics are apparently continuous and widely overlap at low FeO*/MgO ratios. In fact, it may be that the composition fields for the abyssal tholeiites are completely included in those of

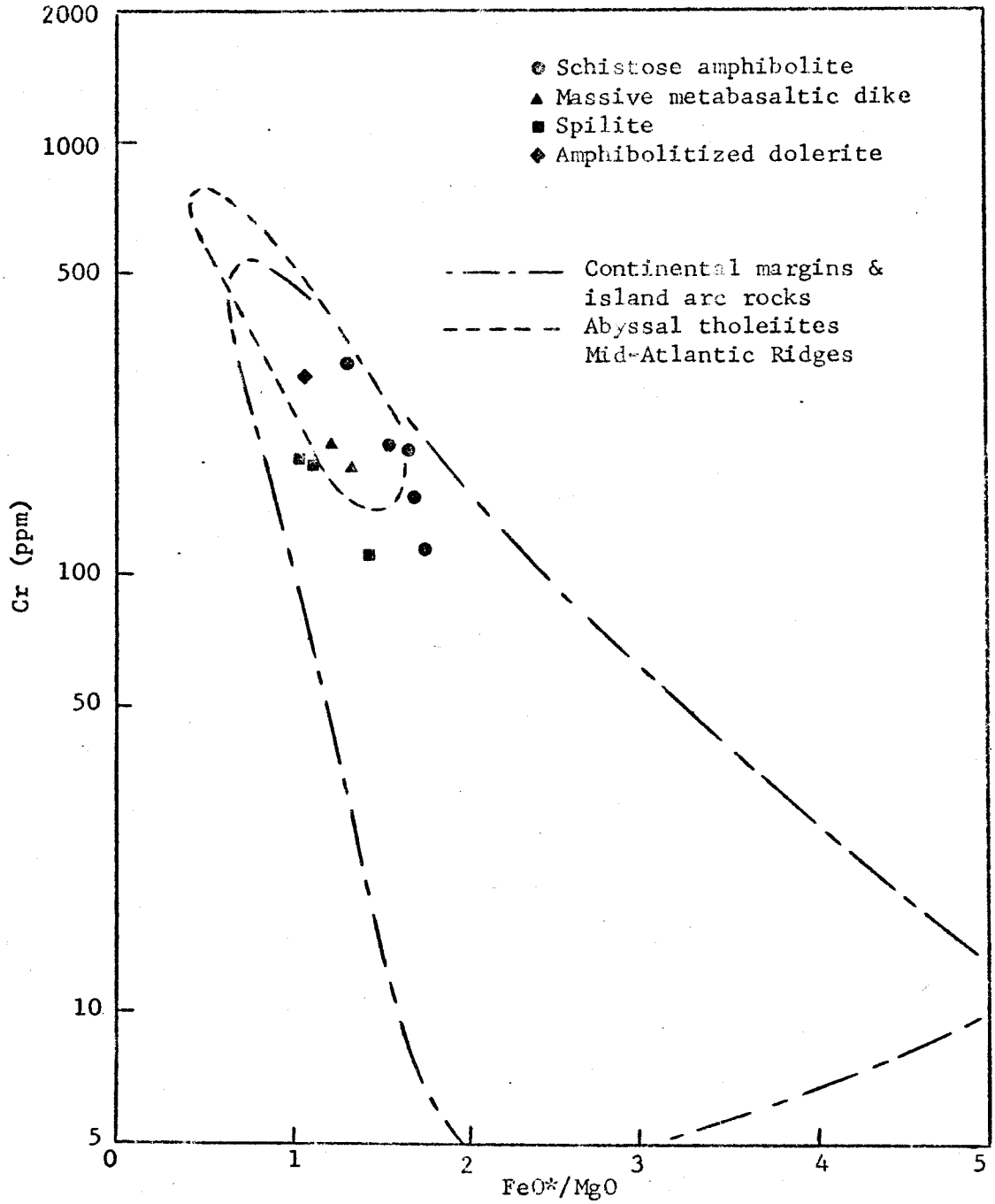

Figure 23A. Cr against FeO*/MgO ratios for the abyssal tholeiites from the mid-Atlantic ridge, the continental margins and island arc volcanics from calc-alkalic series of New Zeland and Japan, Hakone calc-alkalic and tholeiitic series, and calc-alkalic series of northern Chile, and the Bermeja complex.

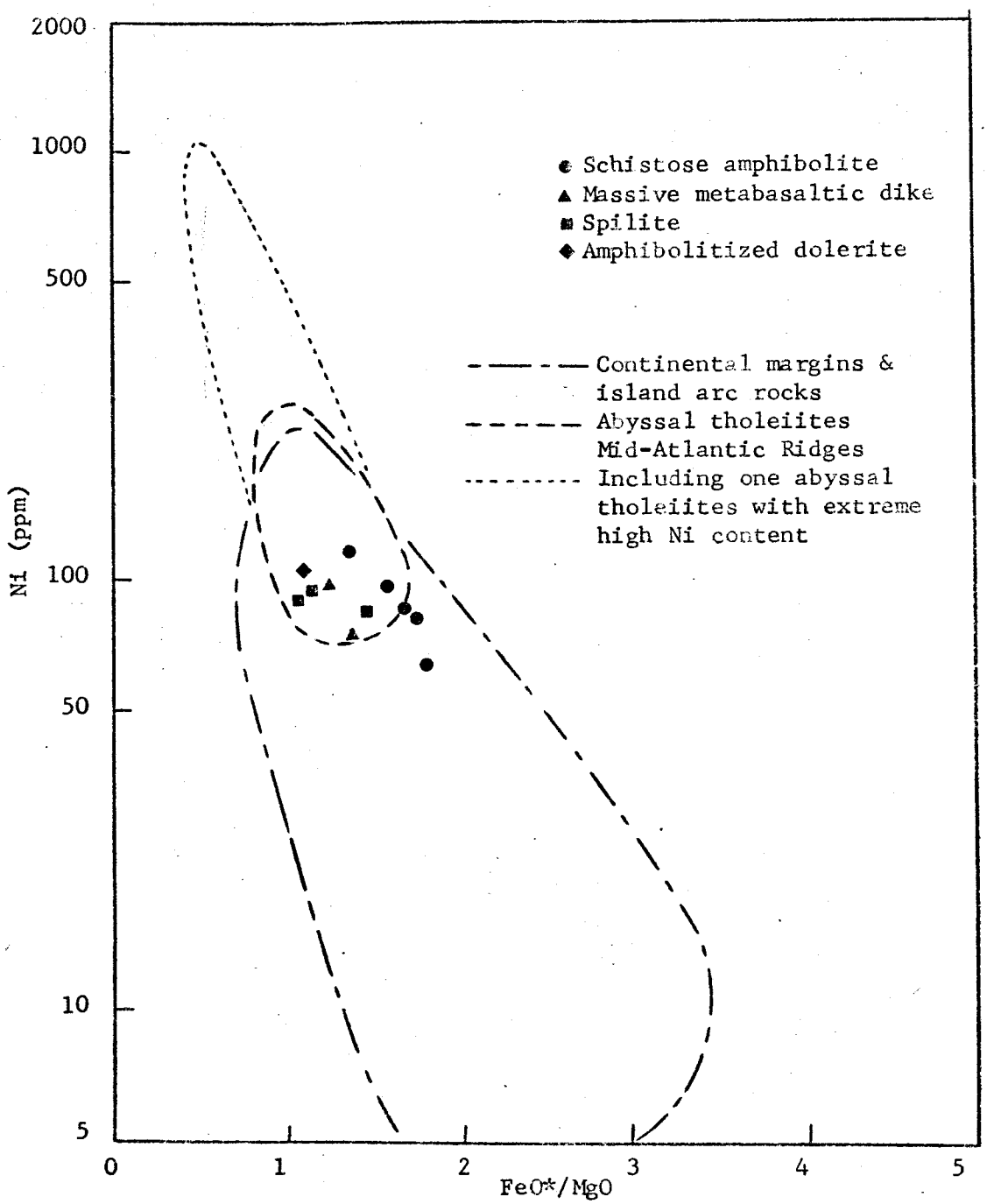

Figure 23B. Ni against FeO*/MgO ratios for the abyssal tholeiites from the mid-Atlantic ridge, the continental margins and island arc volcanics from calc-alkalic series of New Zeland and Japan, Hakone calc-alkalic and tholeiitic series, and Calc-alkalic series of northern Chile, and the Bermeja complex.

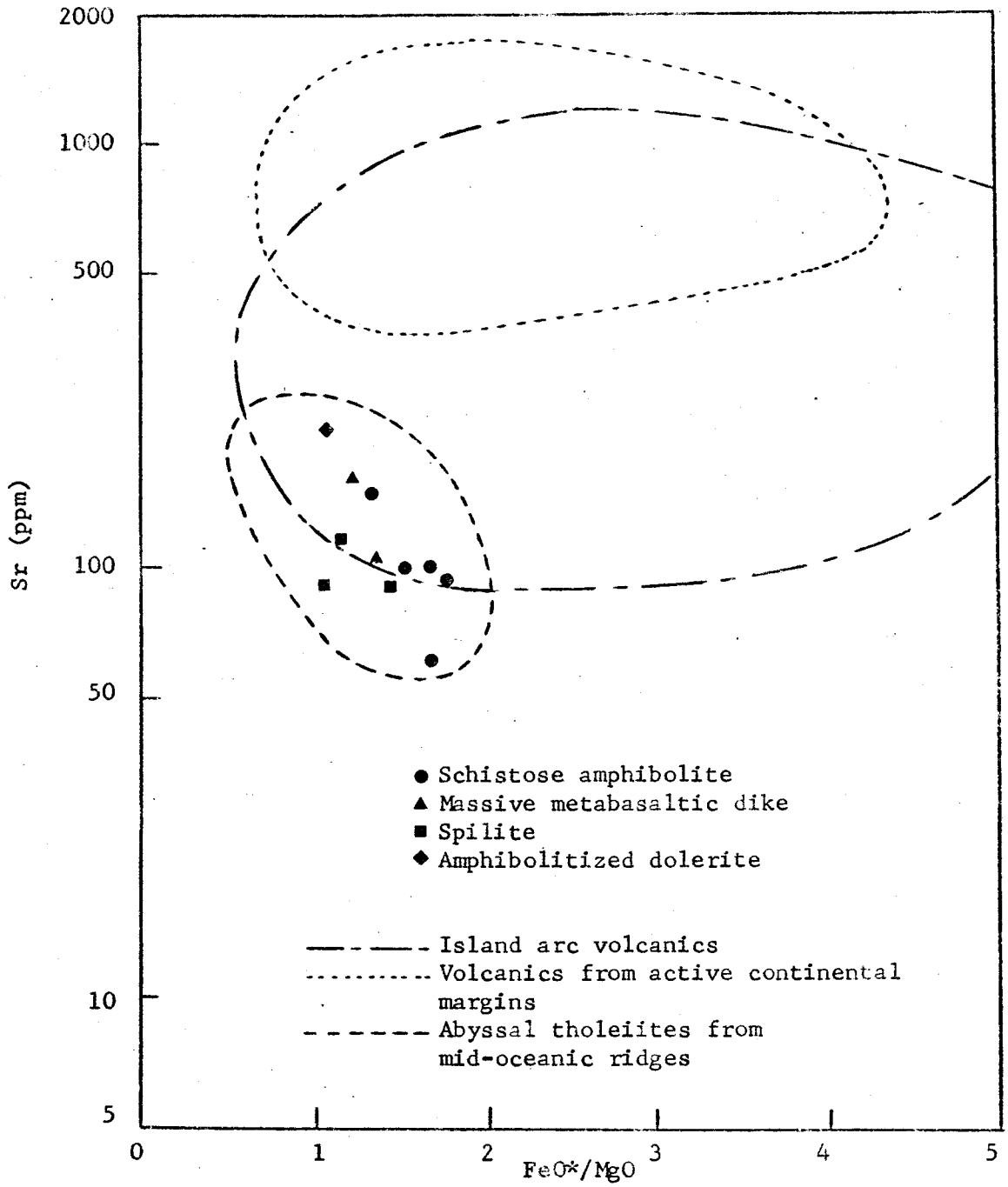

Figure 23C. Sr against FeO*/MgO ratios for the abyssal tholeiites from mid-oceanic ridges, volcanics from active continental margins, island arc volcanics, and the Bermeja complex.

the island arc volcanic rocks. In actuality, the majority of volcanic rocks in island arcs and continental margins have FeO*/MgO ratios higher than 1.5, while most abyssal tholeiites have a FeO*/MgO ratio smaller than 1.5. Thus, a comparison of randomly selected samples of island arc volcanics and abyssal tholeiites commonly leads to finding of compositional differences related to different FeO*/MgO ratios instead of true differences between the two groups of rocks where FeO*/MgO ratios are the same. The Cr and Ni contents tend to be lower at higher FeO*/MgO ratios in island arc and continental margin volcanics, therefore, Cr and Ni contents are not promising for distinguishing volcanic rocks of island arcs and continental margins from abyssal tholeiites, particularly when the FeO*/MgO ratio of the rock is low and the concentrations of these trace elements are high. The Cr and Ni contents in the analyzed basaltic rocks from the Bermeja complex are plotted against FeO*/MgO ratios in Figures 23A-B, respectively. Most analyses of these rocks fall in the common composition field of abyssal tholeiites and island arc volcanics, with FeO*/MgO ratios in the range 1.0 to 1.8. Thus, for the reasons discussed above, Cr and Ni contents are not diagnostic in indicating the origins of the parental rocks for these particular metamorphosed tholeiitic rocks from the Bermeja complex.

In Figure 23C, the distribution fields of Sr concentrations in abyssal tholeiites from mid-oceanic ridge, volcanics from active continental margins, and island arc

volcanics are shown. Although the Sr content of abyssal tholeiites is generally lower than that in the island arc volcanics, the composition field for both rock types overlap. The Sr contents of basaltic rocks from the Bermeja complex range from 60 to 215 ppm and fall within the composition field of the abyssal tholeiite. However, eight out of the eleven analyses of these basaltic rocks are also included in the composition field of the island arc volcanics, although the limited published analyses of the island arc volcanics with low-Sr content in this range are rare. Therefore, it appears, on the basis of the Sr content, that the basaltic rocks from the Bermeja complex are more similar to the abyssal tholeiites than island arc volcanics. However, this is not conclusive.

V. SECULAR COMPOSITIONAL CHANGES OF THE VOLCANIC ROCKS IN PUERTO RICO AND OTHER ISLANDS IN EASTERN WEST INDIES AND THE SIGNIFICANCE OF THE BERMEJA COMPLEX

The association of the radiolarian chert, serpentinized peridotite, pillow lava, and metamorphosed tholeiitic rocks of the Bermeja complex was considered as an ophiolite assemblage by some authors (Hess, 1960; 1964; Donnelly, 1971; Mattson, 1973a, b), who suggested that this ophiolitic complex is a fragment of oceanic crust and the underlying upper mantle which was created at a mid-oceanic ridge. In the past decade, the ophiolite problem has played an important role in the interpretation of tectonic history in relation to sea-floor spreading and plate tectonics. Therefore, it is important to find evidence to support or disprove the existing hypothesis of the "ophiolite association" of the Bermeja complex. On the basis of major element analyses from the literature and new major and trace element analyses presented here for the metabasaltic rocks from the Bermeja complex, the interpretation discussed in the previous sections have led to an undecisive conclusion. The mode of origin of oceanic crust of the Bermeja complex is, therefore, neither proved nor disproved by our discussion at this step. However, in this section, we will examine the compositional variations of the volcanic rocks of pre-Middle Cretaceous to Tertiary age, from the thick island arc

volcanic pile in the central belt of Puerto Rico and in other islands in the eastern West Indies, for their significance regarding the genesis of the Bermeja complex. It will be shown that the Puerto Rican volcanic pile and volcanics from the eastern West Indies as a whole have a regular pattern of island arc volcanism, with a gradual variation in composition with time and stratigraphic level, whereas the metabasaltic rocks from the Bermeja complex show a very close resemblance to the earliest tholeiitic rocks generated in the span of island arc evolution or to the oceanic crust.

A. Compositional Variation of Island Arc Volcanic Rocks

Three rock series can be chemically distinguished for the volcanic rocks of island arcs, tholeiitic, calc-alkalic, and alkalic series (Nockolds and Allen, 1953; 1954; 1956; Kuno, 1959; Miyashiro, 1972, 1973b, in press). However, the distinctions between the series and their mutual relationships in space and time have not been agreed upon among previous works. It has been recognized nevertheless that, in a well developed island arc, the rock series follow a regular pattern of variation in composition across the arc, that is, tholeiitic rocks occur on the oceanic or trench side, followed inland by calc-alkalic and alkalic rocks (Jakes and White, 1971; Miyashiro, 1972). Jakes and White (1969), Gill (1970), and Jakes and White (1971, 1972) noted that there is a variation in composition with time and

stratigraphic level in rock series of the island arcs. The rocks generated in the earliest stage are tholeiitic, varying widely in SiO_2 content (Baker, 1968; Jakes and Gill, 1970; Jakes and White, 1971, 1972), usually including basalts and basaltic andesite of the tholeiitic series. In later stages of island arc evolution, calc-alkaline rocks are erupted along with tholeiitic rocks. Joplin (1964) and Jakes and White (1969, 1971, 1972) considered that the "shoshonitic association", appearing with tholeiites and calc-alkaline rocks, is the latest stage of the arc magma evolution. However, Miyashiro (in press) recognized that the rocks of the alkalic series are abundant only in arcs subject to a very slow rate of plate convergence. The high-K shoshonitic rocks in Puerto Rico and Fiji are suggested to be the products of magmatism related to the spreading episodes behind the arc, instead of an inherent stage in island arc magma evolution (Donnelly, 1973).

Although it is difficult to generalize about true distribution of rock types in island arcs, former workers suggested that the lower or earliest parts of island arcs, may be built mainly of rocks of the tholeiitic series, whereas the higher or later stratigraphic levels of island arcs are composed mainly of rocks of the tholeiitic and calc-alkalic series. Jakes and White (1971) suggested that the whole island arc crust has a primary stratification with respect to K, Rb, Ba, Sr, REE, SiO_2, FeO/MgO, and K_2O/Na_2O resulting from such stratigraphical variations.

B. The Characteristics of Tholeiitic, Calc-alkalic, and Alkalic Series

In the study of the Hawaiian basaltic rocks, MacDonald and Katsura (1964) used a alkali-silica diagram to distinguish tholeiitic and alkalic series rocks. The proposed boundary line in this diagram is useful in the recognition of the alkalic and non-alkalic rock series, where the alkali contents in the rocks are not subjected to changes through any secondary processes.

The distinction between the tholeiitic and calc-alkalic series can be based on critical differences in some chemical features. In FeO^*/MgO - SiO_2 diagram, a typical tholeiitic trend (such as the Skaergaard intrusion) shows that the SiO_2 content remains nearly constant or even decreases slightly during the early stage of fractional crystallization of the magma. The average trend of fractional crystallization for abyssal tholeiites from mid-oceanic ridges is a nearly horizontal line on a FeO^*/MgO - SiO_2 diagram (Miyashiro et al., 1970; Shido et al., 1971). In other tholeiitic magmas, the SiO_2 contents increase slowly with increasing FeO^*/MgO ratios, as represented by curves with gentle slopes in the FeO^*/MgO - SiO_2 diagram, while the SiO_2 contents of the magmas of the calc-alkalic series increase more rapidly with increasing FeO^*/MgO ratios, and are represented by curves with steeper slopes. A dividing line, passing through two points, (FeO^*/MgO = 0.5 and SiO_2 = 46 %) and

(FeO*/MgO = 3.0 and SiO_2 = 62 %), in the FeO*/MgO - SiO_2 diagram (see Figure 26), was proposed by Miyashiro (1973, in press), with the tholeiitic and calc-alkalic series having gentler and steeper slopes, respectively, than this dividing line. The position of Miyashiro's dividing line is arbitrary, however, probably all the magmatic trends showing FeO* enrichment in the early stage of crystallization will be classed in the tholeiitic series. For the FeO*/MgO ratios greater than 2.0, the rocks falling on the lower and the upper side of the dividing line are generally regarded as belonging to the tholeiitic and calc-alkalic series, respectively.

The tholeiitic series is also characterized by an enrichment in FeO* reaching a maximum during fractional crystallization, while the calc-alkalic series shows a monotonic decrease of FeO*. Therefore a dividing curve can also be established on a FeO*/MgO - FeO* diagram (see Figure 26). Generally, the higher a rock series lies on the FeO*/MgO - SiO_2 diagram, the lower the same series tends to lie on the FeO*/MgO - FeO* diagram.

The change of TiO_2 during fractional crystallization also contrasts the two rock series. Typical tholeiitic magmas show enrichment in TiO_2 reaching a maximum with increasing FeO*/MgO ratios, whereas typical calc-alkalic magmas show decreasing TiO_2 contents. As will be mentioned later, the Cretaceous volcanic rocks in the central belt of Puerto Rico have been subjected to more or less low grade

metamorphism, during which migration of elements in the rock might have taken place. However, the FeO*, MgO, SiO_2, and TiO_2 contents usually suffer relatively little change during metamorphism and other secondary processes. Therefore the above relations are particularly useful in the study of the compositional variation of the metabasaltic rocks of the Bermeja complex and the Cretaceous volcanic rocks in Puerto Rico.

C. Stratigraphy and Composition of Pre-Middle Cretaceous to Late Tertiary Volcanic Rocks of Puerto Rico and Other Islands of the Eastern West-Indies

A location map of the eastern West Indies is shown in Figure 24. The principal references on the stratigraphy of Puerto Rico and other islands of interest here are Kaye (1959), Berryhill et al., (1960), Mattson (1960), Briggs and Gelabert (1962), Donnelly (1966), Robson and Tomblin (1966), Mattson (1967), Pease (1968), McIntyre et al., (1970), Donnelly (1970), and Seiders (1971). In this section, I restrict the stratigraphic discussions to the formations for which chemical data are available from the literature.

About 120 chemical analyses of Middle Cretaceous to Early Tertiary volcanic rocks of Puerto Rico and about 40 analyses of Mid-Cretaceous to Late Tertiary volcanic rocks from other islands in the eastern West Indies were examined (Kayes, 1959; Mattson, 1960; Lidiak, 1965; Jolly, 1970;

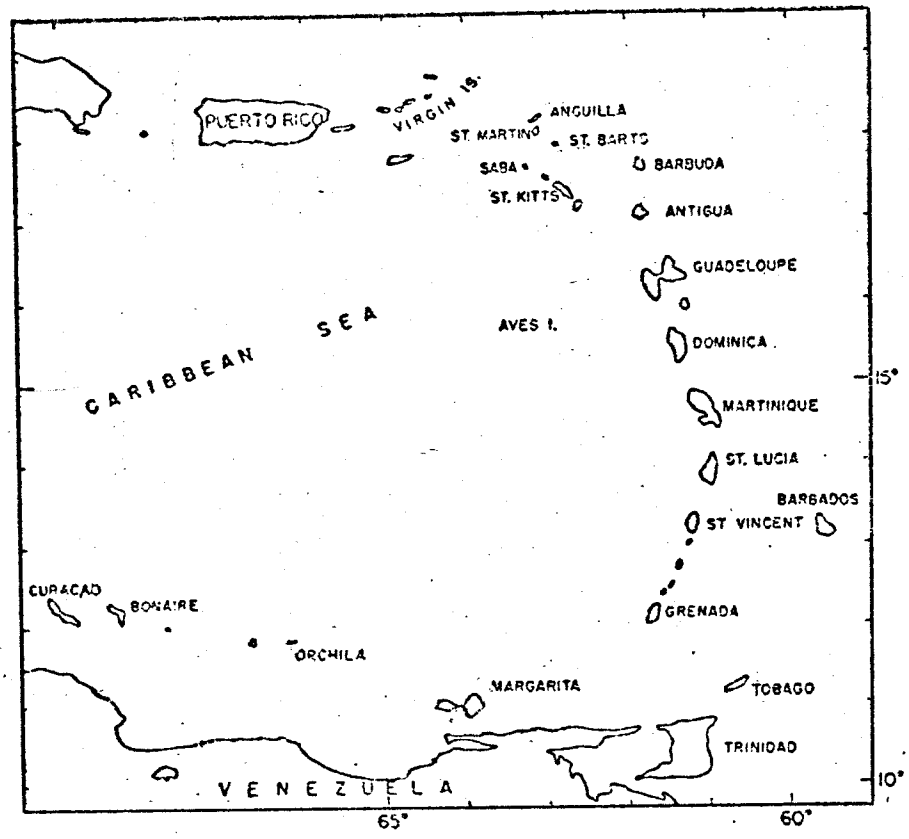

Figure 24. Location map showing the Eastern West-Indies.

Donnelly, 1971; Jolly, 1971). The stratigraphic distribution of these analyses is shown in Table 15.

The Water Island Formation of the Virgin Islands is considered by Donnelly (1966) to be the stratigraphically lowest group of volcanic rocks in the eastern West Indies. It consists of flows, with minor non-explosive pyroclastic material, and was subjected to deuteric processes modified by later, low-grade metamorphic effects (Donnelly, 1966, 1971). An age of pre-Albian was assigned to this formation, although a precise age has not been determined. In the Virgin Islands, the Water Island Formation is terminated by an angular unconformity. This formation was suffered by extensive but not universal low-grade metamorphism (Donnelly, 1966). In central Puerto Rico, the apparent temporal equivalent of the Louisenhoj Formation of the Virgin Islands is the thick Pre-Roble Formation, which is dominantly middle Cretaceous (Albian to Cenomanian) in age. The principal volcanic unit of the Pre-Robles is an augite-andesite breccia. A precise age for the Cerro Gordo and Santa Olaya Formations is in doubt. However, some of these rocks appear to underlie strata of Albian age, and are regarded as Pre-Albian in age (Lidiak, 1970). Flows and pyroclastics of porphyritic basalt, andesitic basalt, and andesite are the main compositional types for these rocks. Unconformably overlying the Pre-Roble is a group of middle Cretaceous volcanic rocks of the Roble Formation and the apparently coeval Rio Orocovis group. These formations may range approximately from Albian

Table 15. Sources and numbers of chemical analyses of Middle Cretaceous to Late Tertiary volcanic rocks from Puerto Rico and other islands in eastern West Indies.

Location	Age	Formation	Kaye (1959)	Mattson* (1960)	Lidiak** (1965)	Jolly (1970)	Donnelly (1971)	Jolly (1971)	Total
Lesser Antilles	Late Tertiary	(LA)					15		15
Puerto Rico	Late Cretaceous to Early Tertiary	Figuera (Fi)	2		4		1		7
		Rio de la Plata			4				4
		Blacho					1		1
	Albian to Santonian(?)	Mayaguez (Mg)		2					2
		Rio Loco (RL)		6					6
		Rio Orocovis (RO)			37		5		42
		Roble (Rb)				14	2	8	24
	Pre-Albian to Cenomanian(?)	Santa Olaya (SO)			15		2		17
		Cerro Gordo (CG)			6		1		7
		Pre-Roble (PR)					2		2
St. Thomas & St. John	Pre-Albian to Cenomanian(?)	Louisenhoj (Lj)					3		3
		Water Island (WI)					26		26

* Rocks from south-western Puerto Rico
** 59 of 66 analyses are partial chemical analyses.

to Santonian in age, although there may be some age overlap between them and the Pre-Roble. Rocks of this age crop out in north-central and central Puerto Rico, and consist of lavas (largely pillow lavas), augite andesite breccias, and wackes and other sedimentary rock types. The Perchas and Los Negros units of the Rio Orocovis Formation consist of porphyritic augite flows, tuffs, and breccias of basalt and basaltic andesite composition. The Avispa unit of the Rio Orocovis shows essentially continuous chemical variation from basaltic andesite to rhyodacite. The Roble Formation essentially consists of augite andesite. Many of the lava units (Roble and Rio Orocovis Formations) of this age, including the Lapa Lava, Avispa Lava, and Perchas Lava, are characterized by high potassium contents. Burial has incipiently metamorphosed to low grades many of the rocks of this age which has resulted in element redistribution to varying degree (Lidiak, 1965; Jolly, 1970). Following this interval, a variety of andesite and dacitic igneous types were erupted during the Latest Cretaceous to Early Tertiary time. These include the Blacho and Rio de la Plata Formations, and Figuera Volcanics. Basalts are very subordinate in the eruptives of this period.

In southwestern Puerto Rico, the Cenomanian to Turonian Rio Loco Formation (Mattson, 1960), lies unconformably upon the Bermeja complex. It consists of essentially bronzite andesite porphyry lavas (more than half with pillow forms), and subordinate tuff and breccia. A volcanic-sedimentary

rock group resting conformably upon the Rio Loco or unconformably the Bermeja complex is known as the Mayaguez group in southwestern Puerto Rico (Mattson, 1960). The age of this group probably ranges from Turonian or Santonian to Maestrichtian. The volcanic rocks in this group consist of basalt porphyry lavas and andesite breccia.

The volcanic-sedimentary sequence of Puerto Rico has been intruded at several times in the Late Cretaceous and Eocene by varied plutonic complex which range petrographically from olivine gabbro through diorite and tonalite and granodiorite and quartz monzonite. Associated dike rocks are dominantly hornblende and pyroxene andesite and diabase. These intrusive plutonic rocks are excluded from our present discussion.

In the Lesser Antilles, with a few exceptions the oldest volcanic rocks are Eocene in age. The Miocene to Recent volcanic rocks are dominantly hypersthene andesite with lesser amounts of hornblende-andesite, dacite, and basalt (Robson and Tomblin, 1966; Donnelly, 1971).

As mentioned above, many of the Late Cretaceous volcanic rocks appear to have been subjected to weak burial metamorphism. As a result, Na and K may have migrated to a considerable extent during the metamorphism. Hence, the alkali contents cannot be safely included in the determination of the original characteristics of these rocks. All the volcanics are assumed to be rocks of non-alkalic series, except for some well established K-rich shoshonitic lavas

of Upper Cretaceous age in central Puerto Rico. The chemical analyses of the non-alkalic series rocks of the individual formations were plotted and variation trends were then defined in terms of FeO^*/MgO - SiO_2, FeO^*/MgO - FeO^*, and FeO^*/MgO - TiO_2 diagrams if the number of available analyses permitted. The analyses were then assigned to either the tholeiitic or calc-alkalic series, based on these trends and the position of dividing lines between the two series in the diagrams which have been discussed in the previous section. The percentages of each rock series among all the volcanics in an individual formation or in an age period were calculated from the available chemical analyses, as an estimate of the proportion of the rock series in the formation or in an age period for this island arc. However, such estimates will be poor for a formation or an age period represented by a biased collection of rocks or only small numbers of analyses.

Brief comments are made below on individual formations in approximate order of decreasing age. Here, the rock types basalt, andesite, and dacite are defined with respect to a SiO_2 content smaller than 52 %, 52 to 63 %, and higher than 63 %, respectively.

(1) Water Island Formation and Louisenhoj Formation

The Water Island Formation of St. Thomas and St. John, U. S. Virgin Islands, has been well documented (Donnelly, 1966; Hekinian, 1971; Donnelly, 1971, 1972). These rocks of a spilite-keratophyre association consist of flows , with minor non-explosive pyroclastic material. Due to the

apparent alkali exchange of the keratophyre flows with sea water (Donnelly, 1966) and the similarity with the Late Cretaceous K-rich rocks in central Puerto Rico (Lidiak, 1965), we exclude the keratophyre from our present discussion.

About two thirds of the available analyses of the spilite of the Water Island Formation and the breccia of Louisenhoj Formation belong to the tholeiitic series, and are predominantly basalt. The remainder are andesites of the calc-alkalic series. The average trends for FeO* and TiO_2 for the two series are shown in Figure 25G.

(2) Pre-Roble Formation, Cerro Gordo Formation, and Santa Olaya Formation

The thick pre-Roble Formations in central Puerto Rico are the temporal equivalent of the Louisenhoj Formation in the Virgin Islands. Although the available analyses belong to basalts of the tholeiitic series, there are too few to define clear variation trends.

The massive andesitic flows of the Cerro Gordo Formation, exposed in north-central Puerto Rico are andesite and dacite of the calc-alkalic series.

The Santa Olaya Formation, extending from the eastern part of the Corozal quadrangle eastward into the Aguas Buenas quadrangle in north-central Puerto , is composed mainly of massive and pillow flows interlayered with pyroclastic tuffs and breccias. The rocks are predominantly tholeiitic basalt. About 15 percent of the available analyses belong to the calc-alkalic series.

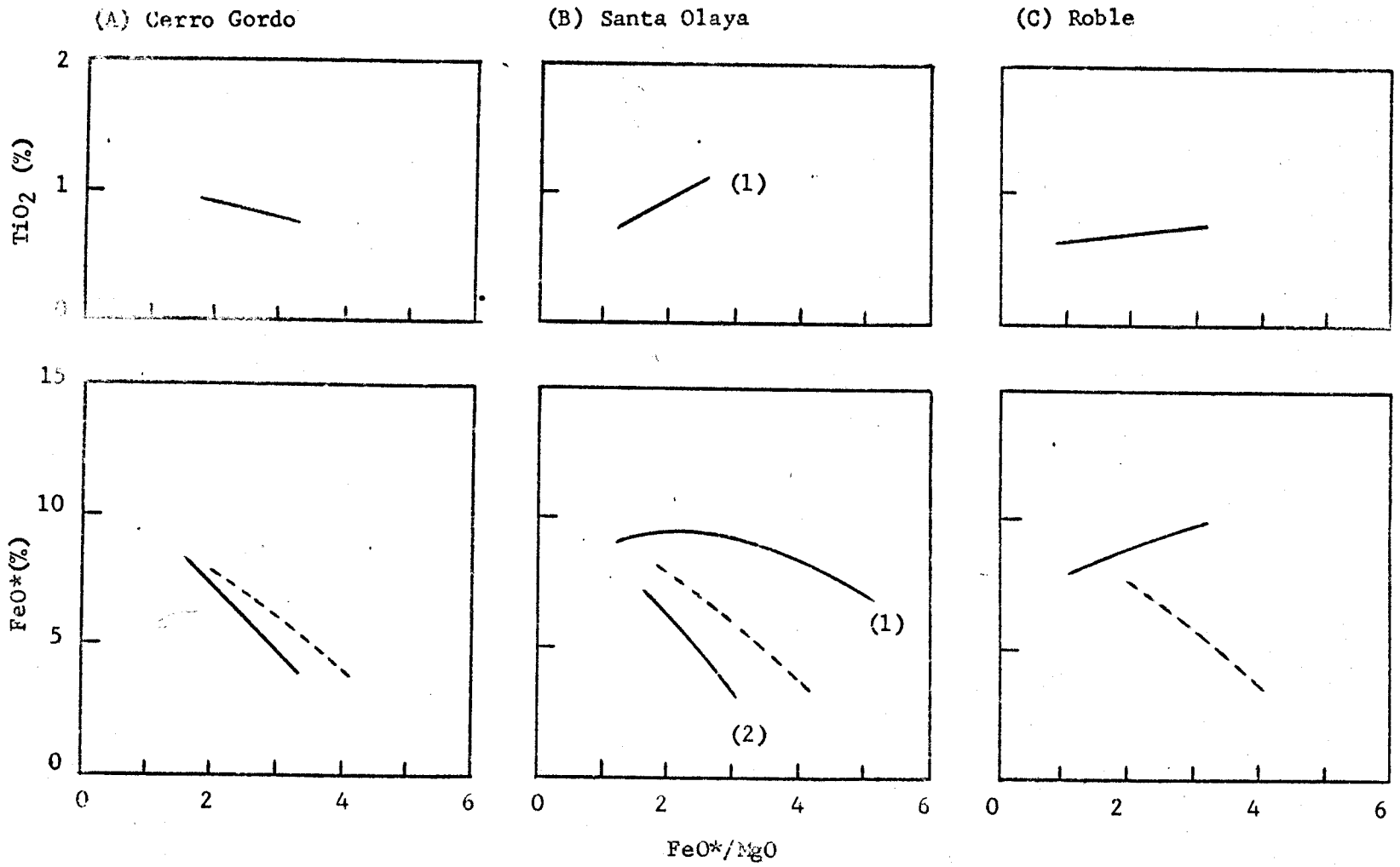

Figure 25 A-C. The average trends show the changes of FeO* and TiO_2 contents with FeO*/MgO ratio in the Puerto Rican volcanic rocks. Broken curve is the boundary between fields of tholeiitic and calc-alkalic series. When the TiO_2 content is not available for analyses, the range of FeO*/MgO ratio of trend in the diagram of FeO*/MgO - TiO_2 may be smaller than that in the diagram of FeO*/MgO - FeO*.

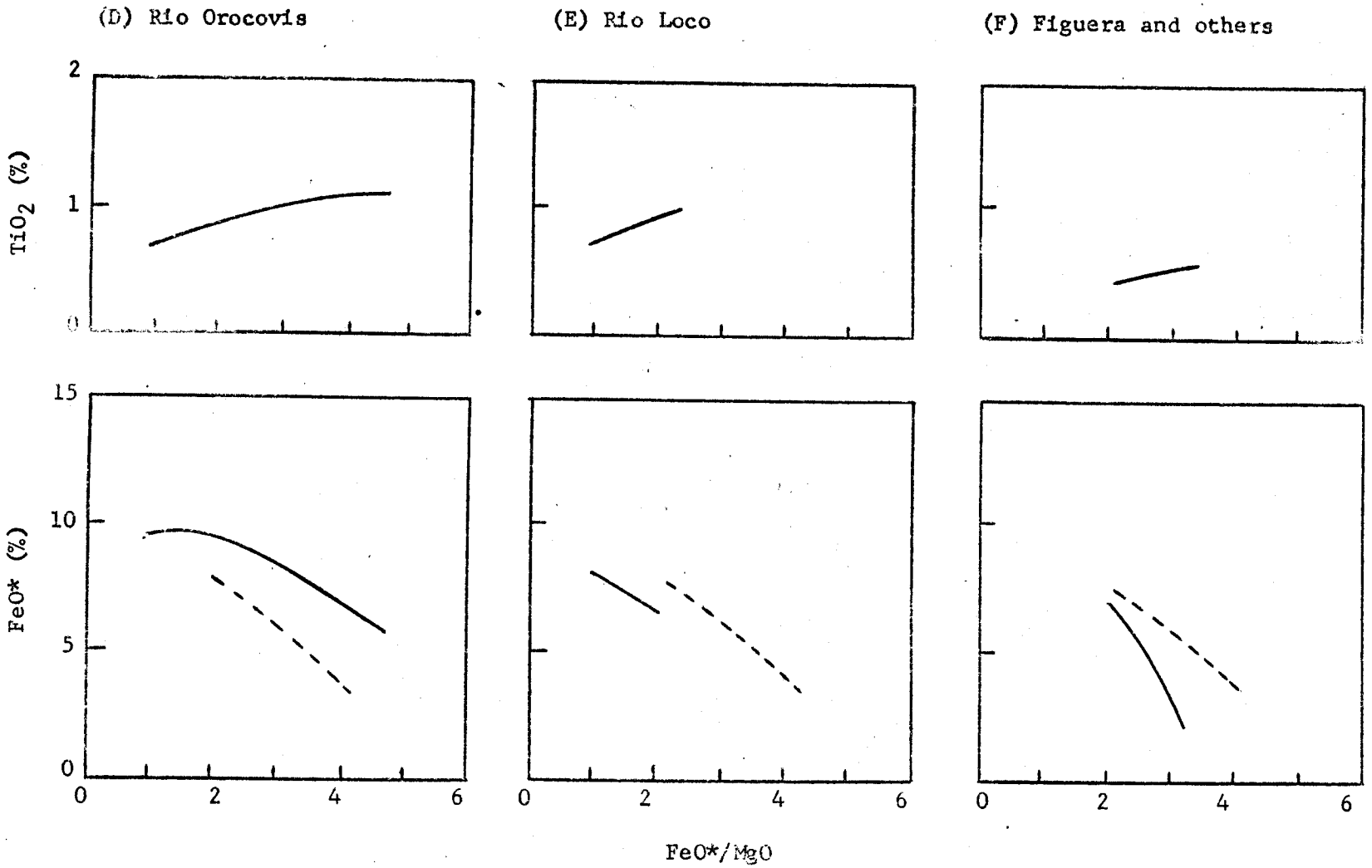

Figures D-F. The average trends show the changes of FeO* and TiO_2 contents with FeO*/MgO ratio in the Puerto Rican volcanic rocks. Broken curve is the boundary between fields of tholeiitic and calc-alkalic series.

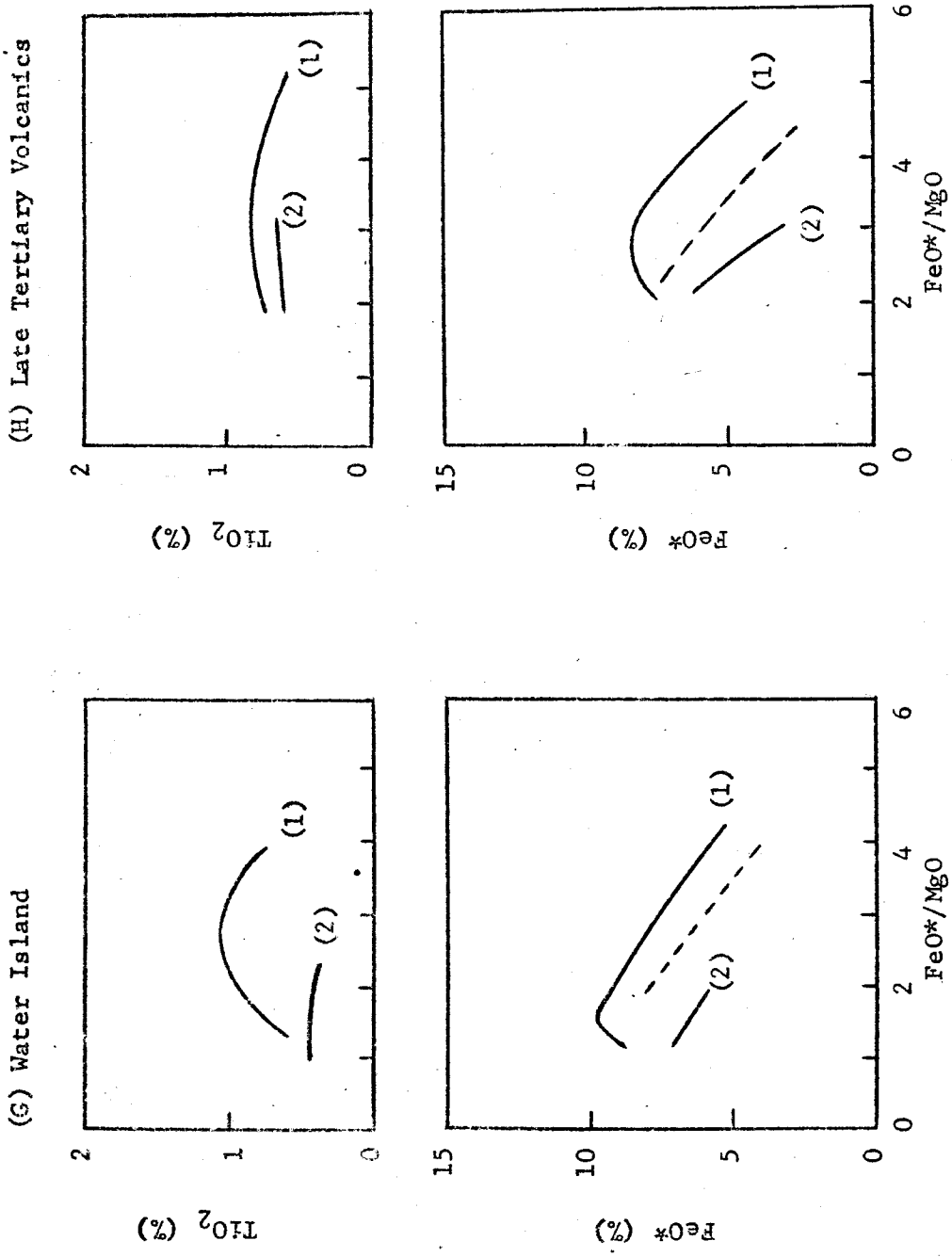

Figures 25G-H. The average trends show the changes of FeO* and TiO_2 contents with FeO*/MgO ratio in the volcanic rocks in eastern West Indies. Broken curve is the boundary between fields of tholeiitic and calc-alkalic series.

The average variation trends of FeO* and TiO_2 contents for the calc-alkalic series of Cerro Gordo and the tholeiitic and calc-alkalic series of Santa Olaya are shown in Figure 25A-B, respectively.

(3) Roble Formations and Rio Orocovis Formations

The lavas of these Late Cretaceous formations are commonly pillowed, and several (Lapa Lava, Avispa Lava, and Perchas Lava) are enriched in potassium (ranging in some cases above 6 percent K_2O). Jolly (1971) made a careful study of one of the more conspicuous lavas, the Lapa Lava in south central Puerto Rico, and concluded that the high potassium content is largely original, although metasomatic enrichment may occur in some cases. Moreover, using trace analyses of K, Th, and U Donnelly et al., (1971) showed that the variation trends of these elements for basic igneous rock series for the Greater and Lesser Antilles are rather smooth, with the conspicuious exception of the K-rich lava series of the Roble and Rio Orocovis Formations. Nevertheless, contents of these elements for these high-K rocks are all coherent, from which he also concluded that the process that resulted in high potassium contents was probably a one-stage process affecting all three elements in a similar fashion. Donnelly et al., (1971) regarded that these K-rich mafic magmas were probably generated by fusion at a green depth, due to a change in the slope of the Benioff plane during the Roble-Rio Orocovis period. However, the difficulties for this interpretation, and cast doubt on an origin of these

high-K mafic magmas through inherent island arc magmatism. Thus, these K-rich lava series have been excluded from the present discussion of the island arc evolution.

The Las Tetas Lava of the Roble Formation, exposed mainly in the northwestern quarter of the Cayey quadrangle, is well documented (Jolly, 1970, 1971). Most rocks of the Las Tetas Lava and the low-K member of the Rio-Orocovis Formation are basalts and andesites of the tholeiitic series. The average variation trends for these rocks are shown in Figure 25C-D.

(4) Rio Loco Formation and Mayaguez Formation

The Rio Loco Formation, exposed in south-western Puerto Rico (Mattson, 1960) is a possible equivalent of the Roble Formation. All the available analyses belong to the andesite of the calc-alkalic series. There are not enough analyses available to characterize the Mayaguez Formation, which conformably overlies the Rio Loco. However, it may include tholeiitic andesite and basalt (?). The variation trends for the calc-alkalic series of the Rio Loco are shown in Figure 25E.

(5) Rio de la Plata Formation and Figurera Volcanics

The epiclastic volcanic debris with minor lava flows of the Rio de la Plata Formation are exposed in the western part of the Naranjito quadrangle. Because of their unusually high K_2O content (over 3 % in most cases), they are excluded from the present discussion. The predominant rocks of the Figurera Volcanics of north-central Puerto Rico

and other minor volcanic units of the early Tertiary in Puerto Rico are dacite of the calc-alkalic series. Andesite of the tholeiitic series is rare. Figure 25F shows the average variation trends of the calc-alkalic series.

(6) Late Tertiary Volcanic Rocks of the Lesser Antilles

The Late Tertiary volcanic rocks exposed in St. Lucia, St. Kitts, St. Vincent, Montserrat, St. Martin, and Dominica of the Lesser Antilles (Figure 24) belong to both of calc-alkalic and tholeiitic series, in about a 3 to 2 proportion. Most rocks of the calc-alkalic series are andesite, with rare dacite. Andesite is also predominant for the tholeiitic series, with rare tholeiitic basalt. The average variation trends of FeO* and TiO_2 for both series are shown in Figure 25H.

Figure 26A-C show plots of FeO*/MgO - SiO_2 and the average variation trends of FeO* and TiO_2 with FeO*/MgO ratio for the available analyses of non-alkalic rocks of Pre-Albian to Cenomanian, Albian to Santonian, and Late Cretaceous to Tertiary formations, respectively.

D. The Possible Role of the Bermeja Complex in the Island Arc Evolution

In this section, the similarity of the metabasaltic rocks of the Bermeja complex to the expected earliest-stage arc tholeiites will be pointed out; these latter rocks in turn may be chemically continuous toward the studied arc

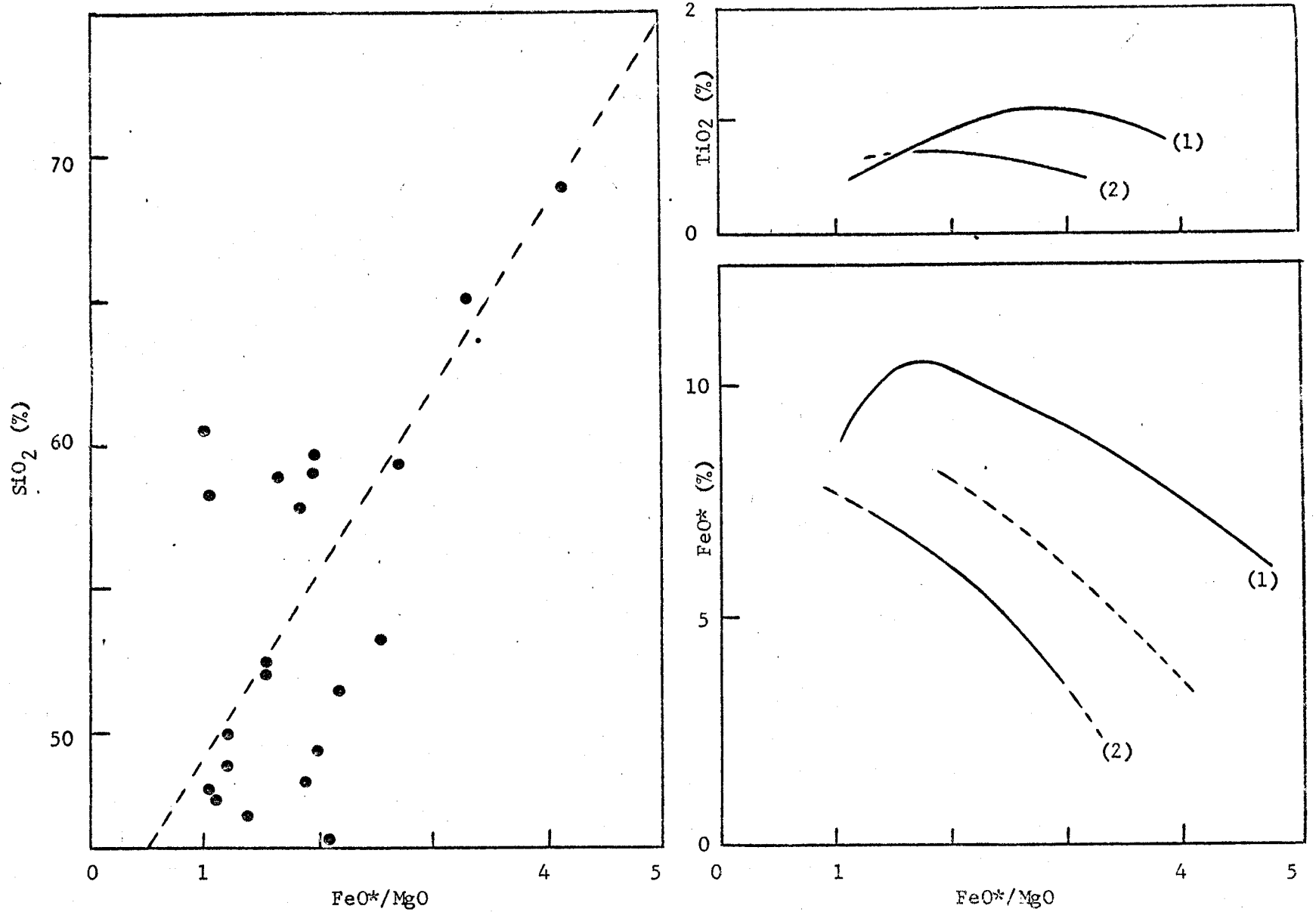

Figure 26A. Changes of SiO_2, FeO*, and TiO_2 contents with FeO*/MgO ratio in the non-alkalic rocks of Pre-Albian to Cenomanian age. Broken curve is the boundary between fields of tholeiitic and calc-alkalic series. When the TiO_2 content is not available for analyses, the range of FeO*/MgO ratio of trend in the diagram of FeO*/MgO - TiO_2 may be smaller than that in the diagram of FeO*/MgO - FeO*.

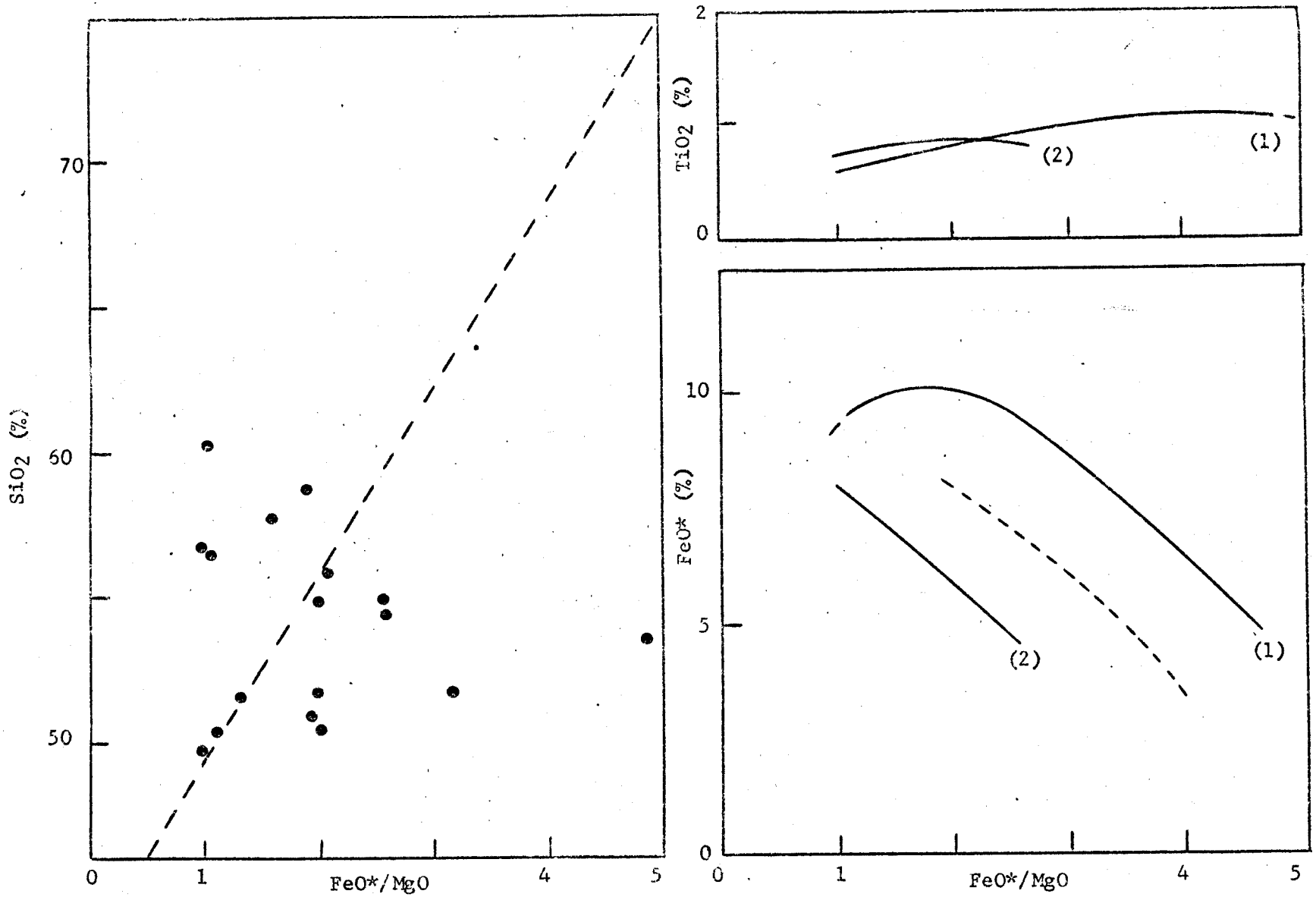

Figure 26B. Changes of SiO_2, FeO*, and TiO_2 contents with FeO*/MgO ratio in the non-alkalic volcanic rocks of Albian to Santonian age. Broken curve is the boundary between fields of tholeiitic and calc-alkalic series.

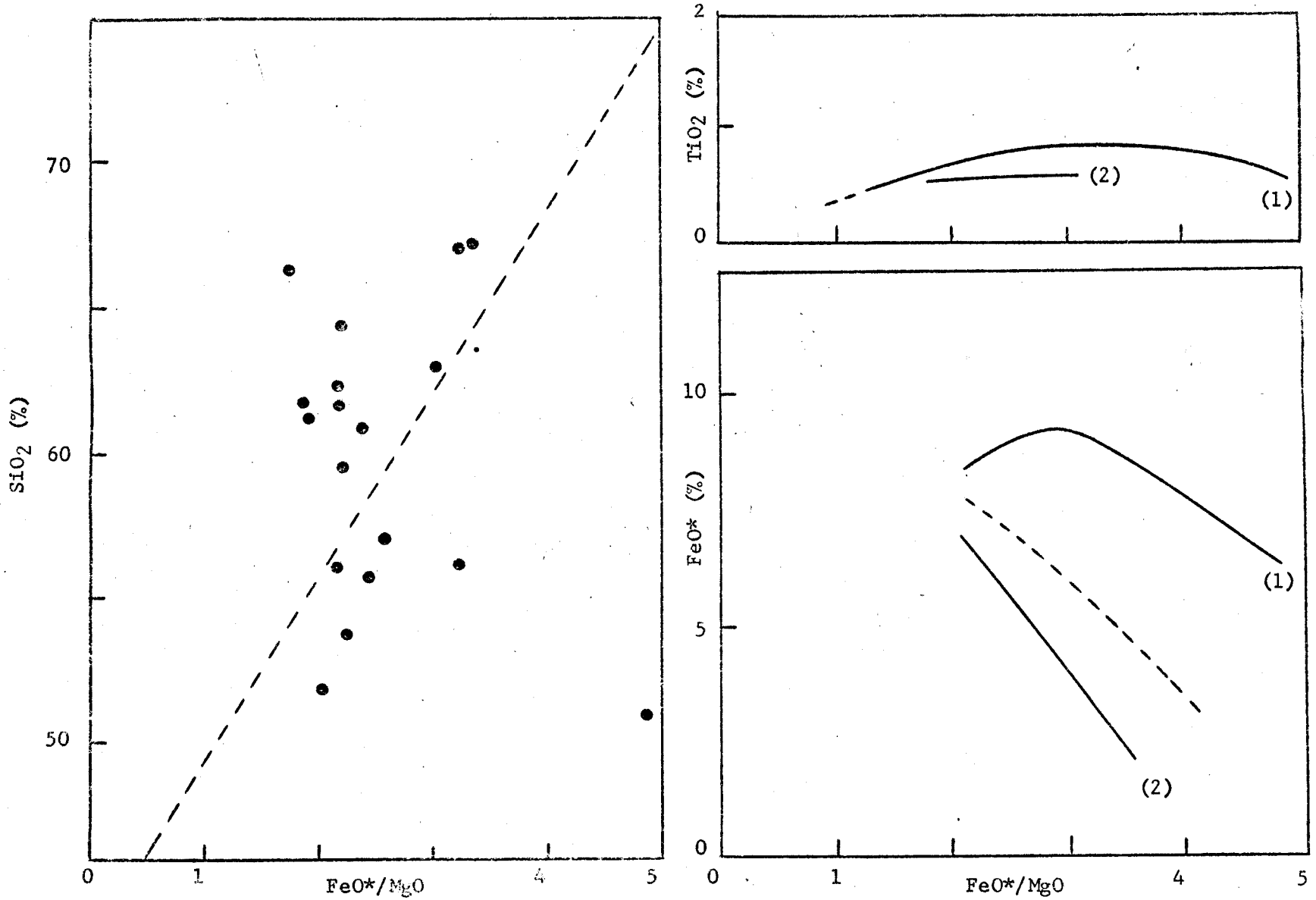

Figure 26C. Changes of SiO_2, FeO*, and TiO_2 contents with FeO*/MgO ratio in the non-alkalic volcanic rocks of Late Cretaceous to Late Tertiary age. Broken curve is the boundary between fields of tholeiitic and calc-alkalic series.

tholeiites.

Some island arcs, composed mainly of rocks of the tholeiitic series, are represented by the Kermadec (Brother and Searle, 1970; Brother and Martin, 1970), Tongas (Bauer, 1970; Baker et al., 1971; Bryan et al., 1972), and North Marianas (Tanakadate, 1940, Schmidt, 1957; Stark, 1963). The low-K tholeiites of island arcs usually have slightly lower TiO_2 and Na_2O contents than common abyssal tholeiites. For these arcs, there is commonly a long submarine history prior to the stage of evolution of rocks for which chemical data are available. Unfortunately, for this unknown initial period of island arc formation we have no data. However, by the extrapolation of the available variation data of arc volcanics back to the presumed initial stage, the tholeiitic rocks thus generated would closely resemble abyssal tholeiites of the mid-oceanic ridge systems, probably even in the TiO_2 and Na_2O contents (Miyashiro, in press). The island arc tholeiites may not rarely have FeO*/MgO ratio higher than 2.0, which is extremely rare in the abyssal tholeiites.

The frequency distributions of SiO_2 percentages (anhydrous basis) and FeO*/MgO ratios in analyzed rocks of the Bermeja complex and of tholeiitic series in the Kermadec arc as well as in abyssal tholeiites and associated rocks in mid-oceanic ridges are compared in Figure 27. For the Bermeja complex, group I (schistose amphibolite) and group II (meta-basaltic dike, spilite, and amphibolitized dolerite) are shown by full and broken lines, respectively. The distributions

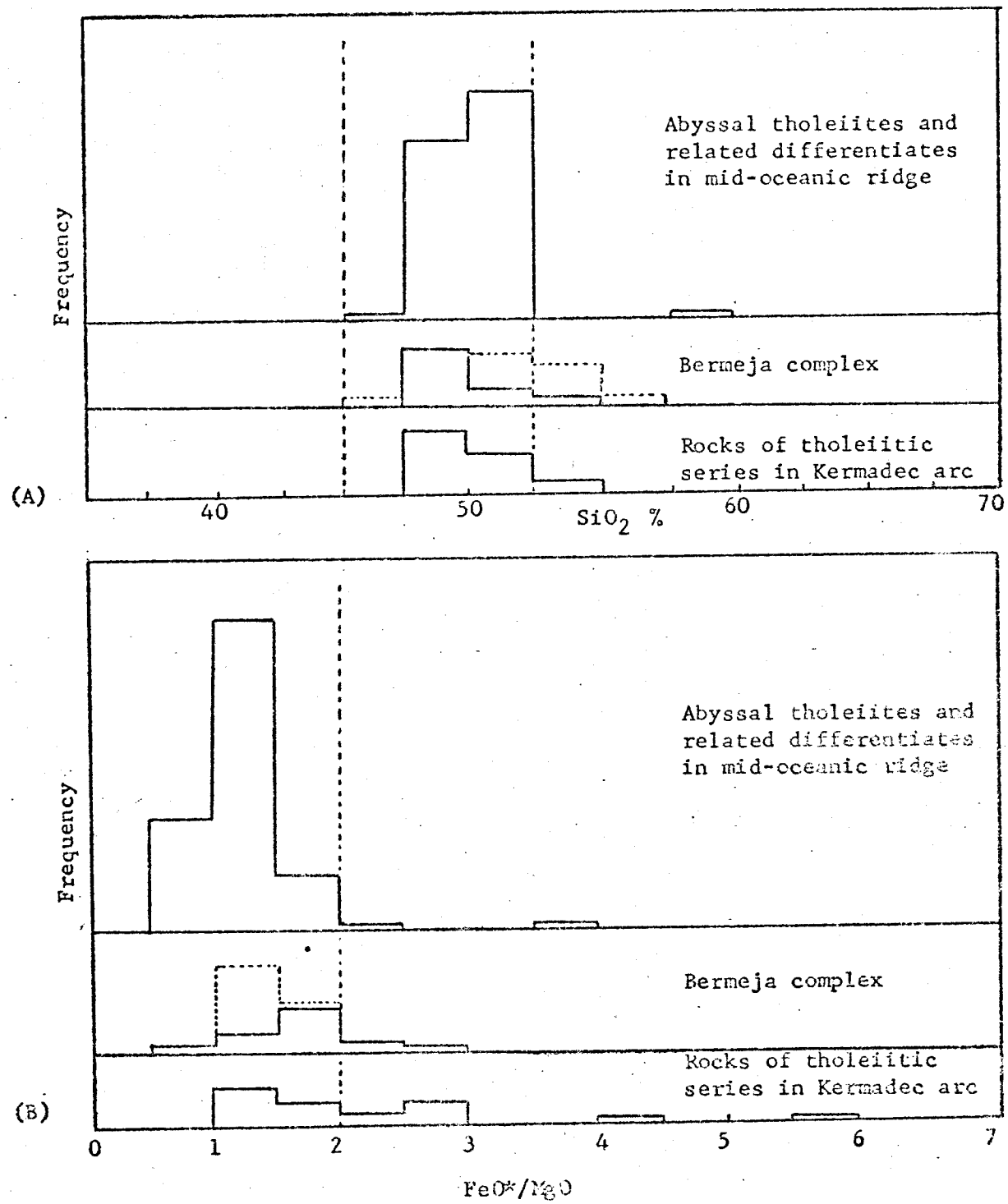

Figure 27 A-B. Frequency distributions of SiO_2 percentage and FeO*/MgO ratios in the analyzed rocks of Bermeja complex (Group I and II are shown by full and broken lines, respectively), rocks of tholeiitic series in Kermadec arc, and in abyssal tholeiites (after Miyashiro, 1973b, Figure 5).

of the older group I of the Bermeja complex and the combined patterns of group I and II are intermediate between those of the Kermadec tholeiites and the abyssal tholeiites. The Kermadec arc has an oceanic-type crust, about 15 Km thick (Karig, 1970). About 90 percent of the rocks of Macauley and Raoul Islands of the arc belong to the tholeiitic series (Miyashiro, in press). The average SiO_2 percentage and FeO*/MgO ratio of the Bermeja complex is intermediate to those of the Kermadec tholeiite and abyssal tholeiites. Thus, the Bermeja complex may represent either oceanic crust beneath the island arc, or the earliest volcanic products of the island arc evolution. If the complex is a volcanic product of the island arc, it is an earlier stage than the tholeiites of the Kermadec arc.

In the discussion of the following section the assumption will be made that the Bermeja complex represents the initial-stage arc tholeiites.

E. Compositional Variation of the Volcanic Rocks in Puerto Rico and Other Islands in Eastern West-Indies

In the previous section, the approximate composition of the rocks of the non-alkalic series for the individual formations was briefly discussed. However, only small numbers of analyses are available for many of the formations. This lowers the reliability of such approximations apart from the problem of possibly biased collections of rocks,

In this section, the formations are divided into three age groups, on the basis of their approximate equivalence in stratigraphic level. These groups comprise Pre-Albian to Cenomanian, Albian to Santonian, and Late Cretaceous to Tertiary age, respectively. These age intervals are chosen simply for convenience in the present discussion. Each formation has been assigned to the corresponding age group, although it is recognized that some age overlap within and between the formations and groups does exist. As a result of this grouping, larger numbers of analyses are obtained for each group, which it is hoped will improve the reliability of average composition data calculated for each group. For the tholeiitic series, the percentage of tholeiitic basalt and the tholeiitic andesite in the tholeiitic series tends to decrease and increase, respectively, with decreasing age of the groups. The percentages of tholeiitic basalt and of the andesite of the calc-alkalic series among all the non-alkalic volcanics decrease and increase, respectively, with decreasing age. The mean SiO_2 percentage and mean FeO*/MgO ratio also tend to increase with decreasing age and consequently increasing degree of development of this island arc. It is important to see that the variation trends for this island arc appear to be continuous, with the Bermeja complex assumed to situatein a position representing an initial stage in the history of arc evolution.

1. Proportion of Tholeiitic and Calc-alkalic Series Rocks

The approximate volume proportions of rock types among all non-alkalic volcanics of each time period are estimated in Table 16A. The Bermeja complex is also included and considered to represent rocks generated in the initial-stage of the island arc evolution. For the purposes of comparison, the Puerto Rican volcanics and volcanic rocks of Puerto Rico and other islands in eastern West-Indies are treated separately as shown in Tables 16A-B and 17A-B. The main reason for the grouping of the non-alkalic volcanics in Puerto Rico, Virgin Islands, and the Lesser Antilles is simply to demonstrate the gradual temporal compositional variations. It is more important, however, to recognize that the Puerto Rico - Virgin Islands region and the Lesser Antilles have different spatial directions (trends), and so probably have different tectonic histories (Malfait and Dinkelman, 1972). For example, when the direction of relative movement of the Caribbean plate is to the east, orogenic activities in Puerto Rico and unlikely but are probable in the Lesser Antilles, and vice versa for relative plate movement to the north. Therefore, grouping together the volcanic rocks of both Puerto Rico and the Lesser Antilles in Tables 16A-B and 17A-B, may juxtapose two possibly tectonicly independent groups of rocks. The variation trends shown in these tables, thus, may or may not show any tectonic significance, but are believed to

Table 16A. Volume proportions of rock types among all non-alkalic volcanics of each age group. The proportions are estimates based on frequencies among our new analyses and analyses taken from literature. The figure in the parathensis shows the number of analysis.

	Series (100 %)					
	Tholeiitic			Calc-alkalic		
	Basalt	Andesite	Dacite	Basalt	Andesite	Dacite
	Puerto Rican Volcanics					
Pre-Albian Bermeja complex (25)	76	24	0	0	0	0
Pre-Albian to Cenomanian (20)	74	0	0	0	13	13
Albian to Santonian (17)	35	24	0	6	35	0
Late Cretaceous to Early Tertiary (18)	0	25	0	0	0	75
	Puerto Rico and Other Islands in Eastern West Indies					
Pre-Albian Bermeja complex (25)	76	24	0	0	0	0
Pre-Albian to Cenomanian (33)	57	5	5	23	5	5
Albian to Santonian (17)	35	23	0	7	35	0
Late Cretaceous to Late Tertiary (33)	11	32	0	0	32	25

Table 16B. Volume proportions of rock types among all non-alkalic volcanics of the accumulated age groups. The proportions are estimated based on frequencies among our new analyses and analyses taken from literatures. The figure in the parathensis shows the number of analysis.

	Series (100 %)					
	Tholeiitic			Calc-alkalic		
	Basalt	Andesite	Dacite	Basalt	Andesite	Dacite
	Puerto Rican Volcanics					
Pre-Albian Bermeja complex (25)	76	24	0	0	0	0
Pre-Albian to Cenomanian (45)	73	21	0	0	3	3
Pre-Albian to Santonian (62)	60	22	0	2	14	2
Pre-Albian to Early Tertiary (80)	55	21	0	2	14	8
	Puerto Rico and Other Islands in Eastern West Indies					
Pre-Albian Bermeja complex (25)	76	24	0	0	0	0
Pre-Albian to Cenomanian (58)	65	18	2	2	11	2
Pre-Albian to Santonian (75)	57	19	2	9	11	2
Pre-Albian to Late Tertiary (108)	46	22	2	7	16	7

carry temporal significance in respect to the development of the overall island arc. For the Puerto Rican volcanics the age group from Pre-Albian to Cenomanian includes the Pre-Roble, Cerro Gordo, and Santa Olaya formations, the age group from Albian to Santonian includes the Roble, Rio Orocovis, Rio Loco, and Mayaguez formations, and the age group from Late Cretaceous to Early Tertiary includes the Figuera and other Early Tertiary volcanic units. For the volcanic rocks of Puerto Rico and of other islands in the eastern West Indies, the Water Island and the Louisenhoj formations are added to the group of Puerto Rico volcanics of Pre-Albian to Cenomanian age, and the Late Tertiary Lesser Antilles volcanics are combined with the youngest group of Puerto Rican volcanics.

The oldest Pre-Albian Bermeja complex contains about 75 % tholeiitic basalt and 25 % tholeiitic andesite. In the Middle Cretaceous, about half of the volcanics are tholeiitic basalt, and one quarter is calc-alkalic basalt. The remainder includes equal amounts of tholeiitic series andesite and dacite and calc-alkalic andesite and dacite. Toward the Late Cretaceous, basalt and andesite of the tholeiitic series respectively tend to decrease and increase in proportion. These trends are more pronounced during the Tertiary, in which equal proportions of andesites of both the tholeiitic and calc-alkalic series are predominant (about one third each), with approximately one forth dacite of the calc-alkalic series and one tenth of tholeiitic basalt.

For the Puerto Rican volcanics, most of the tholeiitic series rocks are basalt in the Middle Cretaceous. The proportion of basalt in the tholeiitic series decreases gradually while that of andesite increases with decreasing age. In the Late Cretaceous to Early Tertiary period, andesite is the only tholeiitic series representative. For the calc-alkalic series, the proportion of the more silicious types also increases with decreasing age. The variations in proportions of rock types in the tholeiitic and calc-alkalic volcanic series of the whole eastern West Indies also have a trend similar to those of the Puerto Rican volcanics. In the Middle Cretaceous basalt is predominant in the calc-alkalic series, while during the Late Cretaceous, andesite is most abundant, and in the Tertiary, there are about equal amounts of andesite and dacite.

In Table 16B, the estimated volume proportions of rock types in the whole non-alkalic volcanics of the accumulated by age groups from the Pre-Albian are shown. This may represent the distribution of rock types for non-alkalic volcanic rocks below a certain different stratigraphic level. It may also indicate the nature of compositional variation occurring with island arc evolution, the latter being represented by the thickness of the crust underlying the arc (Miyashiro, in press). As shown in Table 16B, the proportion of tholeiitic basalt tends to decrease with an accumulating thickness of volcanic rocks in the arc, while proportion of andesite and dacite of the calc-alkalic series tends to

increase slightly with evolution of the island arc. The proportion of tholeiitic andesite among all volcanics, however, remains nearly unchanged. As suggested by the present data, the whole island arc volcanic of the eastern West-Indies (as shown in the bottom row of Table 16B) may have better development of basalt and andesite of calc-alkalic series and tholeiitic dacite and andesite, and lesser development of tholeiitic basalt than those of the Puerto Rican volcanics. However, this comparison may not be significant due to the possible sampling bias.

The estimated volume proportions of tholeiitic and calc-alkalic series in each stratigraphic group are shown in Table 17A. In the earliest stage, all volcanic rocks belong to the tholeiitic series. Then, the proportion of tholeiitic series and calc-alkalic series gradually decrease and increase, respectively, with decreasing age. During the Tertiary, the calc-alkalic series appears to be more prevalent than the tholeiitic series. A similar trend can also be seen in Table 17B, in which the estimated accumulated percentages of tholeiitic and calc-alkalic series at various stages of island arc evolution are shown, Estimated total volcanics from the initial stage up to Tertiary age (as shown in the last row of Table 17A-B) consist of about two thirds tholeiitic series and one third calc-alkalic series. However, among the Puerto Rico volcanics there appears to be a somewhat larger proportion of tholeiitic series than among all volcanic rocks of the eastern West Indies. This is probably

Table 17A-B. Volume proportion of tholeiitic and calc-alkalic series of each age group (A) and the accumulated age group (B).

	Puerto Rican Volcanics		Puerto Rico and Other Islands in Eastern West Indies	
	Series (100 %)		Series (100 %)	
	Tholeiitic	Calc-Alkalic	Tholeiitic	Calc-Alkalic
(A)				
Pre-Albian Bermeja complex	100	0	100	0
Pre-Albian to Cenomanian	75	25	67	33
Albian to Santonian	59	31	58	32
Late Cretaceous to Tertiary	25	75	43	57
(B)				
Pre-Albian Bermeja complex	100	0	100	0
Pre-Albian to Cenomanian	94	6	85	15
Pre-Albian to Santonian	82	18	78	22
Pre-Albian to Tertiary	76	24	70	30

a reflection of the fact that Late Tertiary volcanics, which have well developed calc-alkalic series are dominant in the Lesser Antilles.

2. Frequency Distribution of SiO_2 Content

The SiO_2 content in non-alkalic volcanic rocks of some formations in Puerto Rico roughly increases with decreasing age of the formation, although the trend is weak (not shown in figure). A better definition is seen when the rocks are divided into the same three groups as those previously used in this section. The frequency distributions on this basis using the average SiO_2 content for each group are shown in Figure 28A. They are arranged in approximate order of decreasing age from the bottom to the top of the diagram. It is seen that the SiO_2 content increases gradually from the oldest Bermeja complex toward younger group, although wide variations are present in most of the formations or age units. The accumulated frequency distribution of SiO_2 content at certain stages of island arc evolution as expressed by various stratigraphic levels for the Puerto Rico volcanics are shown in Figure 28B. It is shown that the SiO_2 content gradually increases with the degree of development of the arc volcanics. Figure 28C-D show the gradual variation of SiO_2 content for all non-alkalic volcanic rocks in the eastern West Indies, on the basis of separate age intervals and cumulatively. The increase in the average SiO_2 content with decreasing age is similarily expressed in these diagrams.

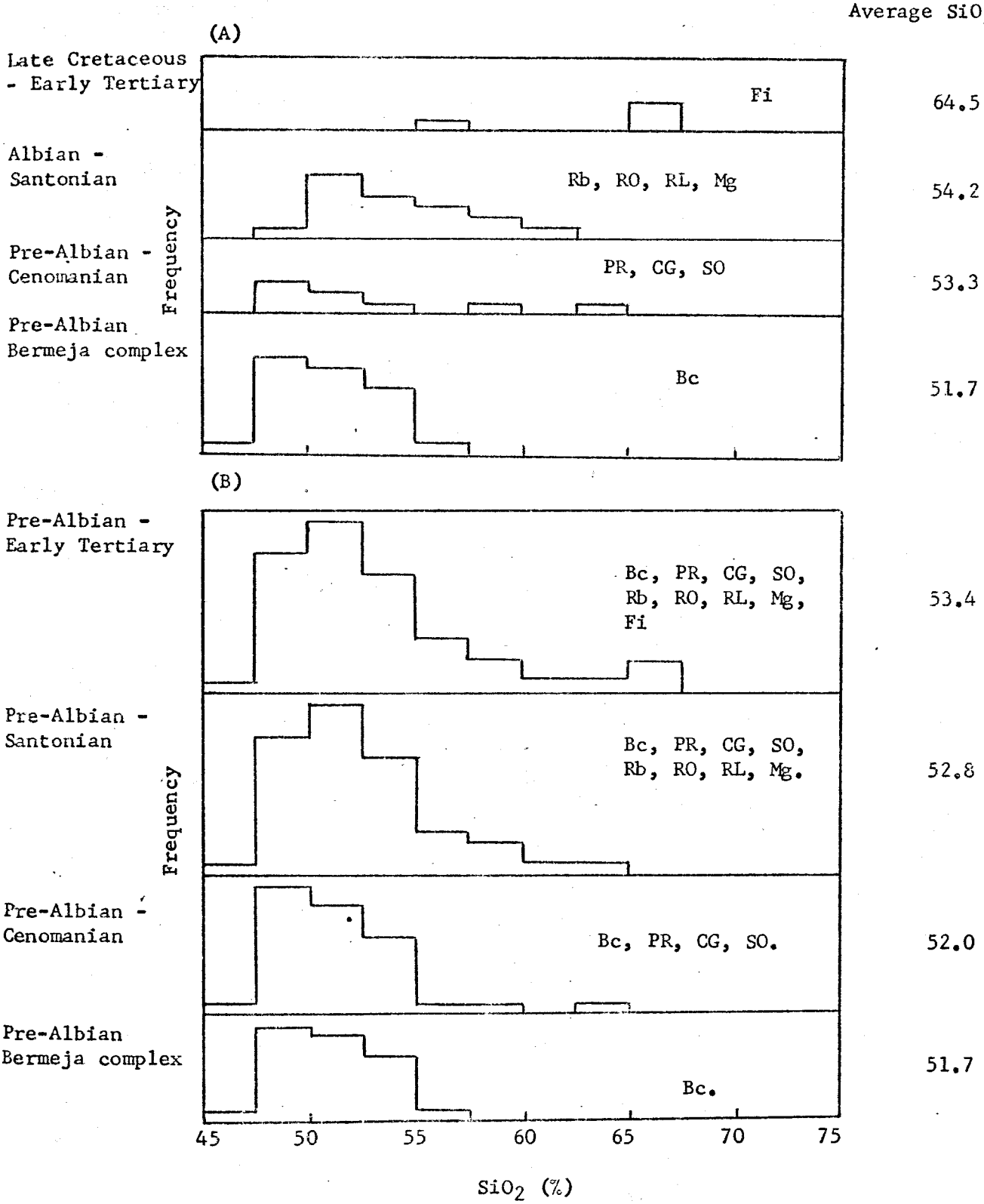

Figure 28 A-B. Frequency distribution of SiO_2 (%) (anhydrous) in the analyzed non-alkalic volcanic rocks in Puerto Rico. Symbols are the same as those in Table 15.

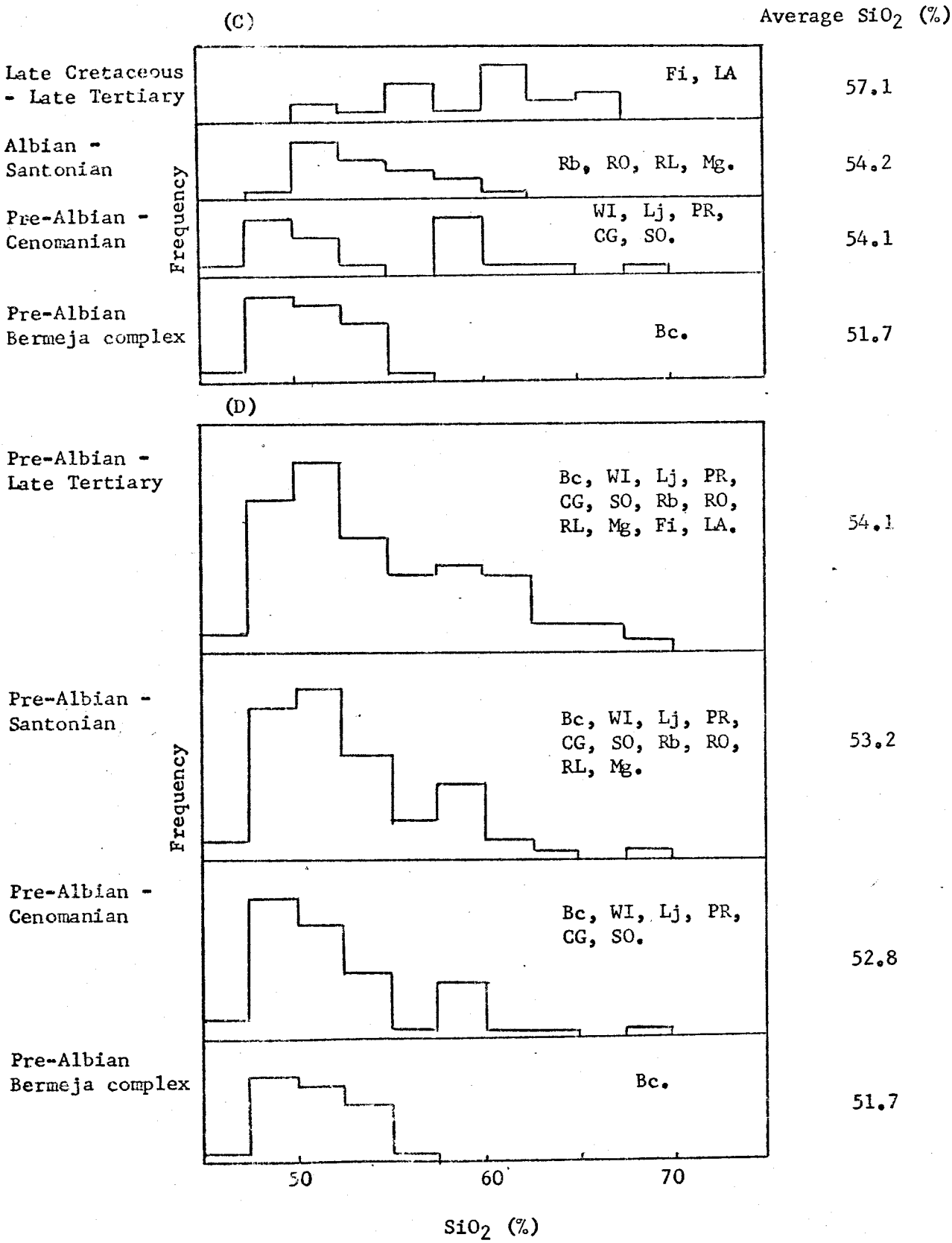

Figure 28 C-D. Frequency distribution of SiO_2 (%) (anhydrous) in the analyzed non-alkalic volcanic rocks in the eastern West-Indies. Symbols are the same as those in Table 15.

Thus, the increase in the proportion of calc-alkalic series rock (as discussed above in this section) is accompanied by an apparent increase in the proportion of more silicic volcanic rocks among the non-alkalic volcanics, as shown in these diagram.

3. Frequency Distribution of FeO*/MgO Ratio

Figure 29A-D show the frequency distributions of FeO*/MgO ratios in the volcanic rocks plotted on a corresponding basis as for Figure 28A-D, respectively. The available data for most formations (not shown in figure) are not numerous enough to allow any definite conclusion on the trend of variation of FeO*/MgO among them with decreasing age. However, it is important to see that the overall FeO*/MgO ratio does tend to increase with advancing development of this island arc, as expressed by the estimated averages for formations of similar age grouped together (Figure 29A,C) and for the accumulated rocks up to various stratigraphic levels (Figures 29B,D).

Thus, the increase in the average SiO_2 content of the non-alkalic volcanic rocks with the advancing development of this island arc may be ascribed not only to the increasing proportion of calc-alkalic series rocks, but also to the apparently more advanced stage of fractional crystallization of magma, or to contamination of magmas by rocks of more granitic composition, both of which tend to increase not only the SiO_2 content, but also the FeO*/MgO

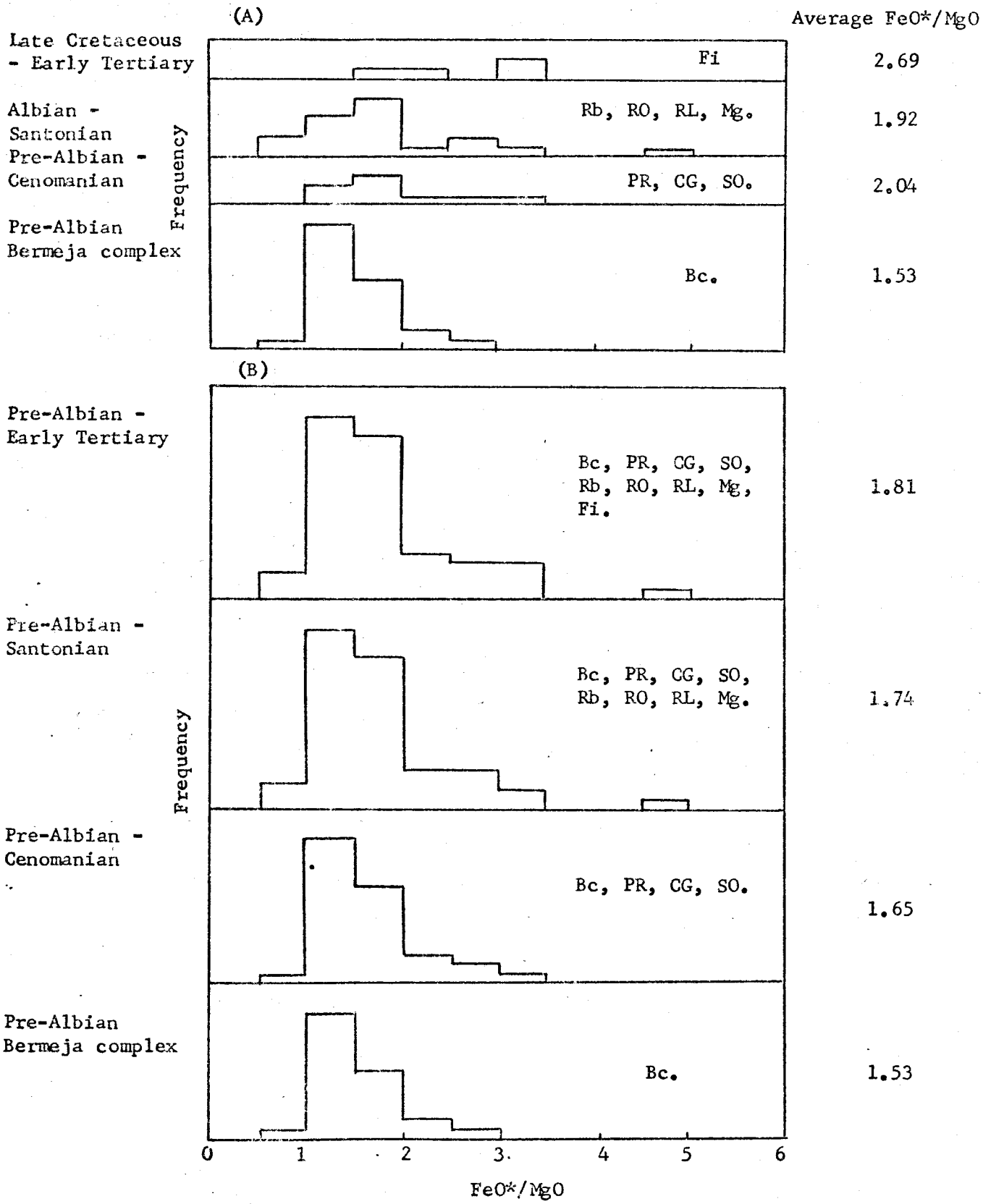

Figure 29 A-B. Frequency distribution of FeO*/MgO ratio for the analyzed non-alkalic volcanic rocks in Puerto Rico. Symbols are the same as those in Table 15.

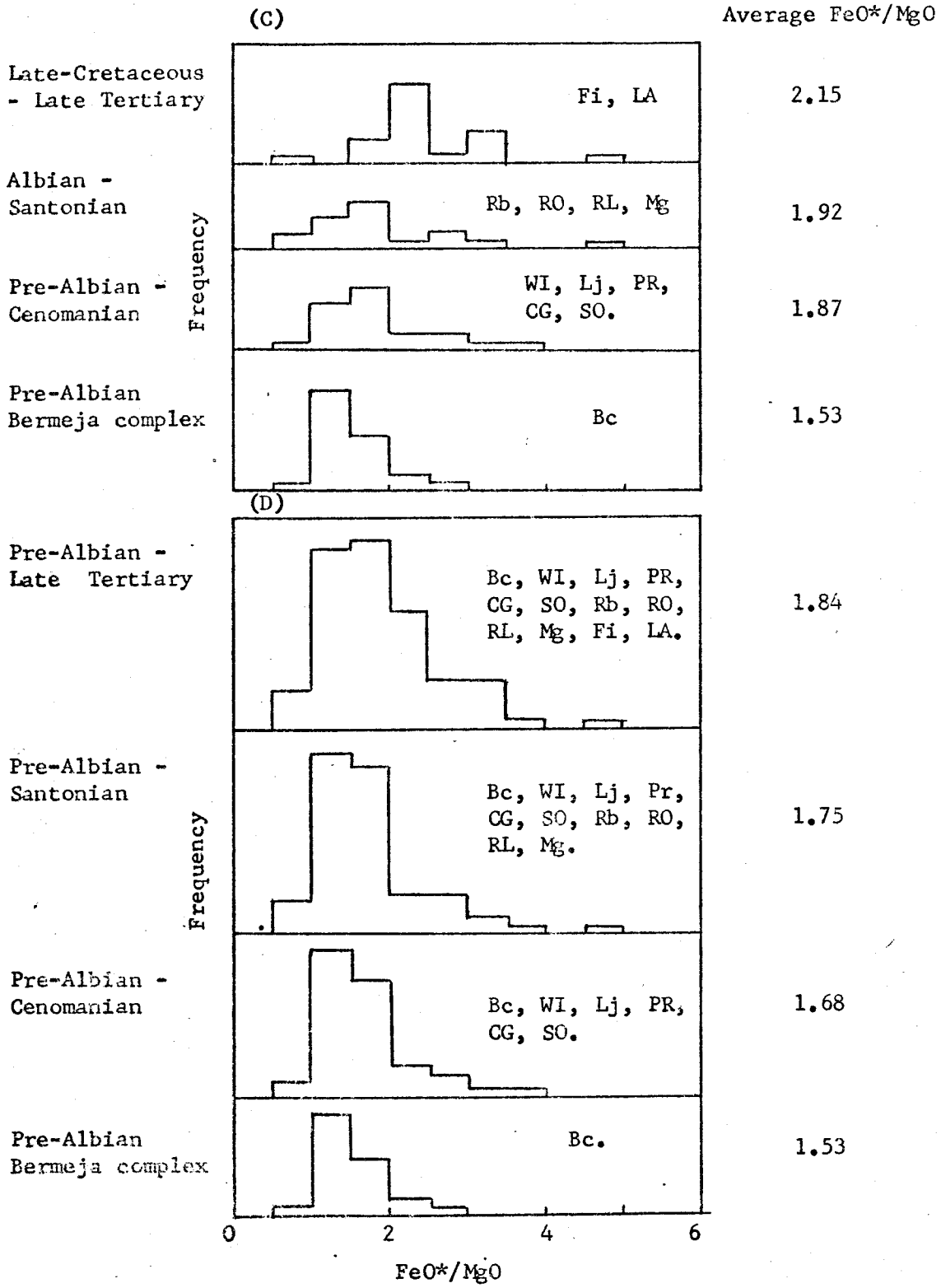

Figure 29 C-D. Frequency distribution of FeO*/MgO ratio for the analyzed non-alkalic volcanic rocks in the eastern West Indies. Symbols are the same as those in Table 15.

ratio.'

In summary, the rock types, the proportion of the tholeiitic and calc-alkalic series, and the average SiO_2 content and FeO*/MgO ratio appear to change gradually in regular patterns, from the earliest generated Bermeja complex through the volcanic rocks of the upper stratigraphic levels of Puerto Rico and the eastern West-Indies. These compositional variations may be naturally continuous, and show the trends of evolution of this island arc. The Bermeja complex may represent either the metamorphosed derivatives of the oldest initial-stage arc tholeiites, presumably the major rocks forming the basement underlying the thick volcanic pile of Puerto Rico, or an ancient oceanic crust beneath the island arc.

F. Comparison with Other Similar Island Arc Systems

The island arc of the Central Kuriles has a composition similar to the Puerto Rico - Virgin Islands non-alkalic volcanic rock suite in the proportions of the tholeiitic and calc-alkalic series, and in the frequency distributions of SiO_2 percentages and FeO*/MgO ratios.

The Kurile arc is divided into the South, Central, and North portions (Gorshkov, 1970). The Central Kuriles have an oceanic crust a little less than 15 km thick (Gorshkov, 1970), and a single arc structure. It is composed both of tholeiitic and calc-alkalic series rocks. The percentage

of calc-alkalic series rocks among all volcanics is about 32 percent (Miyashiro, in press).

The frequency distributions of SiO_2 percentages and FeO*/MgO ratios in analyzed rocks of the non-alkalic volcanics of Puerto Rico and of the combined volcanics of Puerto Rico and Virgin Islands, as well as the volcanics of the Central Kuriles are compared in Figures 30A-B. The Puerto Rico and the Central Kuriles distributions have similar ranges, though that for Puerto Rico shows a larger proportion of low-SiO_2 and low-FeO*/MgO rocks. Data for all non-alkalic volcanics in the Puerto Rico and Virgin Islands region resemble that of the volcanics of the Central Kuriles to a slightly greater extent than for Puerto Rico alone. The frequency distribution differences between these two arc systems, however, may be a reflection of different degrees of development of their contained rock series. The percentage of tholeiitic series rocks is higher in Puerto - Virgin Islands (75 %) (the Bermeja complex included), or lower (60 %) (the Bermeja complex not included) than in the Central Kuriles (68 %).

Miyashiro (in press) noted that the percentage of calc-alkalic series rocks among all volcanics in the South and North Kuriles, which have a thicker and more continental-type crust (18 - 30 Km), is greater (48 - 57 percent) than in the Central Kuriles. Thus, the percentage of calc-alkalic series rocks may tend to increase with, and reflect, the development of a continental-type crust in the Kuriles arc.

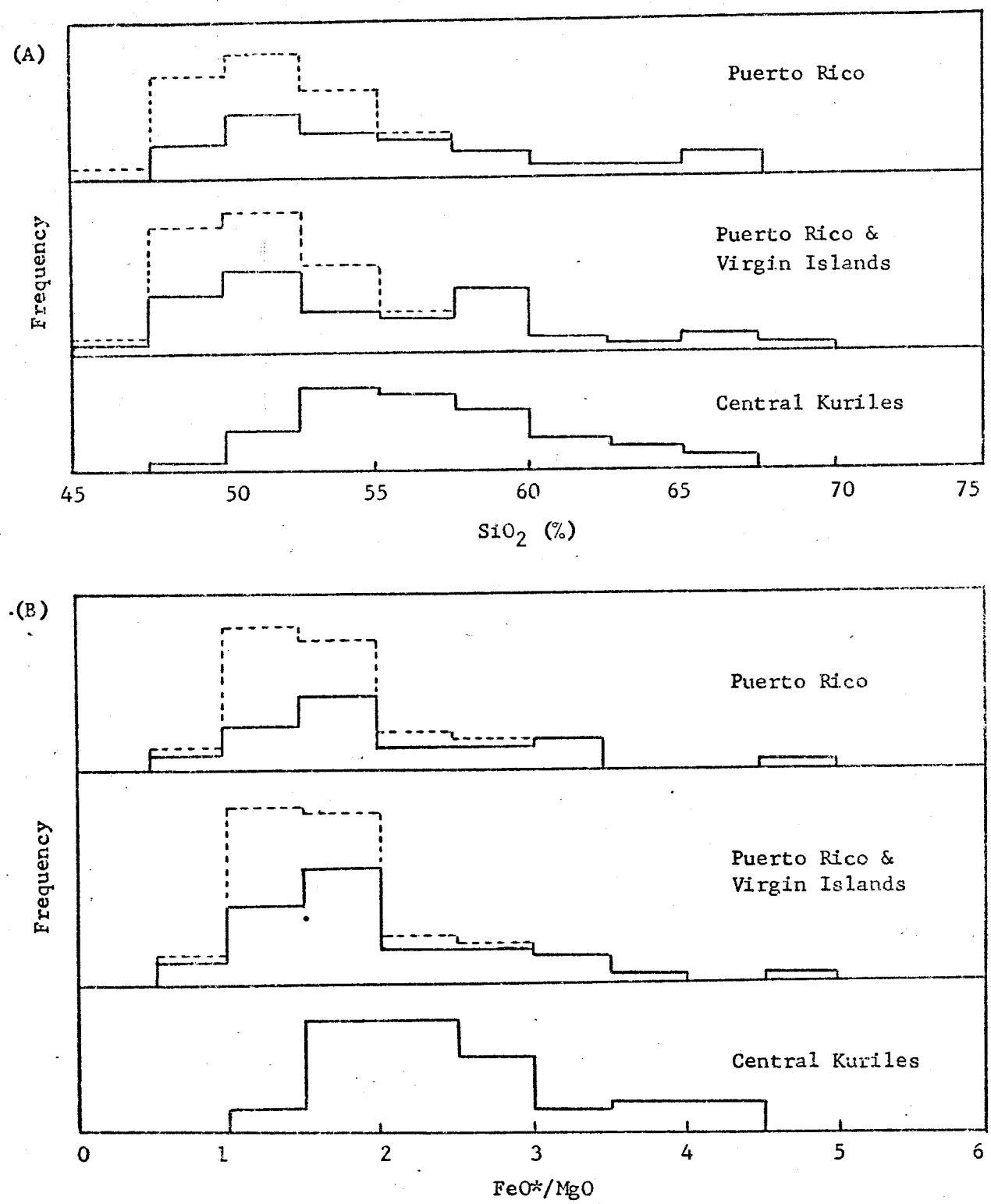

Figure 30 A-B. Frequency distributions of SiO_2 percentage and FeO*/MgO ratios in the volcanic rocks in Puerto Rico, Puerto Rico and Virgin Islands (Broken line: the Bermeja complex included; solid lines: the Bermeja complex not included), and Central Kuriles.

This conclusion may, moreover, be true for most island arc systems around the world (Miyashiro, in press). Because tholeiitic series rocks of the Puerto Rico - Virgin Islands region are similar in abundance as in the Central Kuriles, the eastern Greater Antilles may have a crustal thickness of around 15 Km. From an analysis of gravity data, Talwani et al., (1959) deduced a maximum thickness of 30 Km for a "root" beneath the eastern Greater Antilles. However, a more direct investigation of the crust beneath Puerto Rico by seismic refraction would provide invaluable data for a more detailed estimation of the physical and chemical nature of the crust-mantle system of this island arc.

APPENDIX A-D: PETROGRAPHIC DATA OF ANALYZED SAMPLES OF THE BERMEJA COMPLEX

Sample localities and petrography of analyzed samples of the Bermeja complex, including schistose amphibolites (A), massive metabasaltic dikes (B), spilites (C), amphibolitized dolerite (D), and serpentinized peridotite (E) are described below.

A. Schistose Amphibolite

The following five samples of schistose amphibolites were analyzed and shown in Tables 10 and 14.

Ba-8a-1: The schistose amphibolite was sampled on a stream cut, about 20 m north of the bridge on route 303 at Las Palmas. The rocks are deep green colored and well foliated, having a segregation layering consisting of white layers of plagioclase and quartz that alternate with dark green layers rich in hornblende, with an average grain size of 0.8 mm. Dominant minerals are hornblende, plagioclase, and quartz; accessories are scattered magnetite, sphene, and apatite. Hornblende is subhedral prismatic (averaging 1 mm in length), elongated parallel to the foliation with well developed cleavage. The plecchroism is X = pale yellow, Y = deep yellowish green, and Z = bluish green. The extinction angle (C∧Z) is about 22°. The optic angle ($2V_X$) as measured on a universal stage is 81°. Refractive index determinations

of n_X and n_Y are 1.652 and 1.676, respectively. Plagioclase is either twinned or untiwined, usually very slightly zoned with an average composition of An_{34} as determined on a universal stage by the maximum extinction angle method. It commonly shows undulatory extinction, occurring as anhedral and slightly flattened grains (averaging 0.8 mm in longest dimension, which is subparallel to the foliation) associated with smaller anhedral quartz grains (averaging 0.5 mm) in the light-colored layers that alternate with the dark colored layers rich in hornblende. Plagioclase is usually slightly clouded in appearance and altered to white micas. Accessory sphene, apatite, and opaque minerals are interstitial or inclusions in hornblende.

Ba-8a-4: Sample from a stream cut, about 55 m north of the bridge on route 303 at Las Palmas. The rock is generally similar to sample Ba-8a-1 and consists dominantly of hornblende, plagioclase, and quartz, with minor iron oxides (magnetite), apatite, and sphene. Hornblende: n_X = 1.658, n_Z = 1.682. Pleochroism X = straw yellow, Y = yellowish green, Z = bluish green, $2V_X = 80^\circ$. The composition of plagioclase is An_{40}.

7717-85: Sample obtained 110 m north and 350 south of the contacts with the serpentinite at Las Palmas. In general the rock is megascopically and microscopically similar to sample Ba-8a-1, except for a finer average grain size (averaging 0.6 mm). The essential minerals include hornblende, plagio-

clase, quartz, and sphene. The plagioclase (An_{36}) is slightly to moderately altered to white micas. A small amount of epidote minerals in megascopic veinlets was sawed out before chemical analysis. Hornblende: $2V_X = 80^\circ$, pleochroism X = pale yellow, Y = yellowish green, Z = pale bluish green, $n_X = 1.644$, $n_Z = 1.666$.

7917-45: Sample obtained 400 m north and 80 m south of the contacts with the serpentinite at Las Palmas. The rock is similar to sample Ba-8a-1. It contains essentially hornblende, plagioclase, and quartz, with minor iron oxides, sphene, and apatite. Hornblende: $2V_X = 74^\circ$, pleochroism X = pale yellow, Y = yellowish green, Z = green to pale bluish green, $n_X = 1.660$, $n_Z = 1.682$. Plagioclase is An_{34} and is locally slightly altered to white micas.

7917-66: Sample obtained 120 m north and 400 m south of the contacts with the serpentinite at Las Palmas. Generally, the rock is similar to sample Ba-8a-1, with dominant hornblende, plagioclase, and quartz, and minor iron oxides, sphene, and apatite. The pleochroism of the hornblende is deeper than that of sample Ba-8a-1, showing X = pale yellow, Y = deep yellowish green to brownish green, and Z = bluish green to brownish bluish green, with $2V_X = 76^\circ$ and $n_X = 1.656$ and $n_Z = 1.680$. Plagioclase (An_{40}) is slightly to moderately altered to white micas. Small veinlets filled with tiny epidote grains and quartz, were mostly removed before chemical analysis.

B. Massive Metabasaltic Dike

Two samples of massive metabasaltic dike were analyzed and shown in Tables 11 and 14.

Ba-8b-2: The massive metabasaltic dike was sampled on the stream cut, about 65 m north of the bridge on route 303 at Las Palmas. The dike, which is intruded into schistose amphibolite, has a deep green groundmass set with light colored,randomly oriented, prismatic phenocrysts. Under the microscope, it contains about 20 percent of porphyroblasts and relict phenocrysts (0.5 to 1.5 mm) in a fine grained intersertal groundmass. The essential minerals include amphibole and plagioclase, with minor amount of iron oxides, and prehnite. The amphibole occurs as simple crystals of hornblende (0.5 mm), as groups of subradiated fibrous actinolite after original mafic minerals (probably olivine and/or pyroxene) or as small subhedral prismatic hornblende in the groundmass. Generally, the cleavage of the hornblende is not well developed. Hornblende: $2V_X = 67^\circ$, optic axis Z = pale bluish green, $n_X = 1.646$, $n_Z = 1.668$. Actinolite : $2V_X = 70^\circ$, very faint pleochroic, $n_Y = 1.656$. Plagioclase laths in phenocrysts from 0.5 mm to 1.5 mm are usually dusty in appearance and slightly to moderately altered to tiny hornblende grains and also commonly replaced by epidote minerals (clinozoisite). Some less altered crystals are either twinned or untwinned with slight zonning, with an average composition of An_{33}. Tiny granules of magnetite occur throughout the

rock. Veinlets are filled with tiny prehnite,plagioclase, and quartz (?), mostly are sawed away and not included in the prepared sample for the chemical analysis.

Ba-10: The dike rock was sampled in a small road cut about 0.25 mile west of a 69.1 m benchmark at Las Palmas. The rock is megascopically similar to sample Ba-8b-2. The rock consists essentially of hornblende, plagioclase, with minor epidote, sphene, iron oxides (magnetite), and prehnite. The original phenocrysts of plagioclase and mafic minerals is less than 15 percentage. A weak foliation is defined by a subparallel arrangement of elongate hornblende grains, which are subhedral prismatic and range from very small to 0.3 mm. The pleochroism of hornblende shows X = pale yellow, Y = yellowish green, and Z = pale bluish green to pale brownish green. $2V_X$ is about 73°, n_X and n_Z are 1.644 and 1.664, respectively. Plagioclase phenocrysts are usually dusty in appearance and are replaced by tiny hornblende. Some less altered plagioclase has a composition of An_{35} as determined on universal stage. Anhedral but elongated magnetite grains tend to be parallel to the weakly developed foliation. Veinlets, which were mostly sawed out before chemical analysis, consist of epidote, plagioclase, prehnite, and lesser amounts of chlorite.

C. Spilite

Three samples of spilite were analyzed and shown in

Tables 12 and 14.

Ba-1b: The spilite was sampled 4 m away from the sheared contact zone with foliated serpentinite on the east wall of the water outlet cut at the northwestern corner of the quarry about 0.7 mile by road east of Mayaguez on route 105. It is massive grayish green rock with an average grain size of 0.7 mm. Slickensides, joints, and calcite veinlets are visible on the outcrops. The rock is intersertal in texture and consists dominantly of albite laths and interstitial augite and chlorite, with minor amounts of calcite, epidote, prehnite, white micas, and iron oxides (magnetite). The plagioclase is slightly clouded and altered to white micas, chlorite, and epidote. The composition is albite (An_{4-6}) as determined by universal stage. The interstitial augite commonly exhibits undulatory extinction and the optical angle is thus difficult to determined. $n_Y = 1.684$. The veinlets consist mostly of calcite and minor prehnite, chlorite, epidote, and anhedral albite, and were carefully sawed out during the preparation of the sample for chemical analysis.

Ba-3: The spilite was sampled about 2 m up on the western wall of the quarry about 0.7 mile by road east of Mayaguez on route 105. The rock is massive and grayish green with an average grain size of 0.6 mm, and an intersertal texture. Major minerals include albite laths, augite, and chlorite, with minor epidote, magnetite, and prehnite. Plagioclase is clear and only very slightly replaced by

the same. Augite: $2V_Z = 50^\circ$, $n_Y = 1.686$. The original interstitial glass (?) is completely replaced by chlorite. Calcite veinlets were mostly removed before chemical analysis.

Ba-6: The spilite was sampled about 15 m above the bottom of the wall at the eastern side of the quarry about 0.7 miles by road east of Mayaguez on route 105. The rock is massive with a pale grayish green matrix spotted with dark green pyroxenes with an average grain size of 1 mm. The spilite has intersertal texture, and consists mainly of albite laths and interstitial clinopyroxene and chlorite, with small amounts of iron oxides (magnetite), calcite, white micas, prehnite, and epidote. The plagioclase (An_4) is slightly clouded and replaced by white micas, chlorite, epidote, and prehnite. Clinopyroxene is augite with $2V_Z = 53^\circ$, $n_Y = 1.686$. It sometimes altered to yellowish brown granular aggregates and yellowish green prismatic crystals of epidote associated with or without magnetite and chlorite. Calcite veinlets were mostly removed before chemical analysis.

D. Amphibolitized Dolerite

Ba-7a: The amphibolitized dolerite was sampled in the quarry about 0.7 miles by road east of Mayaguez on route 105. The rock is deep grayish green with subophitic texture and average grain size of 0.8 mm. It contains mostly zoned plagioclase (An_{45-70}) and hornblende, with accessory relic clinopyroxene, iron oxides, and white micas. The calcic-core

of the plagioclase is clouded and slightly altered to white micas. The pleochroism of hornblende is X = pale yellow, Y = yellowish green, and Z = green to pale bluish green, occuring as subhedral to anhedral crystals ranging from 0.1 to 1 mm in the interstices between plagioclase. The average optical angle ($2V_X$) is 70°. n_X and n_Y are 1.642 and 1.662, respectively. Small relic clinopyroxene occur rarely in the cores of large hornblende grain with $2V_Z = 59^\circ$. Irregularly shaped iron oxides are associated with or embedded in the hornblende. Rock analyses are shown in Tables 12 and 14.

E. Serpentinized Peridotite

B-2: The serpentinite is from the MASOC test hole core near Mayaguez, Puerto Rico (Burk, ed., 1964), at a depth of 19.49 m. The rock is a dark greenish brown and is about 80 percent serpentinized. It originally contained about 75 per cent olivine and 25 percent pyroxene. The original orthopyroxene (about 20 percent), usually anhedral and equidimensional, is up to 4 mm in size, while the anhedral clinopyroxene (about 5 percent) is up to 2 mm. The relict orthopyroxene (about 15 percent) is enstatite with $2V_Z$ of 88° and $n_X = 1.664$, $n_Z = 1.676$. Closely spaced thin exsolution lamellae of clinopyroxene, oriented parallel to the (100) plane of enstatite are common. The clinopyroxene lamellae usually pinch out towards the edge of the enstatite grains, however, they may extend beyond the borders of fresh enstatite

in serpentine. The relict clinopyroxene (< 5 percent) is diopside with a $2V_Z$ of 56° and n_Y = 1.678. Relict olivine is rare (< 5 percent) with $2V_Z$ of 86°, but the refractive index is difficult to determine. Translucent spinel of a golden brown color occurs as scattered interstitial crystals about 0.6 mm in size, rimmed by opaque minerals (magnetite ?). Spinel constituted about 2 percent of the original rock, as judged from its relict interstitial texture. Serpentinized peridotite analyses are shown in Tables 13 and 14.

REFERENCES CITED

Abbey, S., 1972, "Standard samples" of silicate rocks and minerals - A review and compilation: Geol. Surv. Can. Paper, p. 72-130

Amstutz, G. C., 1968, Spilites and spilitic rocks: in Poldervaart treatis on rocks of basaltic composition, v. 2 (H. H. Hess; and A. Poldervaart, eds.), Interscience Publishers, p. 373-753, New York, 1968

Baker, P. E., 1968, Comparative volcanology and petrology of the Atlantic island arcs: Bull. Volcan., v. 32, p. 189

_____and Harris, P. G., and Reay, A., 1971, The geology of Tofua Island, Tonga: Royal Soc. New Zealand Bull., v. 8, p. 67-79

Bauer, G. R., 1970, The geology of Tofua Island, Tonga: Pacific Science, v. 24, p. 333-350

Berkey, C. P., 1915, Geological reconnaissance of Puerto Rico: N. Y. Acad. Sci. Ann., v. 26, pt. 1, p. 1-70

Berryhill, H., Briggs, R. P., and Glover, L., III, 1960, Stratigraphy, sedimentation, and structure of Late Cretaceous rocks in eastern Puerto Rico - Preliminary report: Am. Assoc. Petroleum Geologists Bull., v. 44, p. 137-155

Bertin, E. P., 1970, Principles and practice of X-ray spectrometric analysis: New York, Plenum Press, 679 p.

Bowin, C. O., Nalwalk, A. J., and Herney, J. R., 1966, Serpentinized peridotite from the north wall of the

Puerto Rico Trench: Geol. Soc. America Bull., v. 77, p. 357-270

Briggs, R. P., 1961, Preliminary geologic map of Puerto Rico and adjacent islands: U. S. Geol. Survey open file report.

_____and Akers, J. P., 1965, Hydrogeologic map of Puerto Rico and adjacent areas: U. S. Geol. Survey Hydrogeologic Investigations Atlas HA-197

_____and Gelabert, P., 1962, Preliminary report of the geology of the Barranquitos quadrangle, Puerto Rico: U. S. Geol. Survey Misc. Geol. Inv. Map I-336

Brothers, R. N., and Martin, K. R., 1970, The geology of Macauley Island, Kermadec group, Southwest Pacific: Bull. Volcanol., v. 34, p. 330-346

_____and Searle, E. J., 1970, The geology of Raoul Island, Kermadec group, Southwest Pacific: Bull. Volcanol., v. 34, p. 7-37

Bryan, W. B., Stice, G. D., and Ewart, A., 1972, Geology, petrography, and geochemistry of the volcanic islands of Tonga: Jour. Geophys. Research, v. 77, p. 1566-1585

Burns, R. G., 1970, Site preferences of transition metal ions in silicate crystal structures: Che. Geol., v. 5, p. 275-283

Campbell, A. S., and Fyfe, W. S., 1965, Analcime-albite equilibria: Am. J. Sci., v. 263, p. 8070816

Challis, G. A., 1969, Discussion on the paper "The origin of ultramafic and ultrabasic rocks" by Wyllie, P. J.:

Techtonophysics, v. 7, p. 495-505

Coombs, D. S., 1954, The nature and alteration of some Triassic sediments from Southland, New Zealand: Trans. R. Soc. Z. Z. 82, p. 65-109

_____1961, Some recent work on the lower grades of metamorphism: Austral. J. Sci., v. 24, p. 203-215

_____Ellis, A. J., Fyfe, W. S., and Taylor, A. M., 1959, The zeolite facies, with comments on the interpretation of hydrothermal syntheses: Geochim. Cosmochim. Acta, v. 17, p. 53-107

_____Horodyski, R. J., and Naylor, R. S., 1970, Occurrence of prehnite-pumpellyite facies metamorphism in northern Maine: Am. J. Sci., v. 268, p. 142-156

Dengo, G., 1972, Review of Caribbean serpentinites and their tectonic implications: Geol. Soc. Amer. Mem. 132, p. 303-312

Donnelly, T. W., 1960, The geology of St. Thomas and St. John, Virgin Islands: Trans. 2nd Caribbean Geol. Conf. p. 153-155

_____1964, Evolution of eastern Greater Antillean Island Arc: Amer. Assoc. Petrol. Geol. Bull., v. 48, p. 680-696

_____1966, Geology of St. Thomas and St. John, U. S. Virgin Island: in Hess, H. H., ed., Caribbean Geological Investigation: Geol. Soc. America Mem. 98, p. 85-176

_____1970, Summary of the Cretaceous stratigraphy of north-central Puerto Rico: in Donnelly, T. W., ed., Inter-

national Field Institute in the Eastern Caribbean: Natl. Sci. Foundation - Am. Geol. Inst., p. 1-5

_____1972, Deep-water, shallow-water, and subaerial island-arc volcanism: an example from the Virgin Islands: Geol. Soc. America Mem. 132, p. 401-414

_____1973, Evolution of island-arc magmas: The Caribbean and South-west Pacific compared:

_____Rogers, J. J. W., Pushkar, P., and Armstrong, R. L., 1971, Chemical evolution of the igneous rocks of the Eastern West Indies: An investigation of thorium, uranium, and potassium distribution, and lead and strontium isotopic ratios: Geol. Soc. America Mem. 130, p. 181-224

Emmons, R. C., 1953, Selected petrogenic relationships of plagioclase Geol. Soc. Amer. Mem. 52, 142p.

Ernst. W. G., 1965, Mineral parageneses in Franciscan metamorphic rocks, Panoche Pass, California: Bull. Geol. Soc. Am., v. 76, p. 879-914

_____Seki, Y., Onuki, H., and Gilbert, M. G., 1970, Comparative study of low-grade metamorphism in the California Coast ranges and the outer metamorphic belet of Japan: Geol. Soc. America Mem. 124, 276 p.

Flanagan, F. J., 1967, U. S. Geological Survey silicate rock standards: Geochim. Cosmochim, Acta, v. 31, p. 280-308

Gill, J. B., 1970, Geochemistry of Viti Levu, Fiji, and its evolution as an island arc: Contrib. Mineral. Petrol., v. 27, p. 179-203

Glover, L., 1967, Geology of the Coamo quadrangle, Puerto Rico: Ph. D. Dissert., Princeton Univ. Princeton, New Jersey, 363 p.

_____1971, Geology of the Coamo area, Puerto Rico: U. S. Geol. Survey Prof. Paper 636

Gorshkov, G. W., 1970, Volcanism and the upper mantle. Investigations in the Kurile Island arc: New York, Plenum Press, 385 p.

Green, D. H., 1964, The petrogenesis of the high-temperature peridotite intrusion in the Lizard area, Cornwall: Journ. Petrology, v. 5, p. 134-188

_____1967, High-temperature peridotite intrusions: in Wyllie, P. J., ed., Ultramafic and related rocks, p. 212-222, New York, John Wiley 1967.

Gunn, B. M., 1971, Trace element partition during olivine fractionation of Hawaiian basalts: Chem. Geol., v. 8, p. 1-13

Harris, P. G., Reay, A., and White, L. G., 1967, Chemical composition of the upper mantle: J. Geophys. Res., v. 72, p. 6359-6369

Hart, S. R., 1970, Chemical exchange between sea water and deep ocean basalts: Earth Planet Sci. Lett., v. 9, p. 269-279

_____and Nalwalk, A. J., 1970, K, Rb, Cs, and Sr relation-

ships in submarine basalts from the Puerto Rico trench: Geochim. Cosmochim. Acta, v. 34, p. 145-155

Hekinian, R., 1971, Petrological and geochemical study of spilites and associated rocks from St. John, U. S. Virgin Islands: Geol. Soc. America Bull., v. 82, p. 659-682

Henderson, P., and Dale, I. M., 1970, The partitioning of selected transition element ions between olivine and groundmass of oceanic basalts: Chem. Geol., v. 5, p. 267-274

Hess, H. H., 1955, The oceanic crust: J. Marine Res., v. 14, p. 423-439

_____1960, Caribbean research project: Progress report: Geol. Soc. America Bull., v. 71, p. 236-240

_____1964, The oceanic crust, the upper mantle and the Mayaguez serpentinized peridotite: in Burk, C. A., ed., A study of serpentinite: Nat. Acad. Sci. - Natl. Research Council: Pub. 1188, p. 169-175

_____1966, Caribbean research project, 1965, and bathymetric chart: Geol. Soc. Amer. Mem. 98, p. 1-10

_____and Maxwell, J. C., 1953, Caribbean research project: Geol. Soc. America Bull., v. 64, p. 1-6

_____and Otalora, G., 1964, Mineralogical and chemical composition and their bearing upon the origin of the serpentinite near Mayaguez, in Burk, C . A., ed., A study of serpentinite: Nat. Acad. Sci. - Natl. Research Council: Pub. 1188, p. 152-168

Hubbard, B., 1923, The geology of the Lares district, Puerto Rico: N. Y. Acad. Sci., Scientific Survey of Puerto Rico and the Virgin Islands, v. 2, pt. 1, p. 1-115

Jakes, P., and Gill, J. B., 1970, Rare earth elements and the island arc tholeiitic series: Earth Planet. Sci. Lett., v. 9, p. 17-28

_____and White, A. J. R., 1969, Structure of the Melanesian arcs and correlation with distribution of magma types: Tectonophysics, v. 8, p. 223

_____and White, A. J. R., 1971, Composition of island arcs and continental growth: Earth Planet. Sci. Lett., v. 12, p. 244-230

_____and White, A. J. R., 1972, Major and trace element abundances in volcanic rocks of orogenic areas: Geol. Soc. Amer. Bull., v. 83, p. 29-40

Jolly, W. T., 1970a, Zeolite and prehnite-pumpellyite facies in south central Puerto Rico: Contr. Mineral. and Petrol. v. 27, p. 204-224

_____1970b, Lapa lava member of the Robles formation, south central Puerto Rico in Donnelly, T. W., ed., International Field Institute in the Eastern Caribbean: Natl. Sci. Foundation - Am. Geol. Inst., p. 1-2

_____1971, Potassium-rich igneous rocks from Puerto Rico: Geol. Soc. Amer. Bull., v. 82, p. 399 -408

Jopline, G. A., 1968, The shoshonite association: A review: Geol. Soc. Australia Jour., v. 15, p. 275-294

Karig, D. E., 1970, Ridges and basins of the Tonga-Kermadec

Island arc system: Jour. Geophys. Research, v. 75, p. 239-254

Kay, R., Hubbard, N. J., and Gast, P. W., 1970, Chemical characteristics and origin of oceanic ridge volcanic rocks: J. Geophys. Res., v. 75, p. 1585-1613

Kaye, C., 1959, Geology of the San Juan metropolitian arean, Puerto Rico: U. S. Geol. Survey Prof. Paper 317-A, p. 1-4E

Kuno, H., 1959, Origin of Cenozoic petrographic provinces of Japan and surrounding areas. Bull. Volcanol. Ser. 2, v. 20, p. 37-76

Lidiak, E. G., 1965, Petrology of andesitic, spilitic, and Keratophyric flow rock, north-central Puerto Rico: Bull. Geol. Soc. Am., v. 76, p. 57-88

_____1970, Volcanic rocks in the Puerto Rican Orogen, in Donnelly, T. W., ed., International Field Institute in the Eastern Caribbean: Natl. Sci. Foundation - Am Geol. Inst., p. 1-7

Liou, J. G., 1970, Synthesis and stability relations of wairakite, $CaAl_2Si_4O_{12}.2H_2O$: Contr. Mineral. Petrol., v. 27, p. 257-282

Macdonald, C. A., and Katsura, T., 1964, Chemical composition of Hawaiian lavas: Jour. Petrology, v. 5, p. 82-133

Malfait, B. R., and Dinkelman, M. G., 1972, Circum-Caribbean tectonic and igneous activity and the evolution of Caribbean plate: Geol. Soc. America Bull., v. 83, p. 251-272

Matsuda, T., and Kuriyagawa, S., 1965, Lower grade metamorphism in the eastern Akaishi Mountains, central Japan: Tokyo Univ. Earthquake Res. Inst. Bull., v. 43, p. 209-235

Mattson, P. H., 1960, Geology of the Mayaguez area, Puerto Rico: Geol. Soc. America Bull., v. 71, p. 319-362

_____1964, Petrography and structure of serpentinite from Mayaguez, Puerto Rico, in Burk, C. A., ed., A study of serpentinite: Nat. Acad. Sci. - Nat. Res. Council Pub. 1188, p. 7-24

_____1966, Geological characteristics of Puerto Rico, p. 124-138, in Poole, W. H., ed., Continental margins and island arcs: Canada Geol. Survey Paper 66-15

_____1967, Cretaceous and lower Tertiary stratigraphy in west-central Puerto Rico: U. S. Geol. Survey Bull. 1257-B, p. B1-1335

_____1970, Road logs in western Puerto Rico, p. 1-26, in Donnelly, T. W. ed., International Field Institute in the Eastern Caribbean: Nat. Sci. Foundation: Amer. Geol. Inst., Washington.

_____1973a, Middle Cretaceous nappe structures in Puerto Rican ophiolites and their relation to the tectonic history of the Greater Antilles, Geol. Soc. America Bull., v. 84, p. 21-38

_____1973b, Middle Cretaceous nappe structures in Puerto Rican ophiolites and their relation to the tectonic history of the Greater Antilles: Reply: Geol. Soc.

America Bull., v. 84, p. 3757-3760

_____Pessagno, E. A., 1971, Caribbean Eocene volcanism and Atlantic Ocean layer A: Science, v. 174, p. 138-139

_____Pessagno, E. A., and Helsley, C. E., 1972, Outcropping layer A and A" correlatives in the Greater Antilles: Geol. Soc. Amer. Mem. 132, p. 57-66

_____and Schwartz, D. P., 1971, Control of intensity of deformation in Puerto Rico by mobile serpentinized peridotite basement: Geol. Soc. America Mem. 130, p. 97-106

McIntyre, D. H., Aaron, J. M., and Tobisch, O. T., 1970, Cretaceous and Lower Tertiary stratigraphy in southwestern Puerto Rico: U. S. Geol. Survey Bull. v. 1294-d, p. D1-D16.

Melson, W. G., Jarosewich, E., Bowen, V. T., and Thompson, G, 1967, St. Peter and St. Paul Rocks: a high-temperature mantle-derived intrusion: Science, v. 155, p. 1532-1535

Mayerhoff, H. A., 1933, Geology of Puerto Rico: University of Puerto Rico Monograph, Ser. B. no. 1, 306 p.

Mitchell, G. J., 1922, Geology of Ponce district, Puerto Rico: N. Y. Acad. Sci., Scientific Survey of Puerto Rico and the Virgin Islands, v. 1, pt. 3, p. 229-300

Miyashiro, A., 1966, Some aspects of peridotite and serpentinite in orogenic belts: Jap. Jour. Geol. Geogr., v. 37, p. 45-61

_____1972, Metamorphism and related magmatism in plate

tectonics: Am. Jour. Sci., v. 272, p. 629-656

_____1973a, Paired and unpaired metamorphic belts: Tectonophysics, v. 17, p. 241-254

_____1973b, The troodos ophiolitic complex was probably formed in an island arc: Earth Planet. Sci. Lett., v. 19, p. 218-224

_____1973c, Metamorphism and metamorphic belts: New York, John Wiley & Sons, 492 p.

_____in press, Volcanic rocks series in island arcs

_____and Shido, F., 1970, Progressive metamorphism in zeolite assemblages: Lithos,, v. 3, p. 251-260

_____Shido, F., and Ewing, M., 1969a, Diversity and origin of abyssal tholeiite from the Mid-Atlantic Ridge near 24° and 30° north latitude: Contri. Mineral. and Petrol., v. 23, p. 38-52

_____Shido, F., and Ewing, M., 1969b, Composition and origin of serpentinites from the Mid-Atlantic Ridge: Contr. Mineral. and Petrol., v. 23, p. 117-127

_____Shido, F., and Ewing, M., 1970, Crystallization and differentiation in abyssal tholeiites and gabbros from mid-oceanic ridges: Earth Planet. Sci. Lett., v. 7, p. 361

_____Shido, F., and Ewing, M., 1971, Metamorphism in the Mid-Atlantic ridge near 24° and 30° N: Phil. Trans. Sco. Lond. A., v. 268, p. 589-603

Molnar, P., and Sykes, L., 1969, Tectonics of the Caribbean and Middle America regions from focal mechanisms and

seismicity: Geol. Soc. America Bull., v. 80, p. 1639-1684

Nockolds, S. R., and Allen, R., 1953, 1954, 1956, the geochemistry of some igneous rock series, I, II, III: Geochim. Cosmochim. Acta, v. 4, p. 105-142; v. 5, p. 245-285; v. 9, p. 34-77

Otalora, G., 1964, Zeolites and related minerals in Cretaceous rocks of east-central Puerto Rico: Am. Jour. Sci., v. 262, p. 726-734

Pease, M., 1968, Cretaceous and lower Tertiary stratigraphy of the Naranjito and Agnos Buenos quadrangles and adjacent areas, Puerto Rico: U. S. Geol. Survey Bull., v. 1253, p. 1-57

Renz, O., and Verspyck, G. W., 1962, The occurrence of geneissic amphibolite in southwest Puerto Rico: Geologie, en Mijnbouw, v. 41, p. 315-320

Robson, G., and Tomblin, J., 1966, Catalogue of the active volcanoes of the world including Solfatara fields: Part XX. West Indies: Internat. Assoc. Volcanology Rome, p. 1-56

Schmidt, R. G., 1957, Geology of Saipan, Mariana Islands, part 2, Chapter B, Petrology of the volcanic rocks: U. S. Geol. Survey Prof. Paper 280-B-D, p. 127-176

Seiders, V. M., 1971, Cretaceous and lower Tertiary stratigraphy of the Gurabo and El Yuque quadrangles, Puerto Rico: U. S. Geol. Survey Bull. 1294-F, p. F1-F58

Seki, Y., Oki, Y., Matsuda, T., Mikami, K., and Okumura, K.,

1969. Metamorphism in the Tanzawa Mountains, Central Japan: J. Japanese Assoc. Min. Petr. Econ. Geol., v. 61, p. 1-29, 50-75

_____Onuki, H., Oba, T., and Mori, R., 1971, Sanbagawa metamorphism in the central Kii Peninsula: Jap. J. Geol. Geogr., v. 41, p. 65-78

Shido, F., Miyashiro, A., and Ewing, M., 1971, Crystallization of abyssal tholeiites: Contr. Mineral. and Petrol., v. 31, p. 251-266

Stark, J. T., 1963, Petrology of the volcanic rocks of Guam: U. S. Geol. Survey Prof. Paper 403-C, C1-32

Talwani, M., Sutton, G. H., and Worzel, J. L., 1959, A crustal section across the Puerto Rico Trench: Jour. Geophys. Res., v. 64, p. 1545-1555

Tanakadate, H., 1940, Volcanoes in the Mariana Islands in the Japanes mandated South Sea: Bull. Volcanol., ser. 2, v. 6, p. 199-223

Thompson, A. B., 1970, Laumontite equilibria and the zeolite facies: Am. J. Sci., v. 269, p. 267-275

Thompson, G., 1973, Trace-element distributions in fractionated oceanic rocks, 2 Gabbros and related rocks: Chem. Geol., v. 12, p. 99-111

_____Shido, F., and Miyashiro, A., 1972, Trace element distribution in fractionated oceanic basalt: Chem. Geol. v. 9, p. 89-97

Tilley, C. E., 1947, The dunite-mylonites of St. Pauls' Rocks (Atlantic): Am. J. Sci., v. 245, p. 483-491

_____1966, A note on the dunite (peridotite) mylonites of St. Paul's Rocks (Atlantic): Geol. Mag.,v. 103, p. 120-123

Tobisch, O. T., 1968, Genessic amphibolite at Las Palmas, Puerto Rico, and its significance in the early history of the Greater Antilles island arc: Geol. Soc. America Bull., v. 79, p. 557-574

Utada, M., 1965, Zonal distribution of authigenic zeolites in the Tertiary pyroclastic rocks in Mogami district, Yamagata prefecture. Tokyo Univ. Coll. Gen. Educ. Sci. Paper, v. 15, p. 173-216

Walper, J. L., 1973, Middle Cretaceous nappe structure in Puerto Rican Ophiolites and their relation to the tectonic history of the Greater Antilles: Discussion: Geol. Soc. America Bull., v. 84, p. 3755-3756

White, A. J. R., Jakes, P., and Christie, D. M., 1971, Composition of greenstones and the hypothesis of sea-floor spreading in the Archaean: Geol. Soc. Australia Spec. Pub., v. 3, p. 47-56

Yoder, H. S., Jr. and Tilley, C. E., 1962, Origin of basalt magmas and experimental study of natural and synthetic rock systems: Jour. Petrology, v. 3, p. 342-532